

University of Groningen

Relevance, targets, and clinical translation of near-infrared fluorescence imaging in breast cancer

Pleijhuis, Rick Gert-Jan

IMPORTANT NOTE: You are advised to consult the publisher's version (publisher's PDF) if you wish to cite from it. Please check the document version below.

Document Version

Publisher's PDF, also known as Version of record

Publication date:

2013

[Link to publication in University of Groningen/UMCG research database](#)

Citation for published version (APA):

Pleijhuis, R. G-J. (2013). Relevance, targets, and clinical translation of near-infrared fluorescence imaging in breast cancer Groningen: s.n.

Copyright

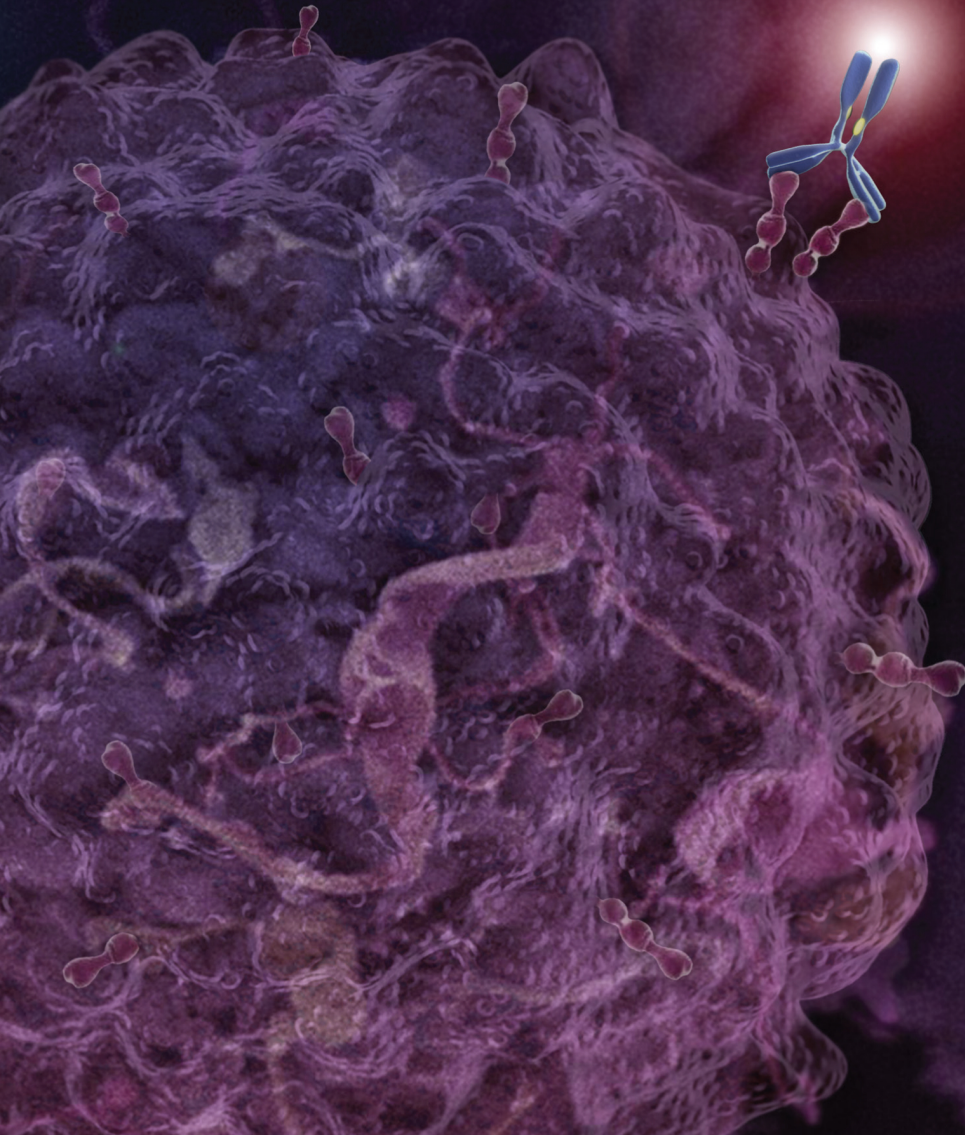
Other than for strictly personal use, it is not permitted to download or to forward/distribute the text or part of it without the consent of the author(s) and/or copyright holder(s), unless the work is under an open content license (like Creative Commons).

Take-down policy

If you believe that this document breaches copyright please contact us providing details, and we will remove access to the work immediately and investigate your claim.

Downloaded from the University of Groningen/UMCG research database (Pure): <http://www.rug.nl/research/portal>. For technical reasons the number of authors shown on this cover page is limited to 10 maximum.

Relevance, targets, and clinical translation of near-infrared fluorescence imaging in breast cancer



Relevance, targets, and clinical translation
of near-infrared fluorescence imaging
in breast cancer

R.G. Pleijhuis

COLOFON

Pleijhuis, R.G.

Relevance, targets, and clinical translation of near-infrared fluorescence imaging
in breast cancer

Thesis, University of Groningen, The Netherlands

ISBN: 978-90-367-6660-9 (printed version)

ISBN: 978-90-367-6659-3 (electronic version)

Cover design: R.G. Pleijhuis

Lay-out: R.G. Pleijhuis

Printed by: Gildeprint Drukkerijen - Enschede

© Copyright 2014 R.G. Pleijhuis, The Netherlands

All rights reserved. No part of this thesis may be reproduced, stored in a retrieval system, or transmitted in any form or by any means, without prior permission of the author.

Publication of this thesis was financially supported by: University of Groningen, University Medical Center Groningen (UMCG), Groningen University Institute for Drug Exploration (GUIDE), and Koninklijke Nederlandsche Maatschappij tot Bevordering der Geneeskunst (KNMG) district XVII.



rijksuniversiteit
groningen

**Relevance, targets, and clinical translation
of near-infrared fluorescence imaging
in breast cancer**

Proefschrift

ter verkrijging van de graad van doctor aan de
Rijksuniversiteit Groningen
op gezag van de
rector magnificus, prof. dr. E. Sterken
en volgens besluit van het College voor Promoties.

De openbare verdediging zal plaatsvinden op

maandag 20 januari 2014 om 12:45 uur

door

Rick Gert-Jan Pleijhuis

geboren op 26 augustus 1987
te Almelo

Promotores:

Prof. dr. G.M. van Dam

Prof. dr. T. Wiggers

Copromotores:

Dr. J.S. de Jong

Dr. W. Helfrich

Beoordelingscommissie:

Prof. dr. E.G.E. de Vries

Prof. dr. P.J. van Diest

Prof. dr. C.W.G.M. Löwik

Paranimfen:

Kasper Veldhuis

Arnoud Potgieser

Aan mijn ouders

TABLE OF CONTENTS

Chapter 1	General introduction and outline of the thesis	9
Chapter 2	Obtaining adequate surgical margins in breast-conserving therapy for patients with early-stage breast cancer: current modalities and future directions	15
Chapter 3	A validated web-based nomogram for predicting positive surgical margins following breast-conserving surgery as a preoperative tool for clinical decision-making	37
Chapter 4	Segmentation-based comparative analysis of planar optical signals (SCAPOS): a platform to detect and correct for discrepancies in tumor demarcation in planar fluorescence imaging	57
Chapter 5	Near-infrared fluorescence (NIRF) imaging in breast-conserving surgery: assessing intraoperative techniques in tissue-simulating breast phantoms	69
Chapter 6	Optical imaging for lymph node surveillance in breast cancer patients: intraoperative detection as a step-up approach towards tumor-targeted imaging	81
Chapter 7	A systematic review and meta-analysis of sentinel lymph node identification in breast cancer and melanoma: a plea for tracer mapping	93
Chapter 8	Selecting tumor markers for targeted imaging applications in breast cancer: the next step in patient-tailored interventions	127
Chapter 9	Identifying tumor markers in lymph node metastases for targeted imaging applications in breast cancer patients	159
Chapter 10	Summary	181
Chapter 11	Conclusions & future perspectives	185
Chapter 12	Nederlandse samenvatting	193
ADDENUM		
	List of abbreviations	198
	Dankwoord	200
	List of publications	202
	Curriculum vitae	203

Chapter

1

General introduction & outline of the thesis

R.G. Pleijhuis

INTRODUCTION

Optical imaging has a substantial impact on basic and translational medical research through the development of optical imaging modalities for visualization of a wide variety of cellular and molecular processes *in vivo*.¹ Optical imaging is considered safe, fast, inexpensive, makes use of non-ionizing radiation, and enables real-time anatomical and functional imaging.² It has the potential to become a powerful and practical tool for a wide array of applications in medicine and in particular in cancer research and treatment, such as noninvasive early detection, image-guided biopsy, intraoperative procedures, image-guided pathology, and therapeutic monitoring of cancer.³

This thesis focuses on the development of near-infrared fluorescence imaging applications to complement the surgical treatment of breast cancer. In addition, the identification of suitable tumor targets is described for targeted imaging applications.

Basic principles of optical imaging

In optical imaging, information is obtained through measuring photons originating from a certain area of interest. Photons can either be emitted as a product of a (bio)chemical reaction or as a result of the excitation of fluorescent molecules. Although the amount of photons emitted is typically small and therefore undetectable with the human eye, a highly sensitive charged-coupled device (CCD) camera can be applied to image emitted photons noninvasively.⁴ Optical signals are influenced by several variables when propagating through tissue, including absorption and scattering of photons. There are many molecular components in biological tissue that can absorb photons, collectively known as endogenous tissue chromophores. Examples of such chromophores include hemoglobin, melanin, nucleic acids, water molecules, and lipids, which all have their own unique spectrum.⁵ In the visible and ultraviolet spectral range (<650 nm), scattering and absorption of photons by tissue chromophores limit effective light penetration to several millimeters. In the near-infrared (NIR) spectral range (650–900 nm), tissue penetration is up to several centimeters as scattering and photon absorption by tissue chromophores are minimized. At longer wavelengths (>900 nm), tissue penetration decreases again due to absorption of photons by water molecules. The optimal spectral window for imaging purposes therefore lies between 650 nm and 900 nm, also known as the *diagnostic window* (Fig. 1).

Near-infrared fluorescence optical imaging

In near-infrared fluorescence (NIRF) imaging, an external light source of a certain wavelength is used to excite a target fluorescent molecule. Upon excitation, the fluorescent molecule emits a photon of lower energy at a longer wavelength, which can subsequently be detected by a highly sensitive CCD camera system.⁶

Due to the favorable optical characteristics of photons in the NIR spectral region, NIRF imaging seems of particular interest for clinical translation.⁷ Already, vibrant developments have been made in both imaging systems and tumor-targeted fluorescent probes that are potentially suitable for human use and may improve the way cancer is managed and monitored.^{8,9} NIRF imaging could be applied for noninvasive detection and visualization of tumors, improving the way cancer is managed and monitored. Moreover, image-guided surgery could assist surgeons in localizing the tumor and evaluating the extent of surgery intraoperatively in real-time. As fluorescent probes translate from preclinical studies to patients, potential applications of optical imaging in clinical care are expected to expand rapidly in the near future.¹⁰

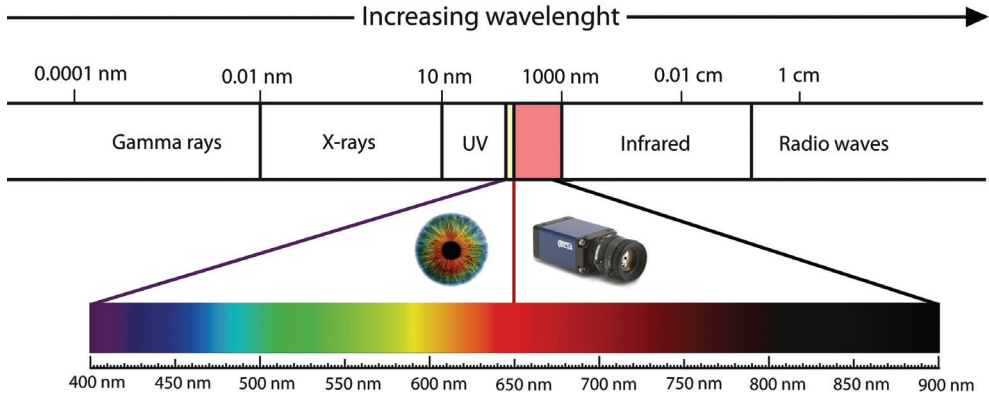


Figure 1. Overview of the spectrum of wavelengths, indicating the spectral range that is visible to the human eye (400–650 nm) and the near-infrared spectral range (650–900 nm) that requires a highly sensitive CCD camera for detection.

Near-infrared fluorescence optical imaging in breast cancer

Breast cancer is the most common form of malignancy in women in the Netherlands, with the number of newly diagnosed patients approximating 15,000 on an annual basis.¹¹ In the case of clinical $T_{1-2}N_{0-1}M_{0-x}$ breast carcinoma, breast-conserving surgery followed by radiotherapy is considered standard treatment. The surgeon hereto removes the primary tumor together with a small rim of normal breast tissue, guided by palpation and/or visual inspection. However, in 20% to 40% of the patients who underwent breast-conserving surgery, positive surgical margins are reported, which is considered an important risk factor for local recurrence.¹² In the case of more than focal positive margins, a second operation and/or additional radiotherapy is therefore indicated, leading to increased complication rates, psychological distress, and healthcare costs.¹³ New approaches are needed to decrease the rate of positive surgical margins while preserving cosmetic outcome.

OUTLINE

Chapter 2 comprises a review of the different techniques that are currently available as well as potential future techniques for obtaining negative surgical margins in breast cancer treatment.

Chapter 3 describes the development and validation of a predictive tool (*BreastConservation!* nomogram) to support both patients and clinicians in clinical decision-making by estimating the risk of positive margins prior to surgery. The tool is based on data obtained from twenty hospitals in the Northern- and Eastern region of the Netherlands.

Chapter 4 focuses on the potential of NIRF imaging in demarcating cancerous tissue. NIRF imaging was performed in a xenograft breast cancer mouse model using tumor-targeted fluorescent probes. Tumor delineation was compared between NIRF imaging and bioluminescence imaging as a gold standard for tumor tissue using the novel *segmentation-based comparative analysis of planar optical signals* (SCAPOS) analysis tool.

Chapter 5 describes the development of a breast phantom model with optical characteristics similar to normal breast tissue. In a feasibility study, breast phantoms were applied to simulate pre- and intraoperative NIRF imaging applications using a novel intraoperative NIRF camera system.

Fluorescence-guided sentinel lymph node detection

In addition to breast-conserving surgery, a sentinel lymph node biopsy is generally performed for staging purposes in patients with clinically negative lymph nodes. Hereto, the first-draining lymph node is removed and evaluated for the presence of possible lymph node metastases. Intraoperatively, the surgeon is guided by a combination of vital blue dye and radioisotope, which is regarded standard-of-care for localizing the sentinel lymph node.

Chapter 6 describes an alternative technique for intraoperative visualization of the sentinel lymph node using a nonspecific fluorescent dye in combination with an intraoperative NIRF imaging system. A technical feasibility study was performed in ten patients to serve as a step-up towards targeted imaging of lymph node metastases using tumor-targeted fluorescent agents.

Chapter 7 comprises a systematic review of conventional techniques used for sentinel lymph node mapping in breast cancer and melanoma patients. In addition, NIRF-guided sentinel lymph node mapping is judged on its merits and variables influencing sentinel lymph node detection are described.

Tumor-targeted imaging in breast cancer

To exploit the full potential of NIRF imaging, targeted fluorescent probes should be used that are directed towards specific markers exclusively expressed on tumor cells. Numerous studies have reported the feasibility of fluorescent probes to specifically target tumor lesions with excellent signal-to-noise ratios.⁸ Because targeted probes usually consist of relatively large molecules, e.g., monoclonal antibodies conjugated to a fluorescent dye, their target should ideally be expressed on the tumor cells' outer membrane to ensure good accessibility.

Although the portfolio of tumor markers known to play a role in breast cancer is large and still expanding, a single tumor-targeted agent that can be applied to all breast cancers is not yet available and is unlikely to become available in the future. A panel of targeted agents is therefore needed to make patient-tailored optical imaging accessible to the general population. As the development of targeted agents is time-consuming and costly, a selection of those markers that bear particular potential for clinical translation is desirable.

Chapter 8 describes the evaluation of ten promising membranous and/or extracellular tumor markers for targeted NIRF imaging in breast cancer. For the majority of tumor markers assessed, targeted agents are already available for clinical use, facilitating clinical translation.

In addition to intraoperative localization of the primary tumor, identification of possible lymph node metastases could be a potent application of targeted NIRF imaging. **Chapter 9** focuses on tumor marker expression of lymph node metastases, comparing expression levels with corresponding primary tumors.

In **Chapter 10** and **Chapter 11**, the results of the studies are summarized and suggestions for future approaches to intraoperative imaging and tumor targeting are discussed.

REFERENCES

1. Tsien RY. The green fluorescent protein. *Annu Rev Biochem.* 1998; 67:509-44.
2. Keereweer S, Kerrebijn JD, van Driel PB et al. Optical image-guided surgery – where do we stand? *Mol Imaging Biol.* 2010; 13(2):199-207.
3. Solomon M, Liu Y, Berezin MY, Achilefu S. Optical imaging in cancer research: basic principles, tumor detection, and therapeutic monitoring. *Med Princ Pract.* 2011; 20(5):397-415.
4. Zinn KR, Chaudhuri TR, Szafran AA, et al. Noninvasive bioluminescence imaging in small animals. *ILAR J.* 2008 ;49(1):103-115.
5. Ntziachristos V. Fluorescence molecular imaging. *Annu Rev Biomed Eng.* 2006; 8:1-33.
6. Luker GD, Luker KE. Optical imaging: current applications and future directions. *J Nucl Med.* 2008; 49(1): 1-4.
7. Taruttis A, Ntziachristos V. Translational optical imaging. *AJR Am J Roentgenol.* 2012; 199(2):263-271.
8. Mieog JS, Vahrmeijer AL, Hutteman M et al. Novel intraoperative near-infrared fluorescence camera system for optical image-guided cancer surgery. *Mol Imaging.* 2010; 9(4):223-231.
9. Themelis G, Yoo JS, Soh KS, Schulz R, Ntziachristos V. Real-time intraoperative fluorescence imaging system using light-absorption correction. *J Biomed Opt.* 2009; 14;064012.
10. van Dam GM, Themelis G, Crane LM et al. Intraoperative tumor-specific fluorescence imaging in ovarian cancer by folate receptor- α targeting: first in-human results. *Nat Med.* 2011; 17(10):1315-1319.
11. <http://tinyurl.com/lo7ec8z> (Version: 2.0, Evidence based 2012-02-13, justification: NABON, type: nation-wide guideline).
12. Jacobs L. Positive margins: the challenge continues for breast surgeons. *Ann Surg Oncol.* 2008; 15(5): 1271-1272.
13. Jeevan R, Cromwell DA, Trivella M et al. Reoperation rates after breast conserving surgery for breast cancer among women in England: retrospective study of hospital episode statistics. *BMJ.* 2012; 345:e4505.

Chapter

2

Ann Surg Oncol. 2009; 16:2717–2730

Obtaining adequate surgical margins in breast-conserving therapy for patients with early-stage breast cancer: current modalities and future directions

R.G. Pleijhuis
M. Graafland
J. de Vries
J. Bart
J.S. de Jong
G.M. van Dam

ABSTRACT

Inadequate surgical margins represent a high risk for adverse clinical outcome in breast-conserving therapy (BCT) for early-stage breast cancer. The majority of studies report positive resection margins in 20% to 40% of the patients who underwent BCT. This may result in an increased local recurrence (LR) rate or additional surgery and, consequently, adverse affects on cosmesis, psychological distress, and healthcare costs. In the literature, various risk factors are reported to be associated with positive margin status after lumpectomy, which may allow the surgeon to distinguish those patients with a higher a priori risk for re-excision. However, most risk factors are related to tumor biology and patient characteristics, which cannot be modified as such. Therefore, efforts to reduce the number of positive margins should focus on optimizing the surgical procedure itself, because the surgeon lacks real-time intraoperative information on the presence of positive resection margins during breast-conserving surgery.

This review presents the status of pre- and intraoperative modalities currently used in BCT. Furthermore, innovative intraoperative approaches, such as positron emission tomography, radioguided occult lesion localization, and near-infrared fluorescence optical imaging, are addressed, which have to prove their potential value in improving surgical outcome and reducing the need for re-excision in BCT.

INTRODUCTION

Breast cancer is the most common form of cancer and second leading cause of death in women in Europe and the United States.^{1,2} During the last 30 years, wide-spread mammographic screening and technological developments have led to a rapid increase in the diagnosis of small, nonpalpable breast cancer.^{3,4} Breast-conserving therapy (BCT), consisting of lumpectomy and irradiation therapy, has become the standard treatment for T₁-T₂ breast tumors and is regarded generally sufficient in appropriately selected patients.^{5,6}

Large randomized clinical trials (RCT's) have reported no significant difference in disease-free and overall survival between BCT and traditional mastectomy.⁷⁻⁹ BCT is considered to be associated with a diminished psychological burden compared to mastectomy, offers better cosmetic results, and reduces wound infection risk.¹⁰ The most important disadvantage of BCT is the life-long risk for local recurrence (LR), in which case additional surgery is necessary.¹¹ Large clinical trials have reported LR rates between 6% and 16%.¹²⁻¹⁴

Accurate localization is essential for adequate surgical removal of breast tumors, in which an optimal balance between good cosmetic results and preservation of resection margins is the primary goal. Obtaining tumor free surgical margins decreases the incidence of LR of the primary tumor.^{11,15,16} However, previous studies have shown that the number of patients exposed to BCT in whom tumor cells were present at or near the cut edge of the surgical specimen after resection of the primary tumor ranged from 5% to 82%, with the majority of studies indicating positive margins in 20% to 40% of the patients.^{10,17-21} To obtain tumor free margins, mutilating additional surgical procedures have to be performed.^{11,15,16}

Alternatively, intraoperative radiation therapy can be applied as a boost to the tumor bed or, postoperatively, to the biopsy scar.^{22,23} Boost radiation, as an additive to standard whole-breast radiation therapy, reduces the LR rate; the absolute effect of radiation therapy is of greatest benefit to women with higher risk of LR (P<0.0001).²³⁻²⁷ Adverse effects associated with boost radiation include decreased cosmetic outcome, delayed wound healing, and altered postoperative mammographic and ultrasonographic findings at the original tumor site in case of detection of recurrent disease.²⁷⁻³⁰

BCT still has limitations in achieving an acceptable therapeutic outcome.¹⁰ This review outlines the major challenges currently encountered intraoperatively and demarcates risk factors for positive resection margins and LR. In addition, current imaging modalities and future directions in achieving the highest feasible percentage of negative surgical margins in BCT are addressed.

CLINICAL IMPACT OF POSITIVE MARGINS

To assess strategies to decrease LR rates after BCT, several RCTs were performed and revealed numerous and varying risk factors that might be associated with LR (Table 1). A large meta-analysis of 72 trials, containing information on >42,000 patients, assessed that local surgical control at 5 years showed a significant improvement in disease-free survival and overall mortality at 15 years follow-up.²⁴

The influence of "close" margins, usually defined as tumor cells being present >0 and within ≤2 mm from the cut edge, is still controversial.⁴ Several studies reported close margins to be a significant risk factor for increased rates of LR, as well as the apparent quantity of cancerous cells approaching the cut edge.³¹⁻³⁴

Table 1. Independent risk factors for local recurrence.

Author	Year	No. of patients	Study design	LR rate (%)	Follow-up (m)	Analysis	Risk factors for local recurrence	P-value
Yildirim et al. ⁴²	2008	1217	Retrospective	5.2	74	Multivariate	Age ≤ 35 years (vs. >35 years) Invasive tumor size >20 mm (vs. ≤ 20 mm) Positive lymph node status (vs. negative)	<0.0001 0.03 0.04
Kreike et al. ¹¹	2008	1026	Retrospective	11.1	160	Multivariate	Positive margin status (<1 mm) (vs. negative (≥ 1 mm)) Presence of vascular invasion (vs. absence)	0.0002 0.004
Jobsen et al. ^{37,a}	2007	2126	Prospective	6.0	83	Multivariate	Positive margin status for DCIS (0 mm) (vs. negative (>0 mm))	0.002
Gülben et al. ^{146,b}	2007	120	Retrospective	13.3	28	Multivariate	Partial clinical response (vs. stationary) No. of positive lymph nodes 1–3 (vs. ≥ 4)	0.007 0.013
Komoike et al. ¹²	2006	1901	Retrospective	9.0	107	Multivariate	Age ≤ 35 years (vs. >35 years) Radiotherapy (vs. none) Positive margin status (<5 mm) (vs. negative (≥ 5 mm))	<0.0001 <0.0001 0.0004
Nottage et al. ¹³	2006	1540	Prospective	6	37	Multivariate	Radiotherapy (vs. none) Intraductal disease (vs. none) Hormonal therapy (vs. none) Histological grade unknown (vs. grade I) Age <40 years (vs. ≥ 40 years)	<0.0001 0.01 0.01 0.01 0.05
Aziz et al. ¹⁴⁷	2006	1430	Retrospective	12.6	60	Multivariate	Radiotherapy (vs. none) Tamoxifen (vs. none) Tumor size >20 mm (vs. ≤ 20 mm) Lymphovascular invasion (vs. none)	<0.0001 <0.0001 0.03 0.05
Céfaro et al. ¹⁴⁸	2006	969	Retrospective	4.1	63	Multivariate	Age <50 years (vs. ≥ 50 years) Tumor size >30 mm (vs. ≤ 30 mm) Unknown margin status (vs. known) Positive margin (0 mm) (vs. negative (>0 mm)) Hormonal therapy (vs. chemotherapy)	<0.001 <0.01 <0.01 <0.05 <0.05
Vargas et al. ³³	2005	367	Retrospective	8.2	84	Multivariate	Age <45 years (vs. ≥ 45 years) No visible mass on mammogram (vs. visible) Electron boost energy ≤ 9 Mev (vs. >9 Mev) Positive or close margin (<2 mm) (vs. negative (≥ 2 mm))	<0.001 0.003 0.01 0.02

IC, invasive carcinoma; DCIS, ductal carcinoma in situ; LR, local recurrence

^a Only women aged >40 years were included.

^b Only women with stage IIIB non-inflammatory breast cancer were included.

Table 2. Independent risk factors associated with positive margins.

Author	Year	No. of patients	Study design	Positive margins (%)	Definition ^c	Analysis	Risk factors for positive margin	P-value
Kurniawan et al. ³⁹	2008	1 648	Retrospective	13.5	0 mm	Multivariate	Multifocal disease (vs. unifocal) Tumor size ≥ 30 mm (vs. < 30 mm) Microcalcifications on mammogram (vs. none)	< 0.0001 < 0.0001 0.001
Smitt et al. ¹⁴⁹	2007	395	Retrospective	43.1	0 mm	Chi-square	Excisional biopsy (vs. core/needle biopsy) Presence of EIC (vs. absence) Age ≤ 45 years (vs. > 45 years) ER status negative (vs. positive) Lobular histological type (vs. other)	< 0.0001 0.002 0.02 0.02 0.02
Cabioglu et al. ^{40a}	2007	264	Retrospective	20	0 mm	Multivariate	Diagnosis by excisional biopsy (vs. other) Multifocality (vs. unifocality) Tumor size > 20 mm (vs. ≤ 20 mm)	< 0.0001 0.020 0.028
Aziz et al. ¹⁴⁷	2006	1 430	Retrospective	14.3	0 mm	Multivariate	Age < 50 years (vs. ≥ 50 years)	< 0.0001
Dillon et al. ^{41b}	2006	612	Retrospective	34	< 5 mm	Chi-square	No preoperative diagnosis (vs. yes) Presence of EIC (vs. absence) Referred from screening (vs. symptomatic) Lobular histological type (vs. other) Large tumor size (vs. small)	< 0.001 0.002 0.018 0.024 0.04
Chagpar et al. ²⁰	2004	2 658	Prospective	12.4	0 mm	Multivariate	T ₃ tumor (vs. T ₁₋₂) Lobular histological type (vs. ductal)	< 0.001 0.036

EIC, extensive intraductal component; ER, estrogen receptor

^a Risk factors associated with close or positive margin.

^b Risk factors associated with compromised margin (being defined as tumor-free margin: ≥ 1 mm en < 5 mm).

^c Definition of positive surgical margins as stated in the study.

In a recent trial conducted by Zavagno et al., 431 patients who underwent re-excision due to margin involvement were evaluated from a total of 1,520 patients who underwent BCT.³⁵ The authors found LR rates after positive margins and close margins to be 51.8% and 34.1%, respectively ($P=0.001$). However, no correlation was found between the distance of the tumor from the cut edge (range: 0.08–3 mm) and LR rate. These findings are consistent with the results of most of the studies performed on the correlation between margin width and LR rate, as reviewed by Singletary.⁴ Margin closeness is therefore currently not seen as an indication for re-excision.

Zavagno et al. suggest that residual disease in close margin involvement may be largely due to the existence of multiple cancerous foci and not to margin closeness by itself.³⁵ Breast tumors are shown to grow multifocally in 59%, of which 71% grow at a distance >2 cm from the reference tumor.³⁶ Therefore, margin status as such may be considered an important judgment factor in planning re-excision, but cannot be seen as an indicator for the presence of residual tumor in the surrounding tissue.³⁵ Adequate perioperative imaging of cancerous foci may be of great value to the surgeon.

Singletary reviewed 34 studies on margin status and LR, in which a total of $>15,000$ patients were assessed.⁴ In 30 of 34 reviewed studies, persistent microscopic inadequate (R1) or macroscopic inadequate (R2) surgical margins were highly significant for LR compared with negative margins ($P=0.0001$), depicting the relevance of margin status on the outcome of BCT. In a study by Jobsen et al. of approximately 2,300 patients, the LR rate was found to be related to positive margin status and young age.³⁷ The authors found the 10-year LR-free survival rate for young women (≤ 40 years) with positive margins to be significantly lower compared with negative margins (34.6% vs. 84.4%, respectively; $P=0.008$). The effect of positive margin status for invasive carcinoma seems to be limited to young women and is not only restricted to local control, but also to distant metastases and survival.³⁷

Because positive margin status is found to be an important risk factor for LR, substantial efforts have been made to understand the causes of the relatively high percentage of positive margins after BCT. A number of risk factors for positive margin status in itself have been identified over the years (Table 2). Again, young age is reported to be a strong risk factor for positive margin status.^{20,37-41} Vrieling et al. reported that tumor size was significantly larger in young patients (≤ 40 years) compared with older patients ($P=0.001$).³⁸ Furthermore, re-excisions occurred more often in younger patients (34–35% vs. 20–28%; $P=0.001$), which was probably related to a more frequent incomplete excision at the first attempt (24–26% vs. 14–21%; $P=0.001$). Vicini et al. suggested that a lesser extent of the excision, for cosmetic reasons, might be the cause of less optimal margin resection in younger patients.³⁴ When adequate negative margins were obtained, no difference in LR was seen in different age groups.

Other reported risk factors for positive margin status are large tumor size, multifocality, and lobular histological type.^{17,20,39-43} Furthermore, the number of positive lymph nodes (N-status) is reported to be a risk factor.⁴⁴ However, it should be noted that there is a strong variability in the reported findings of these studies.

An explanation for the high rate of positive margins reported in literature might be the restricted visibility of the tumor and coexisting ductal carcinoma in situ (DCIS) during surgery. In order to give an adequate perspective on the problems surrounding the pre- and intraoperative visibility of the tumor, the techniques currently used are summarized in the following sections and judged on their merits.

CURRENT MODALITIES OF IMAGING BREAST CANCER IN BCT

Clinical aspects in patient selection

Approximately one third of all diagnosed breast cancers is clinically occult. As a consequence, additional techniques have to be used to localize the tumor adequately. By current standards, the tumor is visualized with X-ray mammography or ultrasonography before the surgical procedure. However, during the lumpectomy procedure, the surgeon relies mostly on palpation of the tumor.⁴⁵ Palpation of the tumor alone is considered inadequate for optimal lumpectomy due to a few basic shortcomings: difficulty to detect occult or multicentric disease and difficulty in differentiating between malignant tissue and fibrosis. Furthermore, tumors in younger women are harder to detect because of the firmer nature of the breast tissue.⁴² Therefore, most institutions use additional intraoperative techniques to evaluate surgical margins, which may assist in obtaining margin negativity. Because none of these techniques fully guarantee the detection of a negative margins status, preoperative imaging is an absolute necessity for adequate BCT.

Preoperative mammography

Due to widespread mammographic screening programs, radiographic X-ray mammography is currently the most common way of detecting breast malignancy. Mammography gives an accurate assessment of tumor size and borders. It also provides information on the presence of multicentricity, multifocality, and microcalcification, which is considered to be a sign for the presence of DCIS.^{46,47} In a recent meta-analysis on the efficacy of mammography for the detection of tumors, sensitivity and specificity rates of 94% and 61% were found, respectively.⁴⁸ Although mammography is an adequate technique for breast cancer detection, it has a relatively high rate of nonspecific findings.⁴⁹ Furthermore, it does not give any functional information nor does it provide quantitative information on tissue function or composition.⁵⁰ Because of the aforementioned shortcomings, ultrasound was introduced as an addition to mammography for preoperative tumor assessment. While radiography provides information on tissue density and microcalcifications, ultrasound gives a more accurate image of tumor size and growth pattern. Although both imaging modalities act complementary, they fail to assess tumor size and growth pattern in a substantial percentage of patients. Deurloo et al. found an underestimation in tumor extent of 23% in patients considered eligible for BCT, largely due to failure in assessing diffuse and multinodular tumors.^{51,52} Especially patients of younger age present difficulties. An earlier study found failure to meet malignancy criteria in 13% of patients assessed preoperatively by ultrasound alone.⁵³

Preoperative magnetic resonance imaging

Magnetic resonance imaging (MRI) is a highly sensitive imaging technique, which is reported to be a substantial improvement in detecting multinodular disease and assessment of tumor spread compared with conventional techniques.^{54,55} MRI provides highly sensitive information on DCIS.⁵⁶ In a trial conducted in Belgium, MRI detected intraductal extent in 34 out of 50 (68%) patients who were reported to have an intraductal component, compared with 48.5% in mammography and 34.2% in ultrasound.⁵⁷ Furthermore, MRI has an accurate capability to differentiate between malignant tissue and fibrosis, enabling assessment of breast tissue after irradiation or chemotherapy for the presence of recurrent disease.⁵⁸ MRI is equally accurate in distinguishing malignancies in younger women with more extensive fibroglandular tissue.

In a meta-analysis of 2,160 patients from 16 studies, Houssami et al. showed that MRI detects additional disease in 16% of patients with breast cancer, leading to conversion of local excision to mastectomy in 1.1% (95% confidence interval (CI), 0.3–3.6) and to otherwise extended surgery in 5.5% (95% CI, 3.1–9.5).⁵⁹ The authors reported a relatively high false positive ratio (true positive to false positive ratio of 1.91 (95% CI, 1.09–3.34)), for which further research on its clinical value is necessary. Nevertheless, MRI has been shown to have a profound clinical impact on selection of patients for BCT and is currently regarded as the preferred imaging modality for preoperative assessment and clinical decision making.

It should be emphasized that several studies have shown that MRI assessment before surgery fails to improve postoperative margin status and subsequent LR, even compared with conventional imaging modalities.^{60,61} The intraoperative limitation may be due to the limited provision of real-time margin assessment.⁶²

INTRAOPERATIVE TUMOR LOCALIZATION

Because of the limited intraoperative capabilities of the current preoperative imaging techniques, more invasive imaging and surgical guidance techniques have been developed to assess tumor localization intraoperatively. These techniques are addressed in the next section.

Wire-guided localization

For more than 20 years, the standard technique for intraoperative tumor localization of clinically occult tumors has been wire-guided localization (WGL), in which a wire is introduced in the tumor guided by ultrasound, X-ray mammography, or MRI. After resection, the excised lump can be evaluated mammographically for localization of the tumor and microcalcifications. However, the WGL procedure has been criticized for the last 5 years. Burkholder et al. recently analyzed the success rate of WGL in a retrospective study of 511 patients and found positive to close (<3 mm) margins in 21.3% of the patients, of which 26.7% had to undergo re-excision.⁶³ Similar percentages were found by Schmidt-Ullrich et al.⁶⁴ Two recent studies reported that WGL resulted in positive margins in 38% to 43% of the patients who underwent BCT.^{3,65}

An important disadvantage of WGL is that the guide-wire does not provide a clear three-dimensional perspective on the various tumor edges and does not influence surgical margins as such. Furthermore, the guide-wire is prone to move before or during surgery and may for this reason lead to inadequate information on tumor localization. The WGL procedure is time consuming and uncomfortable for the patient, resulting in increased levels of stress and arousal.⁶⁶ Because WGL results in an unacceptable high rate of positive margins, other techniques have been developed for intraoperative tumor detection.

Intraoperative ultrasound guided resection

Current trends in BCT are moving toward the direction of one combined diagnostic and therapeutic procedure, a so-called ‘theranostic’ procedure, in which effective visualization plays a more prominent role. One of these theranostic procedures is intraoperative ultrasound (IOUS)-guided excision. In this technique, the patient is examined with ultrasound (US) before and during surgery to improve tumor assessment. After surgery, the excised tissue is examined using US to assess margin status. In case of positive or close margins, the patient’s cavity margins are shaved in order to remove any residual disease.⁶⁷

Several studies investigating the use of IOUS in BCT showed positive margin rates between 3% and 11%.⁶⁸⁻⁷¹ Rahusen et al. compared IOUS to WGL in a prospective study in 48 patients.⁷⁰ The authors reported that positive or close margin status (≤ 1 mm) was improved significantly using IOUS compared to WGL (11% vs. 45%, respectively; $P < 0.007$). However, Klimberg et al.

showed that only half (50%) of the nonpalpable breast tumors can be visualized by ultrasonography.⁷² Another problem of IOUS is the unreliability in detecting DCIS lesions, because ultrasonography is not suitable for the detection of microcalcifications.⁷³

Karni et al. reported on a radiofrequency-based intraoperative margin assessment device (MarginProbe™, Dune Medical Devices Ltd., Israel), which is able to detect malignant tissue within the surgical specimen up to a depth of 1 mm.⁷⁴ The MarginProbe™ displays device readings as 'negative' or 'positive' margin, the latter indicating excision of additional breast tissue. Sensitivity and specificity rates of the MarginProbe™ were reported to be 71% and 68%, respectively.⁷⁴ Recently, Allweis et al. showed re-excision rates to be lower if the surgeon had a MarginProbe™ at his disposal during breast-conserving surgery compared with the control group, although not statistically significant (12.6% vs. 18.6%; $P=0.098$).⁷⁵ However, this reduction in re-excision rate might, in part, have been due to the excision of larger tissue volumes in the device group compared with the control group (107 cm³ vs. 94 cm³; $P=0.066$).

Intraoperative specimen radiography

Another technique for evaluation of surgical margins is intraoperative specimen radiography. After excision by the surgeon, the specimen is evaluated by X-ray radiography. If microcalcifications occur close to the edges of the specimen, the surgeon may decide to shave the associated cavity edges in order to remove any residual malignant disease. However, the use of radiographic X-ray mammography is limited due to limitations in detecting small, noncalcified lesions and a high rate of nonspecific findings.⁷⁶ Lee and Carter examined postexcision specimen radiographs of 125 patients and found a sensitivity, specificity, and overall accuracy for detecting margin positivity of 49%, 77%, and 62%, respectively.⁷⁷ They concluded that intraoperative specimen radiography could not be relied on solely but presents a valuable addition to BCT.

Cryoprobe-assisted localization

Cryoprobe-assisted localization (CAL) is a technique of particular value in small, nonpalpable tumors. This technique makes use of an ultrasound-guided cryoprobe, which is inserted into the breast and freezes the tumor, thereby turning the tumor into a small, palpable sphere that can be more easily located and excised. Tafra et al. compared the capability of CAL in achieving negative margins to conventional WGL in a prospective trial in 310 patients.⁷⁸ No significant differences were found between the CAL and WGL arms in positive surgical margin status (28% vs. 31%; $P=0.691$) and re-excision rates (19% vs. 21%; $P=0.764$). However, it did reduce the amount of healthy surrounding tissue excised and therefore improved cosmetic outcome ($P<0.001$). Furthermore, excision time and ease were significantly improved using the CAL method ($P<0.001$).

INTRAOPERATIVE PATHOLOGICAL EXAMINATION

Frozen section analysis

Frozen section analysis (FSA) is a commonly applied technique for intraoperative pathological margin assessment in many oncologic procedures. The excised specimen is frozen, sliced, and analyzed microscopically.⁷⁹ Because of the relative ease and the wide experience gained, this technique has been applied frequently to assess tumor margins during lumpectomy. The procedure is performed directly after the tumor has been excised. In case FSA indicates residual disease, the wound can be re-opened immediately for additional cavity shaving, thus preventing a costly re-excision procedure at a later stage. The FSA procedure takes an average of 30 minutes, which adds significantly to the operating time.⁸⁰

Reported sensitivity rates for detecting residual disease ranged between 65% and 78%, whereas specificity rates ranged between 98% and 100%.^{40,81,82} The relatively high variance in sensitivity might be explained by differences in experience between pathologists.

Several studies retrospectively analyzed the influence of FSA on BCT outcome and found that 24% to 27% of the patients underwent additional tissue excision based on FSA, whereas 5% to 9% required a second re-excision procedure after definitive histopathological examination.^{80,82,83} FSA during BCT did not improve overall LR rates (3.8% and 1.2%, respectively).^{80,83} Considering the costs of the FSA procedure (the average Medicare charge for FSA is estimated at US\$90), these low re-excision rates clearly indicate the benefits of the procedure compared with permanent pathological evaluation alone. Nevertheless, in evaluating small tumors (diameter <10 mm) and presence of DCIS, the technique is less reliable.^{80,81} Other disadvantages of FSA are the prolonged duration of operation time and the requirement of a relatively large part of the specimen, which compromises definitive evaluation by the pathologist for histological aspects and tumor staging. In conclusion, although FSA is a relatively safe and cost-effective procedure that reduces the rate of re-excisions significantly, its reliability for negative margin status is questionable due to relatively high variance in diagnostic sensitivity.

Intraoperative touch preparation cytology

Intraoperative touch preparation cytology (IOTPC) or 'imprint cytology' is a promising alternative to FSA. The technique is based on the histological characteristics of the cell surface of malignant cells, which stick to glass surfaces, whereas benign mammary fat tissue does not. To assess margin status, a glass slide is brought against the borders of the excised specimen. Next, cells sticking to the glass surface are fixated, stained and microscopically evaluated.⁸⁴ Several studies have concluded that IOTPC is inexpensive, accurate, quick and saves tissue for permanent sectioning and histopathological examination.⁸⁴⁻⁸⁶

Klimberg et al. evaluated IOTPC for accuracy in diagnosis as well as margin assessment during surgery in a prospective trial in 428 patients.⁸⁴ They reported a diagnostic sensitivity and specificity of 96% and 100%, respectively, and a margin status sensitivity and specificity of both 100%. Weinberg et al. compared the efficacy of IOTPC to other histopathological assessment techniques such as definitive histopathological assessment and intraoperative FSA in a database of 1,713 patients.⁸⁷ They reported that intraoperative margin assessment using IOTPC significantly reduced LR rates compared with conventional methods (2.8% vs. 8.8%; $P < 0.0001$).

Although the overall results seem promising, IOTPC is not as commonly used as might be expected based on reported LR rates and detection rates of positive margins. A possible explanation might be the likelihood of artifacts caused by draught and surface cautery.⁴ Also, IOTPC is proven less effective in distinguishing lobular carcinoma.⁸⁵ Another important shortcoming of IOTPC is that close margins are not taken into account, since only superficial tumor cells are detected with the technique. Therefore, no information is gathered on margin width, multifocality, and quantity of cancerous cells approaching the cut edge.

STANDARDIZED CAVITY SHAVING

To avoid the earlier-mentioned difficulties in intraoperative cytological or histological techniques, some authors suggested that standardized surgical cavity shaving could achieve the intended reduction in positive-margin rates.⁸⁸ Hereto, all cut edges are shaved systematically after excision of the primary tumor to remove any residual disease.

Huston et al. compared the number of systematically shaved cavity edges to the achieved definitive histopathological margin status and found an inverted correlation between the rate of positive margin status and the total volume of breast tissue removed.⁸⁹ Similar results were found by Janes et al.⁹⁰ Because cavity shaving requires additional tissue resection, cosmetic outcome, and thereby one of the primary objectives of BCT, is comprised as a consequence.^{89,90} Furthermore, standardized cavity shaving still does not provide certainty in achieving negative margins due to the lack of intraoperative assessment of margin status.

FUTURE DIRECTIONS

Because most of the current techniques result in a relatively high rate of positive resection margins together with a clear impact on LR rates and cosmetic results, new innovative surgical approaches and methods for intraoperative margin assessment are needed.^{6,10} In the following section, innovative applications of radioguided surgery and optical imaging are addressed.

Positron emission tomography imaging

¹⁸F-fluoro-2-deoxy-D-glucose (¹⁸F-FDG) positron emission tomography (PET) imaging is considered a powerful imaging modality for diagnosis, staging, and monitoring of various malignancies, including breast cancer.⁹¹

The oncologic applications of PET are still expanding with the development of new positron-emitting radiopharmaceuticals and imaging techniques.⁹² Recently, the suitability of ¹⁸F-FDG as a tracer for tumors has led to an interest in its use in PET-guided BCT (Fig. 1). The radiopharmaceutical ¹⁸F-FDG demarcates sites of high glucose metabolic activity, such as tumors, inflammation, and infection.⁹³ Because breast cancers frequently overexpress the facilitative glucose transporter GLUT1, uptake of the glucose analogue ¹⁸F-FDG may be increased in breast cancer cells.^{94,95}

Hand-held PET-probes have become available, which allow for the detection of high-energy gamma rays during surgery and may facilitate localization of breast carcinoma by offering the surgeon real-time, intraoperative evaluation of tumor localization and margin status.^{96,97} The use of hand-held probes for the detection of ¹⁸F-FDG accumulating tumors has been shown previously for various malignancies.^{91,92,97-99}

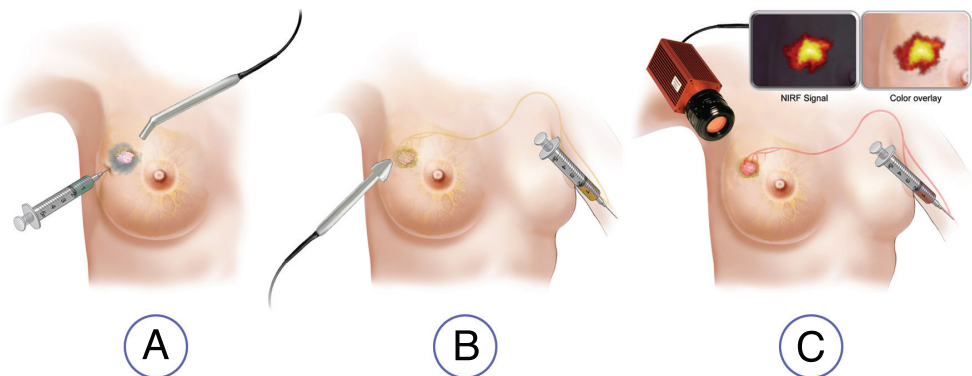


Figure 1. New evolving imaging modalities for intraoperative margin assessment in breast-conserving therapy: **(A)** radioguided occult lesion localization (ROLL), **(B)** positron emission tomography (PET); and **(C)** near-infrared fluorescence (NIRF) optical imaging.

Sensitivity and specificity of PET are relatively high for ^{18}F -FDG-avid breast tumors.^{100,101} However, because of limited spatial resolution of PET-imaging, small tumors (<1 cm) are difficult to detect, whereas breast screening programs and technological developments have led to a considerable reduction in the size of breast cancers being detected.^{97,102,103} The same limited spatial resolution is of major concern for the intraoperative detection of positive margins in itself. Also, PET has a limited role in patients with well-differentiated and lobular types of breast cancer.¹⁰⁴ Additionally, PET lacks specificity, because normal physiologic uptake of ^{18}F -FDG can be demonstrated to varying degrees in nonmalignant tissues, such as inflammatory tissue.⁹¹ Finally, PET has the disadvantage of high costs and radiation exposure to primary operating personnel during the intraoperative ^{18}F -FDG PET procedure is expected to be relatively high.^{101,102}

Further development of more specific radiopharmaceuticals may compensate in part for the current limitations associated with ^{18}F -FDG PET imaging. In carefully selected patients, the intraoperative use of a PET-probe may provide a useful tool to improve surgical outcome.⁹³ However, its use in BCT warrants further exploration on feasibility and validation and at this stage cannot be considered to compete with the current techniques.⁹¹

Radioguided occult lesion localization

Radioguided occult lesion localization (ROLL), introduced by Luini et al. in 1996, is an upcoming surgical technique and theranostic tool for intraoperative localization and simultaneous resection of nonpalpable tumors of the breast.¹⁰⁵

The technique makes use of a nonspecific radioisotope, which is injected into the tumor under stereotactic or ultrasonographic guidance. The exact position of the primary tumor can be assessed intraoperatively by use of a hand-held gamma probe. After excision of the primary tumor, the probe can also be used to search for any residual areas of high radioactivity.¹⁰⁶

The injection of the nonspecific radioisotope into the tumor is a fundamental step in the ROLL procedure and has to be very accurate in order to minimize false negative and false positive results. Several studies showed that the radioisotope was correctly positioned in 95% to 100% of patients.^{3,65,106-110} However, spillage of radiotracer within the mammary gland during the ROLL procedure might decrease accuracy of location of the lesion.¹¹¹ Furthermore, the amount of tracer injected needs to correlate with tumor size.

Alternatively, a radioactive iodine (125I) seed can be implanted at the tumor, followed by radioguided localization and excision of the tumor together with the radioactive seed.¹¹² Hughes et al. analyzed 383 patients treated with radioguided seed localization (RSL) compared with 99 patients treated with WGL and considered the technique to be safe, effective, and more patient friendly compared with WGL.¹¹³ Additionally, RSL was reported to reduce the incidence of inadequate surgical margins compared with WGL (26% vs. 57%; $P=0.02$).¹¹² However, although RSL might prove valuable for BCT in the future, experience with this technique is still limited.

Sarlos et al. analyzed the oncologic safety of the ROLL procedure and the effectiveness of tumor localization in a prospective, controlled trial.¹¹⁰ In 20% of the patients with invasive ductal carcinoma (IDC), the tumor was excised inadequately (margin ≤ 1 mm) at the initial surgical procedure. These results are consistent with margin positivity reported by others, ranging from 11% to 17%.^{3,65,114} The detection rate of nonpalpable breast tumors during surgery was found to be 98%.

Although the clinical efficacy of ROLL compared with WGL was found to be similar in two prospective RCTs, there were several aspects in which ROLL exceeded the current standard of WGL.^{3,107} Rampaul et al. concluded that ROLL was less painful for the patient and was an easier technique to perform surgically.¹⁰⁷ Furthermore, the ROLL procedure could be combined with lymphatic mapping and sentinel lymph node biopsy, which makes it more

patient-friendly compared with WGL.^{112,115} ROLL was reported to significantly reduce pre- and intraoperative localization time of nonpalpable breast tumors.³ However, the total duration of the surgical procedure was not reduced by ROLL.^{3,65,107,114} Regarding costs, WGL is probably exceeded by ROLL, although this effect could be leveled off by the potential net savings that accompany a reduction of re-excision rates.³

In conclusion, ROLL seems to be a simple, accurate, and relatively safe technique in comparison with the current standard of WGL.¹⁰⁶⁻¹⁰⁹ Further research is needed to elucidate the position of ROLL for the treatment of nonpalpable breast tumors. Currently, a multicenter clinical trial is being conducted in the Netherlands, in which ROLL is being compared to WGL regarding the percentage of positive margins, cost effectiveness, patient comfort, and cosmetic outcome.¹¹⁶

Near-infrared fluorescence optical imaging

In recent years, significant progress has been made in the development of optical imaging systems and fluorescent contrast agents for clinical applications.¹¹⁷⁻¹¹⁹ Several animal and clinical studies have shown the potential use of near-infrared fluorescence (NIRF) optical imaging to improve the therapeutic outcome of surgery.¹²⁰⁻¹²⁶

It must be emphasized that NIRF imaging on itself is not possible without the use of near-infrared (NIR) fluorescent molecular probes (fluorochromes), for which several groups can be distinguished. One group consists of 'targeted fluorochromes', which are specific for certain tumor markers involved in breast cancer, like vascular endothelial growth factor (VEGF) receptor, epidermal growth factor (EGF) receptor, or the HER2 receptor.¹²⁷⁻¹³² Another group is formed by the 'activatable probes', which show virtually no fluorescence activity in their native state, thereby minimizing background signals.¹¹⁹ However, after activation by a specific enzyme, the probe emits a bright fluorescence signal when appropriately excited (Fig. 2).^{119,121,123} A number of enzymes that play a role in carcinogenesis and tumor spreading can already be visualized with activatable probes, including proteases, such as cathepsin B, cathepsin D, and matrix metalloproteinase 2 (MMP2).^{121,133-137}

An optical imaging technique commonly used is two-dimensional (2D) fluorescence reflectance imaging (FRI), also known as epi-illumination fluorescence imaging. FRI with a hand-held imaging device could complement BCT by visualizing tumor delineation, remnant disease, and pinpointing suspicious lymph nodes, thereby enabling the surgeon to detect (diagnostic) and excise (therapeutic) malignant tissue and possible residual disease at the same time (Figs. 1, 3).^{119,121,122,138}

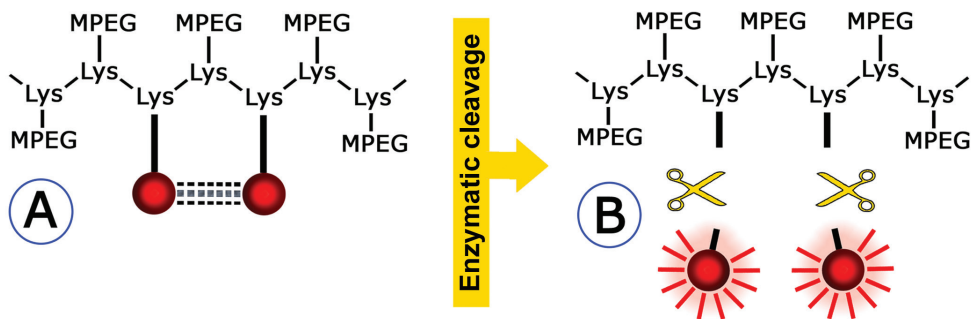


Figure 2. Schematic example of the mechanism behind an activatable probe. The probe is dark in its native state, thereby keeping unwanted background signals to a minimum (A). After cleavage of the backbone carrier by a specific enzyme, the probe will fluoresce when excited with light of a specific wavelength (B).

The use of NIRF optical imaging offers additional advantages: the technology is safe, simple to operate, fast, high resolution (as low as 10 μm), relatively inexpensive, and makes use of non-ionizing radiation.^{119,122,124,139-141} Besides the aforementioned advantages, NIRF optical imaging does have limitations, which originate from the intrinsic characteristics of light propagation through tissue.¹⁴² Especially, besides absorption and scattering of light, autofluorescence can reduce detection sensitivity and imaging performance due to absorbance and subsequent emission of light by intrinsic tissue fluorochromes.^{143,144} Although the use of FRI for noninvasive detection of breast cancer is restricted because of limited depth resolution and a nonlinear dependence between the signal detected on the surface of tissue and the depth of the activity, the technique is well suited for intraoperative imaging applications.^{119,121,122,139} Clinical applications for NIRF optical imaging are expected to expand rapidly, although further work is needed to overcome the aforementioned limitations of the technique.^{117,145}

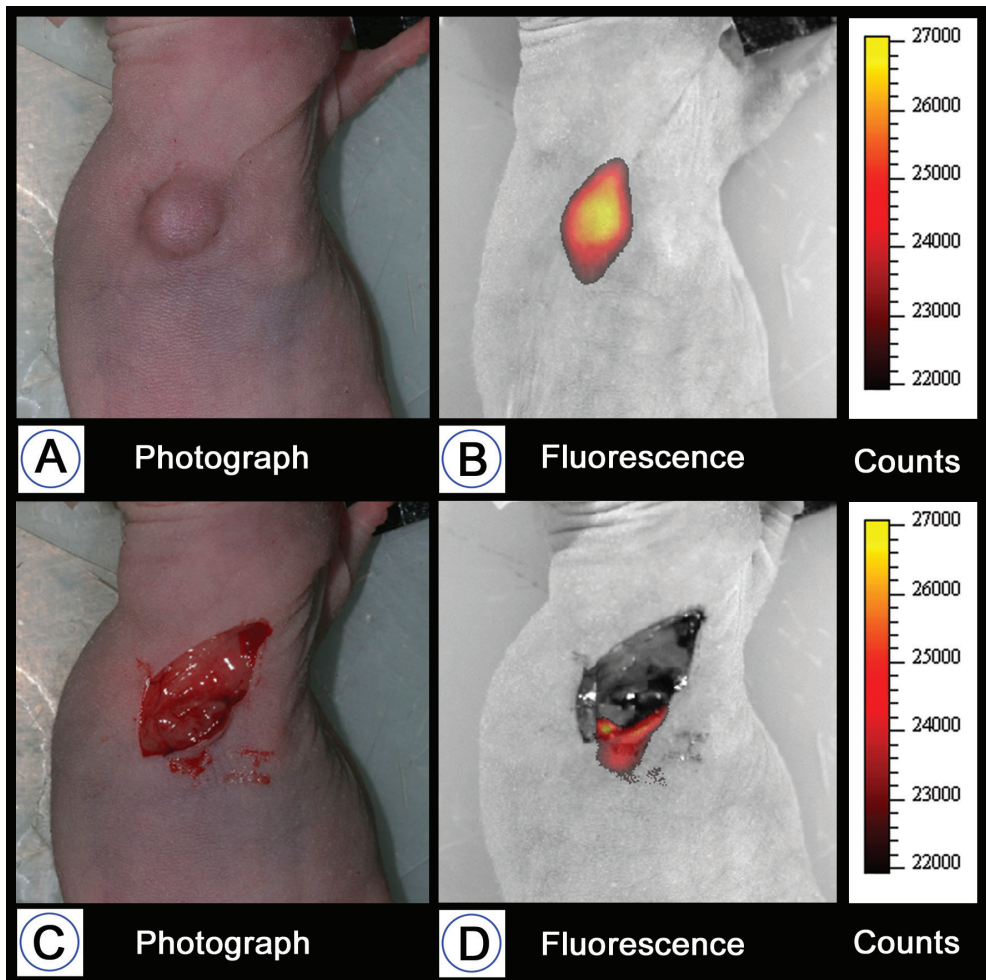


Figure 3. NIRF optical imaging with a protease-activatable fluorescent probe before (**B**) and after (**D**) surgical excision of the primary breast tumor in a nude mouse model. After initial excision of the tumor, a small area of residual disease could be detected (**D**). Normal photographs were taken for comparison (**A**, **C**).

CONCLUSION

Current imaging techniques used in BCT result in positive surgical margins in 20% to 40% of the patients who undergo breast-conserving surgery. Risk factors associated with positive margins are predominantly related to tumor biology factors or patient characteristics and, therefore, cannot be influenced directly to improve surgical outcome. Instead, multidisciplinary research should focus on techniques that provide the surgeon with a so-called 'theranostic' tool, enabling the surgeon to obtain an optimal balance between safe surgical margins and good cosmetic results. Current techniques present significant difficulties in this perspective. New innovative techniques, such as radioguided and NIRF-guided surgery, are emerging. Further studies are being performed to elucidate their potential value in improving surgical outcome and reducing the need for re-excision in BCT.

ACKNOWLEDGEMENT

The authors wish to thank prof. Vasilis Ntziachristos of the Technical University of Munich for revision and editing.

REFERENCES

1. Heron M. Deaths: leading causes for 2004. *Natl Vital Stat Rep* 2007; 56:1-95.
2. Ferlay J, Autier P, Boniol M et al. Estimates of the cancer incidence and mortality in Europe in 2006. *Ann Oncol* 2007; 18:581-592.
3. Medina-Franco H, barca-Perez L, Garcia-Alvarez MN et al. Radioguided occult lesion localization (ROLL) versus wire-guided lumpectomy for nonpalpable breast lesions: a randomized prospective evaluation. *J Surg Oncol* 2008; 97:108-111.
4. Singletary SE. Surgical margins in patients with early-stage breast cancer treated with breast conservation therapy. *Am J Surg* 2002; 184:383-393.
5. Kramer S, Darsow M, Kummel S et al. Breast-conserving treatment of breast cancer - oncological and reconstructive aspects. *Gynakol Geburtshilfliche Rundsch* 2008; 48:56-62.
6. Schwartz GF, Veronesi U, Clough KB et al. Consensus conference on breast conservation. *J Am Coll Surg* 2006; 203:198-207.
7. Blichert-Toft M, Nielsen M, Daring M et al. Long-term results of breast conserving surgery vs. mastectomy for early-stage invasive breast cancer: 20-year follow-up of the Danish randomized DBCG-82TM protocol. *Acta Oncol* 2008; 47:672-681.
8. Fisher B, Anderson S, Bryant J et al. Twenty-year follow-up of a randomized trial comparing total mastectomy, lumpectomy, and lumpectomy plus irradiation for the treatment of invasive breast cancer. *N Engl J Med* 2002; 347:1233-1241.
9. van Dongen JA, Voogd AC, Fentiman IS et al. Long-term results of a randomized trial comparing breast-conserving therapy with mastectomy: European Organization for Research and Treatment of Cancer 10801 trial. *J Natl Cancer Inst* 2000; 92:1143-1150.
10. Jacobs L. Positive margins: the challenge continues for breast surgeons. *Ann Surg Oncol* 2008; 15:1271-1272.
11. Kreike B, Hart AA, van d, V et al. Continuing risk of ipsilateral breast relapse after breast-conserving therapy at long-term follow-up. *Int J Radiat Oncol Biol Phys* 2008; 71:1014-1021.
12. Komoike Y, Akiyama F, Iino Y et al. Ipsilateral breast tumor recurrence (IBTR) after breast-conserving treatment for early breast cancer: risk factors and impact on distant metastases. *Cancer* 2006; 106:35-41.
13. Nottage MK, Kopciuk KA, Tzontcheva A et al. Analysis of incidence and prognostic factors for ipsilateral breast tumor recurrence and its impact on disease-specific survival of women with node-negative breast cancer: a prospective cohort study. *Breast Cancer Res* 2006; 8:R44.
14. Bijker N, Peterse JL, Duchateau L et al. Risk factors for recurrence and metastasis after breast-conserving therapy for ductal carcinoma in situ: analysis of European Organization for Research and Treatment of Cancer Trial 10853. *J Clin Oncol* 2001; 19:2263-2271.
15. Mannell A. Breast-conserving therapy in breast cancer patients: a 12-year experience. *S Afr J Surg* 2005; 43:28-30.
16. Rubio IT, Marco V. The importance of surgical margins in conservative surgery for breast cancer. *Cir Esp* 2006; 79:3-9.
17. Miller AR, Brandao G, Prihoda TJ et al. Positive margins following surgical resection of breast carcinoma: analysis of pathologic correlates. *J Surg Oncol* 2004; 86:134-140.
18. Weng EY, Juillard GJ, Parker RG et al. Outcomes and factors impacting local recurrence of ductal carcinoma in situ. *Cancer* 2000; 88:1643-1649.
19. Park CC, Mitsumori M, Nixon A et al. Outcome at 8 years after breast-conserving surgery and radiation therapy for invasive breast cancer: influence of margin status and systemic therapy on local recurrence. *J Clin Oncol* 2000; 18:1668-1675.
20. Chagpar AB, Martin RC, Hagendoorn LJ et al. Lumpectomy margins are affected by tumor size and histologic subtype but not by biopsy technique. *Am J Surg* 2004; 188:399-402.

21. Cao D, Lin C, Woo SH et al. Separate cavity margin sampling at the time of initial breast lumpectomy significantly reduces the need for reexcisions. *Am J Surg Pathol* 2005; 29:1625-1632.
22. Sacchini V, Beal K, Goldberg J et al. Study of quadrant high-dose intraoperative radiation therapy for early-stage breast cancer. *Br J Surg* 2008; 95:1105-1110.
23. Reitsamer R, Sedlmayer F, Kopp M et al. Concepts and techniques of intraoperative radiotherapy (IORT) for breast cancer. *Breast Cancer* 2008; 15:40-46.
24. Clarke M, Collins R, Darby S et al. Effects of radiotherapy and of differences in the extent of surgery for early breast cancer on local recurrence and 15-year survival: an overview of the randomised trials. *Lancet* 2005; 366:2087-2106.
25. Reitsamer R, Sedlmayer F, Kopp M et al. The Salzburg concept of intraoperative radiotherapy for breast cancer: results and considerations. *Int J Cancer* 2006; 118:2882-2887.
26. Lemanski C, Azria D, Thezenas S et al. Intraoperative radiotherapy given as a boost for early breast cancer: long-term clinical and cosmetic results. *Int J Radiat Oncol Biol Phys* 2006; 64:1410-1415.
27. Kraus-Tiefenbacher U, Bauer L, Kehrler T et al. Intraoperative radiotherapy (IORT) as a boost in patients with early-stage breast cancer: acute toxicity. *Onkologie* 2006; 29:77-82.
28. Morgan DA, Robertson JF. Boost or not. *J Clin Oncol* 2008; 26:1013-1014.
29. Bartelink H, Horiot JC, Poortmans PM et al. Impact of a higher radiation dose on local control and survival in breast-conserving therapy of early breast cancer: 10-year results of the randomized boost versus no boost EORTC 22881-10882 trial. *J Clin Oncol* 2007; 25:3259-3265.
30. Wasser K, Schoeber C, Kraus-Tiefenbacher U et al. Early mammographic and sonographic findings after intraoperative radiotherapy (IORT) as a boost in patients with breast cancer. *Eur Radiol* 2007; 17:1865-1874.
31. Freedman G, Fowble B, Hanlon A et al. Patients with early-stage invasive cancer with close or positive margins treated with conservative surgery and radiation have an increased risk of breast recurrence that is delayed by adjuvant systemic therapy. *Int J Radiat Oncol Biol Phys* 1999; 44:1005-1015.
32. Kunos C, Latson L, Overmoyer B et al. Breast conservation surgery achieving ≥ 2 mm tumor-free margins results in decreased local-regional recurrence rates. *Breast J* 2006; 12:28-36.
33. Vargas C, Kestin L, Go N et al. Factors associated with local recurrence and cause-specific survival in patients with ductal carcinoma in situ of the breast treated with breast-conserving therapy or mastectomy. *Int J Radiat Oncol Biol Phys* 2005; 63:1514-1521.
34. Vicini FA, Kestin LL, Goldstein NS et al. Impact of young age on outcome in patients with ductal carcinoma-in-situ treated with breast-conserving therapy. *J Clin Oncol* 2000; 18:296-306.
35. Zavagno G, Goldin E, Mencarelli R et al. Role of resection margins in patients treated with breast conservation surgery. *Cancer* 2008; 112:1923-1931.
36. Holland R, Veling SH, Mravunac M et al. Histologic multifocality of T_{is} , T_{1-2} breast carcinomas. Implications for clinical trials of breast-conserving surgery. *Cancer* 1985; 56:979-990.
37. Jobsen JJ, van der Palen J, Ong F et al. Differences in outcome for positive margins in a large cohort of breast cancer patients treated with breast-conserving therapy. *Acta Oncol* 2007; 46:172-180.
38. Vrieling C, Collette L, Fourquet A et al. Can patient-, treatment-, and pathology-related characteristics explain the high local recurrence rate following breast-conserving therapy in young patients? *Eur J Cancer* 2003; 39:932-944.
39. Kurniawan ED, Wong MH, Windle I et al. Predictors of Surgical Margin Status in Breast-Conserving Surgery Within a Breast Screening Program. *Ann Surg Oncol* 2008; 84:154-159.
40. Cabioglu N, Hunt KK, Sahin AA et al. Role for intraoperative margin assessment in patients undergoing breast-conserving surgery. *Ann Surg Oncol* 2007; 14:1458-1471.
41. Dillon MF, Hill AD, Quinn CM et al. A pathologic assessment of adequate margin status in breast-conserving therapy. *Ann Surg Oncol* 2006; 13:333-339.
42. Yildirim E. Locoregional recurrence in breast carcinoma patients. *Eur J Surg Oncol* 2008; 35:258-263.

43. Kennecke H, McArthur H, Olivotto IA et al. Risk of early recurrence among postmenopausal women with estrogen receptor-positive early breast cancer treated with adjuvant tamoxifen. *Cancer* 2008; 112:1437-1444.
44. Noh WC, Paik NS, Kim MS et al. Ipsilateral breast tumor recurrence after breast-conserving therapy: A comparison of quadrantectomy versus lumpectomy at a single institution. *World J Surg* 2005; 29:1001-1006.
45. Morrow M, Strom EA, Bassett LW et al. Standard for breast conservation therapy in the management of invasive breast carcinoma. *CA Cancer J Clin* 2002; 52:277-300.
46. Cho KR, Seo BK, Kim CH et al. Non-calcified ductal carcinoma in situ: ultrasound and mammographic findings correlated with histological findings. *Yonsei Med J* 2008; 49:103-110.
47. Ikeda DM, Andersson I. Ductal carcinoma in situ: atypical mammographic appearances. *Radiology* 1989; 172:661-666.
48. Rauscher GH, Johnson TP, Cho YI et al. Accuracy of self-reported cancer-screening histories: a meta-analysis. *Cancer Epidemiol Biomarkers Prev* 2008; 17:748-757.
49. Ikeda DM, Birdwell RL, O'Shaughnessy KF et al. Analysis of 172 subtle findings on prior normal mammograms in women with breast cancer detected at follow-up screening. *Radiology* 2003; 226:494-503.
50. Leff DR, Warren OJ, Enfield LC et al. Diffuse optical imaging of the healthy and diseased breast: a systematic review. *Breast Cancer Res Treat* 2008; 108:9-22.
51. Deurloo EE, Klein Zeggelink WF, Teertstra HJ et al. Contrast-enhanced MRI in breast cancer patients eligible for breast-conserving therapy: complementary value for subgroups of patients. *Eur Radiol* 2006; 16:692-701.
52. Faverly DR, Hendriks JH, Holland R. Breast carcinomas of limited extent: frequency, radiologic-pathologic characteristics, and surgical margin requirements. *Cancer* 2001; 91:647-659.
53. Zonderland HM, Hermans J, Coerkamp EG. Ultrasound variables and their prognostic value in a population of 1103 patients with 272 breast cancers. *Eur Radiol* 2000; 10:1562-1568.
54. Hwang ES, Kinkel K, Esserman LJ et al. Magnetic resonance imaging in patients diagnosed with ductal carcinoma-in-situ: value in the diagnosis of residual disease, occult invasion, and multicentricity. *Ann Surg Oncol* 2003; 10:381-388.
55. Hata T, Takahashi H, Watanabe K et al. Magnetic resonance imaging for preoperative evaluation of breast cancer: a comparative study with mammography and ultrasonography. *J Am Coll Surg* 2004; 198:190-197.
56. Kuhl CK, Schrading S, Bieling HB et al. MRI for diagnosis of pure ductal carcinoma in situ: a prospective observational study. *Lancet* 2007; 370:485-492.
57. Van GM, Schelfout K, Kersschot E et al. MR mammography is useful in the preoperative locoregional staging of breast carcinomas with extensive intraductal component. *Eur J Radiol* 2007; 62:273-282.
58. Bhattacharyya M, Ryan D, Carpenter R et al. Using MRI to plan breast-conserving surgery following neoadjuvant chemotherapy for early breast cancer. *Br J Cancer* 2008; 98:289-293.
59. Houssami N, Ciatto S, Macaskill P et al. Accuracy and surgical impact of magnetic resonance imaging in breast cancer staging: systematic review and meta-analysis in detection of multifocal and multicentric cancer. *J Clin Oncol* 2008; 26:3248-3258.
60. Solin LJ, Orel SG, Hwang WT et al. Relationship of breast magnetic resonance imaging to outcome after breast-conservation treatment with radiation for women with early-stage invasive breast carcinoma or ductal carcinoma in situ. *J Clin Oncol* 2008; 26:386-391.
61. Pengel KE, Loo CE, Teertstra HJ et al. The impact of preoperative MRI on breast-conserving surgery of invasive cancer: a comparative cohort study. *Breast Cancer Res Treat* 2008.
62. Morrow M, Freedman G. A clinical oncology perspective on the use of breast MR. *Magn Reson Imaging Clin N Am* 2006; 14:363-78, vi.
63. Burkholder HC, Witherspoon LE, Burns RP et al. Breast surgery techniques: preoperative bracketing wire localization by surgeons. *Am Surg* 2007; 73:574-578.

64. Schmidt-Ullrich R, Wazer DE, Tercilla O et al. Tumor margin assessment as a guide to optimal conservation surgery and irradiation in early-stage breast carcinoma. *Int J Radiat Oncol Biol Phys* 1989; 17:733-738.
65. Thind CR, Desmond S, Harris O et al. Radio-guided localization of clinically occult breast lesions (ROLL): a DGH experience. *Clin Radiol* 2005; 60:681-686.
66. Kelly P, Winslow EH. Needle wire localization for nonpalpable breast lesions: sensations, anxiety levels, and informational needs. *Oncol Nurs Forum* 1996; 23:639-645.
67. Haid A, Knauer M, Dunzinger S et al. Intra-operative sonography: a valuable aid during breast-conserving surgery for occult breast cancer. *Ann Surg Oncol* 2007; 14:3090-3101.
68. Ngo C, Pollet AG, Laperrelle J et al. Intraoperative ultrasound localization of nonpalpable breast cancers. *Ann Surg Oncol* 2007; 14:2485-2489.
69. Bennett IC, Greenslade J, Chiam H. Intraoperative ultrasound-guided excision of nonpalpable breast lesions. *World J Surg* 2005; 29:369-374.
70. Rahusen FD, Bremers AJ, Fabry HF et al. Ultrasound-guided lumpectomy of nonpalpable breast cancer versus wire-guided resection: a randomized clinical trial. *Ann Surg Oncol* 2002; 9:994-998.
71. Moore MM, Whitney LA, Cerilli L et al. Intraoperative ultrasound is associated with clear lumpectomy margins for palpable infiltrating ductal breast cancer. *Ann Surg* 2001; 233:761-768.
72. Klimberg VS. Advances in the diagnosis and excision of breast cancer. *Am Surg* 2003; 69:11-14.
73. Smith LF, Rubio IT, Henry-Tillman R et al. Intraoperative ultrasound-guided breast biopsy. *Am J Surg* 2000; 180:419-423.
74. Karni T, Pappo I, Sandbank J et al. A device for real-time, intraoperative margin assessment in breast-conservation surgery. *Am J Surg* 2007; 194:467-473.
75. Allweis TM, Kaufman Z, Lelcuk S et al. A prospective, randomized, controlled, multicenter study of a real-time, intraoperative probe for positive margin detection in breast-conserving surgery. *Am J Surg* 2008; 196:483-489.
76. Huynh PT, Jarolimek AM, Daye S. The false negative mammogram. *Radiographics* 1998; 18:1137-1154.
77. Lee CH, Carter D. Detecting residual tumor after excisional biopsy of impalpable breast carcinoma: efficacy of comparing preoperative mammograms with radiographs of the biopsy specimen. *AJR Am J Roentgenol* 1995; 164:81-86.
78. Tafta L, Fine R, Whitworth P et al. Prospective randomized study comparing cryo-assisted and needle-wire localization of ultrasound-visible breast tumors. *Am J Surg* 2006; 192:462-470.
79. Weber S, Storm FK, Stitt J et al. The role of frozen section analysis of margins during breast conservation surgery. *Cancer J Sci Am* 1997; 3:273-277.
80. Riedl O, Fitzal F, Mader N et al. Intraoperative frozen section analysis for breast-conserving therapy in 1016 patients with breast cancer. *Eur J Surg Oncol* 2008; 35:264-270.
81. Cendan JC, Coco D, Copeland EM. Accuracy of intraoperative frozen-section analysis of breast cancer lumpectomy-bed margins. *J Am Coll Surg* 2005; 201:194-198.
82. Olson TP, Harter J, Munoz A et al. Frozen section analysis for intraoperative margin assessment during breast-conserving surgery results in low rates of re-excision and local recurrence. *Ann Surg Oncol* 2007; 14:2953-2960.
83. Camp ER, McAuliffe PF, Gilroy JS et al. Minimizing local recurrence after breast conserving therapy using intraoperative shaved margins to determine pathologic tumor clearance. *J Am Coll Surg* 2005; 201:855-861.
84. Klimberg VS, Westbrook KC, Korourian S. Use of touch preps for diagnosis and evaluation of surgical margins in breast cancer. *Ann Surg Oncol* 1998; 5:220-226.
85. Valdes EK, Boolbol SK, Ali I et al. Intraoperative touch preparation cytology for margin assessment in breast-conservation surgery: does it work for lobular carcinoma? *Ann Surg Oncol* 2007; 14:2940-2945.
86. Bakhshandeh M, Tutuncuoglu SO, Fischer G et al. Use of imprint cytology for assessment of surgical margins in lumpectomy specimens of breast cancer patients. *Diagn Cytopathol* 2007; 35:656-659.

87. Weinberg E, Cox C, Dupont E et al. Local recurrence in lumpectomy patients after imprint cytology margin evaluation. *Am J Surg* 2004; 188:349-354.
88. Malik HZ, George WD, Mallon EA et al. Margin assessment by cavity shaving after breast-conserving surgery: analysis and follow-up of 543 patients. *Eur J Surg Oncol* 1999; 25:464-469.
89. Huston TL, Pigalarga R, Osborne MP et al. The influence of additional surgical margins on the total specimen volume excised and the reoperative rate after breast-conserving surgery. *Am J Surg* 2006; 192:509-512.
90. Janes SE, Stankhe M, Singh S et al. Systematic cavity shaves reduces close margins and re-excision rates in breast conserving surgery. *Breast* 2006; 15:326-330.
91. Hall NC, Pivoski SP, Murrey DA et al. Combined approach of perioperative 18F-FDG PET/CT imaging and intraoperative 18F-FDG handheld gamma probe detection for tumor localization and verification of complete tumor resection in breast cancer. *World J Surg Oncol* 2007; 5:143.
92. Gulec SA, Hoenie E, Hostetter R et al. PET probe-guided surgery: applications and clinical protocol. *World J Surg Oncol* 2007; 5:65.
93. Gulec SA, Daghighian F, Essner R. PET-Probe: Evaluation of Technical Performance and Clinical Utility of a Handheld High-Energy Gamma Probe in Oncologic Surgery. *Ann Surg Oncol* 2006.
94. Brown RS, Wahl RL. Overexpression of Glut-1 glucose transporter in human breast cancer. An immunohistochemical study. *Cancer* 1993; 72:2979-2985.
95. Brown RS, Leung JY, Fisher SJ et al. Intratumoral distribution of tritiated-FDG in breast carcinoma: correlation between Glut-1 expression and FDG uptake. *J Nucl Med* 1996; 37:1042-1047.
96. Schulze T, Bembenek A, Schlag PM. Sentinel lymph node biopsy progress in surgical treatment of cancer. *Langenbecks Arch Surg* 2004; 389:532-550.
97. Strong VE, Humm J, Russo P et al. A novel method to localize antibody-targeted cancer deposits intraoperatively using handheld PET beta and gamma probes. *Surg Endosc* 2008; 22:386-391.
98. Cohn DE, Hall NC, Pivoski SP et al. Novel perioperative imaging with ¹⁸F-FDG PET/CT and intraoperative ¹⁸F-FDG detection using a handheld gamma probe in recurrent ovarian cancer. *Gynecol Oncol* 2008; 110:152-157.
99. Piert M, Burian M, Meisetschlager G et al. Positron detection for the intraoperative localisation of cancer deposits. *Eur J Nucl Med Mol Imaging* 2007; 34:1534-1544.
100. Kaida H, Ishibashi M, Fuji T et al. Improved breast cancer detection of prone breast fluorodeoxyglucose-PET in 118 patients. *Nucl Med Commun* 2008; 29:885-893.
101. Heckathorne E, Dimock C, Dahlbom M. Radiation dose to surgical staff from positron-emitter-based localization and radiosurgery of tumors. *Health Phys* 2008; 95:220-226.
102. Wahl RL. Current status of PET in breast cancer imaging, staging, and therapy. *Semin Roentgenol* 2001; 36:250-260.
103. Perez CA. Conservation therapy in T₁-T₂ breast cancer: past, current issues, and future challenges and opportunities. *Cancer J* 2003; 9:442-453.
104. Kumar R, Alavi A. Fluorodeoxyglucose-PET in the management of breast cancer. *Radiol Clin North Am* 2004; 42:1113-1122, ix.
105. Luini A, Zurrida S, Paganelli G et al. Comparison of radioguided excision with wire localization of occult breast lesions. *Br J Surg* 1999; 86:522-525.
106. De Cicco C, Pizzamiglio M, Trifiro G et al. Radioguided occult lesion localisation (ROLL) and surgical biopsy in breast cancer. Technical aspects. *Q J Nucl Med* 2002; 46:145-151.
107. Rampaul RS, Bagnall M, Burrell H et al. Randomized clinical trial comparing radioisotope occult lesion localization and wire-guided excision for biopsy of occult breast lesions. *Br J Surg* 2004; 91:1575-1577.
108. Machado RH, Oliveira AC, Rocha AC et al. Radioguided occult lesion localization (ROLL) and excision of breast lesions using technetium-99m-macroaggregate albumin and air injection control. *J Exp Clin Cancer Res* 2007; 26:323-327.

109. Cortes RM, Pardo GR, Soriano CA et al. Radioguided occult breast lesion location (ROLL). *Rev Esp Med Nucl* 2005; 24:374-379.
110. Sarlos D, Frey LD, Hauelsen H et al. Radioguided occult lesion localization (ROLL) for treatment and diagnosis of malignant and premalignant breast lesions combined with sentinel node biopsy: A prospective clinical trial with 100 patients. *Eur J Surg Oncol* 2008; 35:403-408.
111. Paredes P, Vidal-Sicart S, Zanon G et al. Radioguided occult lesion localisation in breast cancer using an intraoperative portable gamma camera: first results. *Eur J Nucl Med Mol Imaging* 2008; 35:230-235.
112. Gray RJ, Salud C, Nguyen K et al. Randomized prospective evaluation of a novel technique for biopsy or lumpectomy of nonpalpable breast lesions: radioactive seed versus wire localization. *Ann Surg Oncol* 2001; 8:711-715.
113. Hughes JH, Mason MC, Gray RJ et al. A multi-site validation trial of radioactive seed localization as an alternative to wire localization. *Breast J* 2008; 14:153-157.
114. Nadeem R, Chagla LS, Harris O et al. Occult breast lesions: A comparison between radioguided occult lesion localisation (ROLL) vs. wire-guided lumpectomy (WGL). *Breast* 2005; 14:283-289.
115. van Esser S, Hobbelink MG, van der Ploeg IM et al. Radio guided occult lesion localization (ROLL) for nonpalpable invasive breast cancer. *J Surg Oncol* 2008; 98:526-529.
116. van Esser S, Hobbelink MG, Peeters PH et al. The efficacy of 'radio guided occult lesion localization' (ROLL) versus 'wire-guided localization' (WGL) in breast conserving surgery for nonpalpable breast cancer: a randomized clinical trial - ROLL study. *BMC Surg* 2008; 8:9.
117. Luker GD, Luker KE. Optical imaging: current applications and future directions. *J Nucl Med* 2008; 49:1-4.
118. Tromberg BJ, Pogue BW, Paulsen KD et al. Assessing the future of diffuse optical imaging technologies for breast cancer management. *Med Phys* 2008; 35:2443-2451.
119. Ntziachristos V. Fluorescence molecular imaging. *Annu Rev Biomed Eng* 2006; 8:1-33.
120. von Burstin J, Eser S, Seidler B et al. Highly sensitive detection of early-stage pancreatic cancer by multimodal near-infrared molecular imaging in living mice. *Int J Cancer* 2008; 123:2138-2147.
121. Kirsch DG, Dinulescu DM, Miller JB et al. A spatially and temporally restricted mouse model of soft tissue sarcoma. *Nat Med* 2007; 13:992-997.
122. Tagaya N, Yamazaki R, Nakagawa A et al. Intraoperative identification of sentinel lymph nodes by near-infrared fluorescence imaging in patients with breast cancer. *Am J Surg* 2008; 195:850-853.
123. Sevic-Muraca EM, Sharma R, Rasmussen JC et al. Imaging of lymph flow in breast cancer patients after microdose administration of a near-infrared fluorophore: feasibility study. *Radiology* 2008; 246:734-741.
124. Ogasawara Y, Ikeda H, Takahashi M et al. Evaluation of breast lymphatic pathways with indocyanine green fluorescence imaging in patients with breast cancer. *World J Surg* 2008; 32:1924-1929.
125. Brandt MG, Moore CC, Jordan K. Randomized control trial of fluorescence-guided surgical excision of nonmelanotic cutaneous malignancies. *J Otolaryngol* 2007; 36:148-155.
126. Stummer W, Pichlmeier U, Meinel T et al. Fluorescence-guided surgery with 5-aminolevulinic acid for resection of malignant glioma: a randomised controlled multicentre phase III trial. *Lancet Oncol* 2006; 7:392-401.
127. Backer MV, Levashova Z, Patel V et al. Molecular imaging of VEGF receptors in angiogenic vasculature with single-chain VEGF-based probes. *Nat Med* 2007; 13:504-509.
128. Chen K, Li ZB, Wang H et al. Dual-modality optical and positron emission tomography imaging of vascular endothelial growth factor receptor on tumor vasculature using quantum dots. *Eur J Nucl Med Mol Imaging* 2008; 35:2235-2244.
129. Sampath L, Kwon S, Ke S et al. Dual-labeled trastuzumab-based imaging agent for the detection of human epidermal growth factor receptor 2 overexpression in breast cancer. *J Nucl Med* 2007; 48:1501-1510.
130. Ke S, Wen X, Gurfinkel M et al. Near-infrared optical imaging of epidermal growth factor receptor in breast cancer xenografts. *Cancer Res* 2003; 63:7870-7875.

131. Lee SB, Hassan M, Fisher R et al. Affibody molecules for *in vivo* characterization of HER2-positive tumors by near-infrared imaging. *Clin Cancer Res* 2008; 14:3840-3849.
132. Gee MS, Upadhyay R, Bergquist H et al. Human breast cancer tumor models: molecular imaging of drug susceptibility and dosing during HER2/neu-targeted therapy. *Radiology* 2008; 248:925-935.
133. Weissleder R. Molecular imaging: exploring the next frontier. *Radiology* 1999; 212:609-614.
134. Bremer C, Ntziachristos V, Weitkamp B et al. Optical imaging of spontaneous breast tumors using protease sensing 'smart' optical probes. *Invest Radiol* 2005; 40:321-327.
135. Tung CH, Mahmood U, Bredow S et al. *In vivo* imaging of proteolytic enzyme activity using a novel molecular reporter. *Cancer Res* 2000; 60:4953-4958.
136. Bremer C, Ntziachristos V, Weissleder R. Optical-based molecular imaging: contrast agents and potential medical applications. *Eur Radiol* 2003; 13:231-243.
137. Stanciute D, Didziapetriene J, Kadziauskas J. Expression of matrix metalloproteinases in patients with malignant tumors. *Medicina* 2004; 40:1143-1150.
138. Veisoh M, Gabikian P, Bahrami SB et al. Tumor paint: a chlorotoxin: Cy5.5 bioconjugate for intraoperative visualization of cancer foci. *Cancer Res* 2007; 67:6882-6888.
139. Frangioni JV. New technologies for human cancer imaging. *J Clin Oncol* 2008; 26:4012-4021.
140. Ntziachristos V, Bremer C, Weissleder R. Fluorescence imaging with near-infrared light: new technological advances that enable *in vivo* molecular imaging. *Eur Radiol* 2003; 13:195-208.
141. Ntziachristos V, Ripoll J, Wang LV et al. Looking and listening to light: the evolution of whole-body photonic imaging. *Nat Biotechnol* 2005; 23:313-320.
142. Bremer C, Tung CH, Weissleder R. *In vivo* molecular target assessment of matrix metalloproteinase inhibition. *Nat Med* 2001; 7:743-748.
143. Bornhop DJ, Contag CH, Licha K et al. Advance in contrast agents, reporters, and detection. *J Biomed Opt* 2001; 6:106-110.
144. Soubret A, Ntziachristos V. Fluorescence molecular tomography in the presence of background fluorescence. *Phys Med Biol* 2006; 51:3983-4001.
145. Godavarty A, Eppstein MJ, Zhang C et al. Detection of single and multiple targets in tissue phantoms with fluorescence-enhanced optical imaging: feasibility study. *Radiology* 2005; 235:148-154.
146. Gulben K, Berberoglu U, Cengiz A et al. Prognostic factors affecting locoregional recurrence in patients with stage IIIB noninflammatory breast cancer. *World J Surg* 2007; 31:1724-1730.
147. Aziz D, Rawlinson E, Narod SA et al. The role of reexcision for positive margins in optimizing local disease control after breast-conserving surgery for cancer. *Breast J* 2006; 12:331-337.
148. Cefaro GA, Genovesi D, Marchese R et al. Predictors of local recurrence after conservative surgery and whole-breast irradiation. *Breast Cancer Res Treat* 2006; 98:329-335.
149. Smitt MC, Horst K. Association of clinical and pathologic variables with lumpectomy surgical margin status after preoperative diagnosis or excisional biopsy of invasive breast cancer. *Ann Surg Oncol* 2007; 14:1040-1044.

Chapter

3

Breast. 2013; 22(5):773-779.

A validated web-based nomogram for predicting positive surgical margins following breast-conserving surgery as a preoperative tool for clinical decision-making

R.G. Pleijhuis
A.B. Kwast
L. Jansen
J. de Vries
R. Lanting
J. Bart
T. Wiggers
G.M. van Dam
S. Siesling

ABSTRACT

Background

Breast-conserving therapy, consisting of lumpectomy and adjuvant radiotherapy, is considered standard treatment for early-stage breast cancer. One of the most important risk factors of local recurrence is the presence of positive surgical margins following lumpectomy. We aimed to develop and validate a predictive model (nomogram) to predict for positive margins following the first attempt at lumpectomy as a preoperative tool for clinical decision-making.

Methods

Patients with clinical T₁₋₂N₀₋₁M_{x=0} histology-proven invasive breast carcinoma who underwent BCT throughout the North-East region of the Netherlands between June 2008 and July 2009 were selected from the Netherlands Cancer Registry (n=1,185). Results from multivariate logistic regression analyses served as the basis for development of the nomogram. Nomogram calibration and discrimination were assessed graphically and by calculation of a concordance index, respectively. Nomogram performance was validated on an external independent dataset (n=331) from the University Medical Center Groningen.

Results

The final multivariate regression model included clinical, radiological, and pathological variables. Concordance indices were calculated of 0.70 (95% CI: 0.66–0.74) and 0.69 (95% CI: 0.63–0.76) for the modeling and the validation group, respectively. Calibration of the model was considered adequate in both groups. A nomogram was developed as a graphical representation of the model. Moreover, a web-based application was built to facilitate the use of our nomogram in a clinical setting (<http://www.breastconservation.com>).

Conclusion

We developed and validated a nomogram that enables estimation of the preoperative risk of positive margins in breast-conserving surgery. Our nomogram provides a valuable tool for identifying high-risk patients who might benefit from preoperative MRI and/or oncoplastic surgery.

INTRODUCTION

Breast-conserving therapy (BCT), consisting of lumpectomy and adjuvant radiotherapy, is considered standard treatment for early-stage breast cancer.^{1,2} The presence of a positive (surgical) margin, usually defined as tumor cells being present at the inked margin of the lumpectomy specimen, has been reported to be the most consistent risk factor for local recurrence (LR) following BCT.^{3,4} The percentage of patients with positive margins following the first attempt at lumpectomy ranges from 20% to 40% in the majority of studies.⁵ To reduce the risk of LR in the case of positive margins, additional surgery and/or radiotherapy are required with adverse affects on cosmesis, psychological distress, and healthcare costs.⁶

Previous studies reported large tumor size, lobular histological type, positive N-stage, multifocal disease, lymphovascular invasion, co-existing ductal carcinoma in situ (DCIS), microcalcifications on mammography, and young age to be independent risk factors associated with positive margins following lumpectomy (Supplementary Table 1). To allow for simultaneous consideration of multiple risk factors, statistical tools can be applied to calculate the overall probability of a specific outcome.⁷ These so-called nomograms are tailored to the profile of an individual patient.⁸ User-friendly graphical interfaces and web-based calculators can facilitate the use of nomograms in clinical practice.

Several nomograms have been developed in the field of breast cancer, including one for predicting the risk of positive surgical margins after BCT.⁹ However, this study was based and validated on single-center data, which might impair generalizability of the model. The aims of the current study were i) to develop a user-friendly graphical and web-based nomogram based on multicenter data to predict individual probability of positive margins following the first attempt at lumpectomy based on clinicopathological variables and ii) to validate the nomogram in an independent dataset.

METHODS

Patient population

A modeling and a validation group were constituted for development and validation of the nomogram, respectively. The modeling group consisted of breast cancer patients selected from the Netherlands Cancer Registry (NCR). Based on pathological notification through the PALGA (automated pathology archive) system,¹⁰ trained registration clerks gathered data concerning patient, tumor, and treatment characteristics from the patient files. Additionally, the NCR registered surgical margin status following lumpectomy between June 2008 and July 2009. During this time frame, data was collected from 1,495 patients who underwent BCT in one of 24 institutions throughout the Northern- and Eastern region of the Netherlands.

Supplementary radiological and clinical variables were collected retrospectively for 1,349 patients from 20 out of 24 institutions. Three institutions were excluded due to a relatively limited contribution to the NCR database (<15 patients). One institution did not participate because of a change in the preoperative work-up during the investigated time frame, which might have influenced surgical outcome. Approval was obtained from the institutional review board of all participating institutions prior to initiation of the study.

Women with clinical T₁₋₂N₀₋₁M_{x,0} histology-proven invasive breast carcinoma who underwent BCT were included. Patients with unconfirmed malignancy prior to surgery, undefined margin status, neo-adjuvant treatment, or absence of reported radiological tumor size were excluded. A total of 1,185 out of 1,349 patients (88%) were eligible for the modeling group.

The validation group consisted of 439 patients who underwent BCT at the University Medical Center Groningen (UMCG), Groningen, the Netherlands between July 2004 and June 2008 or July 2009 and May 2011. Patients who underwent BCT between June 2008 and July 2009 were assigned to the modeling group as they were part of the NCR database. Inclusion and exclusion criteria were identical to those applied in the modeling group. A total of 331 patients (75%) were eligible for the validation group.

Clinicopathological evaluation

The following variables were incorporated from the NCR database: surgical margin status, age, preoperative N-stage, preoperative T-stage, tumor location, histological type, histological grade, estrogen receptor (ER) status, progesterone receptor (PR) status, HER2 receptor status, and presence of co-existing DCIS.

Positive surgical margin status was defined as microscopically confirmed invasive carcinoma (IC) and/or DCIS at the inked margin of the lumpectomy specimen following the first attempt at lumpectomy. Staging was performed according to the fifth edition of the TNM atlas. Preoperative T-stage was based on the maximum tumor diameter as measured on MRI (if available) or ultrasonography. Preoperative N-stage was based on clinical and/or radiological examination as well as preoperative histological examination (if available) of the axillary region. Topography and morphology were coded according to the International Classification of Diseases for Oncology (ICD-O).¹¹ Grading of invasive carcinoma was scored according to the Nottingham (Elston-Ellis) modification of the Scarf-Bloom-Richardson grading system. Positivity of estrogen and progesterone receptors was defined as at least 10% of immunostained nuclei of tumor cells. HER2 status was considered positive in case of HER2 3+ (strong and complete membranous expression in >30% of tumor cells) or HER2 2+ (weak complete membranous expression in >10% of tumor cells) confirmed with positive fluorescence in situ hybridization (FISH). Co-existing DCIS was defined as the presence of any DCIS component. All pathological variables were assessed on final pathology due to the fact that no preoperative core needle biopsy (CNB) was routinely performed in the vast majority of patients.

The NCR database was supplemented with data collected from patient files at the participating institutions, including clinical (family history, referral from screening, palpability, breast cup size, and prior surgery to the ipsilateral breast), and radiological variables (BI-RADS classification, suspicion of multifocality, preoperative MRI, microcalcifications, density of the breast, and area of the breast on the preoperative digital mammogram). Family history was recorded as negative, first-degree (FDR), or second-degree relatives (SDR). Tumors were classified as nonpalpable if a needle-localization procedure was required for excision. BI-RADS classification was recorded according to the fourth edition of the *breast imaging reporting and data system*.¹² Suspicion of multifocality was defined as the presence of two or more tumor foci within the same quadrant of the ipsilateral breast as assessed on MRI (if available) or radiography. The presence of microcalcifications was assessed on mammography and reported as present or absent. Density of the breast was assessed on mammograms and reported as one out of four BI-RADS categories: mostly fatty (<25% dense), scattered fibroglandular tissue (25–50% dense), heterogeneously dense (50–75% dense), and extremely dense (75–100% dense).¹² Area of the breast was determined in mm² by manually delineating the breast on the lateral projection of the preoperative digital mammogram. Calculations were performed using the default radiological software package available at each hospital. Last, postoperative variables were scored for the purpose of describing patient and tumor characteristics, including postoperative T-stage, postoperative N-stage, weight of the excised lump, and tumor-to-lump index (defined as the

maximum tumor diameter in mm divided by the weight of the excised lump in grams). Within the validation group, clinicopathological variables were collected from patient files in the UMCG database. Variables were scored identically to those in the modeling group

Statistical analysis

The primary outcome for this study was the proportion of positive surgical margins following lumpectomy. Multivariate logistic regression analysis (MVA) was used to test the association between clinicopathological variables and the likelihood of positive margins. Stepwise backward variable selection was performed to determine informative variables based on the corrected Akaike's Information Criterion (AIC_c).¹³ The nested model with the lowest AIC_c value was used to construct a graphical nomogram. A corresponding web-based calculator was developed. Moreover, a second calculator was developed including solely clinical and radiological variables, which can be applied in the absence of a preoperative CNB.

Model performance was quantified in both the modeling group and the validation group with respect to discrimination and calibration. Discrimination was assessed by calculating the area under the receiver operating characteristic (AUROC) curve, resulting in a so-called concordance index (*c*-index). Calibration was studied graphically after grouping patients into deciles with respect to their predicted probabilities and plotting the mean predicted probabilities against the mean observed probabilities. Bootstrapping was applied to calculate 95% confidence intervals. Overall fit of the model was evaluated using the Hosmer-Lemeshow goodness-of-fit test. Reported *P*-values are two-sided with alpha 5%.

Statistical analyses were performed using the statistical packages SPSS (SPSS for Windows, version 18.0.3, SPSS Inc., Chicago, USA) and STATA Software, version 10.0 (StataCorp, College Station, USA). Graphs were created using GraphPad Prism (GraphPad Prism for Windows, version 5.00, GraphPad Software, San Diego, USA).

RESULTS

Patient and tumor characteristics of the modeling and validation group are listed in Table 1. Positive margins in BCT were present in 19.7% and 24.5% of the patients in the modeling and validation group, respectively (Supplementary Table 2). Marked differences between the modeling and the validation group were observed with respect to age, weight of the excised lump, tumor location, pN-stage, prior surgery to the breast, family history, BI-RADS classification, and presence of DCIS.

Margin positivity ranged from 11% to 38% throughout the 20 institutions that constituted the modeling group. No difference was observed between positive surgical margin rates from university-affiliated and community hospitals ($P=0.883$). Moreover, no significant difference in the occurrence of positive margins was observed between individual hospitals when evaluated using MVA ($P=0.282$). Of the 233 patients with positive margins in the modeling group, 92 (39.5%) patients had a relumpectomy with clear margins, 2 (0.9%) patients had a second lumpectomy with persistent positive margins, 16 (6.9%) patients underwent mastectomy, and 123 (52.8%) patients had no further surgery despite positive margins. Data on further surgical management was available for all 233 (100%) patients.

Data on breast cup size was available for only 101 out of 1,185 patients (8.5%) in the modeling group and 45 out of 331 patients (13.6%) in the validation group (data not shown). We therefore used the area of the breast on the digital mammogram to substitute for cup size, as the correlation between both variables was strong (Spearman's rho: 0.893, $P<0.0001$).

MRI was performed in 122 patients (10.3%) in the model group for preoperative tumor assessment. Ultrasonography was performed in the remaining 1,064 patients (89.7%). In the validation group, preoperative MRI was performed in 31 patients (9.4%), while the remaining 300 patients (90.6%) had ultrasonography. Sentinel lymph node biopsy was performed in the vast majority of patients, including 1,113 (93.9%) patients from the modeling group and 307 (92.7%) from the validation group. Axillary lymph node dissection (ALND) was performed in 293 (24.7%) and 87 patients (26.3%), respectively. A total of 221 (18.6%) and 63 (19.0%) patients received an ALND in addition to a SLNB procedure.

Multivariate analysis

The nested MVA model with the lowest AIC_c (959.6) was selected. Clinicopathological variables constituting the final model were microcalcifications, preoperative MRI, suspicion of multifocality, palpability, preoperative N-stage, preoperative T-stage, density of the breast, histological type, histological grade, ER status, and presence of DCIS. Corresponding odds ratios are listed in Table 2. Non-significant variables were included if they improved accuracy of the model.

Evaluation of the model

The model fitted the data according to the Hosmer-Lemeshow goodness-of-fit test ($\chi^2 = 2.733$, 8 degrees of freedom, $P=0.950$). Discrimination (Fig. 1) and calibration (Fig. 2) were first assessed for the modeling group. The *c*-index was calculated to be 0.70 (95% CI 0.66–0.74, $P<0.001$). Calibration was considered adequate. External validation on the UMCG dataset resulted in a *c*-index of 0.69 (95% CI 0.63–0.76, $P<0.001$; Fig. 1). Calibration was considered acceptable (Fig. 2).

Nomogram and web-based calculators

A graphical nomogram was developed based on the results of MVA (Fig. 3). The underlying statistical formula was also implemented in a web-based calculator, freely accessible at www.breastconservation.com. Additionally, a second web-based calculator was developed including solely clinical and radiological variables that can be used in the absence of a preoperative CNB. Discrimination of this model ranged from 0.62 to 0.64 for the modeling and validation group, respectively (Supplementary Fig. 1). Calibration was considered acceptable for both groups (Supplementary Fig. 2). Both calculators provide the user with a patient-tailored estimation of the preoperative risk of positive margins, stratified as low (<15%), intermediate (15–25%), or high (>25%) risk. The calculators support Internet Explorer, Safari, Firefox, and Google Chrome. An example on how to use the online nomogram is provided on the website.

Table 1. Patient and tumor characteristics for the modeling and validation group.

Characteristic	Modeling group		Validation Group		P-value
	N	%	N	%	
No. of patients	1185	100	331	100	
Age (years)					
Mean (±SE)	59.8 (±0.31)		56.5 (±0.63)		<0.001 ^a
Median	60.3		56.0		
Range	27–95		26–91		<0.001 ^b
≤40	39	3.3	28	8.5	
41–69	919	77.6	255	77.0	
≥70	227	19.2	48	14.5	
Tumor size (mm)					
Mean (±SE)	15.6 (±0.22)		15.2 (±0.48)		0.107 ^c
Median	14.0		13.0		
Range	1.5–58.5		2.1–57.9		0.087
pT _{1a}	54	4.6	22	6.6	
pT _{1b}	243	20.5	81	24.5	
pT _{1c}	599	50.5	164	49.5	
pT ₂	284	24.0	62	18.7	
pT ₃	5	0.4	2	0.6	
Area on mammogram (mm ²)					
Mean (±SE)	17916 (±6807)		17575 (±6937)		0.617
Median	17163		16498		
Range	3551–46895		5212–50619		0.396
≤15000	450	38.0	138	42.4	
15000–25000	554	46.8	142	44.7	
≥25000	181	15.3	45	13.8	
Weight excised lump (gram)					
Mean (±SE)	62.5 (±39.7)		56.3 (±40.0)		0.027
Median	53.0		47.0		
Range	6–277		6–299		0.044
≤50	270	44.5	167	51.0	
51–99	172	28.3	78	23.9	
≥100	165	27.2	82	25.1	
Tumor-to-lump index					
Mean (±SE)	0.338 (±0.012)		0.354 (±0.020)		0.503
Median	0.266		0.288		
Range	0.02–3.67		0.02–4.41		0.132
≤0.25	278	45.8	121	39.2	
0.25–0.50	228	37.6	135	43.7	
≥0.50	101	16.6	53	17.2	
Palpability					0.104
Palpable	637	53.8	195	58.9	
Nonpalpable	548	46.2	136	41.1	
Tumor location					<0.001
LOQ	122	10.3	42	12.7	
UOQ	535	45.1	170	51.4	
UIQ	189	15.9	50	15.1	
LIQ	150	12.7	26	7.9	
Central	103	8.7	6	1.8	

Table continues on the next page

Characteristic	Modeling group		Validation Group		P-value
	N	%	N	%	
Histological type					0.062
Ductal	957	80.8	286	86.4	
Lobular	119	10.0	23	6.9	
Specified ^d	109	9.2	22	6.6	
Histological grade					0.214
Grade I	330	28.1	107	32.8	
Grade II	531	45.2	133	40.7	
Grade III	313	26.6	86	26.5	
ER status					0.661
Positive	1002	85.3	276	84.4	
Negative	172	14.7	51	15.6	
PR status					0.443
Positive	750	71.4	226	69.1	
Negative	300	28.5	101	30.9	
HER2 receptor status					0.486
Positive	125	10.7	40	12.3	
Negative	1041	89.3	290	87.7	
Multifocal disease					0.170
Yes	47	4.0	19	5.7	
No	1138	96.0	312	94.3	
pN-stage					0.004
Positive	310	26.2	113	34.4	
Negative	875	73.8	218	65.6	
Prior surgery to the breast					<0.001
Yes	46	3.9	34	10.3	
No	1139	96.1	297	89.7	
Family history					<0.001
FDR	91	8.9	75	22.8	
SDR	188	18.2	56	17.0	
Negative	749	72.9	199	60.2	
Referred from screening					0.755
Yes	578	49.1	158	47.7	
No	601	50.9	172	52.3	
BI-RADS classification					0.001
II ^e	3	0.3	8	2.5	
III	93	8.1	31	9.7	
IV	611	52.9	155	48.3	
V	447	38.7	127	39.5	
Preoperative MRI					0.680
Yes	122	10.3	31	9.4	
No	1063	89.7	300	90.6	
Microcalcifications					0.542
Yes	245	20.8	74	22.4	
No	937	79.2	257	77.6	

Table continues on the next page

Characteristic	Modeling group		Validation Group		P-value
	N	%	N	%	
DCIS component present					<0.001
Yes	529	44.6	188	56.8	
No	656	55.4	143	43.2	
Breast density					0.816
0–25 %	323	31.0	101	31.2	
25–50%	467	44.9	146	45.0	
50–75%	217	20.8	70	21.6	
75–100%	34	3.3	7	2.2	
Institution					-
University-affiliated	642	54.2	331	100	
Community hospital	543	45.8	-	-	

ER, estrogen receptor; FDR, first-degree relative; LIQ, lower inner quadrant; LOQ, lower outer quadrant; MRI, magnetic resonance imaging; PR, progesterone receptor; SDR, second-degree relative; UIQ, upper inner quadrant; UOQ, upper outer quadrant.

Variables which differ significantly ($P < 0.05$) between both groups are highlighted in grey.

^a Independent-samples *t*-test.

^b Fisher's exact test.

^c Independent-samples *t*-test following logarithmic transformation to promote data normality.

^d Specified histological types included mucinous, medullary, tubular, and papillary carcinomas.

^e BI-RADS classification II with malignancy proven by fine needle aspiration or core needle biopsy.

Table 2. Preoperative clinical, radiological, and pathological variables included in the final model.

Predictor	Odds ratio	95% CI	P-value
Suspicion of multifocal disease (vs. unifocal)	2.81	1.30–6.06	0.008
Preoperative MRI scan absent (vs. available)	1.80	1.02–3.18	0.043
Positive preoperative N-stage (vs. negative)	1.73	0.97–3.07	0.062
Nonpalpable tumor (vs. palpable)	1.51	1.07–2.13	0.020
Microcalcifications on mammogram (vs. none)	1.37	0.95–2.00	0.094
Preoperative T ₂ stage (vs. T ₁)	1.33	0.87–2.02	0.185
Breast density on mammogram	1.22	1.00–1.49	0.053
Presence of DCIS component (vs. absence)	3.11	2.19–4.42	<0.001
Lobular histological type (vs. other)	2.90	1.71–4.91	<0.001
Positive ER status (vs. negative)	1.80	1.04–3.13	0.037
Elston III grade (vs. Elston I/II)	1.44	0.96–2.16	0.082

CI, confidence interval; DCIS, ductal carcinoma in situ; ER, estrogen receptor; MRI, magnetic resonance imaging

Reported odds ratios indicate a ratio of the probability of positive margins following lumpectomy versus the probability of negative margins. Statistical significant P-values (<0.05) variables are highlighted in grey.

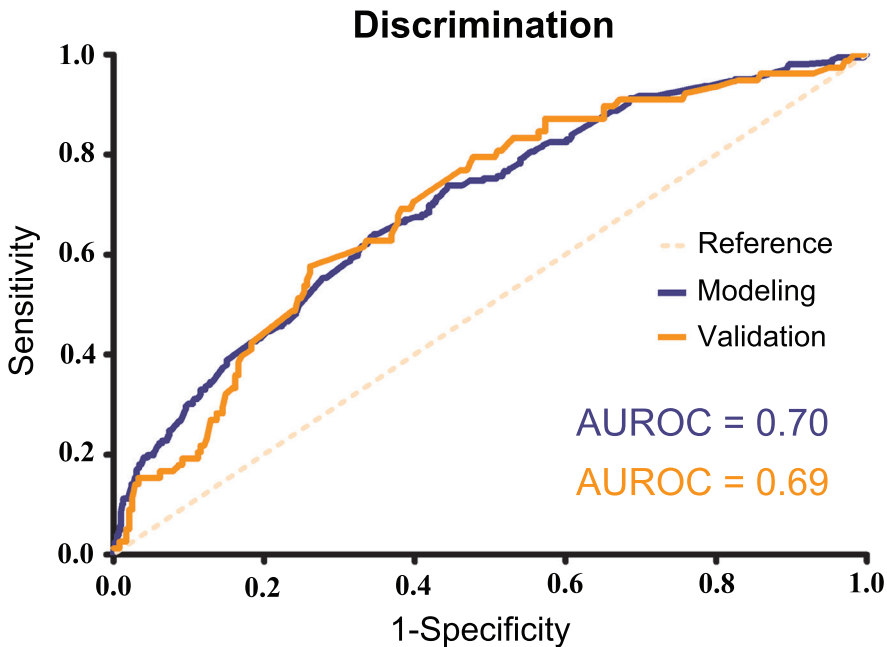


Figure 1. Discrimination of the final model for the modeling and validation group. The area under the receiver-operating characteristic (AUROC) curve, comparable to the concordance index, indicates the discriminative power of the model. The reference line indicates an AUROC value of 0.5, for which the probability of positive surgical margins is equal to the toss of a coin. An AUROC value of 1.0 would resemble perfect discrimination.

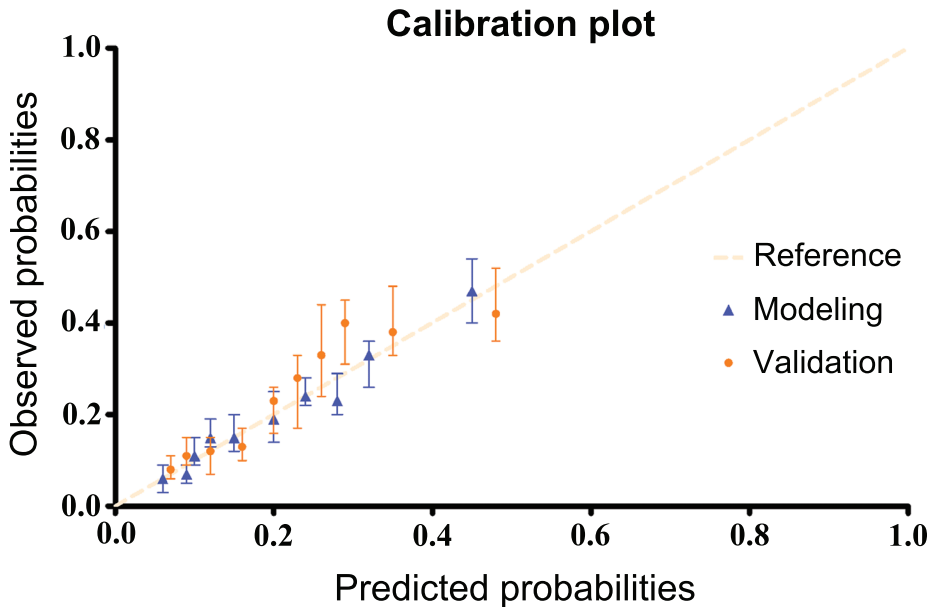


Figure 2. Calibration of the final model in the modeling and validation group. All patients were grouped into deciles (blue triangles and orange dots) based on their predicted probabilities. Mean predicted probabilities were plotted against the actual incidence of positive margins for each decile. Moreover, 95% confidence intervals are shown for both groups. The reference line represents perfect equality of observed frequencies and predicted probabilities.

DISCUSSION

We developed a nomogram and corresponding web-based calculators to estimate the risk of positive margins following lumpectomy using clinicopathological variables. Variables predicting for positive surgical margins on MVA included microcalcifications on mammogram (OR 1.37, $P=0.094$), absence of preoperative MRI (OR 1.80, $P=0.043$), suspicion of multifocality (OR 2.81, $P=0.008$), nonpalpable tumor (OR 1.51, $P=0.020$), positive preoperative N-stage (OR 1.73, $P=0.062$), large tumor size (OR 1.33, $P=0.185$), high density of the breast (OR 1.22, $P=0.053$), lobular histological type (OR 2.90, $P<0.001$), high histological grade (OR 1.44, $P=0.082$), positive ER status (OR 1.80, $P=0.037$), and presence of DCIS (OR 3.11, $P<0.001$). In the absence of preoperative pathological variables (e.g., no CNB available), a second online calculator is available at <http://www.breastconservation.com> that solely includes clinical and radiological variables.

Assessment of pathological variables in the current study was based on final pathology due to the fact that fine needle aspiration biopsy instead of CNB was performed in the vast majority of patients. Nonetheless, CNB may provide important information on preoperative prognostic factors and shows good correlation with findings on final pathology.¹⁴ Histological type can be accurately predicted on CNB and is reported to be concordant with the subsequent surgical specimen in 93% to 100% of the cases.¹⁵ For ER status, reported concordance rates between CNB and the surgical specimen range from 86% to 100%.¹⁶⁻¹⁸ Current evidence shows that histological grade can be assessed on CNB and is concordant with final pathology in approximately 75% of the cases.¹⁹ The highest level of agreement is achieved in high grade carcinomas, with an associated concordance rate of 84%.¹⁴ The presence of co-existing DCIS

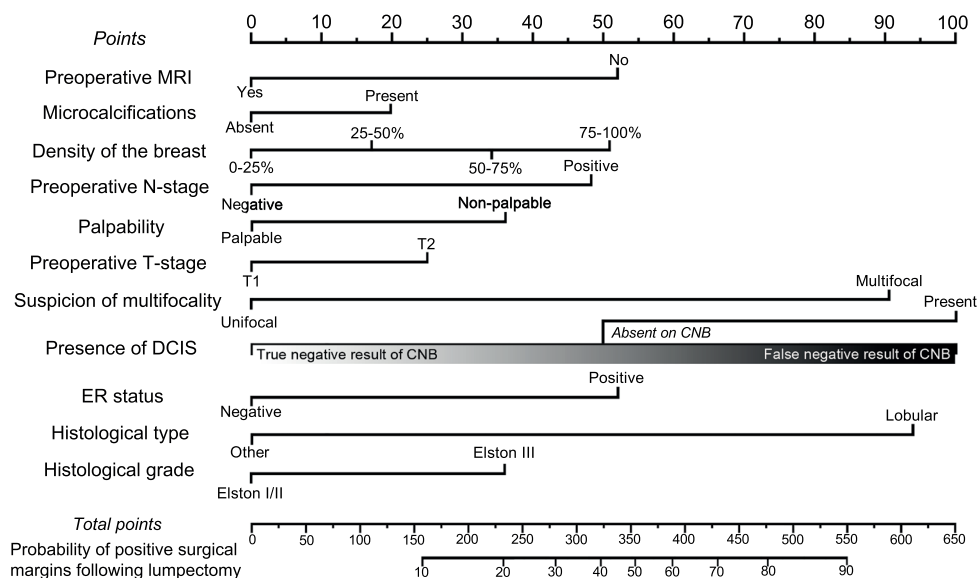


Figure 3. Nomogram including clinical, radiological, and pathological variables for predicting positive surgical margins following the first attempt at lumpectomy.

Instructions for use: Locate the patient's status on the 'preoperative MRI' axis. Draw a line straight upward to the 'points' axis to determine how many points are assigned to the individual patient. Repeat this process for the axes below. Tot up the points achieved for each variable and locate the sum on the 'total points' axis. From here, draw a line straight downward to obtain the probability of positive surgical margins following lumpectomy.

Note: Due to the relatively high frequency of false negative findings when assessing the presence of co-existing DCIS in a core needle biopsy (CNB), absence of DCIS should be interpreted with caution. We therefore recommend to determine a suitable probability interval by calculating the probability of positive surgical margins for both true and false negative outcomes. A more user-friendly web-based version of the nomogram is available at <http://www.breastconservation.com>.

can also be assessed on CNB and is associated with an increased risk of positive margins.²⁰⁻²² However, false negative findings reported in the literature range from 36% to 54%, indicating that the absence of DCIS in the CNB should be interpreted with caution.^{21,23} The risk for false negative results of CNB can be minimized by accurate targeting, sufficient biopsy size, and obtaining a larger number of cores.²⁰ Jimenez et al.²¹ reported that CNB predicts the presence of co-existing DCIS in the subsequent surgical specimen with a sensitivity and specificity of 54% and 92%, respectively. The corresponding negative and positive predictive values were 70% and 85%. To account for the relatively high risk of false negative findings, we recommend determining a suitable probability interval by calculating the probability of positive margins for both true and false negative outcomes when using our nomogram (Fig. 3). The web-based calculator will automatically provide the user with such a probability interval if applicable. The ability to estimate the preoperative risk of positive margins following lumpectomy could support clinicians in counseling patients regarding the likelihood of requiring further surgery, allowing for a more patient-tailored approach. Although broadly supported for positive margins, some authors have also reported an increased risk for LR in the case of close surgical margins.^{4,24} However, the importance of close margins is still a matter of debate.^{25,26} Moreover, consensus over what is the most appropriate margin is lacking, with definitions of close margins ranging from <1 mm to <5 mm distance to the inked margin.²⁷ Because the clinical implications of close margins are uncertain, they were not taken into account in this study.

In patients identified as high-risk (>25%), we advise to perform a preoperative MRI to assist the clinician in defining the extent of local disease and detect areas of co-existing high-grade DCIS that are occult on mammography. Indeed, preoperative MRI was reported to reduce the risk of inadequate tumor excision.²⁸ In the current study, MRI was performed in those patients with preoperative suspicion of multifocal disease or with BRCA1 or BRCA2 mutations. Despite correction for these factors, MRI was found to significantly decrease the risk of positive margins ($P=0.043$; Table 2). However, the true value of MRI in reducing the risk of inadequate tumor excision in patients preoperatively identified as high-risk needs to be assessed in future studies. In addition, high-risk patients might benefit from a more extensive surgical excision. Lovrics et al.²⁹ reported the amount of breast parenchyma excised during BCS to be inversely correlated with the likelihood of positive margins. In the current study, we also found a significant association between low tumor-to-lump index (i.e., relatively small lump compared to size of the tumor) and positive surgical margins ($P=0.002$). However, although excising relatively voluminous specimens is more accurate in predicting margin status than any predictive model, it has profound repercussions on cosmesis. To allow for relatively extensive excisions while maintaining adequate cosmetic results, oncoplastic surgery was suggested as a technique to minimize breast deformities by immediate reconstruction of large resection defects.³⁰ The technique might be of particular value for those patients identified as high risk with our nomogram, although further studies are needed to address this topic.

The rate of positive margins observed in the modeling (19.7%, range: 11%–38%) and the validation group (24.5%) are in line with positivity rates reported in the literature.⁵ The slightly higher positive margin rate in the validation group can partially be explained by the high rate of co-existing DCIS (56.8% vs. 44.6% in the modeling group, $P<0.001$), which is known to increase the risk of positive margins.³¹

Very recently, Shin et al.⁹ reported on a nomogram for predicting positive surgical margins after BCT. The nomogram was based on retrospective single-center data derived from 1,034 Korean breast cancer patients with invasive or in situ breast carcinoma. MVA indicated microcalcifications (OR 1.57, $P=0.034$), dense breasts (OR 4.52, $P=0.005$), 0.5 cm difference in tumor size between MRI and ultrasonography (OR 10.00, $P<0.001$), presence of DCIS (OR 1.58, $P=0.044$), and lobular histological type (OR 3.99, $P=0.015$) to be independent predictors for positive surgical margins. Validation was performed on an independent cohort of 563 patients. The concordance indices of the modeling and the validation groups were reported to be 0.82 (95% CI: 0.79–0.86) and 0.85 (95% CI: 0.80–0.89), respectively. Although the reported concordance indices are relatively high when compared to the current multicenter study, this difference may partly be explained by the relative lack of heterogeneity in single-institution data, impairing generalizability of the model.⁸ Our nomogram was constructed based on multicenter data derived from 20 institutions, including community-based and university-affiliated hospitals. Validation was performed in an independent dataset that showed marked differences when compared to the modeling group, providing sufficient data heterogeneity to assess generalizability of the nomogram.

Several other nomograms are available in the field of breast cancer, including nomograms for predicting the likelihood of cancer spread to the sentinel lymph nodes,³² cancer spread to nonsentinel lymph nodes,³³ and the benefit of systemic adjuvant therapy (*Adjuvant!* Online).³⁴ Moreover, Rudloff et al.³⁵ developed a nomogram (c -index: 0.704) for predicting the 5- and 10-year probability for ipsilateral breast tumor recurrence after BCT for DCIS. The nomogram was developed on the basis of unicenter data derived from 1,681 patients and included ten clinical, pathological, and treatment variables (age at diagnosis, family history, initial presentation, radiation, adjuvant endocrine therapy, nuclear grade, necrosis, margins, number of excisions, and year of surgery). Sanghani et al.³⁶ constructed a web-based nomogram for predicting the probability of ipsilateral breast tumor recurrence after BCT. Data was derived

from 7,811 patients and included both clinical and pathological variables (adjuvant RT or endocrine therapy, age, margin status, number of excisions, and treatment time period). Werkhoven et al.³⁷ developed a comparable nomogram (*c*-index: 0.68) based on data from 1,603 patients. Rouzier et al.³⁸ developed several nomograms that can be applied to predict the probability of successful BCT in patients who underwent neo-adjuvant treatment.

We acknowledge that there are certain limitations to our study. First, our study is subject to limitations that are inherent to retrospective data collection. Second, as discussed earlier, pathological variables were obtained on final pathology due to the fact that preoperative CNB was not routinely performed in the vast majority of patients. We were therefore unable to evaluate the concordance between pathological variables as assessed on CNB and final pathology. However, numerous studies have evaluated this topic with the majority of studies reporting good concordance rates. Third, we used surgical margin status after the first lumpectomy attempt as a primary endpoint. Although information on positive margin rate after a second lumpectomy might be of particular clinical interest, the absolute number of patients with positive surgical margins after a second lumpectomy in our study was considered insufficient to obtain adequate sample size for nomogram development. Larger patient cohorts are therefore needed to address this topic. Last, our nomogram is based on female Dutch inhabitants, who are primarily Caucasian women. We therefore advise caution against extrapolation of the nomogram to different populations.

CONCLUSION

We developed and validated a nomogram to predict the probability of positive surgical margins following lumpectomy using clinicopathological variables. Our nomogram could support clinicians in identifying high-risk patients who might benefit from preoperative MRI and/or oncoplastic surgery.

ACKNOWLEDGEMENTS

The authors wish to thank all employees and cancer registrars who facilitated data collection. Especially, we wish to thank Mr. E. Verbeek for developing the web-based calculators.

REFERENCES

1. Fisher B, Anderson S, Bryant J et al. Twenty-year follow-up of a randomized trial comparing total mastectomy, lumpectomy, and lumpectomy plus irradiation for the treatment of invasive breast cancer. *N Engl J Med* 2002; 347: 1233-1241.
2. Veronesi U, Cascinelli N, Mariani L et al. Twenty-year follow-up of a randomized study comparing breast-conserving surgery with radical mastectomy for early breast cancer. *N Engl J Med* 2002; 347: 1227-1232.
3. Park CC, Mitsumori M, Nixon A et al. Outcome at 8 years after breast-conserving surgery and radiation therapy for invasive breast cancer: influence of margin status and systemic therapy on local recurrence. *J Clin Oncol* 2000; 18: 1668-1675.
4. Leong C, Boyages J, Jayasinghe UW et al. Effect of margins on ipsilateral breast tumor recurrence after breast conservation therapy for lymph node-negative breast carcinoma. *Cancer* 2004; 100: 1823-1832.
5. Pleijhuis RG, Graafland M, de Vries J et al. Obtaining adequate surgical margins in breast-conserving therapy for patients with early-stage breast cancer: current modalities and future directions. *Ann Surg Oncol* 2009; 16: 2717-2730.
6. Jacobs L. Positive margins: the challenge continues for breast surgeons. *Ann Surg Oncol* 2008; 15:1271-1272.
7. Iasonos A, Schrag D, Raj GV et al. How to build and interpret a nomogram for cancer prognosis. *J Clin Oncol* 2008; 26: 1364-1370.
8. Peintinger F. Clinical use of nomograms for breast cancer. *J Surg Oncol* 2011; 103: 745.
9. Shin HC, Han W, Moon HG et al. Nomogram for predicting positive resection margins after breast-conserving surgery. *Breast Cancer Res Treat* 2012; 134: 1115-1123.
10. Casparie M, Tiebosch AT, Burger G et al. Pathology databanking and biobanking in The Netherlands, a central role for PALGA, the nationwide histopathology and cytopathology data network and archive. *Cell Oncol* 2007; 29: 19-24.
11. Fritz A, Percy C, Jack A et al. International Classification of Diseases for Oncology. Geneva: WHO; 2000.
12. American College of Radiology. Breast imaging reporting and data system (BI-RADS). Reston: American College of Radiology 2003; 4th ed.
13. Akaike H. A new look at the statistical model identification. *IEEE Trans Automat Contr* 1974; 19: 716-723.
14. Harris GC, Denley HE, Pinder SE et al. Correlation of histologic prognostic factors in core biopsies and therapeutic excisions of invasive breast carcinoma. *Am J Surg Pathol* 2003; 27: 11-15.
15. Rakha EA, Ellis IO. An overview of assessment of prognostic and predictive factors in breast cancer needle core biopsy specimens. *J Clin Pathol* 2007; 60: 1300-1306.
16. Wood B, Junckerstorff R, Sterrett G et al. A comparison of immunohistochemical staining for oestrogen receptor, progesterone receptor and HER-2 in breast core biopsies and subsequent excisions. *Pathology* 2007; 39: 391-395.
17. Jacobs TW, Siziopikou KP, Prioleau JE et al. Do prognostic marker studies on core needle biopsy specimens of breast carcinoma accurately reflect the marker status of the tumor? *Mod Pathol* 1998; 11: 259-264.
18. Rhodes A, Jasani B, Barnes DM et al. Reliability of immunohistochemical demonstration of oestrogen receptors in routine practice: interlaboratory variance in the sensitivity of detection and evaluation of scoring systems. *J Clin Pathol* 2000; 53: 125-130.
19. Monticciolo DL. Histologic grading at breast core needle biopsy: comparison with results from the excised breast specimen. *Breast J* 2005; 11: 9-14.
20. Bilous M. Breast core needle biopsy: issues and controversies. *Mod Pathol* 2010; 23 Suppl 2: S36-45.
21. Jimenez RE, Bongers S, Bouwman D et al. Clinicopathologic significance of ductal carcinoma in situ in breast core needle biopsies with invasive cancer. *Am J Surg Pathol* 2000; 24: 123-128.

22. Dillon MF, Maguire AA, McDermott EW et al. Needle core biopsy characteristics identify patients at risk of compromised margins in breast conservation surgery. *Mod Pathol* 2008; 21: 39-45.
23. Richter-Ehrenstein C, Muller S, Noske A et al. Diagnostic accuracy and prognostic value of core biopsy in the management of breast cancer: a series of 542 patients. *Int J Surg Pathol* 2009; 17: 323-326.
24. Dillon MF, Hill AD, Quinn CM et al. A pathologic assessment of adequate margin status in breast-conserving therapy. *Ann Surg Oncol* 2006; 13: 333-339.
25. Groot G, Rees H, Pahwa P et al. Predicting local recurrence following breast-conserving therapy for early-stage breast cancer: the significance of a narrow (≤ 2 mm) surgical resection margin. *J Surg Oncol* 2011; 103: 212-216.
26. Houssami N, Macaskill P, Marinovich ML et al. Meta-analysis of the impact of surgical margins on local recurrence in women with early-stage invasive breast cancer treated with breast-conserving therapy. *Eur J Cancer* 2010; 46: 3219-3232.
27. Luini A, Rososchansky J, Gatti G et al. The surgical margin status after breast-conserving surgery: discussion of an open issue. *Breast Cancer Res Treat* 2009; 113: 397-402.
28. Pengel KE, Loo CE, Teertstra HJ et al. The impact of preoperative MRI on breast-conserving surgery of invasive cancer: a comparative cohort study. *Breast Cancer Res Treat* 2009; 116: 161-169.
29. Lovrics PJ, Cornacchi SD, Farrokhyar F et al. The relationship between surgical factors and margin status after breast-conservation surgery for early-stage breast cancer. *Am J Surg* 2009; 197: 740-746.
30. de Lorenzi F. Oncoplastic surgery: the evolution of breast cancer treatment. *Breast J* 2010; 16 Suppl 1: S20-1.
31. Smitt MC, Horst K. Association of clinical and pathologic variables with lumpectomy surgical margin status after preoperative diagnosis or excisional biopsy of invasive breast cancer. *Ann Surg Oncol* 2007; 14: 1040-1044.
32. Bevilacqua JL, Kattan MW, Fey JV et al. Doctor, what are my chances of having a positive sentinel node? A validated nomogram for risk estimation. *J Clin Oncol* 2007; 25: 3670-3679.
33. Coutant C, Olivier C, Lambaudie E et al. Comparison of models to predict nonsentinel lymph node status in breast cancer patients with metastatic sentinel lymph nodes: a prospective multicenter study. *J Clin Oncol* 2009; 27: 2800-2808.
34. Ravdin PM, Siminoff LA, Davis GJ et al. Computer program to assist in making decisions about adjuvant therapy for women with early breast cancer. *J Clin Oncol* 2001; 19: 980-991.
35. Rudloff U, Jacks LM, Goldberg JI et al. Nomogram for predicting the risk of local recurrence after breast-conserving surgery for ductal carcinoma in situ. *J Clin Oncol* 2010; 28: 3762-3769.
36. Sanghani M, Balk E, Cady B et al. Predicting the risk of local recurrence in patients with breast cancer: an approach to a new computer-based predictive tool. *Am J Clin Oncol* 2007; 30: 473-480.
37. Werkhoven E, Hart G, Tinteren H et al. Nomogram to predict ipsilateral breast relapse based on pathology review from the EORTC 22881-10882 boost versus no boost trial. *Radiother Oncol* 2011; 100: 101-107.
38. Rouzier R, Pusztai L, Garbay JR et al. Development and validation of nomograms for predicting residual tumor size and the probability of successful conservative surgery with neoadjuvant chemotherapy for breast cancer. *Cancer* 2006; 107: 1459-1466.

Supplementary Table 1. Studies reporting independent risk factors associated with positive surgical margins in breast-conserving therapy. Studies were included on the basis that they provided odds ratios.

Study	Year	N	Predictor	OR	95% CI	P-value
Park et al. ¹	2011	705	Presence of EIC (vs. absence)	3.85	2.30–6.45	<0.001
			Lobular histological type (vs. ductal)	7.17	2.24–22.98	0.001
			pN ₂ /N ₃ status (vs. pN ₀ /N ₁ status)	2.47	1.20–5.11	0.015
			T ₂ stage (vs. T _{1b} stage)	2.40	0.80–7.21	0.12
			Positive ER status (vs. negative)	1.35	0.80–2.26	0.26
			T ₁ stage (vs. T _{1b} stage)	1.47	0.54–4.02	0.46
			Age >35 years (vs. ≤35 years)	0.96	0.44–2.10	0.91
Sakr et al. ^{2a}	2011	73	Multifocal disease (vs. unifocal)	19.1	4.83–75.5	<0.0001
			Tumor size ^b	1.10	1.02–1.17	0.0095
			Full thickness excision (vs. oncoplastic surgery)	4.57	1.08–19.4	0.039
Kurniawan et al. ³	2008	1648	Tumor size ≥30 mm (vs. <30 mm)	4.22	2.56–6.96	<0.0001
			Multifocal disease (vs. unifocal)	2.85	2.02–4.02	<0.0001
			Microcalcifications on mammogram (vs. none)	1.97	1.33–2.93	0.001
			Presence of DCIS component (vs. absence)	1.45	0.99–2.13	0.059
			Age ≥60 years (vs. <60 years)	0.76	0.44–1.32	0.33
			High histological grade (vs. low)	1.26	0.77–2.04	0.36
			Absence of mammographic mass (vs. presence)	0.93	0.65–1.33	0.681
Cabioglu et al. ⁴	2007	264	Excisional biopsy (vs. other)	7.5	3.1–18.5	<0.0001
			Multifocal disease (vs. unifocal)	3.0	1.2–7.8	0.020
			Tumor size >20 mm (vs. ≤20 mm)	3.3	1.1–9.5	0.028
Aziz et al. ⁵	2006	1430	Age ^c	0.96	0.95–0.98	<0.0001
			Ductal histological type (vs. lobular)	0.67	0.42–1.07	0.09
			Positive ER status (vs. negative)	1.46	0.95–2.25	0.09
			Presence of DCIS component (vs. absence)	1.40	0.93–2.11	0.11
			Positive nodal status (vs. negative)	0.73	0.48–1.11	0.14
			Presence of LVI (vs. absence)	1.35	0.89–2.06	0.16
			Tumor sized	0.97	0.74–1.27	0.82
Chagpar et al. ⁶	2004	2658	Tumor size ^d	0.80	0.72–0.89	<0.001
			Lobular histological type (vs. ductal)	0.61	0.38–0.97	0.036
			Excisional biopsy (vs. FNA and CNB)	1.21	0.91–1.59	0.18
			Age ^c	1.00	0.99–1.01	0.56
			Palpable (vs. nonpalpable)	1.05	0.81–1.35	0.72

CI, confidence interval; CNB, core needle biopsy; DCIS, ductal carcinoma in situ; EIC, extensive intraductal component; ER, estrogen receptor; FNA, fine needle aspiration; LVI, lymphovascular invasion; OR, odds ratio.

^a Risk factors associated with positive margin status for invasive lobular carcinoma.

^b Trend for tumor size at pathology assessment from smaller to larger by 1 mm increments.

^c Trend for age at diagnosis from younger to older by 1 year increments.

^d Trend from smaller to larger across three categories: <1 cm, 1–2 cm, and >2 cm.

REFERENCES WITH SUPPLEMENTARY TABLE 1:

1. Park S, Park HS, Kim SI et al. The impact of a focally positive resection margin on the local control in patients treated with breast-conserving therapy. *Jpn J Clin Oncol* 2011; 41:600-608.
2. Sakr RA, Poulet B, Kaufman GJ et al. Clear margins for invasive lobular carcinoma: a surgical challenge. *Eur J Surg Oncol* 2011; 37:350-356.
3. Kurniawan ED, Wong MH, Windle I et al. Predictors of surgical margin status in breast-conserving surgery within a breast screening program. *Ann Surg Oncol* 2008; 15:2542-2549.
4. Cabioglu N, Hunt KK, Sahin AA et al. Role for intraoperative margin assessment in patients undergoing breast-conserving surgery. *Ann Surg Oncol* 2007; 14:1458-1471.
5. Aziz D, Rawlinson E, Narod SA et al. The role of reexcision for positive margins in optimizing local disease control after breast-conserving surgery for cancer. *Breast J* 2006; 12:331-337.
6. Chagpar AB, Martin RC, 2nd, Hagendoorn LJ et al. Lumpectomy margins are affected by tumor size and histologic subtype but not by biopsy technique. *Am J Surg* 2004; 188:399-402.

Supplementary Table 2. Incidence of positive margins for modeling and validation group by patient and tumor characteristics.

Characteristic	Modeling group			Validation Group		
	N	N	%	N	N	%
No. of patients	1185	233	19.7	331	81	24.5
Age (years)						
≤40	39	8	19.5	28	2	7.1
41–69	919	189	20.2	255	69	27.1
≥70	227	39	17.2	48	10	20.8
T-stage						
pT _{1a}	54	16	29.6	22	9	40.9
pT _{1b}	243	48	19.8	81	16	19.8
pT _{1c}	599	104	17.4	163	35	21.5
pT ₂	284	62	21.8	62	19	30.6
pT ₃	5	3	60.0	2	1	50.0
Area on mammogram (mm ²)						
≤15000	450	90	38.6	138	36	45.6
15001–24999	554	109	46.8	142	34	43.0
≥25000	181	34	14.6	45	9	11.4
Weight excised lump (gram)						
≤50	270	74	56.1	167	41	51.2
51–99	172	30	22.7	78	22	27.5
≥100	165	28	21.2	82	17	21.3
Tumor-to-lump index						
≤0.25	278	49	17.6	121	25	20.7
0.26–0.49	228	49	21.5	135	31	23.0
≥0.50	101	34	33.7	53	22	41.5
Palpability						
Palpable	637	116	18.2	195	42	21.5
Nonpalpable	548	117	21.4	136	39	28.7
Tumor location						
LOQ	122	21	17.2	42	10	23.8
UOQ	535	104	19.4	170	44	25.9
UIQ	189	30	15.9	50	14	28.0
LIQ	150	36	24.0	26	3	11.5
Central	103	21	20.4	6	1	16.7
Histological type						
Ductal	957	184	19.2	286	64	22.4
Lobular	119	33	27.7	23	8	34.8
Specified ^a	109	16	14.7	22	9	40.9
Histological grade						
Grade I	330	48	14.5	107	25	23.4
Grade II	531	111	20.9	133	31	23.3
Grade III	313	72	23.0	86	24	27.9
Estrogen receptor						
Positive	1002	206	20.6	276	62	22.5
Negative	172	25	14.5	51	17	33.3
Progesterone receptor						
Positive	750	139	18.5	226	50	22.1
Negative	300	49	16.3	101	29	28.7
HER2 receptor						
Positive	125	30	24.0	40	9	22.5
Negative	1041	198	19.0	290	71	24.5
No	1063	214	20.1	300	74	24.7

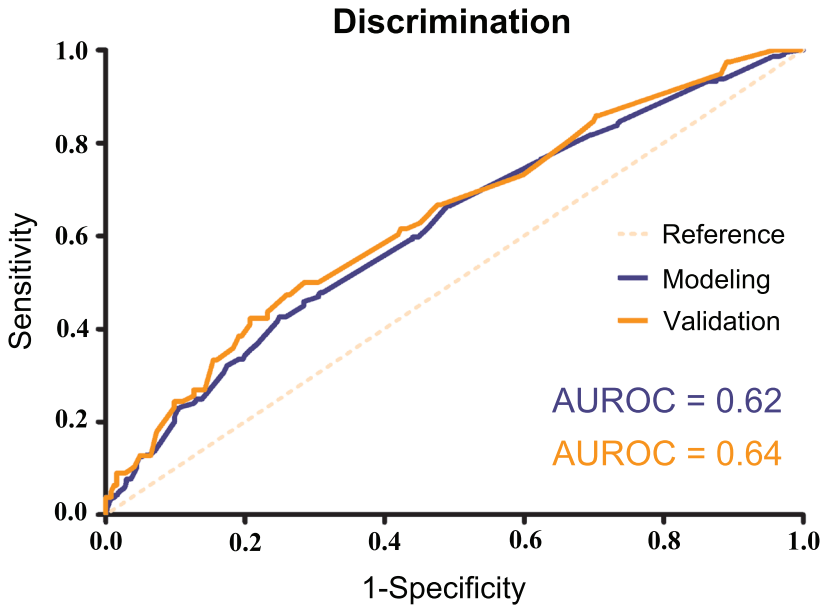
Table continues on the next page

Characteristic	Modeling group			Validation Group		
	N	N	%	N	N	%
No. of patients	1185	233	19.7	331	81	24.5
Age (years)						
Multifocal disease						
Yes	47	17	36.2	19	11	57.9
No	1138	216	19.0	311	69	22.2
pN-stage						
Positive	310	87	28.1	113	29	25.7
Negative	875	146	16.7	218	52	23.9
Prior surgery to the breast						
Yes	46	6	13.0	34	6	17.6
No	1139	227	19.9	297	75	25.3
Family history						
FDR	91	16	17.6	75	19	25.3
SDR	188	35	18.6	56	13	23.2
Negative	749	151	20.2	199	48	24.1
Referred from screening						
Yes	578	109	18.9	158	34	21.5
No	601	124	20.6	172	46	26.7
Unknown	6	0	0	-	-	-
BI-RADS classification						
II ^b	3	2	66.7	8	2	25.0
III	93	19	20.4	31	10	32.3
IV	611	134	21.9	155	39	25.2
V	447	72	16.1	127	29	22.8
Preoperative MRI						
Yes	122	19	15.6	31	7	22.6
No	1063	214	20.1	300	74	24.7
Microcalcifications						
Yes	245	67	27.3	74	29	39.2
No	937	166	17.7	257	52	20.2
DCIS component present						
Yes	529	152	28.7	188	61	32.4
No	656	81	12.3	143	20	14.0
Breast density						
0–25 %	323	60	18.6	101	22	21.8
25–50%	467	90	19.3	146	35	24.0
50–75%	217	49	22.6	70	19	27.1
75–100%	34	10	29.4	7	2	28.6
Institution						
University-affiliated	642	125	19.5	331	81	24.5
Community hospital	543	108	19.9	-	-	-

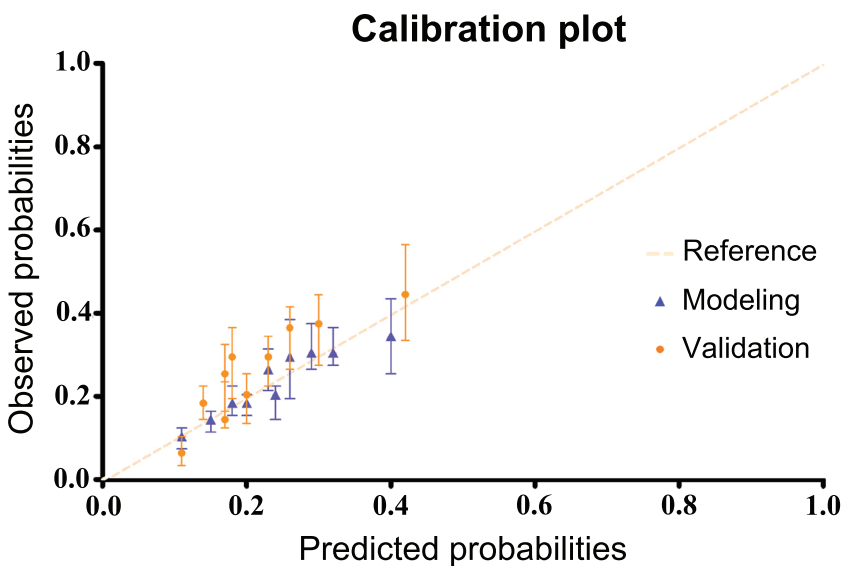
ER, estrogen receptor; FDR, first-degree relative; LIQ, lower inner quadrant; LOQ, lower outer quadrant; MRI, magnetic resonance imaging; PR, progesterone receptor; UIQ, upper inner quadrant; UOQ, upper outer quadrant

^a Specified histological types included mucinous, medullary, tubular, and papillary carcinomas.

^b BI-RADS classification II with malignancy proven by fine needle aspiration or core needle biopsy.



Supplementary Figure 1. Discrimination of the basic web-based calculator for the modeling and validation group. The area under the receiver-operating characteristic (AUROC) curve, comparable to the concordance index (c -index), indicates the discriminative power of the model. The reference line indicates an AUROC value of 0.5, for which the probability of positive surgical margins is equal to the toss of a coin. An AUROC value of 1.0 would resemble perfect discrimination.



Supplementary Figure 2. Calibration of the basic web-based calculator in the modeling and validation group. All patients were grouped into deciles (blue triangles and orange dots) based on their predicted probabilities. Mean predicted probabilities were plotted against the actual incidence of positive margins for each decile. Moreover, 95% confidence intervals are shown for both groups. The reference line represents perfect equality of observed frequencies and predicted probabilities.

Chapter

4

Submitted

Segmentation-based comparative analysis of planar optical signals (SCAPOS): a platform to detect and correct for discrepancies in tumor demarcation in planar fluorescence imaging

R.G. Pleijhuis*
G.C. Langhout*
N.J. Harlaar
G. Themelis
J. Bart
V. Ntziachristos
G.M. van Dam

** Both authors contributed equally*

ABSTRACT*Background*

Near-infrared fluorescence (NIRF) imaging has great potential to improve the outcome of the surgical treatment of solid cancers. With the current diversity in fluorescent agents and the accompanying differences in biodistribution, we aimed to develop a methodology that enables correction for discrepancies in tumor demarcation as a result of the application of different imaging systems and fluorescent probes in NIRF imaging.

Methods

Bioluminescence and NIRF imaging were performed in a breast cancer mouse model using different imaging systems and fluorescent probes in separate groups. Bioluminescence served as a gold standard for cancerous tissue. *Segmentation-based comparative analysis of planar optical signals* (SCAPOS) was applied to correct for false negative NIRF signals in each group.

Results

SCAPOS enabled correction for discrepancies in demarcated tumor areas when using different imaging systems and fluorescent agents. Analysis resulted in a NIRF correction factor of 0.202 and 0.047 for group I and II, respectively ($P=0.018$). SCAPOS-based correction resulted in a decrease in false negative results, i.e., tumor not covered by NIRF, from 9 out of 13 (69%) mice to none (0%).

Conclusion

We exhibited a methodology (SCAPOS) to correct for discrepancies in tumor demarcation due to variation in imaging systems and biodistribution of fluorescent probes.

INTRODUCTION

Innovations in healthcare have come a long way in the past few decades. However, surgical treatment of solid cancers is still regularly confronted with impaired therapeutic outcome as a result from incomplete tumor resection.^{1,2} Currently, intraoperative tumor localization is mainly limited to inspection and palpation. To improve and extend the intraoperative tools available to the surgeon-oncologist, more sensitive optical imaging techniques are being developed.³ Herein, special attention is paid to near-infrared fluorescence (NIRF) epi-illumination imaging, which has great potential for supporting the surgeon intraoperatively by providing real-time feedback on tumor localization and surgical margin status.⁴⁻⁷ The surgeon-oncologist could then detect (diagnostic) and excise (therapeutic) residual disease during the same surgical intervention, also denominated as theranostics.

In NIRF epi-illumination imaging, an external light source is used with a defined wavelength in the near-infrared (NIR) spectral range to illuminate the subject. Immediately after excitation, the fluorescence signal can be detected using a highly sensitive CCD camera.⁸ New developments in NIRF imaging hardware, software, and (tumor-targeted) fluorescent probes have greatly enhanced the possibilities for intraoperative NIRF epi-illumination imaging.³⁻⁷

From literature, little is known on how well NIRF signals correlate with cancerous tissue *in vivo*.⁹ Importantly, Kossodo et al. reported differences in probe biodistribution when simultaneous NIRF imaging was performed with different fluorescent probes, leading to discrepancies in tumor demarcation.¹⁰ Before being broadly applicable for clinical use, thorough assessment and optimization of NIRF imaging is therefore necessary, as differences in the characteristics of imaging systems and biodistribution of fluorescent probes may cause discrepancies in the demarcation of areas designated as tumor tissue. These discrepancies could be estimated in a preclinical setting by comparing signals obtained with NIRF imaging to those obtained with bioluminescence imaging (BLI).

BLI is a highly sensitive method for the detection of cancer cells and can be used as a gold standard for the presence of cancerous tissue. It is widely used in small laboratory animals *in vivo*, permitting real-time, noninvasive monitoring of tumorload at low cost.¹¹⁻¹³ However, BLI necessitates the incorporation of a bioluminescent gene into the tumor cells' DNA, making the technique unsuitable for clinical use.

Sarantopoulos et al. described a validation method for imaging the biodistribution of fluorescent probes *ex vivo* using multispectral epi-illumination cryoslicing imaging.¹⁴ The authors assessed the three-dimensional distribution of fluorescent probes in high resolution by both fluorescence and color imaging. Although this method has great potential for validating the distribution of fluorescent probes in support of imaging studies, its applicability *in vivo* for direct comparison and correction of captured NIRF images seems limited.

In this proof-of-principle study, we aimed to develop a platform to detect and correct for potential discrepancies concerning tumor demarcation in NIRF epi-illumination imaging. Hereto, signals obtained with BLI and NIRF imaging were compared and analyzed with an analytical tool denominated as *segmentation-based comparative analysis of planar optical signals* (SCAPOS). The potential of SCAPOS was evaluated in a xenograft model for human breast carcinoma. To assess its feasibility in various circumstances, SCAPOS was applied using different imaging systems and fluorescent probes.

METHODS

The potential of SCAPOS to detect and correct for discrepancies in tumor demarcation was assessed in a bioluminescent breast cancer mouse model. Both BLI and NIRF imaging were performed to enable calculation of a SCAPOS-based NIRF correction factor. Bioluminescence served as a gold standard for the presence of cancerous tissue.

Cell line

The bioluminescent human breast carcinoma cell line MDA-MB-231-luc-D3H2LN (Caliper Life Sciences, Hopkinton, USA) was used. This cell line is derived from MDA-MB-231-luc human adenocarcinoma cells and stably expresses the firefly luciferase gene, allowing for BLI. Cells were cultured in RPMI 1640 (Invitrogen, Carlsbad, USA) supplemented with 10% fetal calf serum (PAA Laboratories, Pasching, Austria) and 1% L-glutamine (Sigma-Aldrich, St. Louis, USA) at 37 °C in a humidified atmosphere containing 5% CO₂. MDA-MB-231-luc-D3H2LN cells were trypsinized (0.25% trypsin with EDTA), centrifuged, and resuspended in phosphate-buffered saline (PBS; Invitrogen, Carlsbad, USA) to a concentration of 2x10⁶ cells in 200 µl.

Animal model

Experiments were conducted using 15 athymic nude mice (Crl:NU/NU-Foxn1nu, Charles River Research Laboratories, Margate, UK) aged 6 to 8 weeks. Mice were anaesthetized with 2% isoflurane in oxygen. Subsequently, tumor cells (2x10⁶ cells in 200 µl) were orthotopically injected into the pectoral mammary fat pad. Shortly after injection with luciferase-expressing human breast cancer cells, BLI was performed to make sure that inoculation was successful. One mouse was excluded from the study because it did not hatch a tumor. Nine mice (group I) were imaged using a customized intraoperative imaging system in combination with a targeted fluorescent probe. To evaluate the feasibility of SCAPOS in various circumstances, a commercial preclinical imaging system (IVIS® Spectrum) combined with an activatable fluorescent probe was applied in an additional 5 mice (group II). Both groups were randomized into a model and a validation subgroup for determination and validation of the SCAPOS-based NIRF correction factor, respectively. All animal experiments were performed in compliance with the Guide for the Care and Use of Laboratory Animal Resources (1996) and the guidelines of the local Animal Care and Use Committee.¹⁵

Optical imaging systems

Two different optical imaging systems were used. First, a customized clinical prototype NIRF camera system developed at Technical University Munich was applied for both BLI and NIRF epi-illumination imaging.⁵ The system contains an iXon^{EM+} EMCCD camera (ANDOR™ Technology, Belfast, UK) and allows for simultaneous acquisition of color, NIR emission (fluorescence), and NIR excitation (intrinsic) images. The intrinsic images allow for correction of heterogeneous illumination artifacts caused by spatial variation of excitation laser illumination.^{5,16} Second, images were acquired with a commercially available IVIS® Spectrum preclinical system (PerkinElmer Inc., Waltham, USA), which consists of a highly sensitive cooled charged-coupled device (CCD) camera mounted onto a light-tight box. The IVIS® Spectrum is capable of dual bioluminescence/fluorescence imaging.

Near-infrared fluorescent probes

Two commercially available fluorescent probes (MMPsense® 680 and IntegriSense® 680; PerkinElmer, Waltham, USA) were used with excitation and emission profiles in the NIR spectral range. Twenty-four hours prior to NIRF imaging, fluorescent probes were injected in the tail vein under general anesthesia.

Mice in group I (n=9) were injected with 2 nmol of the $\alpha\beta3$ integrin receptor-targeted fluorescent probe IntegriSense® 680 in 100 μL PBS. Overexpression of $\alpha\beta3$ integrin receptor has been shown for various solid cancers and is believed to play an important role in tumor progression, especially for invasive tumors that preferentially metastasize to bone, such as breast carcinoma.^{17,18}

Mice in group II (n=5) were injected with 2 nmol of the activatable fluorescent probe MMPsense® 680 in 100 μL PBS. The probe remains in a quenched state upon injection, in which its fluorescence activity is significantly impaired.⁶ However, when MMPsense® 680 comes into contact with matrix metalloproteinases (MMPs), the probe is activated, enhancing fluorescence activity significantly. MMPs have been shown to be overexpressed in several solid cancers, including breast cancer, and are known to degrade the extracellular matrix and stimulate tumor development, growth, and neovascularization.¹⁹⁻²¹

Bioluminescence and near-infrared imaging

Three weeks following inoculation, both BLI and NIRF imaging were performed under general anesthesia in all mice that hatched a tumor (n=14). To enable BLI, 250 μL D-luciferin (150 mg/kg, Caliper Life Sciences, Alameda, USA) in PBS was injected intraperitoneally 10 minutes prior to imaging. Animals were placed on a low-fluorescence diet (Harlan TD.97184, Madison, USA) in order to reduce autofluorescence from the gastrointestinal tract.

In group I (n=9), the customized clinical camera system was applied for BLI (emission: open; exposure time: 20 s; binning: small) and NIRF imaging (excitation: 673 nm laser; emission: 716 ± 20 nm; exposure time: 5 s; binning: small). One mouse was excluded from the study due to the absence of BLI signal upon imaging.

In group II (n=5), BLI (emission: open; exposure time: 20 sec; f-stop: 1; binning: small) and NIRF imaging (excitation: 675 ± 35 nm, emission: 720 ± 20 , 740 ± 20 , and 760 ± 20 nm; exposure time: 5 sec; binning: small) was performed using the IVIS® Spectrum system.

Histological analysis

After imaging, mice were euthanized by a lethal dose of ketamine. Tissue indicated as cancerous by BLI was excised to confirm the presence of cancer cells by histological analysis. Hereto, tissue specimens were fixed in 10% formalin solution, processed through paraffin, and stained with hematoxylin and eosin for microscopic evaluation by an oncology pathologist (JB).

Preprocessing of captured images

Imaging data acquired with the customized camera system (group I) was corrected for heterogeneous illumination artifacts according to the acquired intrinsic signal.^{5,16} Outliers in pixel intensity were set to mean pixel value. BLI and NIRF images were automatically registered using five reference points and an affine transformation.

Images acquired with the IVIS® Spectrum (group II) were preprocessed using Living Image® version 3.0 analysis software (Caliper Life Sciences, Alameda, USA). Spectral unmixing was performed to separate the authentic MMPsense® 680 fluorescence signal from autofluorescence using the in-built unmix function.²²

Automated tumor demarcation

Following preprocessing of imaging data (Fig. 1-I), automated tumor demarcation of the primary tumor was performed for both BLI and NIRF signals. The methodology consists of several sequential steps (Fig. 1), which can be customized to fit a wide range of images by changing a limited number of parameters.

Images were cropped to a surgical region of interest (ROI) to minimize interference from surrounding organs (Fig. 1-II). Hereto, the center of the BLI signal was selected manually, after which a square ROI was automatically positioned around the specified middle. Second, the borders of the tumor were estimated using Canny Edge detection (Fig. 1-III).²³ Single-pixel thick continuous edges were generated as the outline of a single operation of dilation, filling, and erosion (Fig. 1-IV). Next, a mask was obtained for both BLI and NIRF signals by filling the estimated tumor outline (Fig. 1-V). Both signal masks were combined in a composite image and corresponding labels ('NIRF', 'BLI', and 'NIRF+BLI') were assigned (Fig. 1-VI; 2A).

SCAPOS methodology

SCAPOS was applied to detect and correct for discrepancies in tumor demarcation between NIRF imaging and BLI as the gold standard for the presence of cancerous tissue. In both group I and II, an individual correction factor was calculated for each tumor in the model subgroups by determining the margin required to cover all BLI signal (Fig. 2B) as a proportion of the maximum diameter, automatically indicated by MATLAB.

Regional extension was implemented as morphologic dilatation. Dilution with a correction factor allows for an appropriate safety margin surrounding the NIRF signal, thereby eliminating false negative results (i.e., BLI not covered by NIRF signal). The final SCAPOS-based NIRF correction factor is defined as the mean of the individual correction factors in each group plus the standard deviation of the mean multiplied by three ($\text{mean}_{\text{individual correction factor}} + 3 \times \text{SD}_{\text{mean}}$). When normal distribution of the data is assumed, addition of three standard deviations theoretically leads to the elimination of false negative NIRF signals in a vast majority of cases (>99%). Lastly, the final SCAPOS-based NIRF correction factor was validated on a separate subgroup (Fig. 2C).

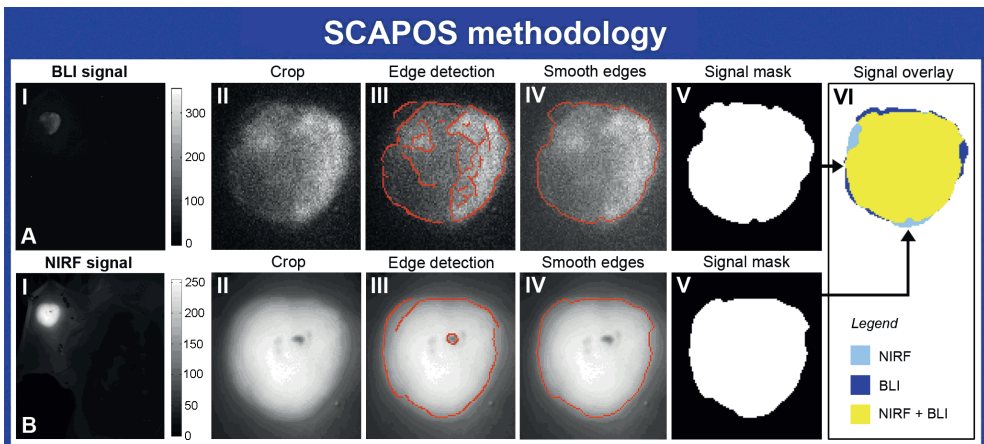


Figure 1. Sequential steps in automated tumor demarcation are shown for a representative mouse (group I). First, bioluminescence (A) and normalized fluorescence (B) images were imported in MATLAB®. Images were cropped to a region of interest (II), followed by automated Canny Edge detection (III) and estimation of a single-pixel thick continuous tumor outline (IV). Next, the estimated tumor outline was filled (V) and segment overlays (VI) were created. Light blue, dark blue, and yellow labels represent NIRF (false positive), BLI (false negative), and overlapping signal (true positive), respectively.

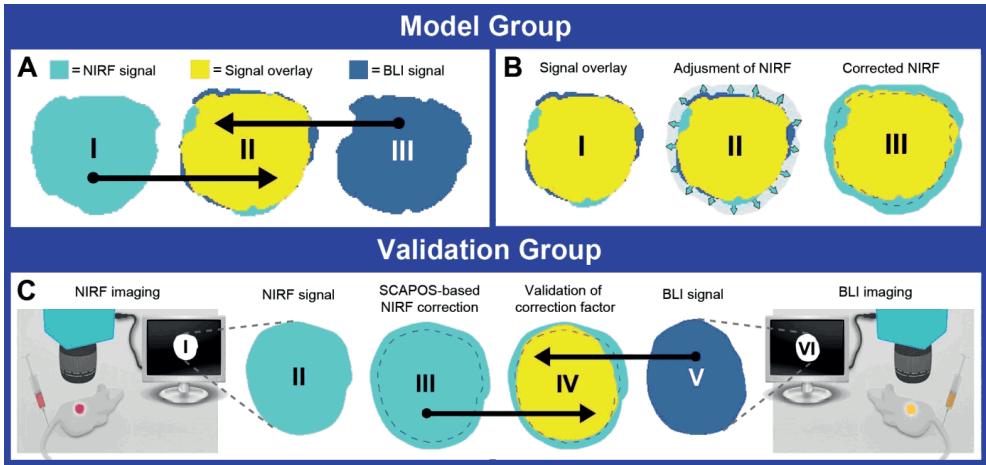


Figure 2. Schematic overview of SCAPOS-based NIRF correction for the model and the validation group. First, a composite image (**AII**, **BI**) was created by combining NIRF (**AI**) and BLI (**AIII**) signal masks. For every tumor in the model group, the NIRF mask was extended (**BII**) until full coverage of the BLI signal mask was obtained (**BIII**). The SCAPOS-based NIRF correction factor as calculated from the model group was applied to the NIRF signal mask of the validation group (**CI-III**). Next, a composite image was created (**CVI**) by combining the corrected NIRF signal (**CIII**) with the BLI signal mask (**CV-VI**) to assess false and true negative proportions.

RESULTS

Animal model

In group I, 9 out of 10 (93%) mice hatched after inoculation, as confirmed by BLI. One mouse was excluded from group I due to the absence of BLI signal upon imaging, leaving 8 mice for SCAPOS analysis in this group. In group II, 5 mice (100%) hatched a tumor. None of the mice showed severe weight loss ($\geq 10\%$ compared to the weight measured on day 0) during the time course of the experiment. Mice were in good condition prior to imaging.

SCAPOS-based NIRF correction

Prior to SCAPOS correction, false negative results were observed in 8 out of 8 mice (100%) in group I and 1 out of 5 mice (20%) in group II. Application of the SCAPOS-based NIRF correction factor resulted in elimination of false negative results in all mice (Fig. 3), i.e., all BLI signal-containing areas were entirely covered by the corrected NIRF signal. The correction factor differed significantly between group I and II (0.20 vs 0.05, $P=0.018$). The mean proportion of false positive NIRF signal following SCAPOS-based NIRF correction was 0.55 (range: 0.53–0.66) for group I and 0.63 (range: 0.62–0.64) for group II (Fig. 3). SCAPOS analysis was performed on a normal laptop within seconds.

Histological analysis

Tissue samples were harvested and sent to the Department of Pathology and Laboratory Medicine for histological analysis. Histology confirmed the presence of tumor cells in all tissue indicated as cancerous by BLI (data not shown).

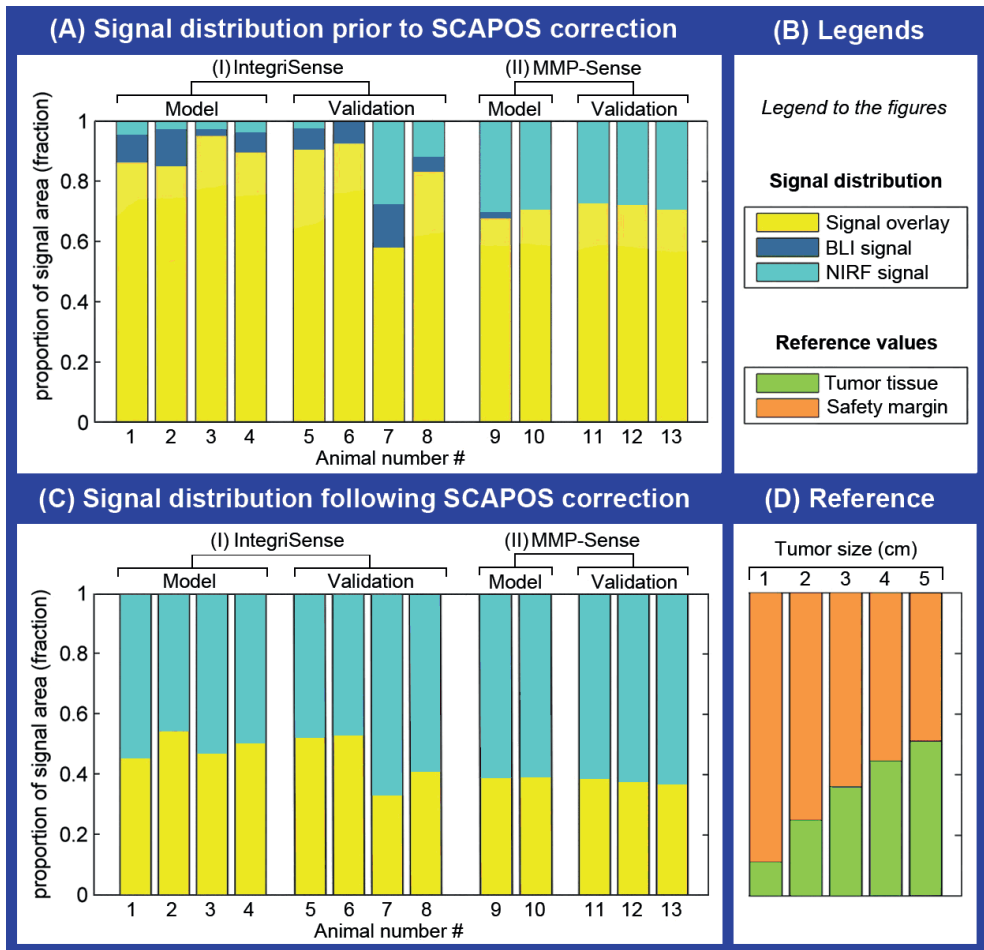


Figure 3. Relative signal distribution prior to (AI, AII) and following (CI, CII) SCAPOS-based NIRF correction. Labels corresponding to the signals are presented (B). Prior to SCAPOS correction, NIRF imaging did not fully cover the BLI signal (i.e., tumor tissue) in all mice from group I (AI) and in one mouse from group II (AII). SCAPOS-based NIRF correction resulted in a full coverage of the BLI signal in all mice while increasing the proportion of false positive results (CI, CII). To put these numbers into perspective, the proportion of healthy breast tissue (orange bars) in relation to cancerous tissue that is normally excised during breast-conserving surgery as a margin of safety is presented for breast tumors (green bars) ranging from 1 to 5 cm in diameter (D). These proportions were based on a gross safety margin of 1 cm healthy breast tissue surrounding the primary tumor, which is considered standard-of-care in breast-conserving surgery.

DISCUSSION

NIRF epi-illumination imaging has great potential for intraoperative applications in which the tumor is localized relatively superficially.^{3,24} Recent developments in imaging systems and fluorescent probes have added to its potential. For a successful introduction of NIRF imaging in the clinic, potential discrepancies in tumor demarcation due to variation between optical imaging systems and the biodistribution of fluorescent probes should be taken into account. The SCAPOS platform described in this paper was developed to detect and correct for these discrepancies.

Automated tumor demarcation indicated substantial differences regarding the occurrence of false negatives (i.e., BLI not detected by NIRF imaging) between group I and II (Fig. 3). NIRF imaging underestimated the amount of BLI in 8 out of 8 mice (100%) in group I, while underestimation was observed in only 1 out of 5 mice (20%) in group II. Parameters used between group I and II differed significantly, making direct comparison inappropriate. However, within groups, the calculation of the false negatives is performed under the same circumstances.

In addition to the difference in imaging systems and preprocessing methods, we suggest an explanation for differences in the biodistribution of the fluorescent probes. IntegriSense® 680 is targeted towards integrins and therefore expected to be quite evenly distributed throughout the tumor.^{17,18} MMPsense® 680 is activated mainly at the tumor border (i.e., invasion sites) and in the zone of inflammation surrounding of the tumor, where the level of MMPs is high.¹⁹⁻²¹ Indeed, Kossodo et al. reported different distribution patterns for integrin-targeted and protease-activated fluorescent probes when simultaneous NIRF imaging was performed.¹⁰

SCAPOS-based NIRF correction decreased the occurrence of false negative results to zero in both groups, indicating that SCAPOS successfully corrected for discrepancies in tumor demarcation. Although it is of the utmost importance in surgical oncology to obtain surgical margins that are free of tumor, the extent of surgery should be as limited as possible to obtain good (cosmetic) outcome.^{3,25} Studies reporting on breast-conserving surgery advise to obtain a gross margin of healthy breast tissue ranging from 1 cm to 3 cm surrounding the tumor.^{26,27} When a 1 cm gross margin is taken into account, the proportion of healthy breast tissue in relation to cancerous tissue excised during breast-conserving surgery ranges from 0.50 to 0.85, depending on the diameter of the primary tumor (Fig. 3D). For a 3 cm gross margin, this proportion even ranges from 0.83 to 0.98. Noteworthy, the proportion of false positive NIRF signal (i.e., healthy tissue indicated as cancerous) following SCAPOS-based NIRF correction ranged from 0.53 to 0.66. The SCAPOS-based correction factor therefore did not exceed the generally applied surgical margin of safety that is considered standard-of-care in breast-conserving surgery (Fig. 3).

Considerations concerning SCAPOS

Part of the automated tumor demarcation was based on Canny Edge detection, which identifies high-contrasting regions delineating the tumor.²³ Due to this characteristic of the Canny Edge algorithm, factors that decrease contrast (e.g., autofluorescence, background signals, and increasing tumor depth) might pose difficulties in automated tumor delineation. As a consequence, best results are obtained after preprocessing captured images. Furthermore, the proposed method is relatively insensitive to changes in exposure time, injected doses of fluorescent probes, and image resolution. The first two mainly influence the total signal intensity, while the distribution of the signal is influenced only marginally. Therefore, the Canny Edge algorithm is likely to mark the same border. The influence of the image resolution is low, because the correction factor is expressed as a proportion of the diameter of the demarcated area. The used parameters for the Canny Edge algorithm influence the number of indicated edges, but again not their position.

Interference of autofluorescence (especially from the gastrointestinal region) is increased in small animals compared to humans because of the smaller distance between conflicting organs and the high content of fluorophores in animal chow. This may pose difficulties on differentiating tumor from background signal. The distorting effects of autofluorescence can be minimized by: i) providing the animals with a low-fluorophore chow, ii) preprocessing of imaging data (e.g., spectral unmixing), and iii) selection of a specific ROI for image analysis.

In order to assess the feasibility of SCAPOS in various circumstances, we chose to use different imaging systems and fluorescent probes. Several preprocessing steps were regarded as system depended, as they are performed on the imaging system itself. Changing more than one variable between groups prohibits definite conclusions concerning possible causal relations. However, the scope of the current study was solely to demonstrate the methodology of SCAPOS instead of quantifying variations between imaging systems or biodistribution of fluorescent probes. Although study size was small, this proof-of-principle study is deemed sufficient to exhibit the basic principle of SCAPOS. Our methodology could theoretically be applied to most solid cancers. However, further studies are needed to validate SCAPOS in larger study populations and different settings.

CONCLUSION

We exhibit a generally applicable platform denominated as *segmentation-based comparative analysis of planar optical signals* (SCAPOS) to optimize tumor demarcation in planar NIRF imaging. SCAPOS could provide a useful step in the translation of NIRF imaging applications towards the clinic by detecting and correcting for variation in the hardware/software of imaging systems and the biodistribution of fluorescent probes that may cause discrepancies in the demarcation of tumor tissue. Further studies are needed to validate SCAPOS in larger study populations and different settings.

ACKNOWLEDGEMENT

This work was supported by a grant from the Jan Kornelis de Cock Fund.

REFERENCES

1. Jacobs L. Positive margins: the challenge continues for breast surgeons. *Ann Surg Oncol* 2008; 15:1271-1272.
2. Houssami N, Macaskill P, Marinovich ML et al. Meta-analysis of the impact of surgical margins on local recurrence in women with early-stage invasive breast cancer treated with breast-conserving therapy. *Eur J Cancer* 2010; 46:3219-3232.
3. Keereweer S, Kerrebijn JD, van Driel PB et al. Optical image-guided surgery – where do we stand? *Mol Imaging Biol* 2011; 13:199-207.
4. Troyan SL, Kianzad V, Gibbs-Strauss SL et al. The FLARE intraoperative near-infrared fluorescence imaging system: a first-in-human clinical trial in breast cancer sentinel lymph node mapping. *Ann Surg Oncol* 2009; 16:2943-2952.
5. Themelis G, Yoo JS, Soh KS, Schulz R, Ntziachristos V. Real-time intraoperative fluorescence imaging system using light-absorption correction. *J Biomed Opt* 2009; 14:064012.
6. Kirsch DG, Dinulescu DM, Miller JB et al. A spatially and temporally restricted mouse model of soft tissue sarcoma. *Nat Med* 2007; 13:992-997.
7. Mieog JS, Vahrmeijer AL, Hutteman M et al. Novel intraoperative near-infrared fluorescence camera system for optical image-guided cancer surgery. *Mol Imaging Biol* 2010; 9:223-231.
8. Ntziachristos V. Fluorescence molecular imaging. *Annu Rev Biomed Eng* 2006; 8:1-33.
9. Nahrendorf M, Keliher E, Marinelli B et al. Hybrid PET-optical imaging using targeted probes. *Proc Natl Acad Sci USA* 2010; 107:7910-7915.
10. Kossodo S, Pickarski M, Lin SA et al. Dual *in vivo* quantification of integrin-targeted and protease-activated agents in cancer using fluorescence molecular tomography (FMT). *Mol Imaging Biol* 2010; 12:488-499.
11. Graves EE, Weissleder R, Ntziachristos V. Fluorescence molecular imaging of small animal tumor models. *Curr Mol Med* 2004; 4:419-430.
12. Löwik CW, Kaijzel E, Que I et al. Whole body optical imaging in small animals and its translation to the clinic: intra-operative optical imaging guided surgery. *Eur J Cancer* 2009; 45 Suppl 1:391-393.
13. Shan L, Wang S, Korotcov A, Sridhar R, Wang PC. Bioluminescent animal models of human breast cancer for tumor biomass evaluation and metastasis detection. *Ethn Dis* 2008; 18:52,65-69.
14. Sarantopoulos A, Themelis G, Ntziachristos V. Imaging the biodistribution of fluorescent probes using multispectral epi-illumination cryoslicing imaging. *Mol Imaging Biol* 2011; 13:874-885.
15. Institute of Laboratory Animal Resources (US). Committee on Care and Use of Laboratory Animals, National Institutes of Health (US). Division of Research Resources. Guide for the care and use of laboratory animals. US Department of Health and Human Services, Public Health Service, National Institutes of Health; 1985.
16. Ntziachristos V, Turner G, Dunham J et al. Planar fluorescence imaging using normalized data. *J Biomed Opt* 2005; 10:064007.
17. Rolli M, Fransvea E, Pilch J, Saven A, Felding-Habermann B. Activated integrin $\alpha v \beta 3$ cooperates with metalloproteinase MMP-9 in regulating migration of metastatic breast cancer cells. *Proc Natl Acad Sci USA* 2003; 100:9482-9487.
18. Sloan EK, Pouliot N, Stanley KL et al. Tumor-specific expression of $\alpha v \beta 3$ integrin promotes spontaneous metastasis of breast cancer to bone. *Breast Cancer Res* 2006; 8:R20.
19. Pellikainen JM, Ropponen KM, Kataja VV et al. Expression of matrix metalloproteinase (MMP)-2 and MMP-9 in breast cancer with a special reference to activator protein-2, HER2, and prognosis. *Clin Cancer Res* 2004; 10:7621-7628.
20. Rydlova M, Holubec L, Jr, Ludvikova M, Jr et al. Biological activity and clinical implications of the matrix metalloproteinases. *Anticancer Res* 2008; 28:1389-1397.
21. Chabotiaux V, Noel A. Breast cancer progression: insights into multifaceted matrix metalloproteinases. *Clin Exp Metastasis* 2007; 24:647-656.

22. Xu H, Rice BW. *In vivo* fluorescence imaging with a multivariate curve resolution spectral unmixing technique. *J Biomed Opt* 2009; 14:064011.
23. Pellegrino FA, Vanzella W, Torre V. Edge detection revisited. *IEEE Trans Syst Man Cybern B Cybern* 2004; 34:1500-1518.
24. Cutter JL, Cohen NT, Wang J et al. Topical application of activity-based probes for visualization of brain tumor tissue. *PLoS One* 2012; 7:e33060.
25. Khan SA, Eladoumki dachi F. Optimal surgical treatment of breast cancer: implications for local control and survival. *J Surg Oncol* 2010; 101:677-686.
26. van Dongen JA, Bartelink H, Fentiman IS et al. Factors influencing local relapse and survival and results of salvage treatment after breast-conserving therapy in operable breast cancer: EORTC trial 10801: breast conservation compared with mastectomy in TNM stage I and II breast cancer. *Eur J Cancer* 1992; 28A:801-805.
27. Veronesi U, Volterrani F, Luini A et al. Quadrantectomy versus lumpectomy for small size breast cancer. *Eur J Cancer* 1990; 26:671-673.

Chapter

5

Eur J Surg Oncol. 2011; 37(1):32-39.

Near-infrared fluorescence (NIRF) imaging in breast-conserving surgery: assessing intraoperative techniques in tissue-simulating breast phantoms

R.G. Pleijhuis
G.C. Langhout
W. Helfrich
G. Themelis
A. Sarantopoulos
L.M.A. Crane
N.J. Harlaar
J.S. de Jong
V. Ntziachristos
G.M. van Dam

ABSTRACT*Background*

Breast-conserving surgery (BCS) results in tumor-positive surgical margins in up to 40% of the patients. Therefore, new imaging techniques are needed that support the surgeon with real-time feedback on tumor location and margin status. In this study, the potential of near-infrared fluorescence (NIRF) imaging in BCS for pre- and intraoperative tumor localization, margin status assessment and detection of residual disease was assessed in tissue-simulating breast phantoms.

Methods

Breast-shaped phantoms were produced with optical properties that closely match those of normal breast tissue. Fluorescent tumor-like inclusions containing indocyanine green (ICG) were positioned at predefined locations in the phantoms to allow for simulation of i) preoperative tumor localization, ii) real-time NIRF-guided tumor resection, and iii) intraoperative margin assessment. Optical imaging was performed using a customized clinical prototype NIRF intraoperative camera.

Results

Tumor-like inclusions in breast phantoms could be detected up to a depth of 21 mm using a NIRF intraoperative camera system. Real-time NIRF-guided resection of tumor-like inclusions proved feasible. Moreover, intraoperative NIRF imaging reliably detected residual disease in case of inadequate resection.

Conclusion

We evaluated the potential of NIRF imaging applications for BCS. The clinical setting was simulated by exploiting tissue-like breast phantoms with fluorescent tumor-like agarose inclusions. From this evaluation, we conclude that intraoperative NIRF imaging is feasible and may improve BCS by providing the surgeon with imaging information on tumor location, margin status, and presence of residual disease in real-time. Clinical studies are needed to further validate these results.

INTRODUCTION

Breast cancer is the most frequent malignancy in women worldwide with an estimated 1.4 million new cases in 2010.¹ Breast-conserving therapy (BCT), consisting of breast-conserving surgery (BCS) followed by radiation therapy, has become the standard treatment for T₁-T₂ breast tumors and is generally regarded as sufficient for this subset of patients.² Unfortunately, a majority of studies on the surgical margin status after BCS have shown that positive margins are detected in 20% to 40% of patients, necessitating additional surgical intervention or radiotherapy.³ Two major points for improving outcome after BCS involve i) a more reliable intraoperative tumor localization and ii) improved real-time feedback on the presence of possible residual disease during or after excision of the tumor.⁴ Intraoperative application of an optical imaging technique known as near-infrared fluorescence (NIRF) imaging may improve the clinical outcome of BCS.^{3,5}

Near-infrared fluorescence imaging

In recent years, significant progress has been made in the development of optical imaging systems and fluorophores for clinical applications.^{6,7} Several animal^{5,8-10} and clinical¹¹⁻¹⁵ studies have shown the potential clinical use of NIRF imaging to improve the therapeutic outcome of surgery. Compared to light in the visible spectral range (400–650 nm), application of near-infrared (NIR) light minimizes absorption by physiologically abundant molecules such as hemoglobin and lipids, which increases penetration depth.^{16,17} Additionally, autofluorescence (the intrinsic fluorescence signal present in all living cells due to various normal metabolites and tissue constituents) is strongly reduced in the NIR spectral range. Taken together, these aspects of NIR light make it particularly suitable for use in intraoperative optical imaging applications. However, clinical application of NIRF imaging in BCS is currently limited to the nonspecific intraoperative detection of the sentinel lymph node.^{11,12,14,18-20}

Tumor-targeted near-infrared fluorophores

With the introduction of clinical grade tumor-targeted NIR fluorophores, NIRF imaging may be extended towards the intraoperative detection of the primary tumor.¹⁰ Several target molecules have been identified for breast cancer that may be of value for such an approach, including HER2 receptor,^{9,21,22} vascular endothelial growth factor (VEGF) receptor,^{23,24} endothelial growth factor (EGF) receptor,²⁵ and folate receptor- α .²⁶

In tumor-targeted NIRF imaging, a tumor-targeted NIR fluorophore is administered several hours or days prior to the imaging procedure. Subsequently, an external laser is used to irradiate the breast with light in the NIR spectral range (650–900 nm).¹⁷ Upon excitation, the fluorophore will release photons of a longer NIR wavelength. Because NIR light is invisible to the naked eye, a dedicated optical imaging system is necessary to capture the NIR signal from the surgical field and digitally convert it into a visible image. Recently, we and our co-workers developed a multispectral NIRF intraoperative camera system that is suitable for intraoperative use with NIR fluorophores.²⁷

Simulation of NIRF-guided surgery

In the current preclinical study, we evaluated intraoperative NIRF imaging applications in a simulated clinical setting as a step-up toward NIRF-guided BCS. To this end, we used tissue-simulating gelatin-based breast phantoms that mimic the optical properties of normal breast tissue.^{28,29} Tumor-like fluorescent inclusions of different size and shape were positioned at

predefined sites in the phantoms, allowing for simulation of i) preoperative tumor localization, ii) real-time NIRF-guided tumor resection and iii) intraoperative macroscopic margin assessment. The tumor-like inclusions contain the nonspecific NIR fluorophore indocyanine green (ICG) to simulate the use of tumor-targeted near-infrared fluorophores in BCS.

Currently, ICG (absorption and emission maximum at ~780 and ~820 nm, respectively) is one of the few FDA-approved NIR fluorophores available for clinical use.⁹ Sevick-Muraca et al. have previously shown the feasibility of NIRF imaging following microdose administration of ICG.¹² Although ICG in itself is nonspecific, their findings suggest that comparable microdose concentrations can be used to label cancer cells with tumor-targeted NIR fluorophores for intraoperative NIRF imaging. Importantly, new fluorophores in the NIR spectral range are currently being developed (e.g., IRDye 800CW) with properties more promising for intraoperative use than those of ICG.²⁵

METHODS

Assessment of ICG fluorescence self-quenching

Because increasing concentrations of ICG may not correspond to an increased fluorescence signal due to the phenomenon of self-quenching, different concentrations of ICG in agarose were evaluated for fluorescence activity.^{29,30} Briefly, an ICG stock solution was serially diluted in 10 ml sterile water (ranging from 0.5 μM to 350 μM ICG), after which 2% agarose was added. The mixture was then heated to 70 °C and stirred until the agarose was completely dissolved. After solidification of the agarose mixture for 15 min at 4 °C, fluorescence reflectance imaging (FRI) was performed to determine maximum photon counts/sec (settings: exposure time: 1000 ms, excitation: 780 nm, emission: 820 nm).

Assessment of maximal penetration depth

In order to determine the maximal penetration depth of the NIRF signal, a cubic fluorescent inclusion of 5x5x5 mm containing 14 μM ICG was positioned in phantom tissue at a depth of 30 mm. Subsequently, the surgeon excised 3–4 mm layers of phantom towards the inclusion (remaining depths were 27, 24, 21, 18, 15, 11, 7, and 4 mm, respectively). At all depths, FRI was performed with the intraoperative NIRF camera system (exposure time: 3000–60000 ms, excitation 780 nm, emission 820 nm, binning: small-medium). Maximum photon counts per second exposure time were calculated as well as the full width at half maximum (FWHM) of the fluorescence signal. The FWHM is a measure for scattering and indicates the diameter of the fluorescence signal when the intensity of the signal is reduced to half the maximum. Scattering both contributes to signal loss and loss in resolution. The FWHM indicates the minimal distance between two distinct sources to be recognized as separate.

Tissue-simulation breast phantoms

Composition of the tissue-simulating gelatin-based breast phantoms was aimed at obtaining uniform optical properties that closely match the optical characteristics of normal breast tissue, as described in detail before.²⁹ Additionally, the breast phantoms mimic the elastic properties of human tissue.³¹

Briefly, 10% gelatin 250 (Natural Spices, Watergang, the Netherlands) was dissolved in 11 TBS (50 mmol Tris-HCl, 150 mmol NaCl, pH 7.4). To remove molecular oxygen and prevent microbial infection, 15 mmol NaN_3 (Merck, Darmstadt, Germany) was added. The gelatin slurry

was completely dissolved by heating to 50 °C and subsequently cooled down to 35 °C and maintained at this temperature. Under constant stirring, 170 μmol hemoglobin (Sigma-Aldrich, Zwijndrecht, The Netherlands) and 1% Intralipid® 20% (Sigma-Aldrich) were added. Next, the gelatin mixture was poured in a custom made prechilled breast-shaped mold (end volume 500 ml) to a level that corresponded to the predefined depth of the agarose inclusion. After solidification for 30 min at 4 °C, a tumor-like NIR fluorescent agarose inclusion was positioned on the surface and temporarily fixed with a small needle. Next, the remaining of the warmed gelatin mixture was added to fill up the remaining mold volume, allowing for adherence of both layers. The phantom was then stored in the dark to solidify for another 30 min at 4 °C, after which it was gently removed from its mold.

In total, four breast phantoms were constructed with tumor-like NIR fluorescent agarose inclusions of different size and shape (Fig. 1A) positioned at predefined depths. Imaging of the phantoms was performed directly after production of all four phantoms.

Breast phantom #1 contained 2 similar-sized ($\text{\O}1.0$ cm) sphere-shaped agarose inclusions at different depths (2.0 and 4.0 cm). Phantom #2 contained 2 sphere-shaped inclusions at the same depth (1.5 cm), differing in size ($\text{\O} 0.5$ cm and $\text{\O} 2.0$ cm). Phantom #3 contained 1 sphere-shaped ($\text{\O}1.0$ cm) and 1 prolate sphere-shaped ($\text{\O}1.0$ cm) agarose inclusion at the same depth (1.5 cm). Finally, phantom #4 contained 2 irregular shaped agarose inclusions of similar size ($\text{\O}1.5$ cm) at different depths (1.5 and 3.0 cm).

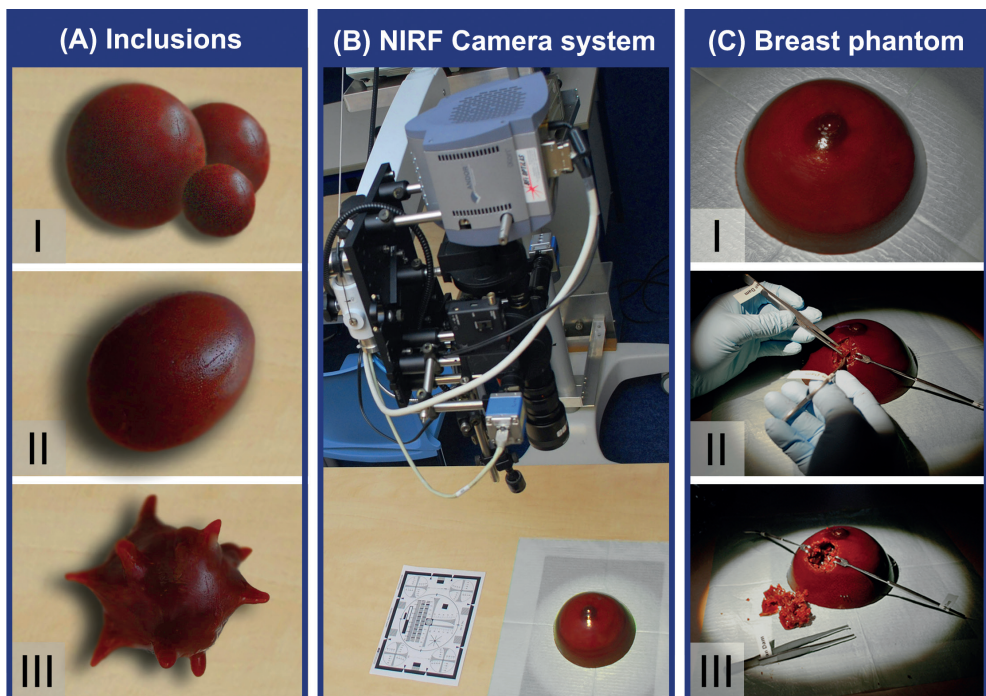


Figure 1. Fluorescent tumor-like agarose inclusions differing in size and shape (AI-III) were integrated in breast-shaped phantoms (CI) prior to surgery. Preoperatively, the location of the tumor-like inclusion was assessed noninvasively using a NIRF camera system (B). Intraoperatively, the inclusion was excised under real-time NIRF guidance or guided solely by visual and tactile information (CII). At the end of the surgical procedure, the NIRF camera system was applied to inspect for residual disease and evaluate the extent of surgery (CIII).

Tumor-like NIR fluorescent agarose inclusions

For tumor-like NIR fluorescent agarose inclusions, 2% agarose (Hispanagar, Burgos, Spain) was used instead of 10% gelatin. Agarose has a higher melting point, which prevents the inclusions from dissolving and leaking ICG (see below) during and after the positioning of the inclusions in the gelatin phantom. In short, a 2% (W/V) agarose slurry was heated to 70 °C and stirred until the agarose was completely dissolved. Subsequently, ICG (ICG-PULSION®; Pulsion Medical Systems, Munich, Germany) was dissolved to a final concentration of 14 µM. Finally, in order to resemble the optical appearance of the surrounding breast phantom tissue, 170 µM hemoglobin, 15 mM NaN₃, and 1% Intralipid® 20% were added to the tumor-like fluorescent inclusions. Tumor-like fluorescent inclusions of different size (range: 0.5 cm to 2.0 cm) and shape (prolate sphere, sphere, and irregular shape, Fig. 1A) were produced. The inclusions were integrated in the breast phantoms as indicated and chilled in the dark for 30 min at 4 °C. Imaging of each individual breast phantom was performed within 6 h.

Near-infrared fluorescence imaging system

A customized NIRF camera system was developed in collaboration with SurgOptix (SurgOptix Inc., Redwood Shores, USA) for real-time intraoperative imaging. The system implements a correction scheme that improves the accuracy of epi-illumination fluorescence images for light intensity variations in tissue. Implementation is based on the use of three cameras operating in parallel. The camera is mounted on a five degrees of freedom bracket, the sixth degree (rotation) can be performed digitally. This camera allows for simultaneous acquisition of color videos and normalized fluorescence images in real-time, yielding a lateral resolution up to 66.58 µm and a variable field of view (FOV) of 13.5W x 11H to 115W x 95H (mm). A description in full detail is provided by Themelis et al.²⁷ The invisible NIRF imaging signal was digitally converted into a pseudocolor and superposed on a color video image of the operating field, allowing for real-time, intraoperative anatomical positioning of the fluorescence signal.

Simulation of intraoperative NIRF imaging

Breast phantoms with tumor-like NIR fluorescent agarose inclusions were used to simulate and evaluate the potential of NIRF imaging applications in BCS (Fig. 1). In all phantoms, the location of the tumor-like fluorescent inclusions was assessed preoperatively with noninvasive NIRF imaging. In phantoms #1 and #2, the tumor-like fluorescent inclusions were subsequently excised using conventional surgical equipment, guided solely by visual inspection, tactile information, and preoperatively obtained NIRF imaging data. The surgeon was asked to indicate when he believed a complete excision of the tumor was reached. Subsequently, the NIRF camera system was applied to assess the feasibility of NIRF-guided macroscopic margin assessment of the surgical cavity and excised tissue fragments. In case of an incomplete excision, the surgeon was asked to perform a re-excision under real-time NIRF guidance. In phantoms #3 and #4, the tumor-like fluorescent inclusions were localized and excised under real-time NIRF guidance. While approaching the tumor-like fluorescent inclusions, the surgeon was supported with both visible and audible information. In short, the detected fluorescent signal was depicted on a TFT-screen and was made quantitatively audible using a digitally generated sound pitch. In this approach, an increase in sound pitch represents an increase in fluorescence signal indicating the approximation of a tumor-like fluorescent inclusion.

RESULTS

ICG fluorescence self-quenching in agarose

To determine the optimal ICG concentration in agarose, a serial range of increasing ICG concentrations was analyzed for fluorescence characteristics. The optimal fluorescence signal was observed at a concentration of approximately 10 μM ICG (Fig. 2). These results are comparable to self-quenching characteristics of ICG as previously determined in gelatin.²⁹

Maximal penetration depth of ICG fluorescence

The maximal tissue penetration depth of a detectable fluorescent ICG inclusion was reached at a depth of 21 mm (Fig. 3C and Supplementary video 2).

Simulation of intraoperative NIRF imaging

Preoperative NIRF-guided localization of tumor-like fluorescent agarose inclusions was performed in 4 different breast phantoms. The various tumor-like inclusions positioned at a depth of ≤ 2.0 cm were detectable with the NIRF camera system (Fig. 4A-I). Tumor-like inclusions positioned at depths of 3.0 and 4.0 cm could not be detected preoperatively.

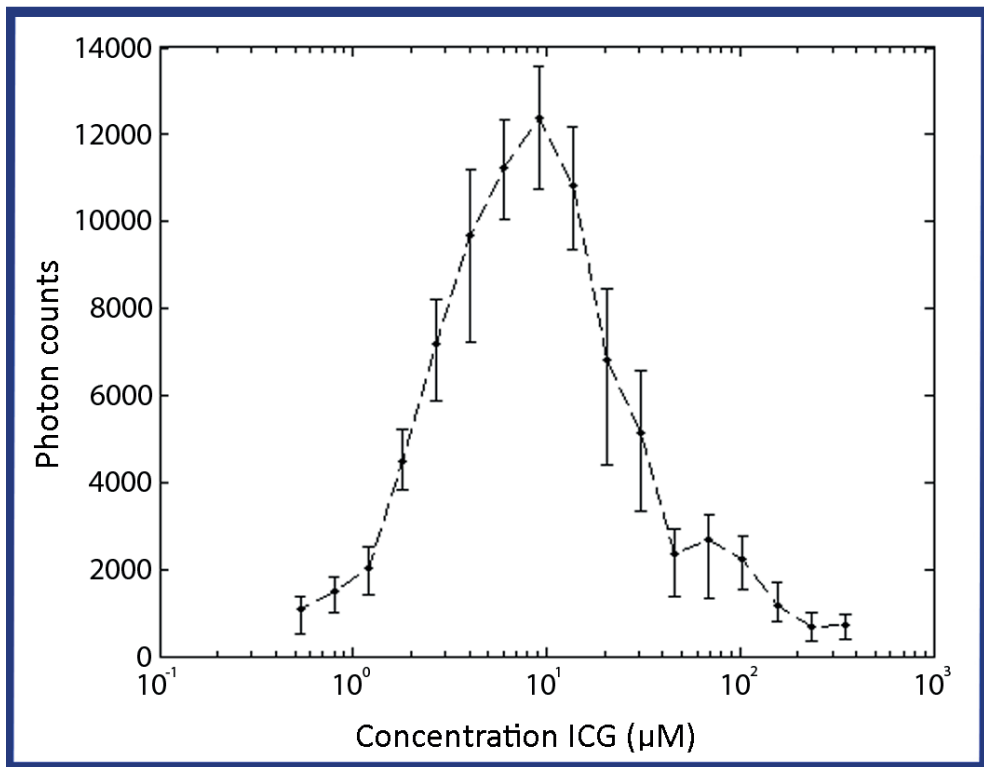


Figure 2. Optimal ICG concentration in 2% agarose was determined in breast phantom tissue. Seventeen different concentrations (each 10 ml, ranging from 0.5 μM to 350 μM) were imaged at once with the intraoperative NIRF camera system. Working distance 45 cm, field of view 160W x 130H (mm), exposure time: 1000 ms.

Tumor-like inclusions in phantom #1 and #2 were excised using conventional techniques for tumor localization. In phantom #1, one out of two tumor-like inclusions proved to be only partially excised, as evidenced by a remnant strong fluorescence signal in the surgical cavity detected by the NIRF camera system (Fig. 4C-III). In phantom #2, the excision of one out of two inclusions was found to be incomplete. In case of residual fluorescence, the surgeon could detect and excise (theranostic procedure) the remnant inclusion under real-time NIRF guidance (Fig. 4C-IV and Supplementary video 1). In all cases, NIRF-guided re-excision resulted in a complete excision, without the need for additional excision of large breast phantom fragments (Fig. 4C-V).

In phantoms #3 and #4, the tumor-like inclusions were located (Fig. 4B) and excised (Fig. 4C) under real-time NIRF guidance. Although the inclusion at 3.0 cm depth in phantom #4 could not be detected preoperatively (Fig. 4B-I), it was detectable using the NIRF camera system after an incision of approximately 1 cm of superficial phantom tissue (Fig. 4B-II). In phantom #3, no residual tumor-like inclusion material could be detected after initial NIRF-guided excision, while the excision of one out of two irregular inclusions in phantom #4 was found to be incomplete. Again, subsequent NIRF-guided re-excision resulted in a complete excision.

During the surgical simulation procedure, the approximation of the surgeon towards tumor-like fluorescent agarose inclusions was guided by both visual information on a TFT screen and audible sound-pitched information (Supplementary videos 1-2). The approach resulted in a clear change in the signal strength of the fluorescence image that was accompanied with an increase of the sound pitch at ~15 mm prior to excision of the tumor-like agarose inclusion. These signals assisted the surgeon in carefully advancing the margins.

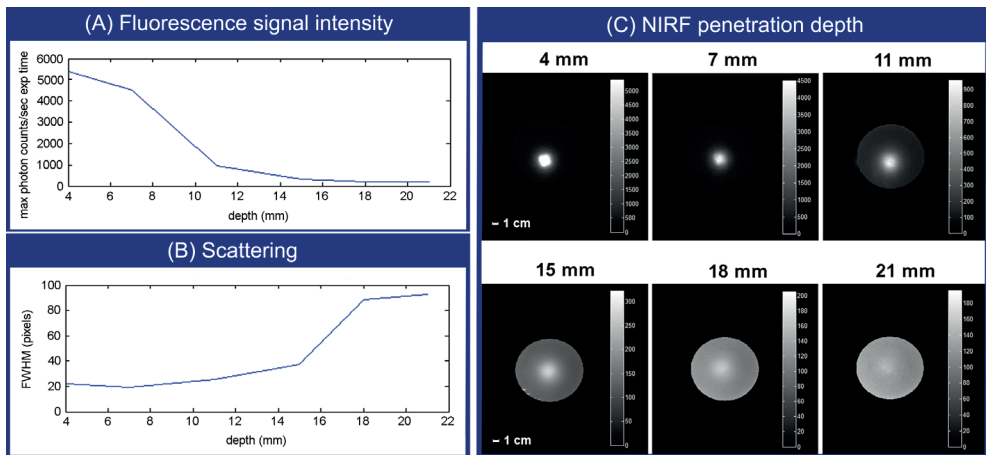


Figure 3. Fluorescent signal intensity related to depth-location in tissue-like phantoms is shown for fluorescent agarose inclusions placed at varying depths in phantom tissue (A). Depth (mm) of the inclusion and maximum photon counts per second exposure time are depicted on the horizontal and vertical axis, respectively. Moreover, scattering of the fluorescence signal is shown (B), with depth (mm) and full width at half maximum (pixels) on the horizontal and vertical axis, respectively. For determination of the NIRF signal penetration depth with the NIRF intraoperative camera system (C), the surgeon repeatedly excised 3–4 mm tissue layers, working his way towards a fluorescent inclusion placed at 30 mm depth in breast phantom tissue. At 30, 27, and 24 mm inclusion depth, no NIRF signal could be detected (not shown). Images were corrected for (normalized) an exposure time of 1000 ms.

Near-Infrared Fluorescence (NIRF) imaging applications

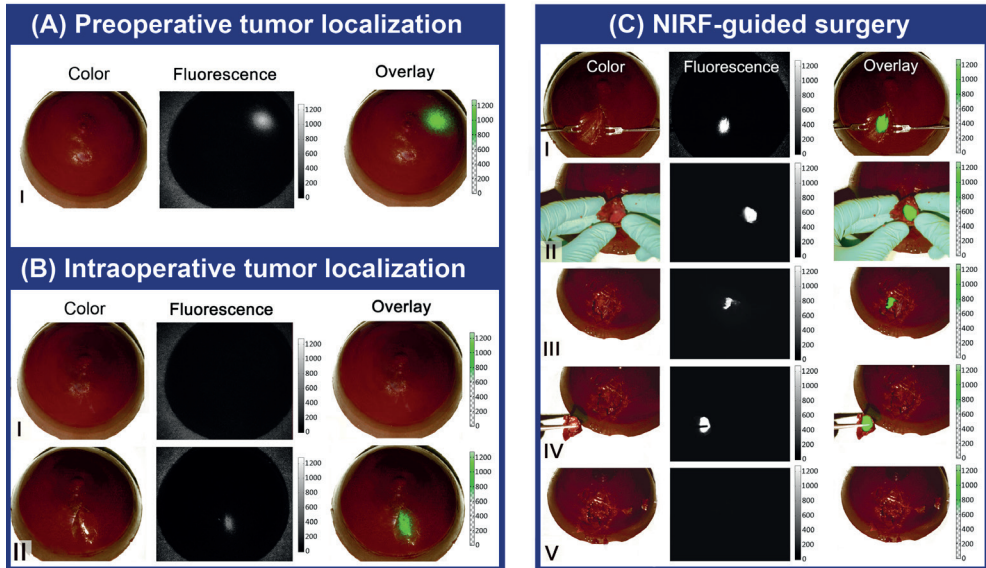


Figure 4. Overview of NIRF applications in breast-conserving surgery. In the case of relatively superficial lesions (≤ 2 cm), NIRF allows for preoperative localization of fluorescent tumor-like inclusions (A). Intraoperative NIRF imaging guides the surgeon towards the tumor-like agarose inclusion (B+C) and allows for intraoperative assessment of surgical margin status (CII-V) and detection of residual disease (CIII). Color bars next to the color overlay indicate a threshold at 800 counts. Pixels with values above the threshold were superposed on the color video (overlay). Exposure time was set to 150 ms for all images.

DISCUSSION

Tissue-like phantoms and tumor-like inclusions

The composition of the breast phantoms was based on data published by De Grand et al., who developed and validated phantoms to mimic the basic optical characteristics (absorption and scattering coefficients) of breast tissue.²⁹ The absorption of photons by both cellular organelles and blood was simulated by hemoglobin, which gives the phantoms a deep red color.^{32,33} Additionally, Intralipid® was added to mimic scattering properties of breast tissue.²⁸ In order to resemble the clinical situation as close as possible, tumor-like fluorescent agarose inclusions were incorporated in the breast phantoms. The agarose-based inclusions simulate the firm-elastic consistency of tumor tissue and allow for surgical margin status assessment, both intraoperatively (NIRF-guided surgery) and *ex vivo* (NIRF-guided macroscopic margin assessment). The relatively low concentration of ICG used in this study resembles the potential application of microdose tumor-targeted fluorophores (ranging from 1 to 100 μM) in BCS. Although the phantoms used in this study are homogeneous, and therefore do not possess the complex structures that characterize mammary tissue, they do provide a tool for assessing the value of theoretical assumptions and indicate generally important features of future clinical NIRF imaging applications in BCS.

Near-infrared fluorescence imaging

NIRF imaging offers a promising technique for real-time NIRF-guided surgery in BCS with little interference in the standard surgical procedure or changes in the design of the operating theatre. The technology is considered safe, fast, makes use of non-ionizing radiation, and has a high resolution.^{3,10} However, NIRF imaging does have limitations originating from the intrinsic characteristics of light propagation through tissue, including scattering and absorbance.¹⁷

Additionally, due to limited depth resolution and a nonlinear dependence of the signal detected and the depth of the fluorescence activity, NIRF imaging by epi-illumination with our current camera system seems of limited value for preoperative localization of tumors. This applies in particular to situations where the tumor is located relatively deep (>2 cm) in fatty and glandular tissue of the breast. However, since the surgeon, by definition, will bring the area of interest closer to the surface during surgery, our multispectral NIRF camera system is well-suited for intraoperative imaging applications.

Nonspecific versus tumor-targeted imaging agents

Several possibilities exist for delivering fluorophores to the tumor. One possibility would be to inject a nonspecific fluorophore (e.g., ICG) into the tumor under stereotactic or ultrasonographic guidance.^{34,35} However, there are some significant drawbacks to this approach. First, the injection of the nonspecific fluorophore into the tumor is a critical step in the procedure and has to be very accurate to minimize false negative and false positive results. Additionally, spillage/leakage of fluorophore within the mammary gland during the procedure will decrease accuracy of both localization of the tumor and macroscopic margin assessment. Therefore, we believe NIRF-guided surgery should ideally be combined with tumor-targeted fluorophores, which provide molecularly-specific detection of cancer cells. In these agents, the NIR fluorophore has been conjugated to a specific targeting ligand or monoclonal antibody. This allows for tumor-specific binding of the fluorophore, increasing SN ratios and minimizing spillage of the fluorophore during the surgical procedure.^{3,10} Several studies have shown the feasibility of using tumor-targeted fluorophores *in vivo* to image tumors intraoperatively, including the use of tumor-targeted ICG-conjugated agents.^{5,9,22,25,26,36,37} However, there are some significant drawbacks, including the heterogeneity of (breast) tumors which should be solved before applying tumor-targeted NIRF imaging in the clinic. In BCS, the preoperative biopsy taken prior to surgery could provide important information on molecular targets for NIRF imaging. As this biopsy is considered standard practice, it will not require an additional invasive procedure, while offering the possibility to determine the expression of different kinds of molecular targets present on the breast cancer cells by immunohistochemical analysis. The surgeon could then look for NIRF agents suited for each individual tumor, offering a more patient-tailored approach.

CONCLUSION

We have preclinically assessed the applicability of NIRF imaging applications in BCS by exploiting tissue-simulating breast phantoms. NIRF-guided intraoperative tumor localization and detection of remnant disease showed feasible. Clinical studies are needed to further validate these results for use in BCS.

ACKNOWLEDGEMENT

This work was supported by a grant from the Jan Kornelis de Cock foundation.

REFERENCES

1. Parkin DM, Bray F, Ferlay J, Pisani P. Global cancer statistics, 2002. *CA Cancer J Clin* 2005; 55(2): 74-108.
2. Schwartz GF, Veronesi U, Clough KB et al. Consensus conference on breast conservation. *J Am Coll Surg* 2006; 203: 198-207.
3. Pleijhuis RG, Graafland M, de Vries J, Bart J, de Jong JS, van Dam GM. Obtaining adequate surgical margins in breast-conserving therapy for patients with early-stage breast cancer: current modalities and future directions. *Ann Surg Oncol* 2009; 16:2717-2030.
4. Singletary SE. Breast cancer surgery for the 21st century: the continuing evolution of minimally invasive treatments. *Minerva Chir* 2006; 61:333-352.
5. Kirsch DG, Dinulescu DM, Miller JB et al. Spatially and temporally restricted mouse model of soft tissue sarcoma. *Nat Med* 2007; 13:992-997.
6. Luker GD, Luker KE. Optical imaging: current applications and future directions. *J Nucl Med* 2008; 49:1-4.
7. Tromberg BJ, Pogue BW, Paulsen KD, Yodh AG, Boas DA, Cerussi AE. Assessing the future of diffuse optical imaging technologies for breast cancer management. *Med Phys* 2008; 35:2443-2451.
8. von Burstin J, Eser S, Seidler B et al. Highly sensitive detection of early-stage pancreatic cancer by multimodal near-infrared molecular imaging in living mice. *Int J Cancer* 2008; 123:2138-2147.
9. Chopra A. Trastuzumab complexed to near-infrared fluorophore indocyanine green. 2004.
10. Keereweer S, Kerrebijn JD, van Driel PB et al. Optical image-guided surgery – where do we stand? *Mol Imaging Biol* 2010; 13:199-207.
11. Tagaya N, Yamazaki R, Nakagawa A et al. Intraoperative identification of sentinel lymph nodes by near-infrared fluorescence imaging in patients with breast cancer. *Am J Surg* 2008; 195:850-853.
12. Sevic-Muraca EM, Sharma R, Rasmussen JC et al. Imaging of lymph flow in breast cancer patients after microdose administration of a near-infrared fluorophore: feasibility study. *Radiology* 2008; 246:734-741.
13. Brandt MG, Moore CC, Jordan K. Randomized control trial of fluorescence-guided surgical excision of nonmelanotic cutaneous malignancies. *J Otolaryngol* 2007; 36:148-155.
14. Ogasawara Y, Ikeda H, Takahashi M, Kawasaki K, Doihara H. Evaluation of breast lymphatic pathways with indocyanine green fluorescence imaging in patients with breast cancer. *World J Surg* 2008; 32:1924-1929.
15. Stummer W, Pichlmeier U, Meinert T, Wiestler OD, Zanella F, Reulen HJ. Fluorescence-guided surgery with 5-aminolevulinic acid for resection of malignant glioma: a randomised controlled multicentre phase III trial. *Lancet Oncol* 2006; 7:392-401.
16. Bremer C, Ntziachristos V, Weissleder R. Optical-based molecular imaging: contrast agents and potential medical applications. *Eur Radiol* 2003; 13:231-243.
17. Ntziachristos V. Fluorescence molecular imaging. *Annu Rev Biomed Eng* 2006; 8:1-33.
18. Troyan SL, Kianzad V, Gibbs-Strauss SL et al. The FLARE intraoperative near-infrared fluorescence imaging system: a first-in-human clinical trial in breast cancer sentinel lymph node mapping. *Ann Surg Oncol* 2009; 16:2943-2952.
19. Kitai T, Inomoto T, Miwa M, Shikayama T. Fluorescence navigation with indocyanine green for detecting sentinel lymph nodes in breast cancer. *Breast Cancer* 2005; 12:211-215.
20. Murawa D, Hirche C, Dresel S, Hunerbein M. Sentinel lymph node biopsy in breast cancer guided by indocyanine green fluorescence. *Br J Surg* 2009; 96:1289-1294.
21. Gee MS, Upadhyay R, Bergquist H et al. Human breast cancer tumor models: molecular imaging of drug susceptibility and dosing during HER2/neu-targeted therapy. *Radiology* 2008; 248:925-935.
22. Lee SB, Hassan M, Fisher R et al. Affibody molecules for *in vivo* characterization of HER2-positive tumors by near-infrared imaging. *Clin Cancer Res* 2008; 14:3840-3849.
23. Backer MV, Levashova Z, Patel V et al. Molecular imaging of VEGF receptors in angiogenic vasculature with single-chain VEGF-based probes. *Nat Med* 2007; 13:504-509.

24. Chen K, Li ZB, Wang H, Cai W, Chen X. Dual-modality optical and positron emission tomography imaging of vascular endothelial growth factor receptor on tumor vasculature using quantum dots. *Eur J Nucl Med Mol Imaging* 2008; 35:2235-2244.
25. Sampath L, Kwon S, Ke S et al. Dual-labeled trastuzumab-based imaging agent for the detection of human epidermal growth factor receptor 2 overexpression in breast cancer. *J Nucl Med* 2007; 48:1501-1510.
26. Segal EI, Low PS. Tumor detection using folate receptor-targeted imaging agents. *Cancer Metastasis Rev* 2008; 27:655-664.
27. Themelis G, Yoo JS, Soh KS, Schulz R, Ntziachristos V. Real-time intraoperative fluorescence imaging system using light-absorption correction. *J Biomed Opt* 2009; 14:064012.
28. Pogue BW, Patterson MS. Review of tissue-simulating phantoms for optical spectroscopy, imaging and dosimetry. *J Biomed Opt* 2006; 11:041102.
29. De Grand AM, Lomnes SJ, Lee DS et al. Tissue-like phantoms for near-infrared fluorescence imaging system assessment and the training of surgeons. *J Biomed Opt* 2006; 11:014007.
30. Yuan B, Chen N, Zhu Q. Emission and absorption properties of indocyanine green in intralipid solution. *J Biomed Opt* 2004; 9:497-503.
31. Lizuka MN, Sherar MD, Vitkin IA. Optical phantom materials for near-infrared laser photocoagulation studies. *Lasers Surg Med* 1999; 25:159-169.
32. Durkin AJ, Jaikumar S, Richardskorum R. Optically dilute, absorbing, and turbid phantoms for fluorescence spectroscopy of homogeneous and inhomogeneous samples. *Appl Spectrosc* 1993; 47:2114-2121.
33. Wagnieres G, Cheng S, Zellweger M et al. An optical phantom with tissue-like properties in the visible for use in PDT and fluorescence spectroscopy. *Phys Med Biol* 1997; 42:1415-1426.
34. Intes X. Time-domain optical mammography softScan: initial results. *Acad Radiol* 2005; 12:934-947.
35. Berridge DL, Mastey LA, Eckstrom PC, Czarnecki DJ. Indocyanine green dye as a tissue marker for localization of nonpalpable breast lesions. *AJR Am J Roentgenol* 1995; 164:1299.
36. Ke S, Wen X, Gurfinkel M et al. Near-infrared optical imaging of epidermal growth factor receptor in breast cancer xenografts. *Cancer Res* 2003; 63:7870-7875.
37. Mieog JS, Hutteman M, van der Vorst JR et al. Image-guided tumor resection using real-time near-infrared fluorescence in a syngeneic rat model of primary breast cancer. *Breast Cancer Res Treat* 2010; 128:679-689.

Chapter

6

Manuscript in preparation

Optical imaging for lymph node surveillance in breast cancer patients: intraoperative detection as a step-up approach towards tumor-targeted imaging

R.G. Pleijhuis
L.M.A. Crane
G. Themelis
W. Kelder
L. Jansen
J. de Vries
B.L. van Leeuwen
A. Sarantopoulos
J.S. de Jong
V. Ntziachristos
G.M. van Dam

ABSTRACT*Introduction*

The sentinel lymph node (SLN) procedure is widely accepted as a method for lymph node staging in cT₁₋₂N₀ breast carcinoma. In the case of a positive SLN, remaining axillary lymph nodes (ALNs) are generally removed. However, these ALNs do not contain metastases in 40% to 80% of the patients, indicating substantial overtreatment. In this paper, near-infrared fluorescence (NIRF) imaging is outlined as a technique for intraoperative detection of the SLN. Moreover, the potential of intraoperative detecting of tumor load within the SLN for a one-step SLN/ALN dissection is outlined.

Methods

Ten (10) women with biopsy-proven cT₁₋₂N₀ breast carcinoma underwent the standard SLN-procedure (preoperative injection with radiolabeled colloid and intraoperative injection with patent blue). Additionally, all patients received a peritumoral injection with 1 ml (0.5 mg/ml) indocyanine green (ICG) intraoperatively. The SLN was visualized with a customized multispectral NIRF camera system.

Results

The SLN was successfully identified in all patients. Total numbers of lymph nodes detected with radiolabeled colloid, patent blue and ICG were 18, 9, and 14, respectively. The use of the NIRF optical imaging system did not interfere with the standard operative procedure. No adverse reactions were encountered.

Conclusion

The intraoperative detection of the SLN with a NIRF optical imaging system is technically feasible. In the near future, tumor-targeted optical contrast agents may allow for a one-stage intraoperative evaluation of lymph node tumor status and intraoperative decision making towards an ALN dissection.

INTRODUCTION

Breast cancer is the leading type of cancer in women with an estimated 1.4 million new cases worldwide in 2010.¹ Treatment of primary breast cancer depends on the resection of the primary tumor and identification of cancer spread to the lymph nodes (LNs). Both are independent prognostic factors for survival and recurrence of the disease.² For identification of tumor involvement in axillary lymph nodes (ALNs), the first-draining node, also denominated as the sentinel lymph node (SLN), is removed and analyzed by histology.³ The best results for intraoperative SLN localization are obtained with a combination of radiolabeled colloid (technetium-99m) and vital blue dye (e.g., patent blue).^{4,5} The intraoperative use of a gamma probe combined with visual inspection of the surgical field (i.e., blue-stained lymphatic vessels and SLNs) leads to a successful identification of the SLN in 97% of the patients.⁴ However, there are disadvantages to both the blue dye and the radiolabeled colloid, including allergy to the blue dye, a shine-through effect at the injection site of the radiocolloid, difficulties with detecting SLNs in obese patients, and the need for appropriate logistics for radioactive matter.⁶⁻⁸

As an alternative technique, several groups have reported on the use of the fluorescent optical contrast agent indocyanine green (ICG) for intraoperative SLN identification.⁹⁻¹⁵ ICG has been used in patients for the last three decades for the study of organ perfusion and ophthalmology and has a safe and well-known pharmacological profile. When excited at the appropriate wavelength, ICG will emit photons in the near-infrared (NIR) spectral range (~820 nm). Because NIR light is invisible to the human eye, a dedicated optical imaging system is needed to visualize the fluorescence signal within the surgical field. Such a system was recently presented by Troyan et al. in a study on lymphatic mapping in breast cancer.¹⁵ The described camera is capable of visualizing fluorescence signals originating from the SLNs in real-time, superposing them on color images of the surgical field for orientation. At the University Medical Center Groningen (UMCG), we recently introduced a similar imaging device, that allows for intraoperative video-rate near-infrared fluorescence (NIRF) imaging of lymphatic vessels and SLNs. In addition, our system is capable of multispectral imaging and is equipped with an algorithm for instant normalization of imaging data.¹⁶

In the current pilot study, our imaging system is applied for lymphatic mapping with ICG alongside the routine technique using blue dye and radiolabeled colloid in early-stage breast cancer patients. After describing the camera system and its use in a clinical setting, we discuss the potential of targeted NIRF imaging for intraoperative detection of tumor load within lymph nodes, allowing for a one-step SLN/ALN dissection procedure.

METHODS

A total of ten women diagnosed with biopsy-proven stage I-II breast cancer who were scheduled to undergo sentinel lymph node biopsy (SLNB) for staging and treatment of their disease, were included in this study. Exclusion criteria were defined as pregnant or breast feeding condition, age younger than 21, significant renal (serum creatinin ≥ 400 $\mu\text{mol/L}$), cardiac or pulmonary disease (ASA III-IV), history of iodine allergy or anaphylactic reactions to insect bites or medication, present or former hyperthyroidism, and recent surgery on the armpit. Informed consent was obtained prior to surgery and all information regarding the patients was anonymized. The study was approved by the Institutional Review Board (IRB) of

the UMCG and the National Committee for Clinical Research (CCMO). This study was performed in accordance with the ethical standards of the Helsinki Declaration and was registered prior to execution at the Dutch Trial Registry no. 2083.

Preoperative procedure

Technetium-99m labeled colloid was routinely administered in four equally-divided peritumoral injections (total volume: 0.4 ml) one day prior surgery. Additionally, a preoperative lymphoscintigram was obtained to determine the definitive position of the SLN and its lymphatic drainage pattern from the primary tumor.

Surgical procedure

After the induction of general anesthesia, the patient was injected peritumorally into the breast parenchyma with a 2 ml mixture of patent blue and ICG. The mixture consisted of 1 ml undiluted patent blue (Guerbet, Roissy-Charles-de-Gaulle, France) added to 0.5 mg (0.65 mmol) indocyanine green (Pulsion, Munich, Germany) dissolved in 1 ml of sterile water (B. Braun Medical, Hillcross, Martindale). The total volume of the mixture was equally divided over four peritumoral injections.

Immediately after injection, fluorescence images were acquired with the NIRF camera and displayed on two wide-screen monitors, of which one was in direct vision of the operating surgeon (Fig. 1). Images of the injection site and the axillary area were acquired with video-rate acquisition. During the surgical procedure, the SLN was identified in the usual way with the combination of a hand-held gamma probe and visual inspection. After an incision was made on the site with the highest count, as determined by the gamma probe, the NIRF camera system was directed at the surgically exposed area to capture an image and quantify fluorescence activity. The radioactive and/or blue SLNs were subsequently excised. After excision, the axillary basin was reassessed for radioactivity and blue spots as well as for NIRF signals. Residual radioactive and/or blue nodes were removed when necessary. In case of remaining fluorescent hot spots, a maximum of one additional SLN was excised by the surgeon. Nodes that were solid and highly suspicious for metastatic tumor on tactile inspection were also removed, irrespective of radioactivity or patent blue staining. The excised SLNs were imaged *ex vivo* with the NIRF camera system immediately after removal.

All SLNs were sent to the Department of Pathology of the UMCG for histopathological analysis. Postoperatively, patients were monitored for at least 24 hours for the appearance of fever or skin rash, which could be an indication for an allergic or anaphylactic reaction to ICG.

Near-infrared fluorescence camera system

For this study, fluorescence imaging was conducted with a multispectral state-of-the-art intraoperative NIRF camera system (Fig. 1). The system contains a halogen white light source, which illuminates the operating field without interfering with the fluorescence channels. Also, the system contains a laser diode, providing light of a specific wavelength for excitation of the fluorescent optical contrast agent.

After excitation, photons emitted by the fluorescent optical contrast agent can be detected with a highly sensitive charged-coupled device camera (CCD camera 1). Intrinsic fluorescence signals can be detected with a second camera (CCD camera 2). Customized software permits

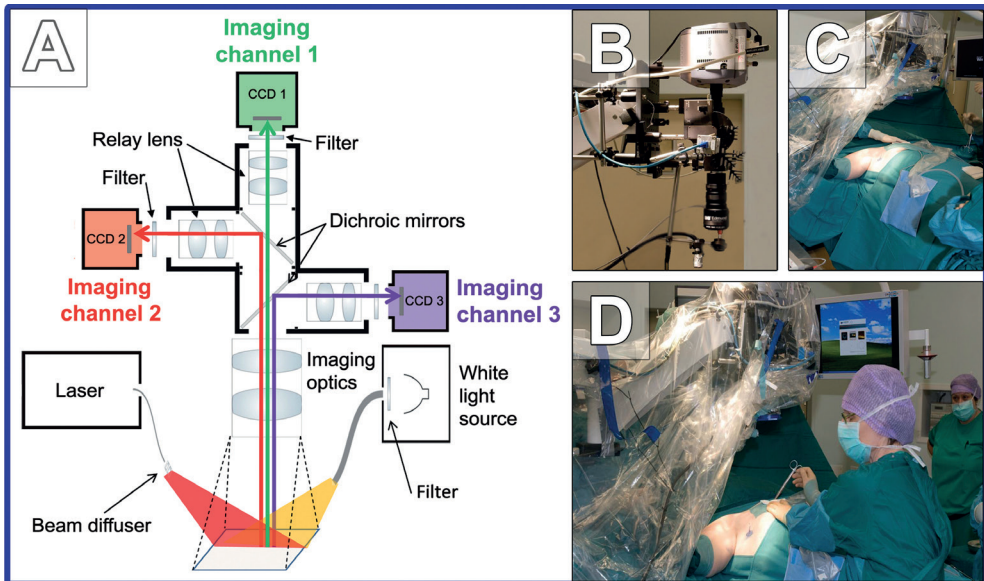


Figure 1. (A) Schematic overview of the clinical (IRB-approved) intraoperative NIRF optical imaging system. (B) Close-up of the intraoperative multispectral fluorescence camera in the operating room. (C+D) Positioning of the camera system covered with sterile draping during the surgical procedure.

simultaneous real-time acquisition of images from both NIRF cameras at up to 15 frames per second (fps). The authentic fluorescence signal from CCD camera 1 can be converted and projected onto a color video image of the operating field obtained with CCD camera 3, allowing for real-time, intraoperative anatomical positioning of the fluorescence signal. For intraoperative use, the entire NIRF camera system was covered in sterile drapes. In order to cover the lens of the camera, a sterile splash shield was used as commonly used in endoscopic surgery. The entire system was granted approval by the Institutional Review Board (IRB) of the UMCG. A detailed description of the technical characteristics of the NIRF camera system used in this study is published previously by Themelis et al.¹⁶

RESULTS

In all patients, a total of 18 SLNs could be identified with an average of 2 SLNs (range: 1–4 SLNs) per patient. Patient characteristics are listed in Table 1. Mean patient age was 65 years. Nine patients (90%) were diagnosed with invasive ductal carcinoma (IDC), one patient with adenoid cystic carcinoma.

Transcutaneous visualization of the SLN was not found feasible in the majority of patients (70%), in part due to spillage of ICG at the injection site. The number of SLNs detected intraoperatively with radiolabeled colloid, patent blue, and ICG were 18 (100%), 9 (50%), and 14 (78%), respectively. Fig. 2 shows the integration of fluorescence signals and color video images of the surgical field as seen by the surgeon on a monitor in the operating room.

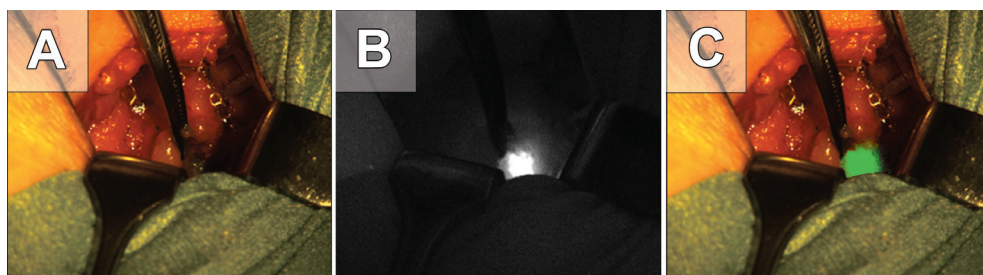


Figure 2. NIRF signal observed during the sentinel lymph node procedure in a breast cancer patient, approximately 5 minutes after peritumoral injection with patent blue and indocyanine green. **(A)** Color image as seen by the surgeon. **(B)** Normalized fluorescence signal. **(C)** Fluorescence signal converted into pseudocolor (green) and superposed on color image for anatomical positioning of the signal. Still images originate from a video taken at 15 frames per second during surgery.

Importantly, NIRF imaging detected 4 out of 4 SLNs containing (micro)metastases, revealed by conventional histopathology. The total duration of the surgical procedure combined with intraoperative NIRF optical imaging was prolonged for 30 minutes. This was mainly due to the learning curve for moving the camera in and out together with the time necessary for data acquisition during the operative procedure. The surgeons judged the camera system in combination with the wide-screen monitors convenient for intraoperative use and comparable to the use of monitors in laparoscopic surgery. It was regarded fairly easy to detect the NIR highlighted SLNs guided by the images on the screen. In addition, the surgeons appreciated the real-time, 'live' images, which gave them a sense of direct feedback on the presence of residual SLNs during the operation. No adverse reactions or wound infections were encountered after the administration of ICG.

DISCUSSION

Systematic studies have shown that tumor cells migrating from the primary tumor metastasize to the first draining lymph node (SLN) before spreading to other ALNs.¹⁷ When histopathological evaluation of the SLN indicates the presence of (micro)metastases, the standard treatment is to perform a complete axillary lymph node dissection (ALND).¹⁸ Histopathological evaluation of excised SLNs at the time of dissection is considered to be a highly accurate method for assessing the spread of the disease.¹⁹

However, in a large meta-analysis of over 7,500 breast cancer patients who underwent SLNB, no additional positive ALNs could be identified following ALND in 47% of the patients who had a positive SLN.²⁰ Furthermore, in 65% to 80% of patients with micrometastases (>0.2 , ≤ 2 mm) in the SLN, no metastases were found in the remaining ALNs.^{21,22} When only isolated tumor cells are present (metastases ≤ 0.2 mm), the percentage of patients with tumor-free ALNs even increases towards 90%.²² Consequently, non-affected ALNs are often needlessly removed due to the fact that the surgeon lacks real-time intraoperative feedback on LN tumor load status. As such, the SLN procedure, although highly specific and sensitive, leads to substantial overtreatment in breast-conserving surgery (BCS) with the known accompanying risks of nerve injury, lymph edema, shoulder dysfunction, and seroma formation.^{18,23-25} There seems

Table 1. Patient characteristics.

Study nr.	Age	Skin type ^a	Histology	Grade	Size (cm)	Location	Lymph nodes	Radioactive ^c	Blue ^c	Fluorescence ^c	Metastasis	ALND ^d
1	66	II ^b	IDC	Elston I	1.3	MUQ	1	+	-	0	+	3/26
							2	+	0	0	+	
							3	+	-	0	-	
							4	0	-	-	-	
2	68	II	IDC	Elston II	1.3	LUQ	5	+	+	+	N/P	
							6	+	0	+		-
3	59	II	IDC	Elston I	1.4	LUQ	7	+	0	+	N/P	
							8	+	-	0		-
4	69	II	IDC	Elston II	0.6	LUQ	9	+	+	+	N/P	
							10	+	+	+		-
5	81	II	IDC	Elston II	2.2	LUQ	11	+	-	0	N/P	
							12	+	+	+		+
6	52	II	IDC	Elston II	1.1	MUQ	13	+	-	0	0/27	
							14	+	+	+		-
7	60	II	ACC	N/A	2.3	LUQ	15	+	0	-	N/P	
							16	0	-	-		-
8	50	II	IDC	Elston I	1.7	LUQ	17	+	-	+	N/P	
							18	+	-	-		-
9	63	II	IDC	Elston II	1.2	LUQ	17	+	-	+	N/P	
							18	+	-	-		-
10	54	II	IDC	Elston II	2.3	LLQ	17	+	-	+	N/P	
							18	+	-	-		-

ACC, adenoid cystic carcinoma; ALND, axillary lymph node dissection; IDC, invasive ductal carcinoma; LUQ, lateral upper quadrant; MUQ, medial upper quadrant; N/A, not applicable; N/P, not performed.

^a Skin types I-VI in accordance with the American Academy of Dermatology.

^b White skin type common in Central European women; sometimes burns; tans gradually.

^c Yes (+), weak (0), no (-)

^d Total number of positive lymph nodes / total number of lymph nodes identified during ALND.

to be a clear need for noninvasive assessment of the SLN tumor burden status. This would significantly reduce comorbidity associated with the unnecessary removal of nonmetastatic ALNs, but could also implicate a one-step procedure in case of a positive SLN for an ALND if the tumor burden is larger than 2 mm. NIRF-imaging with a tumor-specific probe may provide such a lymph node surveillance tool for detecting and assessing the actual SLN status.

Several studies have reported on a near-infrared fluorescence (NIRF) optical imaging system, with which the SLN can be detected noninvasively after subcutaneous injection with the fluorescent optical contrast agent indocyanine green (ICG).^{9,11,13-15,26} ICG flows along with the lymph fluid and accumulates in the SLNs within minutes, enabling rapid detection and visualization of SLNs as fluorescent hot spots. Furthermore, no adverse reactions were reported in any of the conducted trials.^{9,11,13-15,26}

The NIRF camera system at the University Medical Center Groningen enables real-time intraoperative fluorescence imaging of lymphatic vessels and SLNs while capturing color video images of the surgical field simultaneously. NIRF optical imaging enhanced with optical contrast agents that emit in the NIR spectral range (e.g., ICG) offers some considerable advantages to the current SLN procedure: the technique offers a high resolution, is inexpensive, makes use of non-ionizing radiation, and offers high sensitivity and specificity rates.²⁷

The most important limitation of fluorescence imaging is its limited penetration depth (1–2 cm) due to the absorption and scattering of photons when propagating through tissue.²⁸ This may cause difficulties when aiming to visualize SLNs noninvasively or in obese patients. However, by selecting fluorescent optical contrast agents that emit photons in the NIR spectral region, tissue penetration of optical signals can be maximized due to reduced scattering and absorption of photons. In addition, maximal signal-to-noise ratios can be obtained in the NIR spectral region because tissue autofluorescence is minimized.²⁸

In this pilot study, the surgeons appreciated the real-time feedback on the location of the SLNs during the surgical procedure and found the system easy to work with. It was very well possible to excise the NIRF highlighted SLNs guided by the fluorescence signal on the screen. The total operation time was prolonged mainly due to the intraoperative use of the NIRF optical imaging system. However, in the course of these surgeries, we experienced a steep decrease in the time necessary to set up and install the system. We anticipate that, in the near future, the total prolongation of the surgical procedure will not exceed 30 minutes.

The current study shows that NIRF-guided lymphatic mapping with ICG is feasible next to the routine blue dye/radiolabeled colloid technique in early-breast cancer patients. These findings confirm the results reported by others.^{9-13,15} At our institution, intraoperative NIRF imaging will be expanded towards tumor-targeted detection of (micro)metastases in the SLN using NIR dyes like IRDye CW800 (LI-COR Inc., Lincoln, USA) conjugated to tracers of interest. Several studies have shown the feasibility of tumor-labeling with targeted optical contrast agents.²⁹⁻³² Sevick-Muraca et al. have shown the feasibility of NIR optical imaging following microdose administration of ICG. Although ICG is nonspecific, these findings suggest that comparable concentrations can be used for tumor-targeted NIR optical contrast agents for noninvasive SLN status assessment in humans.¹⁴

In the near future, it may be possible to visualize a tumor-targeted optical contrast agent and a nonspecific optical contrast agent with different wavelengths for simultaneous detection and assessment of the SLN. Such a multispectral imaging approach may improve therapeutic outcome of BCS by allowing for a one-step SLN/ALN dissection procedure based on the tumor burden within the SLN, which will ultimately reduce the number of unnecessary ALN

dissections and associated morbidity. The value of multispectral imaging needs yet to be evaluated by studies using uniformly designed and calibrated camera systems and optical agents for tumor-targeted imaging.

ACKNOWLEDGEMENTS

The authors wish to thank Mrs A. Prozee and Mr K. Meijer for logistical support; Dr M. van Oosten, Dr K.T. Buddingh, and Dr G.C. Langhout for help with data collection.

REFERENCES

1. Parkin DM, Bray F, Ferlay J et al. Global cancer statistics, 2002. *Cancer J Clin* 2005; 55:74-108.
2. Carter CL, Allen C, Henson DE. Relation of tumor size, lymph node status, and survival in 24,740 breast cancer cases. *Cancer* 1989; 63:181-187.
3. Giuliano AE, Jones RC, Brennan M et al. Sentinel lymphadenectomy in breast cancer. *J Clin Oncol* 1997; 15:2345-2350.
4. Kargozaran H, Shah M, Li Y et al. Concordance of peritumoral technetium 99m colloid and subareolar blue dye injection in breast cancer sentinel lymph node biopsy. *J Surg Res* 2007; 143:126-129.
5. Kern KA. Concordance and validation study of sentinel lymph node biopsy for breast cancer using subareolar injection of blue dye and technetium-99m sulfur colloid. *J Am Coll Surg* 2002; 195:467-475.
6. Cimmino VM, Brown AC, Szocik JF et al. Allergic reactions to isosulfan blue during sentinel node biopsy: a common event. *Surgery* 2001; 130:439-442.
7. Thevarajah S, Huston TL, Simmons RM. A comparison of the adverse reactions associated with isosulfan blue versus methylene blue dye in sentinel lymph node biopsy for breast cancer. *Am J Surg* 2005; 189:236-239.
8. Tonouchi H, Mohri Y, Tanaka K et al. Laparoscopic lymphatic mapping and sentinel node biopsies for early-stage gastric cancer: the cause of false negativity. *World J Surg* 2005; 29:418-421.
9. Kitai T, Inomoto T, Miwa M et al. Fluorescence navigation with indocyanine green for detecting sentinel lymph nodes in breast cancer. *Breast Cancer* 2005; 12:211-215.
10. Ogasawara Y, Ikeda H, Takahashi M et al. Evaluation of breast lymphatic pathways with indocyanine green fluorescence imaging in patients with breast cancer. *World J Surg* 2008; 32:1924-1929.
11. Tagaya N, Yamazaki R, Nakagawa A et al. Intraoperative identification of sentinel lymph nodes by near-infrared fluorescence imaging in patients with breast cancer. *Am J Surg* 2008; 195:850-853.
12. Hirche C, Murawa D, Mohr Z et al. ICG fluorescence-guided sentinel node biopsy for axillary nodal staging in breast cancer. *Breast Cancer Res Treat* 2010; 121:373-378.
13. Murawa D, Hirche C, Dresel S et al. Sentinel lymph node biopsy in breast cancer guided by indocyanine green fluorescence. *Br J Surg* 2009; 96:1289-1294.
14. Sevic-Muraca EM, Sharma R, Rasmussen JC et al. Imaging of lymph flow in breast cancer patients after microdose administration of a near-infrared fluorophore: feasibility study. *Radiology* 2008; 246:734-741.
15. Troyan SL, Kianzad V, Gibbs-Strauss SL et al. The FLARE() intraoperative near-infrared fluorescence imaging system: a first-in-human clinical trial in breast cancer sentinel lymph node mapping. *Ann Surg Oncol* 2009; 16:2943-2952.
16. Themelis G, Yoo JS, Ntziachristos V. Multispectral imaging using multiple-bandpass filters. *Opt Lett* 2008; 33:1023-1025.
17. Veronesi U, Paganelli G, Viale G et al. A randomized comparison of sentinel-node biopsy with routine axillary dissection in breast cancer. *N Engl J Med* 2003; 349:546-553.
18. Lyman GH, Giuliano AE, Somerfield MR et al. American Society of Clinical Oncology guideline recommendations for sentinel lymph node biopsy in early-stage breast cancer. *J Clin Oncol* 2005; 23:7703-7720.
19. Mabry H, Giuliano AE. Sentinel node mapping for breast cancer: progress to date and prospects for the future. *Surg Oncol Clin N Am* 2007; 16:55-70.
20. Kim T, Aguilar M, Giuliano A. Lymphatic mapping and sentinel lymph node biopsy in early-stage breast carcinoma: A meta-analysis. *Cancer* 2005; 106:4-16.
21. Cserni G, Gregori D, Merletti F et al. Meta-analysis of nonsentinel node metastases associated with micrometastatic sentinel nodes in breast cancer. *Br J Surg* 2004; 91:1245-1252.
22. McCready DR, Yong WS, Ng AK et al. Influence of the new AJCC breast cancer staging system on sentinel lymph node positivity and false negative rates. *J Natl Cancer Inst* 2004; 96:873-875.

23. Kwan W, Jackson J, Weir LM et al. Chronic arm morbidity after curative breast cancer treatment: prevalence and impact on quality of life. *J Clin Oncol* 2002; 20:4242-4248.
24. Ivens D, Hoe AL, Podd TJ et al. Assessment of morbidity from complete axillary dissection. *Br J Cancer* 1992; 66:136-138.
25. Keramopoulos A, Tsiou C, Minaretzis D et al. Arm morbidity following treatment of breast cancer with total axillary dissection: a multivariate approach. *Oncology* 1993; 50:445-449.
26. Tanaka E, Choi HS, Fujii H et al. Image-guided oncologic surgery using invisible light: completed preclinical development for sentinel lymph node mapping. *Ann Surg Oncol* 2006; 13:1671-1681.
27. Pleijhuis RG, Graafland M, de Vries J et al. Obtaining adequate surgical margins in breast-conserving therapy for patients with early-stage breast cancer: current modalities and future directions. *Ann Surg Oncol* 2009; 16:2717-2730.
28. Ntziachristos V. Fluorescence molecular imaging. *Annu Rev Biomed Eng* 2006; 8:1-33.
29. Segal EI, Low PS. Tumor detection using folate receptor-targeted imaging agents. *Cancer Metastasis Rev* 2008; 27:655-664.
30. Wang K, Wang K, Li W et al. Characterizing breast cancer xenograft epidermal growth factor receptor expression by using near-infrared optical imaging. *Acta Radiol* 2009; 50:1095-1103.
31. Zou P, Xu S, Wang A et al. Near-infrared fluorescence labeled anti-TAG-72 monoclonal antibodies for tumor imaging in colorectal cancer xenograft mice. *Mol Pharm* 2009; 6:428-440.
32. Marchal F, Pic E, Pons T et al. Quantum dots in oncological surgery: the future for surgical margin status. *Bull Cancer* 2008; 95:1149-1153.

Chapter

7

Submitted

A systematic review and meta-analysis of sentinel lymph node identification in breast cancer and melanoma: a plea for tracer mapping

M.G. Niebling*
R.G. Pleijhuis*
E. Bastiaannet
A.H. Brouwers
G.M. van Dam
H.J. Hoekstra

** Both authors contributed equally*

ABSTRACT*Introduction*

Sentinel lymph node biopsy (SLNB) has become a widely accepted staging procedure for both breast carcinoma and melanoma. The aim of our study was to systematically review different SLNB techniques and perform a meta-analysis for corresponding identification and false negative rates.

Methods

A systematic review of the literature on SLNB in patients with early-stage breast carcinoma and melanoma was performed. Only articles were included that studied SLNB in early-stage breast carcinoma and melanoma patients, with an original study group. The SLN identification rate and false negative rate were pooled for patients with breast carcinoma or melanoma according to radiocolloid tracer, blue dye, indocyanine green (ICG), or a combination of a radiocolloid tracer with a blue or ICG dye.

Results

Between 1992 and 2012, a total of 154 studies (88 breast carcinoma and 66 melanoma) were reported that met the eligibility criteria. These studies included a total of 44,172 patients. The pooled value for the SLN identification rate in breast carcinoma and melanoma patients using solely blue dye was 85% (range: 65–100%) and 84% (range: 59–100%), using solely radiocolloid 94% (range: 67–100%) and 99% (range: 83–100%), using a combination of blue dye and radiocolloid 95% (range: 76–100%) and 98% (range: 68–100%), using solely ICG 95% (range: 77–100%) and 100% (range: 100–100%), and using a combination of radiocolloid and ICG 96% (range 94.9–96.7%) and 100% (range: 100–100%).

Conclusion

The current meta-analysis provided data that favor the use of radiocolloid solely or radiocolloid combined with a blue dye for the identification of the SLN. Performing SLNB with radiocolloid solely is the technique of choice for experienced surgeons, since blue dye has multiple disadvantages. SLNB using ICG as a fluorescent dye seems a promising technique for the near future.

INTRODUCTION

Breast carcinoma and melanoma are annually diagnosed in 1.38 million and 197,000 people, representing 10.9% and 1.6% of all cancers in the world, respectively.¹ Fortunately, the majority of both cancers are initially diagnosed stage I or II.²

The lymphatic route is a principal way for breast carcinoma and melanoma to metastasize from their original focus. Cancer cells progressing via the lymphatic vessels are trapped in the first lymph node they encounter, denominated as the sentinel lymph node (SLN).^{3,4}

Lymph node metastases can either be detected clinically or through the use of a sentinel lymph node biopsy (SLNB). The concept of the SLN was first described in 1960 by Gould et al. and is based on two basic principles: the existence of an orderly and predictable pattern of lymphatic drainage to a regional lymph node basin, and the functioning of a first lymph node as an effective filter for tumor cells.^{5,6} Clinical implementation of the concept was deployed on a broad scale by Cabanas et al. in penile cancer.⁷

Morton et al. described a method for SLNB in 1992, using peritumoral intradermal injections of blue dye in patients with primary cutaneous melanoma.⁴ The blue-stained lymphatic vessel was followed surgically until it was seen entering a blue-stained lymph node. In 1993, Alex et al. added the use of a radiotracer, injected intradermally around the primary tumor site, followed by imaging and subsequent intraoperative use of a handheld gamma probe to localize and remove the SLN.⁸ In the same year, Krag et al. described the application of this technique in breast carcinoma patients.⁹ Albertini et al. combined both the blue dye and the radioactive tracer in 1996, which is currently the most commonly used technique for SLNB in most centers.¹⁰ The two most widely accepted clinical applications of SLNB are for cutaneous melanoma ≥ 1 mm and T₁₋₂ breast carcinoma.¹¹⁻¹³ SLNB is preferred over direct lymph node dissection (LND) because the risk of morbidity is lower.^{14,15} Moreover, SLNB allows the pathologist to study the few removed SLNs in greater detail for tumor burden compared with examination of the large number of lymph nodes removed by LND.¹⁶

Despite its wide global use, the SLNB procedure has not been standardized internationally due to variation in the method and material used between surgeons and institutions. Although a combination of blue dye and a radiotracer is considered standard-of-care, a significant number of surgeons work with blue dye or a radiotracer alone. In addition, the fluorescent optical contrast agent indocyanine green (ICG) was recently introduced in the clinic as an alternative agent for SLNB guidance.¹⁷

In the present study, a systematic review was performed on peer-reviewed scientific articles to evaluate different SLNB techniques and their corresponding identification- and false negative rates in breast carcinoma and melanoma. In addition, we aimed to identify technical aspects influencing the outcome of the SLNB procedure.

METHODS

Literature search and inclusion/exclusion criteria

A comprehensive, systematic review was conducted in October 2012 of the medical literature published after 1992. Details of the methods of the search and inclusion/exclusion criteria are specified in Supplementary file 1.

Study quality assessment

Authors MGN and RGP performed the quality assessment of selected articles. Study quality was evaluated using the "QUADAS" (*quality assessment of diagnostic accuracy studies*) tool to extract relevant study design characteristics.¹⁸ The core QUADAS items used in this review are outlined in Supplementary file 2. In brief, QUADAS items included: availability of representative spectrum of patients, clear description of selection criteria, adequate reference standard, execution of index and reference test described in sufficient detail, independent interpretation of index test, availability of relevant clinical data, reporting of uninterpretable results, adequate explanation of study withdrawals, availability of adequate reference standard for verification purposes, adequate follow-up, and reporting of false negatives. Each item was scored as 'yes', 'no', or 'unclear'.

Statistical analyses

Univariate and multivariate logistic regression analyses were performed to identify factors associated with SLN identification rate and false negative rate for the different SLNB techniques. Analyses were stratified to technique and performed separately for breast carcinoma and melanoma. Factors included in this analysis were: type of study (prospective or retrospective), study period (1992–2000, 2001–2006, or 2007–2012), age (in years), definition of SLN (radioactivity higher than background or 10% rule), tumor size (in mm), number of SLNs removed, quality of the study (QUADAS score), type of dye (patent blue, isosulfan blue, lymphozuran blue, methylene blue, a combination of blue dyes, ICG, or unknown) or radiocolloid (^{99m}Tc-sulfur colloid, ^{99m}Tc-tin colloid, ^{99m}Tc-phytate, ^{99m}Tc-human serum albumin, ^{99m}Tc-dextran 500, or ^{99m}Tc-tilmanocept), concentration of dye or radiocolloid (in mg/ml or in Mbq), injected volume of dye or radiocolloid (in ml), injection site (peritumoral, parenchymal, subareolar, intradermal, subdermal, combination, or unknown), timing of injection (<15 minutes, 15 minutes–1 hour, 1–10 hours, >10 hours), and massage after injection of dye or radiocolloid. The false negative rate (FNR) was defined as the probability of a negative SLN when the patient has positive lymph nodes in the LND or in the follow-up period of the study.

Calculations were performed using the statistical packages SPSS (IBM SPSS Statistics for Windows, Version 21.0, Armonk, USA). *P*-values <0.05 were considered statistically significant.

Meta-analysis

Identification rate (IR) and FNR were extracted from the studies and pooled (on a study level) according to SLNB technique, breast carcinoma or melanoma, and period (1992–2000, 2001–2006, and 2007–2012). Summary identification rate, false negative rate, and the corresponding 95% confidence interval (CI) were calculated using STATA/SE version 12.0 (StataCorp, College Station, USA) using the metan command. Pooled values were calculated, using either a random-effects or a fixed-effects model, depending on the number of included studies and the amount of heterogeneity observed.

RESULTS

Literature search

Our comprehensive literature search resulted in 335 studies that were selected for further analysis, dating from January 1992 to October 2012. Of these studies, 198 comprised SLNB in breast carcinoma and 137 in melanoma. After thorough review, 154 studies (88 breast

carcinoma and 66 melanoma) met our inclusion criteria (Tables 1–3). A total of 108 out of 154 studies reported on the IR of SLNB using blue dye only, 111 on using radiocolloid only, and 118 on using the combination of blue dye and radiocolloid. Nineteen studies analyzed the IR of SLNB using ICG solely and 12 studies analyzed ICG in combination with radiocolloid. When data from all included articles is aggregated, a total of 44,172 patients underwent SLNB with a median of 103 patients (range: 4–5,611) per study. In the studies where the number of SLNs identified was reported, blue dye identified 12,623 SLNs in 6,052 patients with a mean of 2.09 SLNs per patient, radiocolloid identified 1,6175 SLNs in 7,455 patients with a mean of 2.17 SLNs per patient, blue dye and radiocolloid both identified 37,680 SLNs in 19,917 patients with a mean of 1.89 SLNs per patient. The SLN was positive in 14.6% in SLNs detected with blue dye, 11.5% detected with radiocolloid, and 23.9% detected with both blue dye and radiocolloid. ICG identified 2,697 SLNs in 947 patients with a mean of 2.85 SLNs per patient. Combined with radiocolloid, ICG identified 353 SLNs in 194 patients with a mean of 2.87 SLNs per patient. Table 1 and Table 2 provide an overview of the number of patients per study, the mean SLN, IR, FNR, and the duration of follow-up for all breast carcinoma and melanoma studies, respectively. In Table 3, an overview is shown for SLNB using ICG alone or combined with radiocolloid.

Identification rate and false negative rate

IR and FNR for SLNB using solely blue dye, solely radiocolloid, and these two combined are presented in Table 1 and Table 2, for breast cancer and melanoma patients, respectively. IR and FNR for SLNB for SLNB using ICG, either solely or combined with radiocolloid and/or blue dye, are presented in Table 3. The pooled IR and FNR for all techniques are presented in Table 4 and Table 5, pooled per tumor type for the time periods 1992–2000, 2001–2006, and 2007–2012.

Multivariate analysis

In breast carcinoma, multivariate factors significantly associated with SLN IR were the following: when solely blue dye was used in SLNB (median: 0.87), massage of the breast following injection of blue dye (vs. no massage; OR 3.5, range: 1.2–10.6, $P=0.02$) was identified as an independent factor to increase SLN detection. When solely radiocolloid was used (median: 0.96), a prospective study design (vs. retrospective; OR 6.9, range: 1.3–38.4, $P=0.03$) was associated with a higher SLN detection rate. When radiocolloid and blue dye were combined (median: 0.97), SLN detection rate was found to increase with ascending year of publication since the time period of 1992–2000 (vs. 2001–2006; OR 13.0, range: 1.4–119.1 and 2007–2012; OR 20.0, range: 2.0–203.3, $P=0.04$). No independent factors were identified for SLN detection rate when solely ICG (median: 0.98) or a combination of radiocolloid and ICG (median: 0.96) was used.

In melanoma, multivariate factors significantly associated with SLN IR were the following: when solely ICG was used, the volume of injection (in ml) was associated with SLN IR (OR 9.5, range: 1.1–71.0, $P=0.03$). When radiocolloid and blue dye were combined, the volume of injection of blue dye was identified as an independent factor (OR 19.7, range: 1.3–289.1, $P=0.04$). No significant factors were identified for the use of solely blue dye, radiocolloid, and radiocolloid combined with ICG.

In addition to SLN IRs, logistic regression was performed to identify factors associated with FNRs. Again, analyses were stratified to technique and performed separately for breast carcinoma and melanoma. In both breast carcinoma and melanoma, no univariate or multivariate significant predictive factors were identified for any of the techniques.

Table 1. Identification rates reported in studies for sentinel lymph node biopsy using blue dye, radiocolloid, or a combination of these two in breast carcinoma patients.

Study	Year of publication	Technique	No of patients	Mean SLN	Identification rate (%)	False negative rate (%)	Follow up ^b
Giuliano ⁴⁹	1997	Blue	107		93.5%	0.0%	
Barnwell ⁵⁰	1998	Combi	42	1.0	90.0%	0.0%	
Crossin ⁵¹	1998	Radio	50	2.0	84.0%	2.4%	
Flett ⁵²	1998	Blue	68		82.4%	5.4%	
Kapteijn ⁵³	1998	Blue	30	1.4	86.7%		
Krag ³	1998	Radio	443	2.6	93.2%	11.0%	
Ratanawichitrasin ⁵⁴	1998	Blue	40	1.6	87.5%		
Snider ⁵⁵	1998	Radio	80	2.2	87.5%	7.0%	
Jaderborg ⁵⁶	1999	Combi	79	1.5	81.0%	5.0%	
Kollias ⁵⁷	1999	Blue	19		94.7%		
		Radio	51		68.6%		
		Combi	47		89.0%	6.5%	
Moffat ⁵⁸	1999	Radio	70	2.1	98.6%		
Morgan ⁵⁹	1999	Blue	44		72.7%	16.7%	
Morrow ³⁹	1999	Blue	50		88.0%		
		Combi	42		86.0%		
Veronesi ⁶⁰	1999	Radio	376		98.7%	6.7%	
		Combi	54		68.5%		
Winchester ⁶¹	1999	Radio	180	3.1	90.0%	2.2%	
Canavese ⁶²	2000	Blue	55		65.5%	23.0%	
		Combi	48		94.0%	12.5%	
Cox ⁶³	2000	Blue ^a	1147	2.1	80.3%		
		Radio ^a	1147	2.1	88.6%		
		Combi	1147	2.1	96.0%	1.0%	
Doting ⁶⁴	2000	Combi	136	1.7	93.0%	5.1%	
Fraille ⁶⁵	2000	Radio	132	2.0	96.2%	4.0%	
Lauridsen ³⁸	2000	Blue ^a	80		90.0%		
		Radio ^a	80		92.5%		
		Combi	80	2.0	98.0%	0.0%	
Liu ⁶⁶	2000	Combi	41	1.5	93.0%		
Rodier ⁶⁷	2000	Blue	74		82.4%	8.0%	
Tsugawa ⁶⁸	2000	Blue ^a	48		75.0%		
		Radio ^a	48		66.6%		
		Combi	48		90.0%	4.7%	
Derossis ²²	2001	Blue ^a	2000		82.9%		
		Radio ^a	2000		90.1%		
		Combi	2000		97.0%		
Feggi ⁶⁹	2001	Radio	73	1.0	100.0%		
Mateos ⁷⁰	2001	Blue ^a	65		72.3%	16.7%	20 ^a
		Radio ^a	80	1.2	91.2%	17.0%	
		Combi	80		91.0%		
Sato ⁷¹	2001	Radio	75	1.9	98.7%		
Simmons ⁷²	2001	Blue	30	1.8	90.0%		
Tafra ⁷³	2001	Combi	535	1.6	87.0%	5.2%	
Tanis ⁷⁴	2001	Combi	60	2.2	97.0%		8 ^a
Xavier ⁷⁵	2001	Blue	6		100.0%		
		Combi	50		100.0%	2.0%	
Watanabe ⁷⁶	2001	Radio	87	2.0	100.0%		
Feezor ⁷⁷	2002	Radio	118	1.8	98.3%		
Kern ⁷⁸	2002	Combi	187	2.4	98.0%	0.0%	
Jastrzebski ⁷⁹	2002	Combi	123		88.0%		

Table continues on the next page

Table 1 (continued)

Study	Year of publication	Technique	No of patients	Mean SLN	Identification rate (%)	False negative rate (%)	Follow up ^b
Shimazu ⁸⁰	2002	Blue ^a	62	1.5	79.9%		
		Radio ^a	93		92.5%		
		Combi	93	2.0	96.0%	5.6%	
Nos ⁸¹	2003	Blue	324	2.1	85.5%	11.1%	
Reitsamer ⁸²	2003	Combi	157	2.0	99.0%		
Simmons ⁸³	2003	Blue ^a	112		92.9%		84 [*]
		Radio ^a	112		89.3%		
		Combi	112		96.0%		
Eldrageely ⁸⁴	2004	Blue ^a	164		90.2%		
		Radio ^a	164		94.5%		
		Combi	164	1.5	98.0%		
Gray ⁸⁵	2004	Combi	546	1.3	99.0%		
Lin ³³	2004	Blue	150		82.7%		
		Radio	94		96.8%		
		Combi	76		97.0%		
King ²⁷	2004	Blue ^a	1719		84.3%		
		Radio ^a	1719		97.3%		
		Combi	1719		99.0%		
Nour ⁸⁶	2004	Blue	54		83.3%	0.0%	
Radovanovic ⁸⁷	2004	Blue	50	1.7	68.0%	18.0%	
		Combi	150		83.0%	4.5%	
		Blue ^a	132		84.1%		32 [*]
Radio ^a	132		95.5%				
Combi	132	1.4	97.0%	6.0%			
Hung ⁸⁹	2005	Blue	57	1.8	86.0%	5.0%	
		Combi	61	2.1	100.0%	0.0%	
		Blue	93	1.3	95.7%	20.8%	
Syme ⁹⁰	2005	Combi	257	1.8	89.0%	2.8%	
		Blue ^a	99	2.2	81.8%		
		Radio ^a	99	2.2	98.0%		
Teal ⁹¹	2005	Combi	99	2.2	99.0%		
		Blue ^a	100	1.4	88.0%		
		Radio ^a	100	1.8	96.0%		
Argon ²⁵	2006	Combi	100	1.6	98.0%		
		Blue ^a	141	2.0	96.5%		
		Radio	175	1.1	94.3%	2.5%	
Golshan ⁹²	2006	Combi	758	2.0	89.0%	5.8%	
		Radio	400		95.0%		
		Combi	267		97.0%		
Lo ⁹³	2006	Blue ^a	308	1.7	96.8%		33 [^]
		Radio ^a	308	1.4	95.8%		
		Combi	308	1.9	99.0%		
Zaman ⁹⁶	2006	Combi	32		97.0%	0.0%	
Kargozaran ⁹⁷	2007	Blue ^a	124	1.6	92.7%		23 [^]
		Radio ^a	124	1.7	97.6%		
		Combi	124		98.0%		
Krag ³⁷	2007	Combi	5536	1.3	97.0%		
Nathanson ⁹⁸	2007	Blue ^a	600		89.3%		
		Combi	600		96.0%		
		Blue ^a	449		94.7%		48 [^]
Radio ^a	449		97.1%				
Combi	449	1.8	99.0%				

Table continues on the next page

Table 1 (continued)

Study	Year of publication	Technique	No of patients	Mean SLN	Identification rate (%)	False negative rate (%)	Follow up ^b
Varghese ⁹⁹	2007	Blue	173	1.5	96.5%	3.7%	
		Combi	156	2.5	99.0%	2.5%	
Yen ¹⁰⁰	2007	Radio	213	3.5	97.2%	4.4%	
Bines ²⁶	2008	Radio	208	2.0	93.8%		
		Combi	167	1.9	96.0%		
Mudun ¹⁰¹	2008	Radio	228		97.4%	3.1%	
Thompson ⁴⁰	2008	Combi	236	1.6	96.0%		
Zakaria ¹⁰²	2008	Blue ^a	401		88.0%		
		Combi	401		100.0%		
Climaco ¹⁰³	2009	Combi	46		76.0%		
Koukouraki ¹⁰⁴	2009	Blue ^a	250		94.4%		
		Combi	250		100.0%		
Mathelin ¹⁰⁵	2009	Blue ^a	100	2.7	65.0%		28 [*]
		Radio ^a	100	2.7	94.0%		
		Combi	100	2.7	99.0%		
Hayashida ¹⁰⁶	2010	Blue ^a	640	2.4	79.7%		
		Radio ^a	640	2.4	94.7%		
		Combi	640	2.4	98.0%		
Kang ²³	2010	Radio	1353	2.9	98.4%		
		Combi	2049	2.7	98.0%		
Krikanova ¹⁰⁷	2010	Blue	332		94.6%		
Narui ¹⁰⁸	2010	Blue	234	3.4	99.6%		54 [^]
Straver ¹⁰⁹	2010	Blue ^a	1953		88.3%		
		Radio ^a	1953		95.8%		
		Combi	1953		97.0%		
Yararbas ¹¹⁰	2010	Radio	200		98.0%		
Lida ¹¹¹	2011	Combi	258		99.0%	7.7%	
Mieog ¹¹²	2011	Blue ^a	30	1.5	83.3%		
		Radio ^a	30	1.5	100.0%		

SLN, sentinel lymph node

^a Blue dye and radiocolloid were used in the same procedure. SLN identification rates were recorded separately.

^b Follow-up period in median ([^]) or months (*).

Table 2. Identification rates reported in studies for sentinel lymph node biopsy using blue dye, radiocolloid, or a combination of these two in melanoma patients.

Study	Year of publication	Technique	No of patients	Mean SLN	Identification rate (%)	False negative rate (%)	Follow up ^b
Thompson ¹¹³	1995	Combi	118		87.0%	5.2%	
Albertini ¹¹⁴	1996	Blue ^a	106		69.5%		
		Combi	106	1.9	96.0%	0.0%	60*
Thompson ¹¹⁵	1997	Blue ^a	21		83.0%		
		Radio ^a	21		87.2%		
Wells ¹¹⁶	1997	Combi	21	2.2	91.3%		
		Blue ^a	58	2.3	67.0%		
Bartolomei ¹¹⁷	1998	Combi	36		95.0%	0.0%	12 [^]
		Blue ^a	25		72.0%		
Bedrosian ¹¹⁸	1999	Radio ^a	25	1.5	100.0%	0.0%	11*
		Combi	25		100.0%		
Bostick ¹¹⁹	1999	Blue	23		74.0%		
		Combi	80	1.8	94.7%		
Gennari ¹²⁰	1999	Blue ^a	87		95.1%		
		Radio ^a	87		92.3%		
Gershenwald ¹²¹	1999	Combi	87	1.6	97.6%	0.0%	16*
		Combi	133	1.6	99.0%	3.8%	19 [^]
Morton ¹²²	1999	Combi	612	1.7	95.0%		40 [^]
		Blue	453		94.9%		
Jansen ¹²³	2000	Combi	727		98.3%	3.7%	
		Combi	200	2.2	99.5%	3.9%	
Landi ¹²⁵	2000	Combi	30	2.3	90.0%	9.1%	23*
		Blue	25	1.5	88.0%		
Oliveira Filho ¹²⁶	2000	Combi	425	1.6	99.5%	1.2%	18 [^]
		Blue ^a	64		76.0%		
Temple ¹²⁷	2000	Radio ^a	64		97.0%		
		Combi	64	1.4	100.0%	1.9%	11 [^]
Tremblay ¹²⁸	2000	Combi	56	2.2	98.0%	4.5%	12 [^]
		Radio	36	2.0	97.2%	0.0%	14 [^]
Villa ¹²⁹	2000	Blue ^a	88	1.9	94.3%		
		Radio ^a	49		98.0%		
McMasters ¹³⁰	2001	Combi	49		98.0%		
		Blue ^a	1184		69.0%		
Medina-Franco ¹³¹	2001	Combi	1184	2.4	99.7%	2.0%	
		Blue ^a	38		68.4%		
Neubauer ¹³²	2001	Radio ^a	38		89.5%		
		Combi	38		97.0%	2.9%	15*
Rasgon ¹³³	2001	Radio	41	1.3	95.1%		
		Blue ^a	24		66.7%		
Tavares ¹³⁴	2001	Radio ^a	24	3.0	91.7%		
		Combi	24		92.0%	10.5%	18*
Eicher ¹³⁵	2002	Radio ^a	19		95.0%		
		Combi	19	1.7	95.0%	0.0%	
Ferrone ¹³⁶	2002	Blue ^a	43		27.9%		
		Radio ^a	43		90.7%		
Patel ¹³⁷	2002	Combi	43	3.6	98.0%	0.0%	
		Combi	126	2.0	100.0%		25*
	2002	Blue ^a	48		73.0%		
		Radio ^a	56	2.4	93.0%		
		Combi	48		96.0%	1.9%	20 [^]

Table continues on the next page

Table 2 (continued)

Study	Year of publication	Technique	No of patients	Mean SLN	Identification rate (%)	False negative rate (%)	Follow up ^b
Chao ¹³⁸	2003	Bluea	254	2.1	59.1%		
		Radioa	321	2.8	97.0%	2.2%	16 ^a
Estourgie ¹³⁹	2003	Combi	250	2.3	100.0%	3.2%	72 ^a
Schmalbach ¹⁴⁰	2003	Blue	80	2.2	96.0%	4.5%	25 ^a
Vidal-Sicart ¹⁴¹	2003	Bluea	315		70.1%		
		Radioa	435	1.8	98.8%	1.9%	26 [*]
Weiss ¹⁴²	2003	Bluea	30		67.0%		
		Radioa	30		100.0%		
		Combi	30	1.9	100.0%		
Alex ¹⁴³	2004	Bluea	16		81.3%		
		Radioa	43		97.6%	2.6%	82 [*]
		Combi	16		100.0%		
Chakera ¹⁴⁴	2004	Radioa	241	2.6	98.0%		
		Combi	194	1.7	100.0%	1.1%	15 ^a
Gipponi ¹⁴⁵	2004	Blue	39	1.4	89.7%		
		Combi	126	1.9	100.0%	4.4%	17 ^a
Rossi ¹⁴⁶	2004	Combi	1313	2.0	99.3%	3.5%	31 ^a
Topping ³⁰	2004	Combi	347	2.1	99.0%	1.7%	60 ^a
Shpitzer ¹⁴⁷	2004	Blue	8	1.7	88.0%		
		Combi	22	2.0	96.0%	3.8%	31 ^a
Carlson ¹⁴⁸	2005	Radioa	132	2.1	96.9%	6.4%	35 [*]
MacNeill ¹⁴⁹	2005	Combi	44		93.0%	0.0%	22 [*]
Doting ¹⁵⁰	2006	Bluea	36		63.9%		
		Radioa	36		91.7%		
		Combi	36	2.7	92.0%	6.9%	54 ^a
Gad ¹⁵¹	2006	Combi	278	2.2	98.0%	2.5%	31 ^a
Lin ¹⁵²	2006	Combi	114	4.0	97.0%	4.0%	84 [*]
Oliveira Filho ¹⁵³	2006	Blue	47	1.5	100.0%		
		Radio	47	1.6	100.0%		
		Combi	94	1.6	100.0%	2.7%	20 ^a
Cecchi ¹⁵⁴	2007	Combi	30	1.3	100.0%	21.1%	27 [*]
Kilpatrick ¹⁵⁵	2007	Bluea	316		88.4%		
		Radioa	316		97.4%		
		Combi	316	2.8	97.8%	4.7%	19 [*]
Koskivuo ¹⁵⁶	2007	Combi	305	2.4	97.0%	2.0%	21 [*]
Teltzrow ¹⁵⁷	2007	Radio	106	2.3	89.0%	9.0%	47 [*]
Gomez-Rivera ¹⁵⁸	2008	Combi	111	3.2	100.0%	5.6%	34 ^a
Liu ¹⁵⁹	2008	Bluea	159		60.2%		
		Combi	159		100.0%		
Mattsson ¹⁶⁰	2008	Combi	422	2.1	97.0%	4.2%	12 ^a
Roulin ²⁸	2008	Combi	327	2.0	99.1%	2.8%	34 [*]
Kelly ¹⁶¹	2009	Combi	40		68.0%	9.5%	40 ^a
Kovacevic ¹⁶²	2009	Bluea	40		95.0%		
		Radioa	40		100.0%		
		Combi	40	1.9	100.0%	16.7%	18 [*]
Koskivuo ¹⁶³	2011	Combi	423		96.0%	2.5%	36 ^a
Leong ¹⁶⁴	2011	Radioa	47	2.3	98.9%		
Liu ¹⁶⁵	2011	Combi	571	3.4	100.0%		
Neves ¹⁶⁶	2011	Bluea	93	1.8	47.0%		

Table continues on the next page

Table 2 (continued)

Study	Year of publication	Technique	No of patients	Mean SLN	Identification rate (%)	False negative rate (%)	Follow up ^b
Noro ¹⁶⁷	2011	Blue	47		83.0%		
		Combi	74		95.9%		
Rughani ²⁹	2011	Combi	697	1.9	99.7%	3.0%	46 [^]

SLN, sentinel lymph node

^a Blue dye and radiocolloid were used in the same procedure. SLN identification rates were recorded separately.

^b Follow-up period in median ([^]) or months (*).

Table 3. Identification rates reported in studies combining radiocolloid, vital blue dye, and/or indocyanine green in breast carcinoma and melanoma patients.

Study	Tumor type	Year of publication	Technique	No of patients	Mean SLN	Identification rate (%)	False negative rate (%)	Follow up ^b
Motomura ¹⁶⁸	BC	1999	Green	150	1.7	76.7%	1.1%	
Motomura ¹⁶⁹	BC	2001	Green	93	1.8	83.9%	1.9%	
			G+R	138		94.9%	0%	
Kitai ¹⁷	BC	2005	Green	18	2.8	94.4%		
Tagaya ¹⁷⁰	BC	2008	Greena	25	5.4	100%		6 [*]
			Bluea	25	2.3	92.0%		
Murawa ¹⁷¹	BC	2009	G+R	30		96.7%	0.1%	
Tanaka ¹⁷²	MM	2009	Radio ^a	4		100.0%		
			Green ^a	4		100.0%		
			G+R	4		100.0%		
Hirche ¹⁷³	BC	2010	Green	43	2	97.7%	6.6%	
Abe ¹⁷⁴	BC	2011	Green ^a	128	3.1	100%		
			Blue ^a	128		65.6%		
			G+R+B	4		100.0%		
Aoyama ¹⁷⁵	BC	2011	Green	312	3.4	100%	1.7%	49 [^]
Tagaya ¹⁷⁶	BC	2011	Green	50	3.7	100%		6 [*]
Fujisawa ¹⁷⁷	MM	2011	Blue ^a	6	2	100.0%		
			Radio ^a	5	1.8	100.0%		
			Green ^a	6	2.2	100.0%		
			G+R+B	6	2.2	100.0%		
Namikawa ¹⁷⁸	MM	2011	Blue ^a	49	2	85.7%	5.6%	
			Radio ^a	49	2.5	95.9%	5.6%	
			Green ^a	49	4	61.2%	3.89%	
			G+R+B	49	4	100.0%	0%	20 [^]
Hirche ¹⁷⁹	BC	2012	Green	47	2	97.9%	5.3%	
Polom ¹⁸⁰	BC	2012	G+R	49	2.3	95.9%		
Brouwer ¹⁸¹	MM	2012	Blue ^a	7	1.3	71.4%		
Fujisawa ¹⁸²	MM	2012	Blue ^a	15	1.7	93.0%		
			Radio ^a	15	1.7	100.0%		
			Green ^a	15	2	100.0%		
			G+R+B	15	2	100.0%		
Polom ¹⁸³	MM	2012	Radio ^a	10		100.0%		
			Green ^a	10		100.0%		
			G+R	10	2.3	100.0%		
Stoffels ¹⁸⁴	MM	2012	Radio ^a	22		100.0%		
			Green ^a	22		100.0%		
Uhara ¹⁸⁵	MM	2012	G+R	22	2.8	100.0%	0%	1.3 [*]
			Blue ^a	562		92.3%		
			Radio ^a	562		96.4%		
			Green ^a	67		100.0%		
			G+R+B	562		97.9%		

BC, breast carcinoma; G+R, SLNB using green dye + radiocolloid; G+R+B; SLNB using green dye + radiocolloid + blue dye; MM, malignant melanoma; SLN, sentinel lymph node

^a Blue dye, radiocolloid, and/or indocyanine green were used in the same procedure. SLN identification rates were recorded separately. Indocyanine green was used in 67 out of 562 patients.

^b Follow-up period in median (^) or months (*).

Table 4. Pooled identification rate for sentinel lymph node biopsy for all studies, breast carcinoma studies, and melanoma studies per technique.

Technique	Period	Pooled value		Breast carcinoma		Melanoma	
		Pooled value	95% CI	Pooled value	95% CI	Pooled value	95% CI
Blue dye alone	Whole period	84%	83-86%	85%	83-88%	84%	83-84%
	1992-2000	84%	81-87%	81%	76-86%	91%	91-92%
	2001-2006	81%	78-84%	86%	82-91%	72%	61-84%
	2007-2012	88%	85-91%	87%	84-91%	89%	82-96%
Radiocolloid alone	Whole period	95%	95-96%	94%	93-95%	99%	99-99%
	1992-2000	92%	90-93%	88%	84-91%	100%	100-100%
	2001-2006	95%	94-97%	96%	94-97%	97%	96-97%
	2007-2012	98%	97-98%	97%	96-98%	100%	99-100%
Combination radio-colloid and blue dye	Whole period	96%	96-97%	95%	94-95%	98%	98-98%
	1992-2000	95%	94-95%	91%	88-94%	97%	97-98%
	2001-2006	97%	96-97%	96%	95-96%	99%	98-99%
	2007-2012	98%	97-98%	97%	96-98%	99%	98-99%
ICG	Whole period	99%	98-99%	95%	95-96%	100%	100-100%
	1992-2000	77%*	76-77%	77%*	76-77%	No studies	
	2001-2006	89%	79-99%	89%	79-99%	No studies	
	2007-2012	100%	100-100%	100%	100-100%	100%	100-100%
Combination radio-colloid and ICG	Whole period	99%	99-100%	96%	95-97%	100%	100-100%
	1992-2000	No studies		No studies		No studies	
	2001-2006	95%*	95-95%	95%	95-95%	No studies	
	2007-2012	100%	100-100%	96%	96-97%	100%	100-100%

CI, confidence interval; ICG, indocyanine green.

* Derived from only one study.

Table 5. Pooled false negative rate for sentinel lymph node biopsy in all studies, breast carcinoma studies, and melanoma studies per technique.

Technique	Period	Pooled value		Breast carcinoma		Melanoma	
		Pooled value	95% CI	Pooled value	95% CI	Pooled value	95% CI
Blue dye alone	Whole period	3.4%	3.0–3.8%	3.2%	2.8–3.6%	6.1%*	5.2–7.1%
	1992–2000	3.4%	1.1–5.8%	3.4%	1.1–5.8%	No studies	
	2001–2006	3.5%	1.7–5.3%	3.5%	1.7–5.3%	No studies	
	2007–2012	4.5%	1.3–7.6%	2.9%*	2.7–3.1%	6.1%*	5.2–7.1%
Radiocolloid alone	Whole period	2.6%	1.9–3.3%	2.2%	1.8–2.6%	3.4%	2.6–4.2%
	1992–2000	1.6%	0.7–2.4%	2.0%	1.3–2.7%	0.5%	0.0–1.3%
	2001–2006	2.7%	0.7–4.7%	2.7%	0.7–4.7%	No studies	
	2007–2012	4.5%	3.0–6.0%	2.3%	1.5–3.0%	6.9%	5.5–8.3%
Combination radio-colloid and blue dye	Whole period	2.1%	1.9–2.3%	1.5%	1.3–1.7%	2.6%	2.3–2.9%
	1992–2000	1.9%	1.7–2.1%	1.9%	1.5–2.2%	1.9%	1.6–2.3%
	2001–2006	1.9%	1.5–2.3%	1.1%	0.7–1.6%	2.5%	1.9–3.1%
	2007–2012	3.7%	2.8–4.5%	1.7%	0.0–3.4%	3.4%	3.0–3.8%
ICG	Whole period	4.4%	3.3–5.4%	2.8%	2.3–3.3%	14.3%*	12.9–15.7%
	1992–2000	2.7%*	2.5–2.9%	2.7%*	2.5–2.9%	No studies	
	2001–2006	4.3%*	3.9–4.7%	4.3%*	3.9–4.7%	No studies	
	2007–2012	5.2%	2.6–7.8%	2.5%	2.3–2.7%	14.3%*	12.9–15.7%
Combination radio-colloid and ICG	Whole period	0.1%	0.1–0.1%	0.1%	0.1–0.1%	0.0%	0.0–0.0%
	1992–2000	No studies		No studies		No studies	
	2001–2006	0.0%	0.0–0.0%	0.0%	0.0–0.0%	No studies	
	2007–2012	0.1%	0.1–0.1%	3.3%	0.0–9.8%	0.0%	0.0–0.0%

CI, confidence interval; ICG, indocyanine green.

* Derived from only one study.

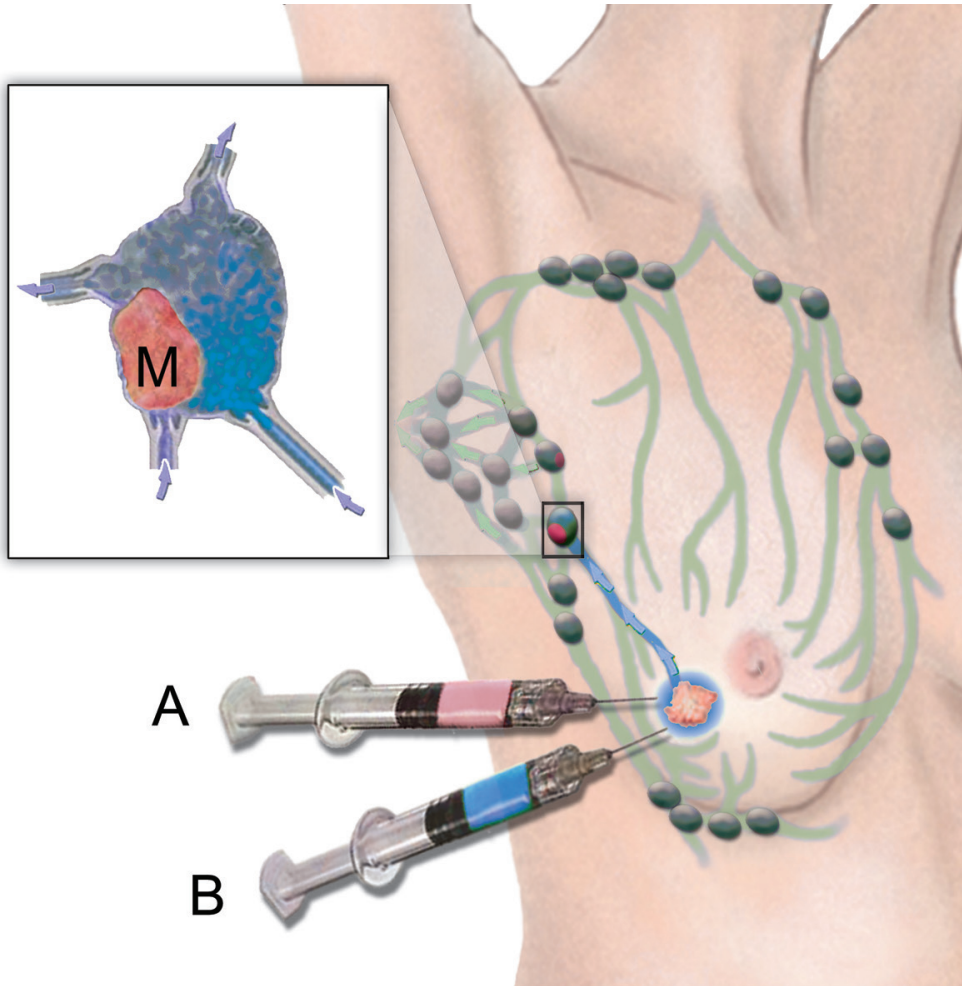


Figure 1. Schematic overview of the sentinel lymph node procedure in a breast cancer patient. Before surgery, the patient is injected peritumorally with a radiocolloid (A) and/or vital blue dye (B). Both substances flow along with the lymphatic fluid and accumulate in the sentinel lymph node. During surgery, the surgeon localizes the sentinel lymph node by visual inspection (blue dye) and a gamma probe (radiocolloid). After excision, the sentinel lymph node is evaluated for the presence of metastases (M) by a pathologist.

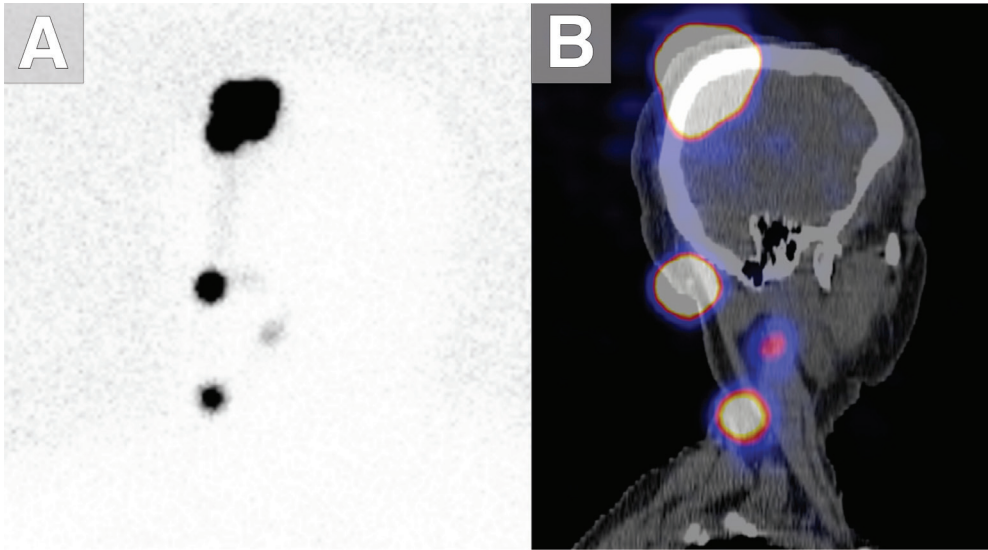


Figure 2. Lymphoscintigraphy (A) and SPECT/CT (B) images of a patient with a primary melanoma on the scalp and lymph nodes metastases in the neck.

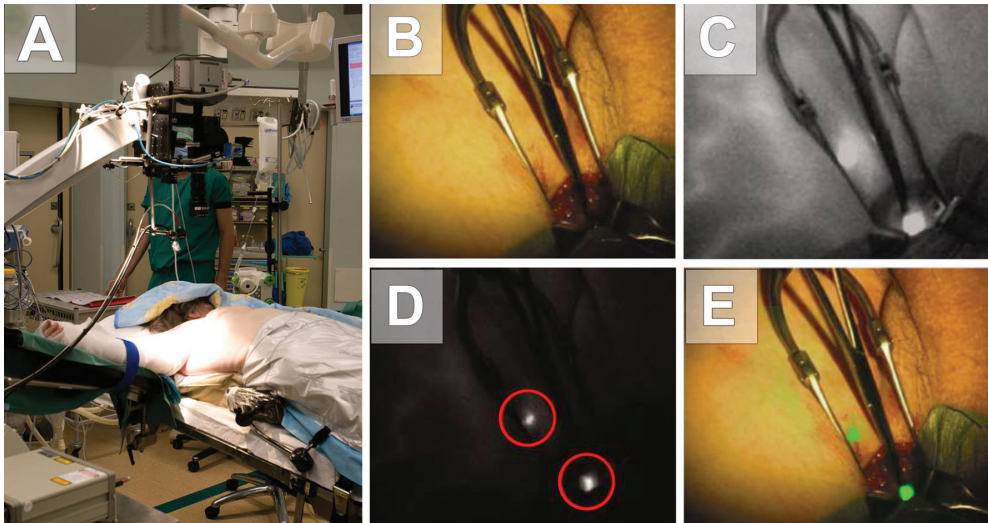


Figure 3. Intraoperative sentinel lymph node localization using a near-infrared fluorescence (NIRF) imaging device in combination with indocyanine green (ICG). The NIRF imaging device is positioned above the patient (A) and can be covered in sterile drapes for intraoperative use (not shown). A color image of the surgical field is shown, representing the axillary region of a breast cancer patient (B). After peritumoral injection with ICG, the NIRF imaging device is applied to visualize the sentinel lymph node (SLN) and corresponding lymphatic vessels (C). By adjusting the threshold for the fluorescent signal, the SLNs (indicated by red circles) become visible (D). For anatomical positioning of the fluorescent signal, the signal can be superposed on a color image of the surgical field as a contrasting pseudocolor (e.g., green; E).

DISCUSSION

SLNB is a widely accepted prognostic procedure in breast carcinoma and melanoma patients. Although a survival benefit compared to watchful waiting with ultrasound is yet to be shown, the status of the SLN is the most important predictor of prognosis and tumor recurrence for early-stage breast carcinoma and melanoma.¹⁹⁻²¹ In contrast to the worldwide acceptance of the procedure, controversies remain regarding the technical aspects of the procedure. The current study represents a systematic review of the published literature on SLNB in breast carcinoma and melanoma patients to evaluate the different SLNB techniques and judge them on their merits.

Identification rates of SLNB using blue dye and radiocolloid

The present study showed that pooled SLN IRs in breast carcinoma/melanoma patients are high for SLNB using solely blue dye (85/84%), solely radiocolloid (94/99%), and blue dye and radiocolloid combined (95/98%) and that FNRs are low (3.2/6.1%, 2.2/3.4%, 1.5/2.6%, respectively). In addition, IRs for all studied techniques steadily increased over time. For SLNB using solely radiocolloid, the IR of SLNB in breast carcinoma/melanoma patients has increased from 88/100% in 1992–2000 to 97/100% in 2007–2012. In the latter period, IR was similar compared to SLNB using a combination of radiocolloid with blue dye (97/99%). The increase in IR during the last 18 years is likely due to the increase in gained experience by the surgeons performing SLNB. Several studies have already reported that with the increase of gained experience by the surgeons, the IR of SLNB with solely radiocolloid also steadily increased with a decline in the marginal benefit offered by using blue dye.^{22,23}

In addition, there are some disadvantages of the use of blue dye. First, the use of blue dye as a guide in SLNB may lead to increasing tissue damage when tracing blue-stained lymphatics to the SLN compared to the use of a gamma probe to guide the path of dissection.²⁴ Second, allergic reactions to blue dye are seen in 0.14% to 3% of the patients, including urticaria, skin rash, erythema, blue hives, cardiovascular collapse, and anaphylactic shock.²⁵⁻³¹ Other side effects are temporary skin tattooing, blue discoloration of the operative field following peritumoral injection, blue-colored urine for up to 24 hr following administration, and a factitious drop in intraoperative oxygen saturation measured by pulse oximetry.²⁴ Furthermore, pregnancy is a relative contraindication due to the unknown teratogenicity and long-term toxicity to the fetus.

However, this should not preclude the use of blue dye by those surgeons who have mastered the technique of blue dye and have produced reliable results with high IRs and low FNRs. SLN mapping with a radiotracer is expensive and prohibited in most developing countries.³² Moreover, not all hospitals are equipped with a cyclotron to produce radioisotopes. SLN mapping using blue dye only should be encouraged in hospitals where radiotracers are not available as the IR for blue dye only is acceptable. Nevertheless, in the current study, the SLN IR when using solely blue dye was found to be 8% lower compared to solely radiocolloid and radiocolloid combined with blue dye. Furthermore, our results indicate that, in the present era, the addition of blue dye to radiotracers does not increase the SLN IR. Taken together with the disadvantages of blue dye, we advise surgeons working in hospitals where radiotracers are available and experienced with the radiocolloid SLNB technique, to perform SLNB using solely radiocolloid.

False negative rate

The pooled FNR for all techniques in all articles was at its peak in the last period (2007–2012), while the IR of SLNB has increased over time. This apparent contradiction might be due to the fact that only few surgeons were experienced with the SLNB procedure shortly after its introduction. When the procedure got widely accepted, less experienced surgeons had to perform SLNB, leading to an increased FNR. It is expected that the FNR will decline when surgeons are more familiar with the SLNB technique.

Type of dye

Apart from the debate on whether SLNB should be performed with blue dye, radiocolloid, or a combination of the two, there are also controversies on the type of dye or radiocolloid. For both breast carcinoma and melanoma studies included in this review, we analyzed different types of blue dye (patent blue, isosulfan blue, lymphozuran blue, or methylene blue) or radiocolloid (^{99m}Tc -sulfur colloid, ^{99m}Tc -human serum albumin, ^{99m}Tc -dextran 500, ^{99m}Tc -phytate, and ^{99m}Tc -tilmanocept). In the present study, univariate or multivariate analysis did not show an association with either the type of blue dye or the type of radiocolloid on IR or FNR. According to these results, the choice of the type of dye/radiocolloid should be based on the surgeon's preference or on the type of dye with the least side effects.

Injection site

Another issue in lymphatic mapping concerns the optimal injection site for dye/radiocolloid in patients with breast carcinoma. Whereas a consensus exists on injection sites for SLNB in melanoma patients (intradermal injection),²⁴ this is currently not the case in breast carcinoma. In the studies included in this review, blue dye and radiocolloid were injected intradermally (18 and 19 studies), subdermally (4 and 4 studies), intraparenchymally (8 and 3 studies), and subareolarly (12 and 12 studies). The present study showed no difference in IR for different injection sites. The choice on injection site can therefore be based on the surgeon's preference, taking previously reported practical advantages of the different injection sites into consideration.^{33–36} The injection of blue dye and radiocolloid in breast carcinoma is presented in Fig. 1.

Injection volume and massage

In breast carcinoma, a larger volume of injected blue dye was associated with a higher SLN IR, although this was only the case when blue dye was combined with radiocolloid. It is unclear why the volume of injected dye is only associated with a higher IR when using the combined technique. When SLNB was performed using solely blue dye, massage of the breast after dye injection was associated with higher IRs. Postinjection massage increases the flow of lymph fluid, significantly increasing the entry of blue dye and radiocolloid into the lymphatic capillaries.²⁴

Lymphoscintigraphy

Lymphoscintigraphy was not used in 4 of 126 studies (3.2%, all breast carcinoma patients) that used radiocolloid solely or in combination with blue.^{37–40} In these studies, only a hand-held gamma probe was used before incision to identify hot spots representing the location of the SLNs. Preoperative lymphoscintigraphy is important for providing a road map to guide the surgeon in identifying the regional nodal basin and estimating the location of SLNs.⁴¹ It is used to identify the lymph drainage basin, determine the number of SLNs, differentiate SLNs from

subsequent nodes, locate the SLN in an unexpected location, and mark the SLN over the skin for biopsy. Moreover, single-photon emission computed tomography/computed tomography (SPECT/CT) has shown important benefits, as a complementary modality for planar lymphoscintigraphy, in sentinel lymph node mapping.⁴² This type of image fusion provides better anatomical benchmarks, provides schematic information about the sentinel node site, and (perhaps most importantly) is easy to understand for surgeons, medical staff, and patients.⁴³ Lymphoscintigraphy and SPECT/CT images of a melanoma patient are presented in Fig. 2.

Definition of sentinel lymph node

Despite ongoing discussions, there is no consensus on the clinical definition of a SLN.²⁴ For this reason, a fair number of studies that used unconventional definitions were excluded from our study.^{10,46-53} In the present review, only studies were included that defined a hot node as 'nodes hotter than the background' or as 'nodes with more than 10% of the hottest node's radioactivity' (Supplementary File 1). The use of either the first or the latter definition did not influence IRs or FNRs for SLNB in both breast carcinoma and melanoma patients, suggesting that less lymph nodes were removed when using the 10% rule while the IR and FNR remained similar.

Near-infrared fluorescence imaging with indocyanine green

As an alternative to the conventional SLNB procedure, SLNB using the fluorescent dye ICG was recently introduced in the clinic.¹⁷ ICG has been used for the last three decades in patients for the study of organ perfusion and ophthalmology and has a safe and well-known pharmacological profile. When excited at the appropriate wavelength, ICG emits photons in the near-infrared fluorescence (NIRF) range of around 800 nm.

Because near-infrared light is invisible to the human eye, a special optical imaging system is needed to visualize the near-infrared signal in the surgical field. Already, several studies have reported on a prototype NIRF optical imaging system, with which the SLN can be detected noninvasively with high accuracy and sensitivity following subcutaneous injection with ICG.^{17,32,44-46} After injection, ICG flows along with the lymph fluid and accumulates in the SLNs within minutes, enabling rapid detection and visualization of SLNs as fluorescent hot spots. No adverse reactions were reported in any of the conducted trials.

NIRF optical imaging enhanced with ICG offers some considerable advantages to the current SLN procedure: the technique offers a high resolution, is relatively cheap, makes use of non-ionizing radiation, and offers high sensitivity and specificity rates.⁴⁷ The most important limitation of fluorescence imaging is the limited penetration depth of optical signals due to the absorption and scattering of photons when propagating through tissue.⁴⁸ The use of fluorescent dyes in the near-infrared spectral range, e.g., ICG, reduces absorption and scattering of photons true tissue, thereby increasing tissue penetration of the optical signal up to several centimeters. Furthermore, tissue autofluorescence in the near-infrared spectral range is minimized, resulting in an increased signal-to-noise ratio.⁴⁸

In the present study, the mean number of identified SLNs per patient when using ICG was considerably higher (ICG: 2.85 SLNs, ICG + radiocolloid: 2.87 SLNs) compared to solely blue dye (2.09 SLNs), solely radiocolloid (2.17 SLNs), or a combination of the two (1.89 SLNs). This difference might be explained by the small molecular size of ICG, facilitating rapid diffusion throughout the lymphatic system. Indeed, IRs up to 100% are described only 5 to 15 minutes following peritumoral injection when using solely ICG. A potential drawback of this rapid spread is that lymph nodes are excised that are not truly sentinel nodes (i.e., no first-draining

lymph nodes), leading to overtreatment and accompanying comorbidity. To solve this problem, ICG can be noncovalently linked to human serum albumin, of which the molecular size is substantially higher.³² In addition to reducing the spread of ICG, the binding to human serum albumin also increases the brightness of the fluorescent signal as it reduces quenching of the fluorescent molecules (i.e., reduction of fluorescent signal due to photons being absorbed by nearby fluorescent molecules).

CONCLUSION

The current meta-analysis provided data that favor the use of radiocolloid solely or radiocolloid combined with a blue dye for the identification of the SLN. Performing SLNB with radiocolloid solely is the technique of choice for experienced surgeons, since blue dye has multiple disadvantages. Moreover, NIRF imaging with ICG as a fluorescent dye seems a promising technique, although hurdles like the limited penetration depth of optical signals still reduces general applicability of the technique.

REFERENCES

1. Ferlay J, Shin HR, Bray F, Forman D, Mathers C, Parkin DM. Estimates of worldwide burden of cancer in 2008: GLOBOCAN 2008. *Int J Cancer*. 2010; 127(12):2893-2917.
2. Dutch comprehensive cancer centers. 2013. <http://ikcnet.nl/>. Accessed July 2013.
3. Krag D, Weaver D, Ashikaga T, et al. The sentinel node in breast cancer: a multicenter validation study. *N Engl J Med*. 1998; 339(14):941-946.
4. Morton DL, Wen DR, Wong JH, et al. Technical details of intraoperative lymphatic mapping for early-stage melanoma. *Arch Surg*. 1992; 127(4):392-399.
5. Gould EA, Winship T, Philbin PH, Kerr HH. Observations on a "sentinel node" in cancer of the parotid. *Cancer*. 1960; 13:77-78.
6. Tanis PJ, Nieweg OE, Valdes Olmos RA, Th Rutgers EJ, Kroon BB. History of sentinel node and validation of the technique. *Breast Cancer Res*. 2001; 3(2):109-112.
7. Cabanas RM. An approach for the treatment of penile carcinoma. *Cancer*. 1977; 39(2):456-466.
8. Alex JC, Krag DN. Gamma-probe guided localization of lymph nodes. *Surg Oncol*. 1993; 2(3):137-143.
9. Krag DN, Weaver DL, Alex JC, Fairbank JT. Surgical resection and radiolocalization of the sentinel lymph node in breast cancer using a gamma probe. *Surg Oncol*. 1993; 2(6):335-340..
10. Albertini JJ, Lyman GH, Cox C, et al. Lymphatic mapping and sentinel node biopsy in the patient with breast cancer. *JAMA*. 1996; 276(22):1818-1822.
11. Tanis PJ, Boom RP, Koops HS, et al. Frozen section investigation of the sentinel node in malignant melanoma and breast cancer. *Ann Surg Oncol*. 2001; 8(3):222-226.
12. Dutch Melanoma Workgroup. Dutch melanoma guidelines. 2012.
13. Quality institute for Health CBO. Dutch breast cancer guidelines. 2008.
14. de Vries M, Vonkeman WG, van Ginkel RJ, Hoekstra HJ. Morbidity after inguinal sentinel lymph node biopsy and completion lymph node dissection in patients with cutaneous melanoma. *Eur J Surg Oncol*. 2006; 32(7):785-789.
15. Kootstra JJ, Dijkstra PU, Rietman H, et al. A longitudinal study of shoulder and arm morbidity in breast cancer survivors 7 years after sentinel lymph node biopsy or axillary lymph node dissection. *Breast Cancer Res Treat*. 2013; 139(1):125-134.
16. Kim T, Giuliano AE, Lyman GH. Lymphatic mapping and sentinel lymph node biopsy in early-stage breast carcinoma: A metaanalysis. *Cancer*. 2006; 106(1):4-16.
17. Kitai T, Inomoto T, Miwa M, Shikayama T. Fluorescence navigation with indocyanine green for detecting sentinel lymph nodes in breast cancer. *Breast Cancer*. 2005; 12(3):211-215.
18. Whiting P, Rutjes AW, Reitsma JB, Bossuyt PM, Kleijnen J. The development of QUADAS: A tool for the quality assessment of studies of diagnostic accuracy included in systematic reviews. *BMC Med Res Methodol*. 2003; 3:25.
19. Singletary SE, Connolly JL. Breast cancer staging: Working with the sixth edition of the AJCC cancer staging manual. *CA Cancer J Clin*. 2006; 56(1):37-47; quiz 50-1.
20. Balch CM, Gershenwald JE, Soong SJ, et al. Final version of 2009 AJCC melanoma staging and classification. *J Clin Oncol*. 2009; 27(36):6199-6206.
21. Gershenwald JE, Thompson W, Mansfield PF, et al. Multi-institutional melanoma lymphatic mapping experience: The prognostic value of sentinel lymph node status in 612 stage I or II melanoma patients. *J Clin Oncol*. 1999; 17(3):976-983.
22. Derossis AM, Fey J, Yeung H, et al. A trend analysis of the relative value of blue dye and isotope localization in 2,000 consecutive cases of sentinel node biopsy for breast cancer. *J Am Coll Surg*. 2001; 193(5):473-478.
23. Kang T, Yi M, Hunt KK, et al. Does blue dye contribute to success of sentinel node mapping for breast cancer? *Ann Surg Oncol*. 2010; 17 Suppl 3:280-285.

24. Bagaria SP, Faries MB, Morton DL. Sentinel node biopsy in melanoma: Technical considerations of the procedure as performed at the John Wayne Cancer Institute. *J Surg Oncol.* 2010; 101(8):669-676.
25. Argon AM, Duygun U, Acar E, et al. The use of periareolar intradermal Tc-99m tin colloid and peritumoral intraparenchymal isosulfan blue dye injections for determination of the sentinel lymph node. *Clin Nucl Med.* 2006; 31(12):795-800.
26. Bines S, Kopkash K, Ali A, Fogg L, Wool N. The use of radioisotope combined with isosulfan blue dye is not superior to radioisotope alone for the identification of sentinel lymph nodes in patients with breast cancer. *Surgery.* 2008; 144(4):606-610.
27. King TA, Fey JV, Van Zee KJ, et al. A prospective analysis of the effect of blue-dye volume on sentinel lymph node mapping success and incidence of allergic reaction in patients with breast cancer. *Ann Surg Oncol.* 2004; 11(5):535-541.
28. Roulin D, Matter M, Bady P, et al. Prognostic value of sentinel node biopsy in 327 prospective melanoma patients from a single institution. *Eur J Surg Oncol.* 2008; 34(6):673-679.
29. Rughani MG, Swan MC, Adams TS, et al. Sentinel lymph node biopsy in melanoma: The Oxford ten year clinical experience. *J Plast Reconstr Aesthet Surg.* 2011; 64(10):1284-1290.
30. Topping A, Dewar D, Rose V, et al. Five years of sentinel node biopsy for melanoma: The St George's melanoma unit experience. *Br J Plast Surg.* 2004; 57(2):97-104.
31. Bezu C, Coutant C, Salengro A, Darai E, Rouzier R, Uzan S. Anaphylactic response to blue dye during sentinel lymph node biopsy. *Surg Oncol.* 2011; 20(1):e55-9.
32. Troyan SL, Kianzad V, Gibbs-Strauss SL, et al. The FLARE intraoperative near-infrared fluorescence imaging system: A first-in-human clinical trial in breast cancer sentinel lymph node mapping. *Ann Surg Oncol.* 2009; 16(10):2943-2952.
33. Lin KM, Patel TH, Ray A, et al. Intradermal radioisotope is superior to peritumoral blue dye or radioisotope in identifying breast cancer sentinel nodes. *J Am Coll Surg.* 2004; 199(4):561-566.
34. Martin RC, Derossis AM, Fey J, et al. Intradermal isotope injection is superior to intramammary in sentinel node biopsy for breast cancer. *Surgery.* 2001; 130(3):432-438.
35. McMasters KM, Wong SL, Martin RC, 2nd, et al. Dermal injection of radioactive colloid is superior to peritumoral injection for breast cancer sentinel lymph node biopsy: Results of a multiinstitutional study. *Ann Surg.* 2001; 233(5):676-687.
36. Rodier JF, Velten M, Wilt M, et al. Prospective multicentric randomized study comparing periareolar and peritumoral injection of radiotracer and blue dye for the detection of sentinel lymph node in breast sparing procedures: FRANSENODE trial. *J Clin Oncol.* 2007; 25(24):3664-3669.
37. Krag DN, Anderson SJ, Julian TB, et al. Technical outcomes of sentinel lymph node resection and conventional axillary-lymph-node dissection in patients with clinically node-negative breast cancer: Results from the NSABP B-32 randomised phase III trial. *Lancet Oncol.* 2007; 8(10):881-888.
38. Lauridsen MC, Garne JP, Hessov I, et al. Sentinel lymph node biopsy in breast cancer: the Aarhus experience. *Acta Oncol.* 2000; 39(3):421-422.
39. Morrow M, Rademaker AW, Bethke KP, et al. Learning sentinel node biopsy: Results of a prospective randomized trial of two techniques. *Surgery.* 1999; 126(4):714-722.
40. Thompson M, Korourian S, Henry-Tillman R, et al. Intraoperative radioisotope injection for sentinel lymph node biopsy. *Ann Surg Oncol.* 2008; 15(11):3216-3221.
41. Thompson JF, Uren RF. Teaching points on lymphatic mapping for melanoma from the Sydney melanoma unit. *Semin Oncol.* 2004; 31(3):349-356.
42. Ho Shon IA, Chung DK, Saw RP, Thompson JF. Imaging in cutaneous melanoma. *Nucl Med Commun.* 2008; 29(10):847-876.
43. Alvarez Paez AM, Brouwer OR, Veenstra HJ, et al. Decisive role of SPECT/CT in localization of unusual periscapular sentinel nodes in patients with posterior trunk melanoma: Three illustrative cases and a review of the literature. *Melanoma Res.* 2012; 22(3):278-283.

44. Fujiwara M, Mizukami T, Suzuki A, Fukamizu H. Sentinel lymph node detection in skin cancer patients using real-time fluorescence navigation with indocyanine green: Preliminary experience. *J Plast Reconstr Aesthet Surg.* 2009; 62(10):e373-8.
45. Themelis G, Yoo JS, Ntziachristos V. Multispectral imaging using multiple-bandpass filters. *Opt Lett.* 2008; 33(9):1023-1025.
46. Keereweer S, Kerrebijn JD, van Driel PB, et al. Optical image-guided surgery – where do we stand? *Mol Imaging Biol.* 2011; 13(2):199-207.
47. Pleijhuis RG, Graafland M, de Vries J, Bart J, de Jong JS, van Dam GM. Obtaining adequate surgical margins in breast-conserving therapy for patients with early-stage breast cancer: Current modalities and future directions. *Ann Surg Oncol.* 2009; 16(10):2717-2730.
48. Ntziachristos V. Fluorescence molecular imaging. *Annu Rev Biomed Eng.* 2006; 8:1-33.
49. Giuliano AE. Intradermal blue dye to identify sentinel lymph node in breast cancer. *Lancet.* 1997; 350(9082):958.
50. Barnwell JM, Arredondo MA, Kollmorgen D, et al. Sentinel node biopsy in breast cancer. *Ann Surg Oncol.* 1998; 5(2):126-130.
51. Crossin JA, Johnson AC, Stewart PB, Turner WW, Jr. Gamma-probe-guided resection of the sentinel lymph node in breast cancer. *Am Surg.* 1998; 64(7):666-669.
52. Flett MM, Going JJ, Stanton PD, Cooke TG. Sentinel node localization in patients with breast cancer. *Br J Surg.* 1998; 85(7):991-993.
53. Kapteijn BA, Nieweg OE, Petersen JL, et al. Identification and biopsy of the sentinel lymph node in breast cancer. *Eur J Surg Oncol.* 1998; 24(5):427-430.
54. Ratanawichitrasin A, Levy L, Myles J, Crowe JP. Experience with lymphatic mapping in breast cancer using isosulfan blue dye. *J Womens Health.* 1998; 7(7):873-877.
55. Snider H, Dowlatshahi K, Fan M, Bridger WM, Rayudu G, Oleske D. Sentinel node biopsy in the staging of breast cancer. *Am J Surg.* 1998; 176(4):305-310.
56. Jaderborg JM, Harrison PB, Kiser JL, Maynard SL. The feasibility and accuracy of the sentinel lymph node biopsy for breast carcinoma. *Am Surg.* 1999; 65(8):699-705.
57. Kollias J, Gill PG, Chatterton BE, et al. Reliability of sentinel node status in predicting axillary lymph node involvement in breast cancer. *Med J Aust.* 1999; 171(9):461-465.
58. Moffat FL, Jr, Gulec SA, Sittler SY, et al. Unfiltered sulfur colloid and sentinel node biopsy for breast cancer: Technical and kinetic considerations. *Ann Surg Oncol.* 1999; 6(8):746-755.
59. Morgan A, Howisey RL, Aldape HC, et al. Initial experience in a community hospital with sentinel lymph node mapping and biopsy for evaluation of axillary lymph node status in palpable invasive breast cancer. *J Surg Oncol.* 1999; 72(1):24-31.
60. Veronesi U, Paganelli G, Viale G, et al. Sentinel lymph node biopsy and axillary dissection in breast cancer: Results in a large series. *J Natl Cancer Inst.* 1999; 91(4):368-373.
61. Winchester DJ, Sener SF, Winchester DP, et al. Sentinel lymphadenectomy for breast cancer: Experience with 180 consecutive patients: Efficacy of filtered technetium 99m sulphur colloid with overnight migration time. *J Am Coll Surg.* 1999; 188(6):597-603.
62. Canavese G, Gipponi M, Catturich A, et al. Sentinel lymph node mapping in early-stage breast cancer: Technical issues and results with vital blue dye mapping and radioguided surgery. *J Surg Oncol.* 2000; 74(1):61-68.
63. Cox CE, Salud C, Whitehead GF, Reintgen DS. Sentinel lymph node biopsy for breast cancer: Combined dye-isotope technique. *Breast Cancer.* 2000; 7(4):389-397.
64. Doting MH, Jansen L, Nieweg OE, et al. Lymphatic mapping with intralesional tracer administration in breast carcinoma patients. *Cancer.* 2000; 88(11):2546-2552.
65. Fraile M, Rull M, Julian FJ, et al. Sentinel node biopsy as a practical alternative to axillary lymph node dissection in breast cancer patients: An approach to its validity. *Ann Oncol.* 2000; 11(6):701-705.

66. Liu LH, Siziopikou KP, Gabram S, McClatchey KD. Evaluation of axillary sentinel lymph node biopsy by immunohistochemistry and multilevel sectioning in patients with breast carcinoma. *Arch Pathol Lab Med.* 2000; 124(11):1670-1673.
67. Rodier JF, Routiot T, Mignotte H, et al. Lymphatic mapping and sentinel node biopsy of operable breast cancer. *World J Surg.* 2000; 24(10):1220-1226.
68. Tsugawa K, Noguchi M, Miwa K, et al. Dye- and gamma probe-guided sentinel lymph node biopsy in breast cancer patients: Using patent blue dye and technetium-99m-labeled human serum albumin. *Breast Cancer.* 2000; 7(1):87-94.
69. Feggi L, Basaglia E, Corcione S, et al. An original approach in the diagnosis of early breast cancer: Use of the same radiopharmaceutical for both nonpalpable lesions and sentinel node localisation. *Eur J Nucl Med.* 2001; 28(11):1589-1596.
70. Mateos JJ, Vidal-Sicart S, Zanon G, et al. Sentinel lymph node biopsy in breast cancer patients: Subdermal versus peritumoral radiocolloid injection. *Nucl Med Commun.* 2001; 22(1):17-24.
71. Sato K, Uematsu M, Saito T, et al. Sentinel lymph node identification for patients with breast cancer using large-size radiotracer particles: Technetium-99m-labeled tin colloids produced excellent results. *Breast J.* 2001; 7(6):388-391.
72. Simmons RM, Smith SM, Osborne MP. Methylene blue dye as an alternative to isosulfan blue dye for sentinel lymph node localization. *Breast J.* 2001; 7(3):181-183.
73. Tafra L, Lannin DR, Swanson MS, et al. Multicenter trial of sentinel node biopsy for breast cancer using both technetium sulfur colloid and isosulfan blue dye. *Ann Surg.* 2001; 233(1):51-59.
74. Tanis PJ, Deurloo EE, Valdes Olmos RA, et al. Single intralesional tracer dose for radio-guided excision of clinically occult breast cancer and sentinel node. *Ann Surg Oncol.* 2001; 8(10):850-855.
75. Xavier NL, Amaral BB, Cerski CT, et al. Sentinel lymph node identification and sampling in women with early breast cancer using 99m tc labelled dextran 500 and patent blue V dye. *Nucl Med Commun.* 2001; 22(10):1109-1117.
76. Watanabe T, Kimijima I, Ohtake T, Tsuchiya A, Shishido F, Takenoshita S. Sentinel node biopsy with technetium-99m colloidal rhenium sulphide in patients with breast cancer. *Br J Surg.* 2001; 88(5):704-707.
77. Feezor RJ, Kasraeian A, Copeland EM, 3rd, et al. Sequential dermal-peritumoral radiocolloid injection for sentinel node biopsy for breast cancer: The university of florida experience. *Am Surg.* 2002; 68(8):684-688. d
78. Kern KA. Concordance and validation study of sentinel lymph node biopsy for breast cancer using subareolar injection of blue dye and technetium 99m sulfur colloid. *J Am Coll Surg.* 2002; 195(4):467-475.
79. Jastrzebski T, Kopacz A, Lass P. Comparison of peritumoral and subareolar injection of Tc99m sulphur colloid and blue-dye for detection of the sentinel lymph node in breast cancer. *Nucl Med Rev Cent East Eur.* 2002; 5(2):159-161.
80. Shimazu K, Tamaki Y, Taguchi T, Takamura Y, Noguchi S. Comparison between periareolar and peritumoral injection of radiotracer for sentinel lymph node biopsy in patients with breast cancer. *Surgery.* 2002; 131(3):277-286.
81. Nos C, Freneaux P, Louis-Sylvestre C, et al. Macroscopic quality control improves the reliability of blue dye-only sentinel lymph node biopsy in breast cancer. *Ann Surg Oncol.* 2003; 10(5):525-530.
82. Reitsamer R, Peintinger F, Rettenbacher L, Prokop E, Sedlmayer F. Subareolar subcutaneous injection of blue dye versus peritumoral injection of technetium-labeled human albumin to identify sentinel lymph nodes in breast cancer patients. *World J Surg.* 2003; 27(12):1291-1294.
83. Simmons R, Thevarajah S, Brennan MB, Christos P, Osborne M. Methylene blue dye as an alternative to isosulfan blue dye for sentinel lymph node localization. *Ann Surg Oncol.* 2003; 10(3):242-247.
84. Eldrageely K, Vargas MP, Khalkhali I, et al. Sentinel lymph node mapping of breast cancer: A case-control study of methylene blue tracer compared to isosulfan blue. *Am Surg.* 2004; 70(10):872-875.

85. Gray RJ, Pockaj BA, Roarke MC. Injection of (99m)tc-labeled sulfur colloid the day before operation for breast cancer sentinel lymph node mapping is as successful as injection the day of operation. *Am J Surg.* 2004; 188(6):685-689.
86. Nour A. Efficacy of methylene blue dye in localization of sentinel lymph node in breast cancer patients. *Breast J.* 2004; 10(5):388-391.
87. Radovanovic Z, Golubovic A, Plzak A, Stojiljkovic B, Radovanovic D. Blue dye versus combined blue dye-radioactive tracer technique in detection of sentinel lymph node in breast cancer. *Eur J Surg Oncol.* 2004; 30(9):913-917.
88. van Wessem KJ, Meijer WS. Sentinel lymph node biopsy in breast cancer: Results of intradermal periareolar tracer injection and follow-up of sentinel lymph node-negative patients. *Breast.* 2004; 13(4):290-296.
89. Hung WK, Chan CM, Ying M, Chong SF, Mak KL, Yip AW. Randomized clinical trial comparing blue dye with combined dye and isotope for sentinel lymph node biopsy in breast cancer. *Br J Surg.* 2005; 92(12): 1494-1497.
90. Syme DB, Collins JP, Mann GB. Comparison of blue dye and isotope with blue dye alone in breast sentinel node biopsy. *ANZ J Surg.* 2005; 75(9):817-821.
91. Teal CB, Slocum JP, Akin EA. Evaluation of the benefit of using blue dye in addition to radioisotope for sentinel lymph node biopsy in patients with breast cancer. *Breast J.* 2005; 11(6):391-393.
92. Golshan M, Nakhli F. Can methylene blue only be used in sentinel lymph node biopsy for breast cancer? *Breast J.* 2006; 12(5):428-430.
93. Lo YF, Hsueh S, Ma SY, Chen SC, Chen MF. Radioguided sentinel lymph node biopsy in early breast cancer: Experience at chang gung memorial hospital. *Chang Gung Med J.* 2006; 29(5):458-467.
94. Povoski SP, Olsen JO, Young DC, et al. Prospective randomized clinical trial comparing intradermal, intraparenchymal, and subareolar injection routes for sentinel lymph node mapping and biopsy in breast cancer. *Ann Surg Oncol.* 2006; 13(11):1412-1421.
95. Takei H, Suemasu K, Kurosumi M, et al. Added value of the presence of blue nodes or hot nodes in sentinel lymph node biopsy of breast cancer. *Breast Cancer.* 2006; 13(2):179-185.
96. Zaman MU, Khan S, Hussain R, Ahmed MN. Sentinel lymph node scintigraphy and radioguided dissection in breast carcinoma: An initial experience at aga khan university hospital. *J Pak Med Assoc.* 2006; 56(4):153-156.
97. Kargozaran H, Shah M, Li Y, et al. Concordance of peritumoral technetium 99m colloid and subareolar blue dye injection in breast cancer sentinel lymph node biopsy. *J Surg Res.* 2007; 143(1):126-129.
98. Nathanson SD, Grogan JK, DeBruyn D, Kapke A, Karvelis K. Breast cancer sentinel lymph node identification rates: The influence of radiocolloid mapping, case volume, and the place of the procedure. *Ann Surg Oncol.* 2007; 14(5):1629-1637.
99. Varghese P, Mostafa A, Abdel-Rahman AT, et al. Methylene blue dye versus combined dye-radioactive tracer technique for sentinel lymph node localisation in early breast cancer. *Eur J Surg Oncol.* 2007; 33(2):147-152.
100. Yen RF, Kuo WH, Lien HC, et al. Radio-guided sentinel lymph node biopsy using periareolar injection technique for patients with early breast cancer. *J Formos Med Assoc.* 2007; 106(1):44-50.
101. Mudun A, Sanli Y, Ozmen V, et al. Comparison of different injection sites of radionuclide for sentinel lymph node detection in breast cancer: Single institution experience. *Clin Nucl Med.* 2008; 33(4):262-267.
102. Zakaria S, Hoskin TL, Degnim AC. Safety and technical success of methylene blue dye for lymphatic mapping in breast cancer. *Am J Surg.* 2008; 196(2):228-233.
103. Climaco F, Coelho-Oliveira A, Djahjah MC, et al. Sentinel lymph node identification in breast cancer: A comparison study of deep versus superficial injection of radiopharmaceutical. *Nucl Med Commun.* 2009; 30(7):525-532.
104. Koukouraki S, Sanidas E, Askoxilakis J, et al. Is there any benefit from sentinel lymph node biopsy using the combined radioisotope/dye technique in breast cancer patients with clinically negative axilla? *Nucl Med Commun.* 2009; 30(1):48-53.
105. Mathelin C, Croce S, Brasse D, et al. Methylene blue dye, an accurate dye for sentinel lymph node identification in early breast cancer. *Anticancer Res.* 2009; 29(10):4119-4125.

106. Hayashida T, Jinno H, Sakata M, et al. Superiority of radioisotope over blue dye for sentinel lymph node detection in breast cancer. *Eur Surg Res.* 2010; 44(2):111-116.
107. Krikanova M, Biggar M, Moss D, Poole G. Accuracy of sentinel node biopsy for breast cancer using blue dye alone. *Breast J.* 2010; 16(4):384-388.
108. Narui K, Ishikawa T, Kito A, et al. Observational study of blue dye-assisted four-node sampling for axillary staging in early breast cancer. *Eur J Surg Oncol.* 2010; 36(8):731-736.
109. Straver ME, Meijnen P, van Tienhoven G, et al. Sentinel node identification rate and nodal involvement in the EORTC 10981-22023 AMAROS trial. *Ann Surg Oncol.* 2010; 17(7):1854-1861.
110. Yararbas U, Argon AM, Yeniay L, Zengel B, Kapkac M. The effect of radiocolloid preference on major parameters in sentinel lymph node biopsy practice in breast cancer. *Nucl Med Biol.* 2010; 37(7):805-810.
111. Lida S, Haga S, Yamashita K, et al. Evaluation of sentinel lymph node biopsy in clinically node-negative breast cancer. *J Nippon Med Sch.* 2011; 78(2):96-100.
112. Mieog JS, Troyan SL, Hutteman M, et al. Toward optimization of imaging system and lymphatic tracer for near-infrared fluorescent sentinel lymph node mapping in breast cancer. *Ann Surg Oncol.* 2011; 18(9):2483-2491.
113. Thompson JF, McCarthy WH, Bosch CM, et al. Sentinel lymph node status as an indicator of the presence of metastatic melanoma in regional lymph nodes. *Melanoma Res.* 1995; 5(4):255-260.
114. Albertini JJ, Cruse CW, Rapaport D, et al. Intraoperative radio-lympho-scintigraphy improves sentinel lymph node identification for patients with melanoma. *Ann Surg.* 1996; 223(2):217-224.
115. Thompson JF, Niewind P, Uren RF, Bosch CM, Howman-Giles R, Vrouenraets BC. Single-dose isotope injection for both preoperative lymphoscintigraphy and intraoperative sentinel lymph node identification in melanoma patients. *Melanoma Res.* 1997; 7(6):500-506.
116. Wells KE, Rapaport DP, Cruse CW, et al. Sentinel lymph node biopsy in melanoma of the head and neck. *Plast Reconstr Surg.* 1997; 100(3):591-594.
117. Bartolomei M, Testori A, Chinol M, et al. Sentinel node localization in cutaneous melanoma: Lymphoscintigraphy with colloids and antibody fragments versus blue dye mapping. *Eur J Nucl Med.* 1998; 25(11):1489-1494.
118. Bedrosian I, Scheff AM, Mick R, et al. ^{99m}Tc-human serum albumin: An effective radiotracer for identifying sentinel lymph nodes in melanoma. *J Nucl Med.* 1999; 40(7):1143-1148.
119. Bostick P, Essner R, Glass E, et al. Comparison of blue dye and probe-assisted intraoperative lymphatic mapping in melanoma to identify sentinel nodes in 100 lymphatic basins. *Arch Surg.* 1999; 134(1):43-49.
120. Gennari R, Stoldt HS, Bartolomei M, et al. Sentinel node localisation: A new prospective in the treatment of nodal melanoma metastases. *Int J Oncol.* 1999; 15(1):25-32.
121. Gershenwald JE, Thompson W, Mansfield PF, et al. Multi-institutional melanoma lymphatic mapping experience: The prognostic value of sentinel lymph node status in 612 stage I or II melanoma patients. *J Clin Oncol.* 1999; 17(3):976-983.
122. Morton DL, Thompson JF, Essner R, et al. Validation of the accuracy of intraoperative lymphatic mapping and sentinel lymphadenectomy for early-stage melanoma: A multicenter trial. multicenter selective lymphadenectomy trial group. *Ann Surg.* 1999; 230(4):453-465.
123. Jansen L, Nieweg OE, Kapteijn AE, et al. Reliability of lymphoscintigraphy in indicating the number of sentinel nodes in melanoma patients. *Ann Surg Oncol.* 2000; 7(8):624-630.
124. Jansen L, Koops HS, Nieweg OE, et al. Sentinel node biopsy for melanoma in the head and neck region. *Head Neck.* 2000; 22(1):27-33.
125. Landi G, Polverelli M, Moscatelli G, et al. Sentinel lymph node biopsy in patients with primary cutaneous melanoma: Study of 455 cases. *J Eur Acad Dermatol Venereol.* 2000; 14(1):35-45.
126. Oliveira Filho RS, Santos ID, Ferreira LM, et al. Is intra-operative gamma probe detection really necessary for inguinal sentinel lymph node biopsy? *Sao Paulo Med J.* 2000; 118(6):165-168.

127. Temple CL, Scilley CG, Engel CJ, et al. Sentinel node biopsy in melanoma using technetium-99m rhenium colloid: The London experience. *Ann Plast Surg.* 2000; 45(5):491-499.
128. Tremblay F, Louffi A, Shibata H, Meterissian S. Sentinel lymph-node biopsy for melanoma of the trunk and extremities: The McGill experience. *Can J Surg.* 2001; 44(6):428-431.
129. Villa G, Agnese G, Bianchi P, et al. Mapping the sentinel lymph node in malignant melanoma by blue dye, lymphoscintigraphy and intraoperative gamma probe. *Tumori.* 2000; 86(4):343-345.
130. McMasters KM, Reintgen DS, Ross MI, et al. Sentinel lymph node biopsy for melanoma: How many radioactive nodes should be removed? *Ann Surg Oncol.* 2001; 8(3):192-197.
131. Medina-Franco H, Beenken SW, Heslin MJ, Urist MM. Sentinel node biopsy for cutaneous melanoma in the head and neck. *Ann Surg Oncol.* 2001; 8(9):716-719.
132. Neubauer S, Mena I, Igleis R, et al. Sentinel lymph node mapping in melanoma with technetium-99m dextran. *Cancer Biother Radiopharm.* 2001; 16(3):265-267.
133. Rasgon BM. Use of low-dose technetium tc 99m sulfur colloid to locate sentinel lymph nodes in melanoma of the head and neck: Preliminary study. *Laryngoscope.* 2001; 111(8):1366-1372.
134. Tavares MG, Sapienza MT, Galeb NA, Jr, et al. The use of 99mTc-phytate for sentinel node mapping in melanoma, breast cancer and vulvar cancer: A study of 100 cases. *Eur J Nucl Med.* 2001; 28(11):1597-1604.
135. Eicher SA, Clayman GL, Myers JN, Gillenwater AM. A prospective study of intraoperative lymphatic mapping for head and neck cutaneous melanoma. *Arch Otolaryngol Head Neck Surg.* 2002; 128(3):241-246.
136. Ferrone CR, Panageas KS, Busam K, Brady MS, Coit DG. Multivariate prognostic model for patients with thick cutaneous melanoma: Importance of sentinel lymph node status. *Ann Surg Oncol.* 2002; 9(7):637-645.
137. Patel SG, Coit DG, Shaha AR, et al. Sentinel lymph node biopsy for cutaneous head and neck melanomas. *Arch Otolaryngol Head Neck Surg.* 2002; 128(3):285-291.
138. Chao C, Wong SL, Edwards MJ, et al. Sentinel lymph node biopsy for head and neck melanomas. *Ann Surg Oncol.* 2003; 10(1):21-26.
139. Estourgie SH, Nieweg OE, Valdes Olmos RA, Hoefnagel CA, Kroon BB. Review and evaluation of sentinel node procedures in 250 melanoma patients with a median follow-up of 6 years. *Ann Surg Oncol.* 2003; 10(6): 681-688.
140. Schmalbach CE, Nussenbaum B, Rees RS, Schwartz J, Johnson TM, Bradford CR. Reliability of sentinel lymph node mapping with biopsy for head and neck cutaneous melanoma. *Arch Otolaryngol Head Neck Surg.* 2003; 129(1):61-65.
141. Vidal-Sicart S, Pons F, Puig S, et al. Identification of the sentinel lymph node in patients with malignant melanoma: What are the reasons for mistakes? *Eur J Nucl Med Mol Imaging.* 2003; 30(3):362-366.
142. Weiss M, Kunte C, Schmid RA, Konz B, Dresel S, Hahn K. Sentinel node mapping in patients with malignant melanoma using melanoma tc-99m colloidal rhenium sulfide. *Clin Nucl Med.* 2003; 28(5):379-384.
143. Alex JC. The application of sentinel node radiolocalization to solid tumors of the head and neck: A 10-year experience. *Laryngoscope.* 2004; 114(1):2-19.
144. Chakera AH, Drzewiecki KT, Eigved A, Juhl BR. Sentinel node biopsy for melanoma: A study of 241 patients. *Melanoma Res.* 2004; 14(6):521-526.
145. Gipponi M, Di Somma C, Peressini A, et al. Sentinel lymph node biopsy in patients with stage I/II melanoma: Clinical experience and literature review. *J Surg Oncol.* 2004; 85(3):133-140.
146. Rossi CR, Testori A, Mocellin S, Campana L, Lejeune F. Melanoma - what is new in sentinel node biopsy and locoregional treatments in 2003? report of a workshop at the third research meeting on melanoma, Milan, Italy, May 2003. *Melanoma Res.* 2004; 14(5):329-332.
147. Shpitzer T, Segal K, Schachter J, et al. Sentinel node guided surgery for melanoma in the head and neck region. *Melanoma Res.* 2004; 14(4):283-287.
148. Carlson GW, Murray DR, Lyles RH, Hestley A, Cohen C. Sentinel lymph node biopsy in the management of cutaneous head and neck melanoma. *Plast Reconstr Surg.* 2005; 115(3):721-728.

149. MacNeill KN, Ghazarian D, McCready D, Rotstein L. Sentinel lymph node biopsy for cutaneous melanoma of the head and neck. *Ann Surg Oncol.* 2005; 12(9):726-732.
150. Doting EH, de Vries M, Plukker JT, et al. Does sentinel lymph node biopsy in cutaneous head and neck melanoma alter disease outcome? *J Surg Oncol.* 2006; 93(7):564-570.
151. Gad D, Hoiland-Carlsen PF, Bartram P, Clemmensen O, Bischoff-Mikkelsen M. Staging patients with cutaneous malignant melanoma by same-day lymphoscintigraphy and sentinel lymph node biopsy: A single-institutional experience with emphasis on recurrence. *J Surg Oncol.* 2006; 94(2):94-100.
152. Lin D, Franc BL, Kashani-Sabet M, Singer MI. Lymphatic drainage patterns of head and neck cutaneous melanoma observed on lymphoscintigraphy and sentinel lymph node biopsy. *Head Neck.* 2006; 28(3):249-255.
153. Oliveira Filho RS, Silva AM, Hochman B, et al. Vital dye is enough for inguinal sentinel lymph node biopsy in melanoma patients. *Acta Cir Bras.* 2006; 21(1):12-15.
154. Cecchi R, Buralli L, Innocenti S, Seghieri G, De Gaudio C. Sentinel lymph node biopsy in patients with thick (= 4 mm) melanoma: A single-centre experience. *J Eur Acad Dermatol Venereol.* 2007; 21(6):758-761.
155. Kilpatrick LA, Shen P, Stewart JH, Levine EA. Use of sentinel lymph node biopsy for melanoma of the head and neck. *Am Surg.* 2007; 73(8):754-759.
156. Koskivuo I, Talve L, Vihinen P, Maki M, Vahlberg T, Suominen E. Sentinel lymph node biopsy in cutaneous melanoma: A case-control study. *Ann Surg Oncol.* 2007; 14(12):3566-3574.
157. Teltzrow T, Osinga J, Schwipper V. Reliability of sentinel lymph-node extirpation as a diagnostic method for malignant melanoma of the head and neck region. *Int J Oral Maxillofac Surg.* 2007; 36(6):481-487.
158. Gomez-Rivera F, Santillan A, McMurphey AB, et al. Sentinel node biopsy in patients with cutaneous melanoma of the head and neck: Recurrence and survival study. *Head Neck.* 2008; 30(10):1284-1294.
159. Liu Y, Truini C, Ariyan S. A randomized study comparing the effectiveness of methylene blue dye with lymphazurin blue dye in sentinel lymph node biopsy for the treatment of cutaneous melanoma. *Ann Surg Oncol.* 2008; 15(9):2412-2417.
160. Mattsson J, Bergkvist L, Abdou A, et al. Sentinel node biopsy in malignant melanoma: Swedish experiences 1997-2005. *Acta Oncol.* 2008; 47(8):1519-1525.
161. Kelly J, Fogarty K, Redmond HP. A definitive role for sentinel lymph node mapping with biopsy for cutaneous melanoma of the head and neck. *Surgeon.* 2009; 7(6):336-339.
162. Kovacevic P, Visnjic M, Vljakovic M, Kovacevic T, Visnjic A. Sentinel node biopsy for skin melanoma. *Vojnosanit Pregl.* 2009; 66(8):657-662.
163. Koskivuo I, Hernberg M, Vihinen P, et al. Sentinel lymph node biopsy and survival in elderly patients with cutaneous melanoma. *Br J Surg.* 2011; 98(10):1400-1407.
164. Leong SP, Kim J, Ross M, et al. A phase 2 study of (99m)tc-tilmanocept in the detection of sentinel lymph nodes in melanoma and breast cancer. *Ann Surg Oncol.* 2011; 18(4):961-969.
165. Liu LC, Parrett BM, Jenkins T, et al. Selective sentinel lymph node dissection for melanoma: Importance of harvesting nodes with lower radioactive counts without the need for blue dye. *Ann Surg Oncol.* 2011; 18(10):2919-2924.
166. Neves RI, Reynolds BQ, Hazard SW, Saunders B, Mackay DR. Increased post-operative complications with methylene blue versus lymphazurin in sentinel lymph node biopsies for skin cancers. *J Surg Oncol.* 2011; 103(5):421-425.
167. Noro S, Yamazaki N, Nakanishi Y, Yamamoto A, Sasajima Y, Kawana S. Clinicopathological significance of sentinel node biopsy in Japanese patients with cutaneous malignant melanoma. *J Dermatol.* 2011; 38(1):76-83.
168. Motomura K, Inaji H, Komoike Y, et al. Sentinel node biopsy in breast cancer patients with clinically negative lymph-nodes. *Breast Cancer.* 1999; 6(3):259-262.
169. Motomura K, Inaji H, Komoike Y, et al. Combination technique is superior to dye alone in identification of the sentinel node in breast cancer patients. *J Surg Oncol.* 2001; 76(2):95-99.

170. Tagaya N, Yamazaki R, Nakagawa A, et al. Intraoperative identification of sentinel lymph nodes by near-infrared fluorescence imaging in patients with breast cancer. *Am J Surg.* 2008; 195(6):850-853.
171. Murawa D, Hirche C, Dresel S, Hunerbein M. Sentinel lymph node biopsy in breast cancer guided by indocyanine green fluorescence. *Br J Surg.* 2009; 96(11):1289-1294.
172. Tanaka R, Nakashima K, Fujimoto W. Sentinel lymph node detection in skin cancer using fluorescence navigation with indocyanine green. *J Dermatol.* 2009; 36(8):468-470.
173. Hirche C, Murawa D, Mohr Z, Kneif S, Hunerbein M. ICG fluorescence-guided sentinel node biopsy for axillary nodal staging in breast cancer. *Breast Cancer Res Treat.* 2010; 121(2):373-378.
174. Abe H, Mori T, Umeda T, et al. Indocyanine green fluorescence imaging system for sentinel lymph node biopsies in early breast cancer patients. *Surg Today.* 2011; 41(2):197-202.
175. Aoyama K, Kamio T, Ohchi T, Nishizawa M, Kameoka S. Sentinel lymph node biopsy for breast cancer patients using fluorescence navigation with indocyanine green. *World J Surg Oncol.* 2011; 9:157.
176. Tagaya N, Aoyagi H, Nakagawa A, et al. A novel approach for sentinel lymph node identification using fluorescence imaging and image overlay navigation surgery in patients with breast cancer. *World J Surg.* 2011; 35(1):154-158.
177. Fujisawa Y, Nakamura Y, Kawachi Y, Otsuka F. A custom made, low-cost intraoperative fluorescence navigation system with indocyanine green for sentinel lymph node biopsy in skin cancer. *Dermatology.* 2011; 222(3):261-268.
178. Namikawa K, Yamazaki N. Sentinel lymph node biopsy guided by indocyanine green fluorescence for cutaneous melanoma. *Eur J Dermatol.* 2011; 21(2):184-190.
179. Hirche C, Mohr Z, Kneif S, Murawa D, Hunerbein M. High rate of solitary sentinel node metastases identification by fluorescence-guided lymphatic imaging in breast cancer. *J Surg Oncol.* 2012; 105(2): 162-166.
180. Polom K, Murawa D, Nowaczyk P, Rho YS, Murawa P. Breast cancer sentinel lymph node mapping using near infrared guided indocyanine green and indocyanine green: human serum albumin in comparison with gamma emitting radioactive colloid tracer. *Eur J Surg Oncol.* 2012; 38(2):137-142.
181. Brouwer OR, Klop WM, Buckle T, et al. Feasibility of sentinel node biopsy in head and neck melanoma using a hybrid radioactive and fluorescent tracer. *Ann Surg Oncol.* 2012; 19(6):1988-1994.
182. Fujisawa Y, Nakamura Y, Kawachi Y, Otsuka F. Indocyanine green fluorescence-navigated sentinel node biopsy showed higher sensitivity than the radioisotope or blue dye method, which may help to reduce false negative cases in skin cancer. *J Surg Oncol.* 2012; 106(1):41-45.
183. Polom K, Murawa D, Rho YS, Spychala A, Murawa P. Skin melanoma sentinel lymph node biopsy using real-time fluorescence navigation with indocyanine green and indocyanine green with human serum albumin. *Br J Dermatol.* 2012; 166(3):682-683.
184. Stoffels I, von der Stuck H, Boy C, et al. Indocyanine green fluorescence-guided sentinel lymph node biopsy in dermatology. *J Dtsch Dermatol Ges.* 2012; 10(1):51-57.
185. Uhara H, Yamazaki N, Takata M, et al. Applicability of radiocolloids, blue dyes and fluorescent indocyanine green to sentinel node biopsy in melanoma. *J Dermatol.* 2012; 39(4):336-338.
186. Nieweg OE, Tanis PJ, Kroon BB. The definition of a sentinel node. *Ann Surg Oncol.* 2001; 8(6):538-541.
187. Morton DL, Bostick PJ. Will the true sentinel node please stand? *Ann Surg Oncol.* 1999; 6(1):12-14.
188. Faries MB, Morton DL. Surgery and sentinel lymph node biopsy. *Semin Oncol.* 2007; 34(6):498-508.

SUPPLEMENTARY FILE 1**Search method and inclusion/exclusion criteria**

A computer-aided search was conducted using the following databases: PubMed/Medline; Database of Abstracts of Reviews of Effects (DARE) database; Embase; and Cochrane. PubMed was searched as the primary source for scientific articles. Search terms included: "breast carcinoma", "breast neoplasm", or "melanoma" in combination with "sentinel lymph nodes", "lymphatic mapping", "lymph node mapping", "radioisotopes", "radiocolloid", "technetium", "patent blue violet", "methylene blue", "isosulfan blue", and "blue dye".

We augmented our computerized literature search by manually reviewing the reference lists of identified studies and relevant reviews. In addition, Google was searched as a complementary source for related studies. Two reviewers (MGN/RGP) independently assessed the eligibility of all identified studies by checking titles and abstracts. Studies that clearly did not meet the inclusion criteria were excluded. Full text articles were retrieved of potentially relevant references. If there was any disagreement between the readers, a consensus was reached by discussion or by consulting a third reviewer (GMD/HJH). Data from the articles was retrieved and imported into a data abstraction spreadsheet (Microsoft Excel SP3, Microsoft Corp., Redmond, USA) specifically designed for the review.

Criteria for inclusion were: original study group, intraoperative SLN identification in early-stage (stage I or II) breast carcinoma and/or melanoma using radiocolloid tracer, blue dye, ICG, or a combination of a radiocolloid tracer with a blue or ICG. Criteria for exclusion were: studies not in the English language, studies that were published before 1992, case reports, reviews and editorials, studies that did not describe the SLN identification rate (IR), and articles lacking a clear definition of the SLN. Duplicate articles on the same group or follow-up studies with an included subset of previously reported patients were also excluded. The final decision regarding inclusion was based on the full article.

The SLN is generally defined as the initial lymph node that directly drains the lymph fluid from the site of the primary lesion.¹ Despite a good understanding of the theoretical definition of a SLN, there is no consensus on the clinical definition of SLNs detected with a radiotracer.² The SLN has been described as the hottest node, first node visualized on lymphoscintigraphy, and the node with radioactivity greater than twice or thrice the background radioactivity.^{1,3} Data from the Sunbelt Melanoma Trial showed that resection of all blue-stained nodes and all nodes with more than 10% of the hottest node's radioactivity (10% rule) was associated with a low estimated false negative rate.^{4,5} In this systematic review, articles were included only when SLNs were defined as all blue nodes and all hot nodes that had radioactive counts greater than the background or when the 10% rule was applied for hot nodes.

REFERENCES:

1. Nieweg OE, Tanis PJ, Kroon BB. The definition of a sentinel node. *Ann Surg Oncol.* 2001; 8(6):538-541.
2. Bagaria SP, Faries MB, Morton DL. Sentinel node biopsy in melanoma: Technical considerations of the procedure as performed at the John Wayne Cancer Institute. *J Surg Oncol.* 2010; 101(8):669-676.
3. Morton DL, Bostick PJ. Will the true sentinel node please stand? *Ann Surg Oncol.* 1999; 6(1):12-14.
4. McMasters KM, Reintgen DS, Ross MI, et al. Sentinel lymph node biopsy for melanoma: How many radioactive nodes should be removed? *Ann Surg Oncol.* 2001; 8(3):192-197.
5. Faries MB, Morton DL. Surgery and sentinel lymph node biopsy. *Semin Oncol.* 2007; 34(6):498-508.

SUPPLEMENTARY FILE 2**QUADAS quality assessment tool**

The following core QUADAS items were assessed in the current review to assess methodological quality:

1. Was the spectrum of patients representative of the patients who will receive the test?
 - *Yes*: at least 80% of patients had early-stage breast carcinoma or melanoma.
 - *No*: less than 80% of patients had early-stage disease.
 - *Unclear*: stage of disease was not clear from the available information; or, in studies which included both early and late disease, we could not clearly distinguish between information on patients with early disease and those with late disease.
2. Where selection criteria clearly described?
 - *Yes*: all relevant information regarding how participants were selected for inclusion in the study has been provided.
 - *No*: selection criteria were not specified.
 - *Unclear*: selection criteria are only partially reported.
3. Is the reference standard likely to correctly classify the target condition?
 - *Yes*: reference standard is carried out adequately to correctly classify the target condition.
 - *No*: reference standard has not been carried out adequately to correctly classify the target condition.
 - *Unclear*: there is insufficient information given to assess whether reference standard had been carried out adequately (e.g., no mention of number of SLN identified).
4. Is the time period between reference standard and index test short enough to be reasonably sure that the target condition did not change between the two tests?
 - Because the reference standard and index test are applied simultaneously in SLN identification, all items will be scored 'yes'.
5. Was the execution of the index test described in sufficient detail to permit replication?
 - *Yes*: for SLN biopsy using blue dye, description of the execution of the test should include type and amount of tracer substance used, site and timing of application of tracer substance, and method of detection of tracer substance.
 - *No*: the description does not include details as stated above.
 - *Unclear*: it is unclear from the available description as to whether the test can be replicated.

6. Was the execution of the reference test described in sufficient detail to permit its replication?
 - *Yes*: for SLN biopsy using radiocolloid tracer, the description includes type and amount of tracer substance used, site and timing of application of tracer substance, method of detection of tracer substance, and use of scintigraphy.
 - *No*: the above details were not clearly stated.
 - *Unclear*: the description is not adequate to allow replication of the test.
7. Were the reference standard results interpreted without knowledge of the results of the index test?
 - *Yes*: identification of SLNs using the reference standard test was interpreted without knowledge on SLN identification using blue dye.
 - *No*: identification of SLNs using the reference standard test was interpreted with knowledge on SLN identification using blue dye.
 - *Unclear*: insufficient details given as to whether the reference standard results were interpreted with or without knowledge of the results of the index test.
8. Were the index test results interpreted without knowledge of the results of the reference standard?
 - *Yes*: the identification of SLNs using blue dye was interpreted without knowledge (blind) on SLN identification using the reference standard.
 - *No*: the identification of SLNs using blue dye was interpreted with knowledge on SLN identification using the reference standard.
 - *Unclear*: no description of when and how the index tests results are interpreted.
9. Were the same clinical data available when test results were interpreted as would be available when the test is used in practice?
 - *Yes*: the same clinical information was available when the test results were interpreted as would be available when the test is used in practice such as age of patients, clinical history, any related investigation results.
 - *No*: different clinical information, or more or less clinical data, were available; e.g., if tests were interpreted without knowledge of standard clinical data as stated above.
 - *Unclear*: insufficient details given as to what clinical information was available.
10. Were uninterpretable/intermediate test results reported?
 - *Yes*: all uninterpretable results were reported.
 - *No*: not all uninterpretable results were reported.
 - *Unclear*: insufficient information to determine whether all uninterpretable results were reported.

11. Were withdrawals from the study explained?

- *Yes*: all withdrawals from the study were explained.
- *No*: not all withdrawals were explained.
- *Unclear*: insufficient information to assess whether all withdrawals were explained.

12. Did the whole or a random selection of the sample receive verification using a reference standard of diagnosis?

- *Yes*: reference standard (intraoperative SLN identification using radiocolloid tracer) has been carried out in the whole population.
- *No*: reference standard has not been carried out in the whole population.
- *Unclear*: no clear information about the proportion of patients receiving verification using the reference standard.

13. Did patients receive the same reference standard regardless of the index test result?

- *Yes*: all the patients received the same reference standard regardless of the result of the index test.
- *No*: not all the patients received the same reference standard regardless of the result of the index test.
- *Unclear*: insufficient information to assess whether all the patients received the same reference standard.

14. Was the reference standard independent of the index test (i.e., the index test did not form part of the reference standard)?

- *Yes*: it is clear that the index test did not form part of the reference standard.
- *No*: it appears that the index test formed part of the reference standard.
- *Unclear*: insufficient information is available.

15. Was the follow-up adequate and was the false negative rate clearly reported?

- *Yes*: follow-up was adequate (at least 12 months or additional lymph node dissection) and the false negative rate was clearly reported.
- *No*: follow-up was not adequate and the false negative was not clearly reported.
- *Unclear*: no clear information was available on the follow-up and the false negative rate.

Chapter

8

Submitted

Selecting tumor markers for targeted imaging applications in breast cancer: the next step in patient-tailored intervention

R.G. Pleijhuis
B. van der Vegt*
L.M.A. Crane*
S.G. Elias
T. van der Sluis
C.P. Schröder
J. de Vries
L. Jansen
G.M. van Dam
J. Bart

** Both authors contributed equally*

ABSTRACT*Introduction*

The use of targeted therapies has substantially increased in breast cancer treatment, exploiting the expression of certain tumor markers in cancerous tissue. In addition to systemic therapy, tumor markers could also be used to specifically deliver optical imaging agents to cancer cells, enabling (noninvasive) tumor visualization. The aim of this study was to identify tumor markers that bear potential for tumor-targeted optical imaging applications in breast cancer patients.

Methods

Ten membranous and/or extracellular tumor markers were assessed on tissue microarrays of invasive breast carcinomas from 449 patients using immunohistochemistry. Markers included $\alpha\beta 3$ integrin receptor, CXCR4, CA-IX, CA-XII, EpCAM, FR- α , HER2, MGB1, Notch1 receptor, and VEGF-A. Tumor markers were prioritized based on the *target selection criteria* (TASC) scoring system, with scores ≥ 18 indicating markers of particular interest.

Results

A total of 439 (97.8%) invasive breast carcinomas were eligible for analysis. Immunohistochemical scoring agreement between observers was 88% (kappa: 0.79, $P < 0.001$). CXCR4, EpCAM, and CA-XII were assigned modified TASC-scores of 21, 18, and 18, respectively, indicating them to be of particular interest for probe development. When combined, at least one of these three markers was expressed in 76.5% of all breast carcinomas. Modified TASC-scores for the remaining tumor markers ranged between 9 and 16 points.

Conclusion

We systematically assessed the potential of ten tumor markers for tumor-targeted optical imaging in breast cancer patients. CXCR4, EpCAM, and CA-XII were identified as markers of particular interest for development of tumor-targeted probes for clinical translation. At least one of these tumor markers was homogeneously expressed in approximately 80% of the patients included in our study.

INTRODUCTION

Breast cancer is the most common malignancy in women worldwide.¹ In the past decade, there has been a substantial change in the treatment of breast cancer, including a steep increase in the use of targeted therapies. Several drugs have been developed to complement breast cancer treatment by targeting intra- and extracellular tumor markers of the oncogenic pathways.² In addition to functioning as targets for systemic therapy, membranous and extracellular tumor markers can also be exploited through targeted delivery of optical imaging agents.^{3,4} Tumor-specific optical imaging is considered safe and offers some advantages over conventional techniques, including high resolution, lack of ionizing radiation, and high sensitivity and specificity.^{5,6} In particular, the use of near-infrared fluorescence (NIRF) holds great promise due to the preferable optical characteristics of near-infrared light, resulting in low background (auto)fluorescence and increased tissue penetration, even in women with dense glandular tissue.⁷

As optical imaging is fundamentally depth limited, one of the most promising applications of optical imaging in breast cancer patients is image-guided surgical excision of the tumor during breast-conserving surgery. With current techniques, breast-conserving surgery results in an inadequate excision of the primary tumor in 20% to 40% of patients.⁸ This relatively high percentage is mainly due to difficulty in localizing the primary tumor and evaluating the extent of surgery during surgical procedures. Tumor-targeted optical imaging could complement surgery by allowing for intraoperative image-guided tumor localization, tumor excision and assessment of surgical margin status in real-time. Several animal and clinical studies have already shown the potential of optical imaging to improve the therapeutic outcome of surgery by localizing the primary tumor and pinpointing remnant disease following tumor resection.^{6,9-11}

Current research on intraoperative NIRF imaging is directed primarily towards the refinement of imaging systems and the development of non-toxic tumor-targeted imaging agents for clinical use.^{4,11,12} A single tumor-targeted imaging agent that can be applied for all types of breast cancers, however, is not yet available and is unlikely to be discovered in the near future due to marked breast cancer heterogeneity. A panel of imaging agents targeting different tumor markers is therefore needed to make patient-tailored optical imaging available for general use.¹³ Because the portfolio of markers known to be associated with breast cancer is still expanding and the development and translation of targeted imaging agents is time-consuming and costly, it is necessary to identify those tumor markers that bear potential for targeted imaging applications. The aim of the current study was to identify those tumor markers that are of particular interest for intraoperative NIRF imaging applications in breast cancer patients. Tissue microarrays (TMAs) were used to enable high-throughput analysis of hundreds of breast carcinoma samples simultaneously.

METHODS

Selection of tumor markers

As optical imaging requires the use of relatively large imaging agents which are unlikely to pass the membrane of tumor cells, we focused on membranous and/or extracellular tumor markers that are known to play a role in breast cancer. From these, we selected a panel of ten markers based on availability of selective targeted agents on the market or in clinical trials to facilitate clinical translation. Evaluated tumor markers included alpha v beta 3 ($\alpha v\beta 3$) integrin receptor, C-X-C-chemokine receptor 4 (CXCR4), carbonic anhydrase (CA) IX and XII, epithelial cell adhesion molecule (EpcAM), folate receptor alpha (FR- α), human epidermal growth factor receptor 2 (HER2), mammaglobin 1 (MGB1), Notch1 receptor, and vascular endothelial growth factor A (VEGF-A).

The $\alpha v\beta 3$ integrin receptor is expressed on activated endothelial cells and tumor cells, and is reported to play a key role in tumor angiogenesis and metastasis.^{14,15} CXCR4 is a membrane-bound cell surface receptor that plays a role in chemotaxis and cell adhesion and is reported to be consistently expressed in human breast cancer cells and metastases.^{16,17} CA-IX and CA-XII are both integral plasma membrane proteins with large extracellular components that belong to the carbonic anhydrase (CA) family of zinc metalloenzymes. The enzymes are involved in the regulation of the microenvironment acidity and tumor malignant phenotype.¹⁸ CA-XII is associated with good prognosis,¹⁹ whereas CA-IX is a marker of poor prognosis in breast cancer.²⁰ EpcAM is a transmembrane protein that is involved in cell-cell adhesion in normal epithelial cells, and is linked to proliferation of tumor cells.²¹ FR- α is a membrane-associated glycoprotein that binds folate with high affinity and is reported to be associated with reduced survival.²² A similar correlation with poor prognosis is reported for the well-known transmembrane tyrosine kinase receptor HER2.²³ MGB1 is a membrane-associated glycoprotein that is expressed in breast cancer and, to a lesser extent, in normal breast tissue.²⁴ MGB1 is also a member of the epithelial secretoglobin family, of which different secretoglobins seem to be involved in cell signaling, immune response, and chemotaxis.²⁵ Notch1 receptor is a cell surface protein with a single transmembrane domain that regulates a number of cellular properties important in cancer, including cell division, differentiation, and survival.²⁶ VEGF-A comprises a group of growth factors that play a key role in angiogenesis.²⁷ VEGF-A, the most important subtype, is associated with invasive tumor growth, metastasis, and reduced survival.²⁸⁻³¹ VEGF-A can be either membrane-bound or present in the interstitial cell space with highest concentrations observed in close proximity of tumor cells.³²

Selection of tumor specimen

A previously described cohort of 449 invasive breast carcinoma specimens collected between January 1996 and December 2005 was obtained from the archive of the Department of Pathology and Medical Biology, University Medical Center Groningen, The Netherlands.³³ Specimens were selected on the availability of sufficient paraffin-embedded tissue. Clinical and histopathological data of patients were gathered from pathology reports and medical charts. All data were anonymized and the study was conducted in accordance with the Declaration of Helsinki and with the rules and regulations posed by the Institutional Review Board (IRB) of the UMCG.

Construction of tissue microarrays

Slides from all sample blocks were evaluated for representative areas containing invasive breast carcinoma. TMAs were prepared as previously described.³⁴ In brief, the most representative area of invasive carcinoma was marked on the original haematoxylin and eosin (H&E) stained section. From this marked section, three 0.6 mm punches were taken from the donor blocks and mounted in a recipient block using a tissue arrayer (Beecher Instruments, Sun Prairie, USA).

Immunohistochemistry

Immunohistochemistry (IHC) was performed for all ten tumor markers to assess functional extracellular marker expression. Briefly, 3 µm thick TMA sections were deparaffinized with xylene and gradually rehydrated through changes of graded ethanol from 100% to distilled water. Endogenous peroxidase activity was blocked by incubating TMAs in phosphate-buffered saline (PBS), pH 6.8, containing 0.3% H₂O₂ for 30 minutes. In the case of VEGF-A, endogenous biotin was additionally blocked using a Blocking Kit (Vector Laboratories, Burlingame, USA). Information concerning the primary antibodies used in this study is shown in Table 1.

Following incubation with the primary antibody, sections were washed with PBS and incubated with secondary and tertiary antibodies where appropriate. FR-α was incubated with mouse MACH3 (Biocare Medical, Walnut Creek, USA). For visualization of the antibody-antigen complex, 3,3-diaminobenzidine (DAB) was used. After a final wash with distilled water, counterstaining was performed with haematoxylin. Sections were then dehydrated through rising concentrations of ethanol, mounted with mounting medium, and coverslipped. Negative controls consisted of sections processed in the same way but with omission of the primary antibody step. Positive control tissue was included as usual.

Digitalization of tissue microarray slides

TMA slides were digitalized using the ScanScope GL Scanner (Aperio Technologies Inc., Vista, USA), creating high-resolution files suitable for IHC scoring. All slides were produced with core images linked to a Microsoft Access™ database containing relevant tissue core information. After importing the digital slides into ImageScope® (Aperio Technologies Inc., Vista, USA), each individual TMA core on the slide was captured using a snapshot tool, coded, and exported as a separate industry-standard TIFF file.

Scoring of immunohistochemistry

In order to eliminate variation in lighting conditions when using a light microscope, manual IHC scoring was performed on digital TMA cores. All cores were randomized prior to IHC scoring to minimize bias effects. Scoring was performed by a single observer (RGP) after extensive training by an experienced pathologist (BvdV). As manual IHC scoring is a time-consuming process, especially for more than 13,000 TMA cores, we chose not to duplicate our results. Instead, data quality was assessed through validation of IHC scoring in a sample of 100 randomly selected TMA cores. Hereto, a senior pathologist (JB) independently performed IHC scoring on all selected TMA cores. IHC scores obtained by the observer and the senior pathologist were compared and the level of agreement was calculated.

Table 1. Information concerning the antibodies used in the current study.

Target	Catalogue number	Clone	Clonality	Species	Supplier	Dilution	Incubation	Antigen retrieval	Secondary step	Supplier	Tertiary step	Supplier
αvβ3	ab7166	BV3	Monoclonal	Mouse	Abcam	1:100	3 h	PASCAL autoclave for 30 sec at 125 °C	MACH3	Biocare Medical	N/A	N/A
CA-IX	SAB1300310	N/A	Polyclonal	Rabbit	Sigma-Aldrich	1:200	1 h	Microwave 10 mM Tris / 1 mM EDTA, pH 9.0	GARPO	DAKO	RAGPO	DAKO
CA-XII	HPA008773	N/A	Polyclonal	Rabbit	Sigma-Aldrich	1:75	1 h	Microwave 10 mM Tris / 1 mM EDTA, pH 9.0	GARPO	DAKO	RAGPO	DAKO
CXCR4	ab2074	N/A	Polyclonal	Rabbit	Abcam	1:50	1 h	No antigen retrieval	GARPO	DAKO	RAGPO	DAKO
EpCAM	IR637	Ber-EP4	Monoclonal	Mouse	Dako	1:100	1 h	0.1% protease for 30 min	RAMPO	DAKO	GARPO	DAKO
FR-α	mAb-343	3D2	Monoclonal	Mouse	Dr. P.S. Low	1:500	3 h	PASCAL autoclave for 30 sec at 125 °C	MACH3	DAKO	N/A	N/A
HER2	NCL-CB11	CB11	Monoclonal	Mouse	Novocastra	1:80	1 h	Microwave 10 mM Tris / 1 mM EDTA, pH 9.0	RAMPO	DAKO	GARPO	DAKO
MGB1	ab101137	31A5	Monoclonal	Mouse	Abcam	1:100	1 h	Microwave 10 mM Tris / 1 mM EDTA, pH 9.0	RAMPO	DAKO	GARPO	DAKO
Notch1	ab44986	A6	Monoclonal	Mouse	Abcam	1:25	3 h	PASCAL autoclave for 30 sec at 125 °C	MACH3	DAKO	N/A	N/A
VEGF-A	sc-152	N/A	Polyclonal	Rabbit	Santa Cruz Biotechnology	1:50	1 h	Microwave 0.1 M Tris / HCL, pH 9.0, avidin / biotin Blocking Kit	GARbio	DAKO	N/A	N/A

ABC, avidin-biotin complex; αvβ3, alpha v beta 3 integrin receptor; CA-IX, carbonic anhydrase IX; CA-XII, carbonic anhydrase XII; CXCR4, C-X-C chemokine receptor 4; EDTA, Ethylenediaminetetraacetic acid; EpCAM, epithelial cell adhesion molecule; FR-α, folate receptor alpha; GARbio, goat anti-rabbit immunoglobulin / biotinylated; GARPO, goat anti-rabbit polyclonal; HER2, human epidermal growth factor receptor 2; HIER, heat induced epitope retrieval; MGB1, mammaglobin 1; N/A, not applicable; RAMPO, rabbit anti-mouse polyclonal; VEGF-A, vascular endothelial growth factor A.

Functional tumor marker expression was assessed by evaluating the proportion of tumor cells showing no (0), weak (1+), moderate (2+) or strong (3+) membranous staining. Evaluation of staining pattern (diffuse or focal) was performed both on a microscopic (within spot) and a macroscopic (between spots) level. To account for tumor heterogeneity, the average proportion and staining intensity were calculated for each tumor. An average membranous staining intensity of $\geq 2+$ in $\geq 10\%$ of tumor cells was considered positive. For VEGF-A and CXCR4, thresholds for positivity were set to staining intensity 3+ in $\geq 10\%$ of tumor cells to correct for background staining in normal breast epithelium. Tumors were excluded from analysis in the event that all (3 out of 3) TMA cores were missing.

Assessment of tumor-to-normal ratio

Tumor markers for tumor-targeted imaging applications should provide adequate tumor-to-normal (T/N) ratios in order to discriminate between tumor and normal breast tissue. For this reason, glandular expression of all ten tumor markers was also evaluated using IHC in a set of 15 TMAs derived from normal breast tissue. Tissue specimens were obtained from patients who underwent mastoplasty in the absence of breast cancer. The T/N ratio was calculated by multiplying the mean staining intensity with the proportion of stained tumor cells for the tumor (three-item severity score; TIS-score) and dividing it by the TIS-score for normal breast tissue. A T/N ratio ≥ 3 was considered adequate for imaging purposes.³⁵

Evaluation of target selection criteria

All markers were ranked according to the *target selection criteria* (TASC) scoring system, which was recently proposed by van Oosten et al. to serve as a directive to gain objectivity and insight in target selection.³⁶ The scoring system is based on seven favorable target characteristics for optical imaging purposes for which each tumor marker is scored: I) extracellular tumor marker localization; II) expression pattern; III) tumor-to-normal ratio (T/N); IV) target expression rate; V) reported successful use *in vivo*; VI) enzymatic activity, and VII) internalization.

TASC was applied to identify tumor markers that are of special interest for targeted imaging. As described above, the scoring system is based on seven favorable target characteristics for which each tumor marker is scored. For each characteristic, 0–6 points are granted in order of importance (Supplementary Table 1). The maximum TASC score that can be obtained is 22 points. If a marker scores a total of ≥ 18 points, it is considered to be a potential target for tumor-targeted optical imaging and should be prioritized with regards to clinical translation. Markers that are granted < 18 points have less favorable characteristics, deeming them less suitable for targeted imaging modalities.

Modified target selection criteria score

The original TASC score is dominated by the percentage of tumors that express the tumor marker on their cell membranes or in the extracellular matrix adjacent to the tumor cells. TASC assigns up to 6 out of 22 points to expression rates as high as 90%, whereas expression rates below 50% are assigned no points (Supplementary Table 1). For intraoperative targeted imaging applications, however, tumor markers expressed in less than 50% of the tumors can still be of value as long as other characteristics crucial for optical imaging are favorable. Importantly, intraoperative imaging allows for analysis of a sample of the tumor prior to the surgical procedure (e.g., by core needle biopsy), enabling assessment on whether or not the individual tumor expresses the specific marker.

As the focus in the present study lies on the identification of tumor markers for intraoperative NIRF imaging applications, we calculated a modified TASC score, in which the marker is granted 0, 3, 5, or 6 points based on an expression rate of 0–10%, 10–25%, 25–50%, or 50–100%, respectively (Supplementary Table 1).

Preoperative biomarker panel

Besides evaluating each marker individually, we also evaluated the proportion of breast cancers that stained positive to at least one of a panel of markers. For this, we evaluated all possible panels of two through nine marker combinations out of the ten prospective markers. All possible marker combinations were evaluated and ranked according to tumor detection rate. Subgroup analyses were performed based on tumor size and grade of differentiation.

Statistical analysis

Descriptive statistics including medians and frequencies were used for the description of clinicopathological characteristics. Fisher's exact test was performed to test for significant differences between the proportion of tumor marker expression and clinicopathological parameters. To account for sampling variability and assess the robustness and generalizability of the biomarker panel results, we performed all combination analyses under 2000-fold bootstrap resampling and report the mean rank of each panel over these bootstrap resamples as well as the chance that a particular biomarker panel belongs to the top 10 best combinations. The kappa statistic was used to compare interobserver agreement between IHC scoring results. Kappa values of 0.40–0.60, 0.61–0.80, and 0.81–0.99 were considered to resemble moderate, substantial, and almost perfect agreement, respectively.³⁷

A two-sided *P*-value of ≤ 0.05 was considered significant. All calculations were performed using Excel (Microsoft® Office Professional Edition 2003 SP3, Microsoft Corporation, Redmond, USA), SPSS 12.01 (SPSS Inc., Chicago, USA), and R version 3.0.1 (R Foundation for Statistical Computing, Vienna, Austria).³⁸

RESULTS

The characteristics of ten membranous and extracellular tumor markers were assessed in our study population that comprised breast cancer specimen of 449 patients. Ten patients (2%) were excluded from the study due to the absence of representative TMA cores for all stains, leaving 439 patients eligible for analysis. Histological types consisted of invasive ductal carcinomas (97%) and other histological types (3%). Additional clinicopathological characteristics are shown in Table 2.

Immunohistochemistry scoring

A representative IHC image for each stain is shown in Fig. 1. Depending on the staining, 62–78% of the tumors were represented by three TMA cores, 17–26% by two TMA cores, and 2–10% by only one TMA core. Acceptable IHC (defined as at least one of the three cores stained sufficiently) was achieved in 423 cases (97%) for CXCR4, 422 cases (96%) for $\alpha v\beta 3$ integrin receptor, 415 cases (95%) for CA-IX, 426 cases (97%) for CA-XII, 427 cases (97%) for EpCAM, 416 cases (95%) for FR- α , 418 cases (95%) for HER2, 427 cases (97%) for MGB1, 424 cases (97%) for Notch1 receptor, and 431 cases (98%) for VEGF-A. In total, 379 (84%) cases had sufficient data for all ten markers.

Table 2. Clinicopathological characteristics of 439 breast cancer patients.

Characteristics	N	%
Age (years), median (range)	58 (27–91)	
<35	11	2.5
35–50	99	22.7
>50	329	74.8
Tumor size (mm), median (range)	23 (1–140)	
<20	228	53.0
20–50	170	39.5
>50	32	7.5
Histological type		
Invasive ductal carcinoma	425	96.8
Other types	14	3.2
Carcinoma in situ present		
Yes	204	46.5
No	235	53.5
Histological grade		
I	115	26.4
II	187	42.9
III	134	30.7
Progesterone receptor		
Positive	264	63.6
Negative	151	36.4
Estrogen receptor		
Positive	318	76.4
Negative	98	23.6
Nodal status		
Positive	198	46.6
Negative	227	53.4

Tumor-to-normal ratios

Expression of all tumor markers was assessed in 15 specimens of normal glandular breast tissue. T/N ratios were calculated using the aforementioned formula (Table 3). For VEGF-A and CXCR4, diffuse cytoplasmic and/or extracellular staining was seen in the majority of normal breast specimen with staining intensities ranging between 1+ and 2+ (Fig. 1). Thresholds for tumor marker positivity were therefore set to 3+ for these two markers in order to maintain adequate tumor-to-normal ratios.

Expression of individual tumor markers

An overview of the expression rates for each individual tumor marker is shown in Table 3. The most frequently expressed tumor markers were CXCR4, CA-XII, and EpCAM, showing diffuse expression in 60.2%, 29.6%, and 22.6% of breast carcinomas, respectively. Individual expression rates for $\alpha\beta 3$ integrin receptor, CA-IX, CA-XII, EpCAM, FR- α , HER2, Notch1 receptor, MGB1, and VEGF-A ranged from 0.3% to 17.4%. Subgroup analysis was performed regarding tumor marker expression for tumor size and grade of differentiation. Results are shown in Supplementary Figs. 1–2. In brief, tumors were found less likely to express VEGF-A with increasing tumor size ($P=0.031$). FR- α ($P<0.001$), CA-IX ($P<0.001$), and HER2 ($P=0.004$) are more frequently expressed in less differentiated breast carcinoma. On the contrary, VEGF-A ($P<0.001$), MGB1 ($P=0.036$), and CA-XII ($P=0.041$) showed higher expression levels in well-differentiated tumors.

Table 3. Selection of potential tumor markers for targeted optical imaging in breast cancer patients according to the target selection criteria (TASC).

Target Selection Criteria (TASC)								
	I	II	III	IV	V	VI	VII	
Tumor marker	Extracellular localization	Expression pattern	T/N ratio (≥3)	Expression rate (moderate to strong)	Pervasively imaged <i>in vivo</i>	Enzymatic activity	Target-mediated internalization	TASC score
	5	4	3	6	2	1	1	22
<i>Max points</i>								
CXCR4	Membranous	Diffuse	4.5	60.2% membranous	Yes	Not described	Yes	18
EpCAM	Membranous	Diffuse	4.2	22.6% membranous	Yes	Not described	Yes	15
CA-XII	Membranous	Mostly diffuse, focal	4.6	29.6% membranous	Yes	Yes	Not described	13
HER2	Membranous	Mostly diffuse, focal	3.1	17.4% membranous	Yes	Not described	Yes	13
VEGF-A	Extracellular	Diffuse	3.1	15.6% extracellular	Yes	Not described	Not described	14
FR-α	Membranous	Diffuse	3.1	6.3% membranous	Yes	Not described	Yes	15
Notch1	Membranous	Diffuse	2.2	0.3% membranous	Yes	Not described	Yes	12
αvβ3	Membranous	Mostly focal, diffuse	3.3	0.8% membranous	Yes	Not described	Yes	11
CA-IX	Membranous	Mostly diffuse, focal	1.1	4.2% membranous	Yes	Yes	Yes	11
MGB1	Membranous	Mostly diffuse, focal	1.7	4.5% membranous	Yes	Not described	Not described	9

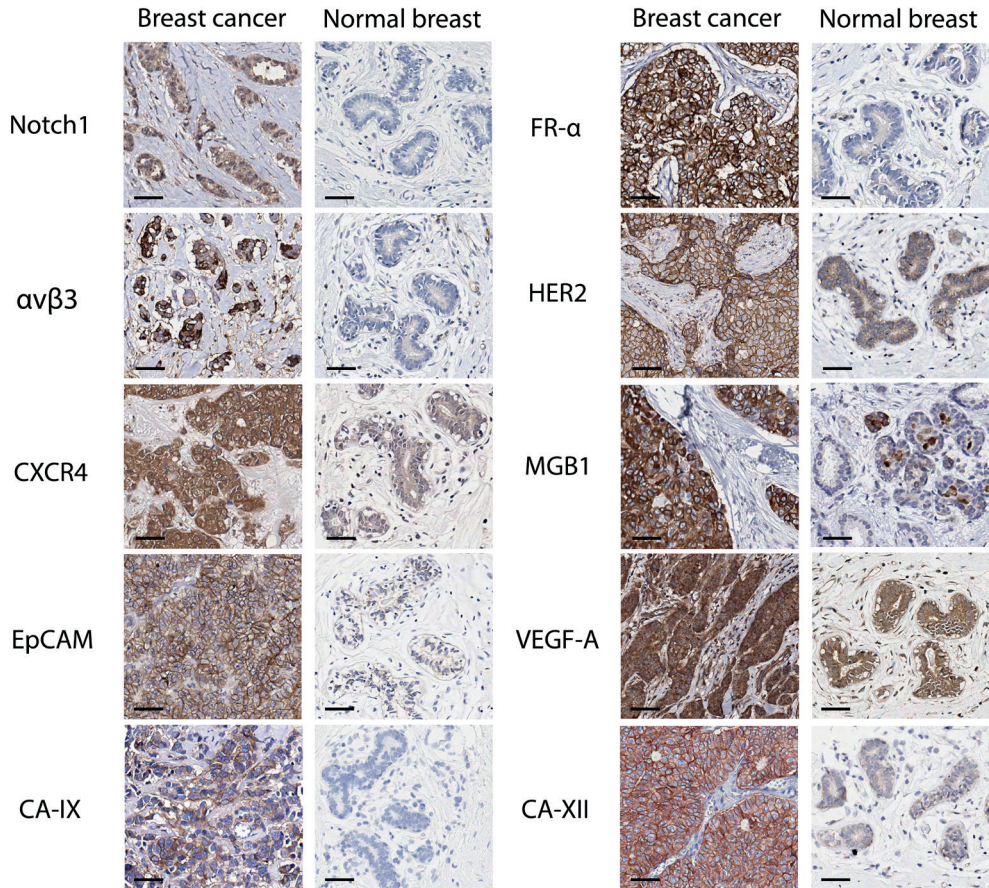
αvβ3, alpha v beta 3 integrin receptor; *CA-IX*, carbonic anhydrase IX; *CA-XII*, carbonic anhydrase XII; *CXCR4*, C-X-C chemokine receptor 4; *EpCAM*, epithelial cell adhesion molecule; *FR-α*, folate receptor alpha; *HER2*, human epidermal growth factor receptor 2; *MGB1*, mammaglobin 1; *VEGF-A*, vascular endothelial growth factor A.

An extended version of this table is available online (Supplementary Tables 1 and 2). Tumor marker characteristics were evaluated through immunohistochemical analysis of breast cancer tissue microarrays. In addition, tumor marker characteristics reported in the literature were taken into account if available.

* Modified TASC score based on alternative threshold for tumor marker expression level.

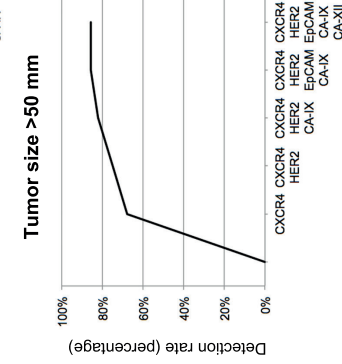
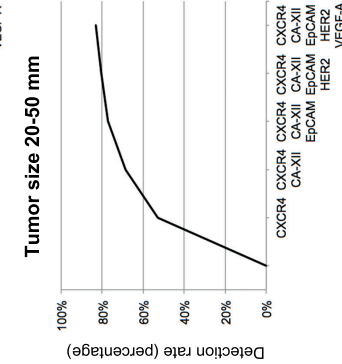
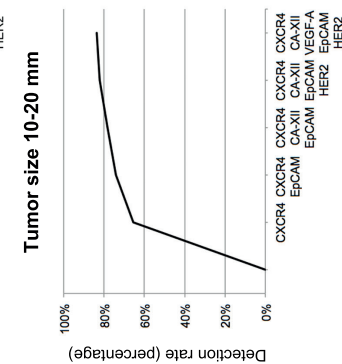
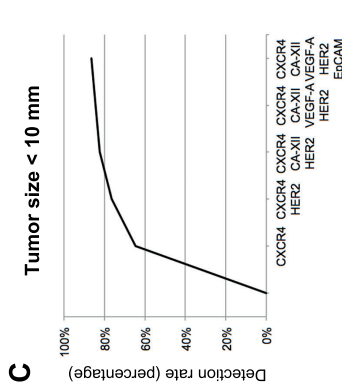
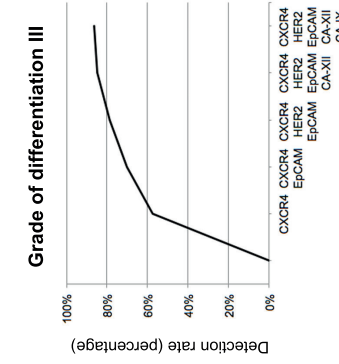
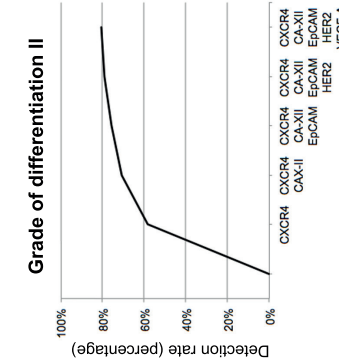
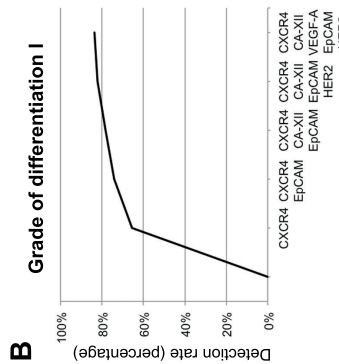
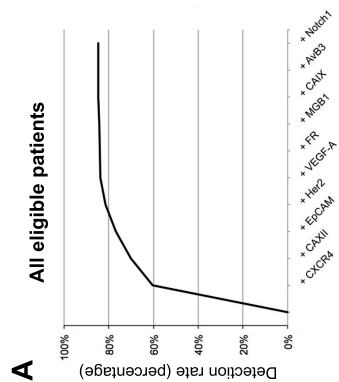
Validation of immunohistochemistry scoring

Overall agreement between IHC scoring by the observer and the senior pathologist was 88%. The corresponding kappa value for interobserver agreement was 0.79 ($P < 0.001$), indicating substantial agreement.³⁷



αvβ3, alpha v beta 3 integrin receptor; *CA-IX*, carbonic anhydrase IX; *CA-XII*, carbonic anhydrase XII; *CXCR4*, C-X-C chemokine receptor 4; *EpCAM*, epithelial cell adhesion molecule; *FR-α*, folate receptor alpha; *HER2*, human epidermal growth factor receptor 2; *MGB1*, mammaglobin 1; *VEGF-A*, vascular endothelial growth factor A.

Figure 1. Extracellular tumor marker expression in breast cancer and normal breast tissue. Immunohistochemical staining of positive breast cancer cases and representative normal breast tissue. The majority of tumor markers showed no to weak staining in normal breast tissue. In the case of *CXCR4* and *VEGF-A*, diffuse weak to moderate cytoplasmic and extracellular staining was observed in part of the normal breast specimen. For *HER2* receptor, weak to moderate cytoplasmic staining was observed in normal breast with no signs of extracellular involvement. Mammaglobin 1 showed intense focal staining in normal breast tissue. Scalebar equals 50 μm .



avb3, alpha v beta 3 integrin receptor; CA-IX, carbonic anhydrase IX; CA-XII, carbonic anhydrase XII; CXCR4, C-X-C chemokine receptor 4; EpcAM, epithelial cell adhesion molecule; FR- α , folate receptor alpha; HER2, human epidermal growth factor receptor 2; MGB1, mammaglobin 1; VEGF-A, vascular endothelial growth factor A.

Figure 2. Optimal combination of tumor markers for breast cancer imaging. The breast cancer detection rate was assessed by calculating the proportion of positive cases, taking into account that a single tumor can express multiple markers. **(A)** Optimal combination of tumor markers for detecting breast carcinoma in the total study population. **(B)** Optimal combination of five markers for tumor detection subdivided to grade of differentiation and **(C)** tumor size. In all subgroups, the proportion of detected breast tumors quickly increases to approximately 80% when markers are added to the panel. After adding 3 to 5 markers, the added value of including additional tumor markers gradually decreases to zero.

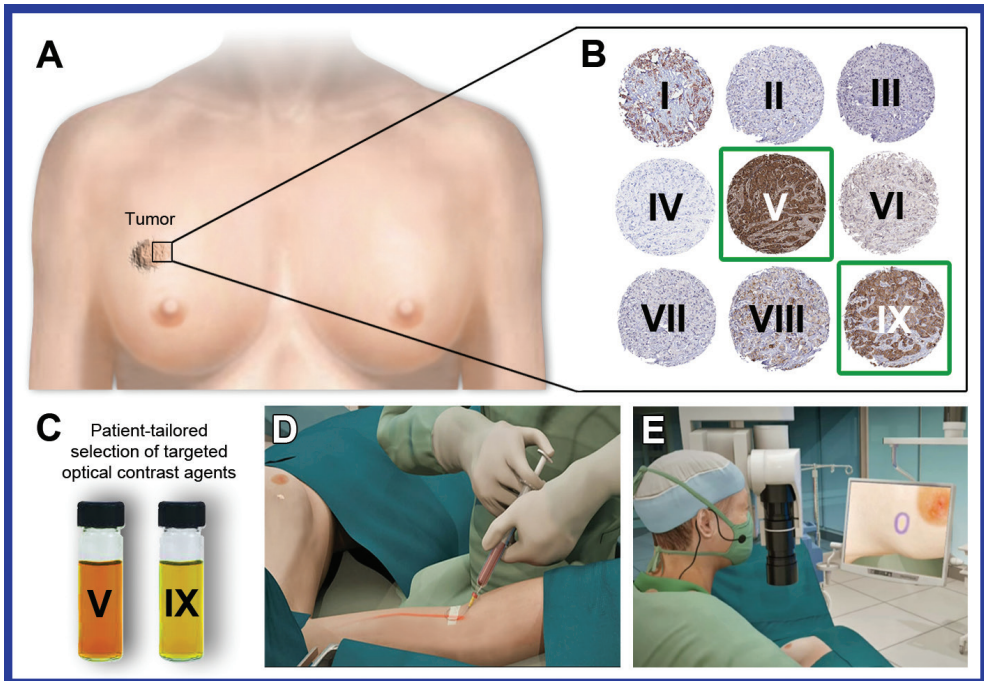


Figure 3. Patient-tailored selection of tumor markers for target optical imaging. Schematic example of the selection of tumor markers for targeted optical imaging applications in an individual breast cancer patient. Prior to imaging, the expression profile of the tumor is assessed for multiple tumor markers using cancerous tissue obtained by core needle biopsy (A). Immunohistochemical analysis is performed to enable selection of tumor markers that show strong and diffuse staining throughout the samples (B). Based on the functional marker expression assay, the appropriate targeted optical contrast agent is selected for the individual patient (C). Several hours after systemic injection with the targeted agent (D), superficial tumors could be visualized noninvasively using a dedicated optical imaging system (E).

Target selection criteria analysis

The (modified) TASC-scores for all ten tumor markers are shown in Table 3. An extended version of this table including an overview of expression rates in tumor and normal breast tissue as reported in the literature is provided in Supplementary Table 2. In brief, CXCR4 (21 points), EpCAM (18 points), and CA-XII (18 points) were identified as the most promising tumor markers for targeted imaging of primary breast tumors of our current panel, fulfilling the TASC criteria of ≥ 18 points. HER2, VEGF-A, and FR- α are considered less suitable with 16, 15, and 15 points, respectively, although they exhibit some favorable characteristics for targeted imaging. The Notch1 receptor (12 points), $\alpha v\beta 3$ integrin receptor (11 points), CA-IX (11 points), and MGB1 (9 points) are regarded unsuitable for targeted imaging based on marker characteristics.

Optimization of preoperative biomarker panel

An optimal combination of markers, i.e., detecting the largest number of breast cancers using the least possible amount of tumor markers, was calculated overall for the total study population. Subgroup analyses were performed for tumor size and grade of differentiation (Fig. 2). When combined, at least one of the three most frequently expressed tumor markers (CXCR4, CA-XII, and EpCAM) was expressed in 76.5% of all breast carcinomas in our cohort.

Beyond the combination of five markers, with an overall combined detection rate of 83%, adding additional markers did not improve the detection rate substantially. Overall, and in subgroups according to grade and tumor size, the maximum combined detection rate varied between 80% to 90%, with different optimal panels between subgroups. The highest detection rates were observed in poorly differentiated breast carcinoma relatively large in size, representing the category of tumors that are considered most aggressive and have the worst prognosis.

Different combinations of equal numbered biomarker panels yielded similar detection rates. For instance, the top 5 best combinations of five markers showed overall detection rates between 82% and 83% (all including CXCR4, CA-XII, EPCAM, and HER2 but varying in the fifth marker; Supplementary Table 4). Nevertheless, the observed top ranking biomarker combinations also proved to be the best ranking biomarker combinations under 2000-fold bootstrap resampling to account for sampling variation and overoptimism, showing the robustness of our findings.

DISCUSSION

In the current study, we aimed to identify tumor markers that are of particular interest for clinical translation towards targeted optical imaging in breast cancer.³⁶ Because the portfolio of markers known to play a role in breast cancer is large and still expanding, we confined our search by focusing on those markers with membranous and/or extracellular expression as reported in the literature. From this group, we selected a panel of ten markers based on the availability of selective targeted agents on the market or in clinical trials (Supplementary Table 4), facilitating the development and translation of tumor-targeted optical contrast agents towards the clinic. Although our study does not cover all potential tumor markers in the field, it does contribute to the identification of promising targets for optical imaging in an objective manner. Further studies are needed to complement our work, judging additional promising markers on their merits for targeted optical imaging applications.

Recently, Vermeulen et al. evaluated the expression of a selected set of tumor markers for targeted molecular imaging in breast cancer patients.³⁵ The most widely expressed tumor marker in their cohort was glucose transporter 1 (GLUT1), which was expressed in 20% of the cases. When a panel of 6 tumor-specific markers was applied (GLUT1, epidermal growth factor receptor, HER2, insulin-like growth factor 1 receptor, hepatocyt growth factor receptor, and CA-IX), 46% of all cases could be detected. This result underlines that no single tumor marker is likely to be sensitive enough to detect all breast cancers. Four tumor markers described by Vermeulen et al. show overlap with the present study (HER2, MGB1, CA-IX, and CA-XII). However, although the authors evaluated membranous expression and T/N ratios for each tumor marker, they did not systematically assess all seven tumor marker characteristics that are part of the TASC scoring system and are considered important for targeted optical imaging.

Tumor maker expression patterns

Membranous staining is of particular interest for targeted optical imaging as imaging agents can more easily target tumor markers situated on the surface of tumor cells or in the extracellular matrix. The expression rates reported in the literature with regards to our tumor marker panel tend to differ substantially between studies (Supplementary Table 2). The majority of studies do not differentiate between cytoplasmic and membranous staining, thus explaining part of the difference. In addition, the use of different antibodies and staining protocols results in heterogeneity in reported expression rates.

Immunohistochemistry

We used IHC as a means to evaluate functional extracellular tumor marker expression on the cell membrane of tumor cells and/or in the extracellular matrix adjacent to tumor cells. IHC can easily be performed on large numbers of tumor samples and is a well-established technique for evaluating marker expression in clinical practice.³⁹ The most important drawbacks of IHC are the lack of assay standardization and variance in the interpretation of IHC stains.^{40,41} Scoring results obtained using IHC should therefore be considered semi-quantitative, as quantifiable internal reference standards for calibration are lacking.⁴² In addition, it is unsure to what extent IHC scoring results are representative for results obtained during *in vivo* imaging. Despite the abovementioned, IHC is considered as a powerful tool for screening purposes and selecting tumor markers of interest for further probe development. In the current study, validation of a randomly selected subset of manual IHC scoring results was performed by a senior pathologist and showed substantial agreement. Although we chose not to duplicate the entire dataset, this result implies that IHC scoring as performed by the single observer was consistent.

Tumor markers for tumor-targeted imaging

The most promising tumor markers identified in the current study using TASC was CXCR4, which showed homogenous extracellular expression in 60.3% of the tumor specimen while maintaining adequate tumor-to-normal ratios. In addition, CA-XII and EpCAM were identified as tumor markers of value for targeted imaging with extracellular expression observed in 29.6% and 22.6% of evaluated breast carcinoma, respectively. Although exhibiting some favorable characteristics for targeted imaging, HER2, VEGF-A, and FR- α did not reach the TASC threshold of ≥ 18 points to be prioritized as markers of particular interest for clinical translation. However, these markers do have considerable value when combined in a panel. The characteristics of $\alpha v \beta 3$ integrin receptor, CA-IX, MGB1, and Notch1 receptor were considered unfavorable for tumor-targeted imaging applications, with TASC scores of 12 and lower.

Already, a number of targeted imaging agents have been described for CXCR4.⁴³ Meincke et al. recently synthesized conjugates of CXCL12 and the near-infrared fluorescent dye IRDye 800CW enabling visualization of tumors *in vivo*.⁴⁴ Nimmagadda et al. succeeded in imaging CXCR4 expressing tumors in mice through the use of AMD3100, which is a clinically approved molecule conjugated to a radionuclide targeted towards CXCR4 (Supplementary Table 4).⁴⁵ Kuil et al. reported the first hybrid CXCR4-targeted imaging agent, which consists of the cyclic peptide Ac-TZ14011 and a multifunctional single attachment point (MSAP) label to which fluorophores can be attached.⁴⁶

Sun et al. successfully labeled anti-EpCAM antibodies with fluorescent dyes of different wavelengths and determined their *in vivo* distribution in a breast cancer xenograft model.⁴⁷ Very recently, Zhu et al. showed that NIRF optical imaging in combination with a fluorescent probe targeted against EpCAM enabled image-guided surgery in an orthotopic model of human prostate cancer.⁴⁸ Accuracy of the technique in detecting tumor margins was reported to be 96%.

To our knowledge, no targeted NIRF imaging of primary breast carcinoma has yet been performed using CA-XII as a target. Tafreshi et al., however, used a NIRF-labeled antibody against CA-XII for noninvasive detection of breast cancer lymph node metastasis in a xenograft mouse model.¹⁸ As few as 1,000 cancer cells could be detected using NIRF imaging, indicating the sensitivity of the technique. Although markers suitable for imaging of lymph node metastasis do not necessarily make good targets for primary breast cancer, the current study suggests that this is the case for CA-XII.

Selection of tumor-targeted agents

Nowadays, core needle biopsy is a common procedure for IHC analysis of ER, PR, and HER2 expression as a lead for patient-tailored therapies. Using IHC, functional expression of those tumor markers throughout the tumor could be identified at diagnosis/prior to imaging and used to select the appropriate targeted optical contrast agent (Fig. 3). This would allow to select those tumor markers that result in the highest signal-to-noise ratio or that exhibit specific favorable characteristics like enzymatic activity or internalization upon binding of the tumor-targeted optical contrast agent.

Development of tumor-targeted agents

In recent years, significant progress has been made in the development of optical imaging systems and non-toxic fluorophores.^{3,4,12,49} Already, a substantial amount of bio-engineered monoclonal antibodies are available for preclinical and clinical use (Supplementary Table 4). Monoclonal antibodies can be conjugated to optical contrast agents with relative ease and therefore facilitate the translation of targeted optical imaging towards the clinic.³⁹ Moreover, the development of so-called 'activatable' probes has added to the potential of optical imaging by providing exceptionally high signal-to-noise ratios. These imaging agents are optically silent in their native state, but become brightly fluorescent upon activation through cleavage by enzymes expressed by the tumor (e.g., CA-IX or CA-XII).⁹

CONCLUSION

Based on the seven tumor marker characteristics that are considered important for tumor-targeted optical imaging applications in breast cancer, we identified CXCR4, EpCAM, and CA-XII as markers of particular interest for development of tumor-targeted probes for clinical translation. At least one of these tumor markers was homogeneously expressed in approximately 80% of the patients included in our study. Although exhibiting some favorable characteristics for targeted imaging, HER2, VEGF-A, and FR- α did not reach the (modified) TASC threshold of ≥ 18 points to be prioritized as markers of particular interest for clinical translation. However, these markers do have considerable value when combined in a panel. The characteristics of $\alpha v\beta 3$ integrin receptor, CA-IX, MGB1, and Notch1 receptor were considered unfavorable for tumor-targeted imaging applications.

ACKNOWLEDGEMENTS

The authors wish to thank Dr. M van Oosten for useful discussions concerning potential tumor markers in breast cancer. We thank professor P.S. Low for his generous gift of mAb-343 for FR- α staining. This work was funded by the UEF-JSM Talent Grant from the University of Groningen. Contribution by the Dutch Cancer Society (KWF research fellowship to SGE) is gratefully acknowledged.

REFERENCES

1. Forouzanfar MH, Foreman KJ, Delossantos AM, et al. Breast and cervical cancer in 187 countries between 1980 and 2010: a systematic analysis. *Lancet* 2011;378:1461-1484.
2. Alvarez RH, Valero V, Hortobagyi GN. Emerging targeted therapies for breast cancer. *J Clin Oncol* 2010;28:3366-3379.
3. Themelis G, Yoo JS, Soh KS, et al. Real-time intraoperative fluorescence imaging system using light-absorption correction. *J Biomed Opt* 2009;14:064012.
4. Keereweer S, Kerrebijn JD, van Driel PB, et al. Optical image-guided surgery—where do we stand? *Mol Imaging Biol* 2011;13:199-207.
5. Ntziachristos V. Fluorescence molecular imaging. *Annu Rev Biomed Eng* 2006;8:1-33.
6. van Dam GM, Themelis G, Crane LM, et al. Intraoperative tumor-specific fluorescence imaging in ovarian cancer by folate receptor-alpha targeting: first in-human results. *Nat Med* 2011;17:1315-1319.
7. Luker GD, Luker KE. Optical imaging: current applications and future directions. *J Nucl Med* 2008;49:1-4.
8. Pleijhuis RG, Graafland M, de Vries J, et al. Obtaining adequate surgical margins in breast-conserving therapy for patients with early-stage breast cancer: current modalities and future directions. *Ann Surg Oncol* 2009;16:2717-2730.
9. Kirsch DG, Dinulescu DM, Miller JB, et al. A spatially and temporally restricted mouse model of soft tissue sarcoma. *Nat Med* 2007;13:992-997.
10. Themelis G, Harlaar NJ, Kelder W, et al. Enhancing surgical vision by using real-time imaging of alphavbeta3 integrin targeted near-infrared fluorescent agent. *Ann Surg Oncol* 2011;18:3506-3513.
11. Keereweer S, Hutteman M, Kerrebijn JD, et al. Translational optical imaging in diagnosis and treatment of cancer. *Curr Pharm Biotechnol* 2012;13:498-503.
12. Ntziachristos V, Yoo JS, van Dam GM. Current concepts and future perspectives on surgical optical imaging in cancer. *J Biomed Opt* 2010;15:066024.
13. van de Ven SM, Elias SG, van den Bosch MA, et al. Optical imaging of the breast. *Cancer Imaging* 2008;8:206-215.
14. Sloan EK, Pouliot N, Stanley KL, et al. Tumor-specific expression of alphavbeta3 integrin promotes spontaneous metastasis of breast cancer to bone. *Breast Cancer Res* 2006;8:R20.
15. Berry MG, Gui GP, Wells CA, et al. Integrin expression and survival in human breast cancer. *Eur J Surg Oncol* 2004;30:484-489.
16. Muller A, Homey B, Soto H, et al. Involvement of chemokine receptors in breast cancer metastasis. *Nature* 2001;410:50-56.
17. Furusato B, Mohamed A, Uhlen M, et al. CXCR4 and cancer. *Pathol Int* 2010;60:497-505.
18. Tafreshi NK, Bui MM, Bishop K, et al. Noninvasive detection of breast cancer lymph node metastasis using carbonic anhydrases IX and XII targeted imaging probes. *Clin Cancer Res* 2012;18:207-219.
19. Pinheiro C, Sousa B, Albergaria A, et al. GLUT1 and CAIX expression profiles in breast cancer correlate with adverse prognostic factors and MCT1 overexpression. *Histol Histopathol* 2011;26:1279-1286.
20. Watson PH, Chia SK, Wykoff CC, et al. Carbonic anhydrase XII is a marker of good prognosis in invasive breast carcinoma. *Br J Cancer* 2003;88:1065-1070.
21. Osta WA, Chen Y, Mikhitarian K, et al. EpCAM is overexpressed in breast cancer and is a potential target for breast cancer gene therapy. *Cancer Res* 2004;64:5818-5824.
22. Hartmann LC, Keeney GL, Lingle WL, et al. Folate receptor overexpression is associated with poor outcome in breast cancer. *Int J Cancer* 2007;121:938-942.
23. Saxena R, Dwivedi A. ErbB family receptor inhibitors as therapeutic agents in breast cancer: Current status and future clinical perspective. *Med Res Rev* 2012; 32:166-215.
24. Watson MA, Dintzis S, Darrow CM, et al. Mammaglobin expression in primary, metastatic, and occult breast cancer. *Cancer Res* 1999;59:3028-3031.

25. Zehentner BK, Carter D. Mammaglobin: a candidate diagnostic marker for breast cancer. *Clin Biochem* 2004;37:249-257.
26. Reedijk M, Odorcic S, Chang L, et al. High-level coexpression of JAG1 and NOTCH1 is observed in human breast cancer and is associated with poor overall survival. *Cancer Res* 2005;65:8530-8537.
27. Ranieri G, Patruno R, Ruggieri E, et al. Vascular endothelial growth factor (VEGF) as a target of bevacizumab in cancer: from the biology to the clinic. *Curr Med Chem* 2006;13:1845-1857.
28. Arias-Pulido H, Chaheer N, Gong Y, et al. Tumor stromal vascular endothelial growth factor A is predictive of poor outcome in inflammatory breast cancer. *BMC Cancer* 2012;12:298.
29. Dhakal HP, Naume B, Synnestevedt M, et al. Expression of vascular endothelial growth factor and vascular endothelial growth factor receptors 1 and 2 in invasive breast carcinoma: prognostic significance and relationship with markers for aggressiveness. *Histopathology* 2012;61:350-364.
30. Cimpean AM, Raica M, Suciuc C, et al. Vascular endothelial growth factor A (VEGF A) as individual prognostic factor in invasive breast carcinoma. *Rom J Morphol Embryol* 2008;49:303-308.
31. Ghosh S, Sullivan CA, Zerkowski MP, et al. High levels of vascular endothelial growth factor and its receptors (VEGFR-1, VEGFR-2, neuropilin-1) are associated with worse outcome in breast cancer. *Hum Pathol* 2008;39:1835-1843.
32. Konecny GE, Meng YG, Untch M, et al. Association between HER-2/neu and vascular endothelial growth factor expression predicts clinical outcome in primary breast cancer patients. *Clin Cancer Res* 2004;10:1706-1716.
33. Hartog H, Horlings HM, van der Veegt B, et al. Divergent effects of insulin-like growth factor-1 receptor expression on prognosis of estrogen receptor positive versus triple negative invasive ductal breast carcinoma. *Breast Cancer Res Treat* 2011;129:725-736.
34. Kononen J, Bubendorf L, Kallioniemi A, et al. Tissue microarrays for high-throughput molecular profiling of tumor specimens. *Nat Med* 1998;4:844-847.
35. Vermeulen JF, van Brussel AS, van der Groep P, et al. Immunophenotyping invasive breast cancer: paving the road for molecular imaging. *BMC Cancer* 2012;12:240.
36. van Oosten M, Crane LM, Bart J, et al. Selecting Potential Targetable Biomarkers for Imaging Purposes in Colorectal Cancer Using TArget Selection Criteria (TASC): A Novel Target Identification Tool. *Transl Oncol* 2011;4:71-82.
37. Viera AJ, Garrett JM. Understanding interobserver agreement: the kappa statistic. *Fam Med* 2005;37:360-363.
38. R Development Core Team (2013). R: A language and environment for statistical computing. R Foundation for Statistical Computing, Vienna, Austria. Available at: <http://www.R-project.org/>.
39. Pakkiri P, Lakhani SR, Smart CE. Current and future approach to the pathologist's assessment for targeted therapy in breast cancer. *Pathology* 2009;41:89-99.
40. Spizzo G, Fong D, Wurm M, et al. EpCAM expression in primary tumour tissues and metastases: an immunohistochemical analysis. *J Clin Pathol* 2011;64:415-420.
41. Camp RL, Chung GG, Rimm DL. Automated subcellular localization and quantification of protein expression in tissue microarrays. *Nat Med* 2002;8:1323-1327.
42. Taylor CR, Levenson RM. Quantification of immunohistochemistry--issues concerning methods, utility and semiquantitative assessment II. *Histopathology* 2006;49:411-424.
43. Kuil J, Buckle T, van Leeuwen FW. Imaging agents for the chemokine receptor 4 (CXCR4). *Chem Soc Rev* 2012;41:5239-5261.
44. Meincke M, Tiwari S, Hattermann K, et al. Near-infrared molecular imaging of tumors via chemokine receptors CXCR4 and CXCR7. *Clin Exp Metastasis* 2011;28:713-720.
45. Nimmagadda S, Pullambhatla M, Stone K, et al. Molecular imaging of CXCR4 receptor expression in human cancer xenografts with [64Cu]AMD3100 positron emission tomography. *Cancer Res* 2010;70:3935-3944.

46. Kuil J, Buckle T, Oldenburg J, et al. Hybrid peptide dendrimers for imaging of chemokine receptor 4 (CXCR4) expression. *Mol Pharm* 2011;8:2444-2453.
47. Sun Y, Shukla G, Pero SC, et al. Single tumor imaging with multiple antibodies targeting different antigens. *BioTechniques* 2012;0:1-3.
48. Zhu B, Wu G, Robinson H, et al. Tumor Margin Detection Using Quantitative NIRF Molecular Imaging Targeting EpCAM Validated by Far Red Gene Reporter iRFP. *Mol Imaging Biol* 2013.
49. Troyan SL, Kianzad V, Gibbs-Strauss SL, et al. The FLARE intraoperative near-infrared fluorescence imaging system: a first-in-human clinical trial in breast cancer sentinel lymph node mapping. *Ann Surg Oncol* 2009;16:2943-2952.

Supplementary Table 1. The target selection criteria (TASC) scoring system

Item	Marker characteristics according to the TASC scoring system*		Score
I	Localization of the marker	Membranous (extracellular domain)	5
		In close proximity of tumor cell (extracellular matrix)	3
		Cytoplasmic	0
II	Expression pattern of the marker	Diffuse expression throughout the tumor	4
		Mostly diffuse, some focal staining	2
		Mostly focal, some diffuse staining	0
III	Tumor-to-normal ratio	Tumor-to-normal ratio >3	3
		TASC definition**	
IV	Percentage of patients in which the marker is expressed	>90%	6
		70–90%	5
		50–69%	3
		10–49%	0
V	Previously imaged with success <i>in vivo</i>		2
VI	Enzymatic activity		1
VII	Internalization		1
		Maximum amount of points	22

* Modified from: van Oosten M, Crane LM, Bart J, van Leeuwen FW, van Dam GM. Selecting potential targetable tumor markers for imaging purposes in colorectal cancer using Target Selection Criteria (TASC): a novel target-identification tool. *Transl Oncol* 2011;4:71-82. Each tumor marker is assigned points on the basis of seven characteristics. A score of ≥ 18 points indicates that the tumor marker is of potential interest and justifies further exploration.

** Modified TASC score based on alternative thresholds for tumor marker expression rate.

Supplementary Table 2. Selection of potential tumor markers for targeted imaging in breast cancer according to the target selection criteria (TASC).

Tumor marker	Target Selection Criteria (TASC) items							
	I	II	III	IV	V	VI	VII	
<i>Max</i>	5	4	3	6	2	1	22	
1 CKCR4	Membranous ¹	Diffuse expression pattern in cancerous tissue Literature (n=8-1808): Mostly diffuse, focal ⁴ Current study (n=423): diffuse	T/N ratio >3 3	Percentage of tumor marker expression in cancerous tissue Literature (n=8-1808): expression in 12-90% of tumors ^{3,7} Proteinatlas (n=12): expression in 100% of tumors Current study (n=423): 60.2% membranous expression	Previously imaged in vivo Animal experiment ^{6,9}	Enzymatic activity Not described	Target internalization Yes ¹¹	Expression in normal breast tissue Literature (n=4-86): 0-55% weak, 0-22% moderate expression ^{3,3} Proteinatlas (n=2): moderate to strong expression Current study (n=10): 50% weak membranous expression
Points	5	4	3	6	2	0	21	
2 EPCAM	Membranous ¹	Literature (n=1715): diffuse ^{3,13} Current study (n=427): diffuse	4.2	Literature (n=17-1715): expression in 35-90% of tumors ^{3,13,31} Proteinatlas (n=34): expression in 60% of tumors Current study (n=427): 22.6% membranous expression	Animal experiment ^{32,33,37} Human trial ³⁸	Not described	Yes ^{30,40}	Literature (n=9-12): weak to moderate expression ^{4,42} Proteinatlas (n=4): weak to moderate expression Current study (n=11): 9% weak membranous expression
Points	5	4	3	3	2	0	18	
3 CA-XII	Membranous ¹	Literature (n=89): Mostly diffuse, focal ^{15,3} Current study (n=428): mostly diffuse, focal	4.6	Literature (n=14-103): expression in 71-80% of tumors ^{5,13} Proteinatlas (n=24): expression in 71% of tumors Current study (n=426): 29.6% membranous expression	Animal experiment ⁴¹	Yes ⁴³	Not described	Literature (n=28-47): in 89-90% weak to moderate, in 0-10% strong expression of ductal epithelium ^{1,5,2} Proteinatlas (n=3): moderate expression Current study (n=12): 8% weak membranous expression
Points	5	2	3	5	2	1	18	
4 Her2	Membranous ⁴⁴	Literature (n=530-2963): mostly diffuse as well as focal ^{16,36} Current study (n=418): mostly diffuse, focal	3.1	Literature (n=83-116,736): expression IHC 1+, 2+/3+ independent from FISH in 9-76% of tumors ^{45,67} Proteinatlas (n=32): expression in 81% of tumors Current study (n=418): 17.4% membranous expression	Animal experiment ^{68,72}	Not described	Yes ⁷³	Literature (n=15-63): no to weak expression ^{45,67} Proteinatlas (n=8): weak to moderate expression Current study (n=11): 36% weak membranous expression
Points	5	2	3	3	2	0	16	
5 VEGF-A	Extracellular matrix ^{13,15}	Literature (n=112-200): mostly diffuse, focal ^{12,16} Current study (n=431): diffuse	3.1	Literature (n=25-611): expression in 18-89% of tumors ^{16,36} Proteinatlas (n=11): expression in 100% of tumors Current study (n=431): 15.0% extracellular expression	Animal experiment ^{75,79} Human trial (NCT01508572)	Not described	Not described	Literature (n=14-211): no to moderate expression ^{32,33,36,80} Proteinatlas (n=2): strong expression Current study (n=12): 58% weak, 42% moderate expression
Points	3	4	3	0	2	0	15	
6 FR-α	Membranous ⁵¹	Literature (n=63): diffuse ⁴⁴ Current study (n=410): diffuse	3.1	Literature (n=7-63): expression in 33-86% of tumors ^{46,46} Proteinatlas: not yet assessed Current study (n=410): 6.3% membranous expression	Animal experiment ⁴⁷ Human trial ⁴⁸	Not described	Yes ⁴⁹	Literature (n=4-5): weak (60%) to moderate (20%) expression ^{45,60} Proteinatlas: not yet assessed Current study (n=12): 25% weak membranous expression
Points	5	4	3	0	2	0	15	
7 Notch1	Membranous ⁶⁹	Literature (n=): diffuse ⁸⁰ Current study (n=424): diffuse	2.2	Literature (n=48-408): expression in 100% of tumors Proteinatlas (n=24): expression in 100% of tumors Current study (n=424): 0.3% membranous expression	Animal experiment ¹⁰⁰	Not described	Yes ¹⁰⁵	Literature (n=22-79): weak to moderate expression ^{101,101,106,106} Proteinatlas (n=2): moderate expression Current study (n=10): 10% weak membranous expression
Points	5	4	0	0	2	0	12	
8 αvβ3	Membranous ²⁶	Literature (n=61): focal, diffuse, confined to the periphery of cell nests ^{6,77} Current study (n=422): mostly focal, diffuse	3.3	Literature (n=5-99): expression in 30-100% of tumors ^{70,82} Proteinatlas (n=24): expression in 87% of tumors Current study (n=422): 0.8% membranous expression	Animal experiment ⁸⁷ Human trial ^{88,88}	Not described	Yes ⁹⁰	Literature (n=6-15): no to moderate expression ^{70,82,87,91} Proteinatlas (n=3): no to moderate expression Current study (n=11): 9% weak membranous expression
Points	5	0	3	0	2	0	11	
9 CA-IX	Membranous ¹	Literature (n=891-103): mostly diffuse, focal ^{1,32} Current study (n=415): mostly diffuse, focal	1.1	Literature (n=14-400): expression in 11-57% of tumors ^{61,62,92,96} Proteinatlas (n=20): no expression Current study (n=415): 4.2% membranous expression	Animal experiment ^{93,97}	Yes ⁹⁴	Yes ⁹⁸	Literature (n=23-47): in 2-74% weak to moderate expression of ductal epithelium ^{1,32} Proteinatlas (n=5): no expression Current study (n=12): 30% weak membranous expression
Points	5	2	0	0	2	1	11	
10 MGB1	Membranous, secreted ^{109,110}	Literature: mostly diffuse as well as focal ¹⁰⁹ Current study (n=427): Mostly diffuse, focal	1.7	Literature (n=36-238): expression in 12-84% of tumors ^{67,108,131,17} Proteinatlas (n=11): expression in 72% of tumors Current study (n=427): 4.5% membranous expression	Animal experiment ¹⁰⁸	Not described	Not described	Literature (n=21-50): weak to moderate staining in 43-63% ^{107,108,110,110} Proteinatlas (n=3): weak to strong staining Current study (n=14): 22% moderate membranous expression
Points	5	2	0	0	2	0	9	

αvβ3, alpha v beta 3 integrin receptor; CA-IX, carbonic anhydrase IX; CA-XII, carbonic anhydrase XII; CXCR4, C-X-C chemokine receptor 4; EPCAM, epithelial cell adhesion molecule; FR-α, folate receptor alpha; HER2, human epidermal growth factor receptor 2; MGB1, mammaglobin 1; VEGF-A, vascular endothelial growth factor-α.

REFERENCES WITH SUPPLEMENTARY TABLE 2

1. Fischer T, Nagel F, Jacobs S, et al. Reassessment of CXCR4 chemokine receptor expression in human normal and neoplastic tissues using the novel rabbit monoclonal antibody UMB-2. *PLoS One* 2008; 3:e4069.
2. Muller A, Homey B, Soto H, et al. Involvement of chemokine receptors in breast cancer metastasis. *Nature* 2001; 410:50-56.
3. Salvucci O, Bouchard A, Baccarelli A, et al. The role of CXCR4 receptor expression in breast cancer: a large tissue microarray study. *Breast Cancer Res Treat* 2006; 97:275-283.
4. Kato M, Kitayama J, Kazama S, et al. Expression pattern of CXC chemokine receptor-4 is correlated with lymph node metastasis in human invasive ductal carcinoma. *Breast Cancer Res* 2003; 5:R144-50.
5. Cabioglu N, Yazici MS, Arun B, et al. CCR7 and CXCR4 as novel biomarkers predicting axillary lymph node metastasis in T1 breast cancer. *Clin Cancer Res* 2005; 11:5686-5693.
6. Andre F, Xia W, Conforti R, et al. CXCR4 expression in early breast cancer and risk of distant recurrence. *Oncologist* 2009; 14:1182-1188.
7. Li YM, Pan Y, Wei Y, et al. Upregulation of CXCR4 is essential for HER2-mediated tumor metastasis. *Cancer Cell* 2004; 6:459-469.
8. Nimmagadda S, Pullambhatla M, Stone K, et al. Molecular imaging of CXCR4 receptor expression in human cancer xenografts with [⁶⁴Cu]AMD3100 positron emission tomography. *Cancer Res* 2010; 70: 3935-3944.
9. Meincke M, Tiwari S, Hattermann K, et al. Near-infrared molecular imaging of tumors via chemokine receptors CXCR4 and CXCR7. *Clin Exp Metastasis* 2011; 28:713-720.
10. Kuil J, Buckle T, Oldenburg J, et al. Hybrid peptide dendrimers for imaging of chemokine receptor 4 (CXCR4) expression. *Mol Pharm* 2011; 8:2444-2453.
11. Haribabu B, Richardson RM, Fisher I, et al. Regulation of human chemokine receptors CXCR4. Role of phosphorylation in desensitization and internalization. *J Biol Chem* 1997; 272:28726-28731.
12. Maae E, Nielsen M, Steffensen KD, et al. Estimation of immunohistochemical expression of VEGF-A in ductal carcinomas of the breast. *J Histochem Cytochem* 2011; 59:750-760.
13. Arias-Pulido H, Chaheer N, Gong Y, et al. Tumor stromal vascular endothelial growth factor A is predictive of poor outcome in inflammatory breast cancer. *BMC Cancer* 2012; 12:298.
14. Nagengast WB, de Vries EG, Hospers GA, et al. *In vivo* VEGF-A imaging with radiolabeled bevacizumab in a human ovarian tumor xenograft. *J Nucl Med* 2007; 48:1313-1319.
15. Stollman TH, Scheer MG, Franssen GM, et al. Tumor accumulation of radiolabeled bevacizumab due to targeting of cell- and matrix-associated VEGF-A isoforms. *Cancer Biother Radiopharm* 2009; 24:195-200.
16. Ghasemi M, Emadian O, Naghshvar F, et al. Immunohistochemical expression of vascular endothelial growth factor and its correlation with tumor grade in breast ductal carcinoma. *Acta Med Iran* 2011; 49:776-779.
17. Cimpean AM, Raica M, Suciuc C, et al. Vascular endothelial growth factor A (VEGF-A) as individual prognostic factor in invasive breast carcinoma. *Rom J Morphol Embryol* 2008; 49:303-308.
18. Hu SE, Zhang YJ, Cui YM, et al. Expression of vascular endothelial growth factor A and C in human breast cancer and their significance. *Ai Zheng* 2005; 24:1076-1079.
19. Konecny GE, Meng YG, Untch M, et al. Association between HER-2/neu and vascular endothelial growth factor expression predicts clinical outcome in primary breast cancer patients. *Clin Cancer Res* 2004; 10: 1706-1716.
20. Lee JS, Kim HS, Jung JJ, et al. Expression of vascular endothelial growth factor in invasive ductal carcinoma of the breast and the relation to angiogenesis and p53 and HER-2/neu protein expression. *Appl Immunohistochem Mol Morphol* 2002; 10:289-295.
21. Dhakal HP, Naume B, Synnestvedt M, et al. Expression of vascular endothelial growth factor and vascular endothelial growth factor receptors 1 and 2 in invasive breast carcinoma: prognostic significance and relationship with markers for aggressiveness. *Histopathology* 2012; 61:350-364.

22. Maae E, Olsen DA, Steffensen KD, et al. Prognostic impact of placenta growth factor and vascular endothelial growth factor A in patients with breast cancer. *Breast Cancer Res Treat* 2012; 133:257-265.
23. Wang Z, Shi Q, Wang Z, et al. Clinicopathologic correlation of cancer stem cell markers CD44, CD24, VEGF-A and HIF-1alpha in ductal carcinoma in situ and invasive ductal carcinoma of breast: an immunohistochemistry-based pilot study. *Pathol Res Pract* 2011; 207:505-513.
24. Kafousi M, Vrekoussis T, Tsentelierou E, et al. Immunohistochemical study of the angiogenetic network of VEGF-A, HIF1alpha, VEGF-AR-2 and endothelial nitric oxide synthase (eNOS) in human breast cancer. *Pathol Oncol Res* 2012; 18:33-41.
25. Noranizah W, Siti-Aishah MA, Munirah MA, et al. Immunohistochemical expression of vascular endothelial growth factor (VEGF-A) and p53 in breast lesions. *Clin Ter* 2010; 161:129-137.
26. Al-Harris ES, Al-Janabi AA, Al-Toriahi KM, et al. Over expression of vascular endothelial growth factor in correlation to Ki-67, grade, and stage of breast cancer. *Saudi Med J* 2008; 29:1099-1104.
27. Terwisscha van Scheltinga AG, van Dam GM, Nagengast WB, et al. Intraoperative near-infrared fluorescence tumor imaging with vascular endothelial growth factor and human epidermal growth factor receptor 2 targeting antibodies. *J Nucl Med* 2011; 52:1778-1785.
28. Cohen R, Stammes MA, de Roos IH, et al. Inert coupling of IRDye 800CW to monoclonal antibodies for clinical optical imaging of tumor targets. *EJNMMI Res* 2011; 1:31.
29. Zhang Y, Hong H, Engle JW, et al. Positron Emission Tomography and Near-Infrared Fluorescence Imaging of Vascular Endothelial Growth Factor with Dual-Labeled Bevacizumab. *Am J Nucl Med Mol Imaging* 2012; 2:1-13.
30. Safwat MD, Habib F, Elayat A, et al. Morphometric and immunohistochemical study of angiogenic marker expressions in invasive ductal carcinoma of human breast. *Folia Morphol (Warsz)* 2009; 68:144-155.
31. Cimino A, Halushka M, Illei P, et al. Epithelial cell adhesion molecule (EpCAM) is overexpressed in breast cancer metastases. *Breast Cancer Res Treat* 2010; 123:701-708.
32. Sun Y, Shukla G, Pero SC, et al. Single tumor imaging with multiple antibodies targeting different antigens. *BioTechniques* 2012; 0:1-3.
33. Spizzo G, Went P, Dirnhofer S, et al. High Ep-CAM expression is associated with poor prognosis in node-positive breast cancer. *Breast Cancer Res Treat* 2004; 86:207-213.
34. Gastl G, Spizzo G, Obrist P, et al. Ep-CAM overexpression in breast cancer as a predictor of survival. *Lancet* 2000; 356:1981-1982.
35. Spizzo G, Fong D, Wurm M, et al. EpCAM expression in primary tumour tissues and metastases: an immunohistochemical analysis. *J Clin Pathol* 2011; 64:415-420.
36. Eder M, Knackmuss S, Le Gall F, et al. 68Ga-labelled recombinant antibody variants for immuno-PET imaging of solid tumours. *Eur J Nucl Med Mol Imaging* 2010; 37:1397-1407.
37. Thurber GM, Weissleder R. Quantitating antibody uptake *in vivo*: conditional dependence on antigen expression levels. *Mol Imaging Biol* 2011; 13:623-632.
38. Schmidt M, Scheulen ME, Dittrich C, et al. An open-label, randomized phase II study of adecatumumab, a fully human anti-EpCAM antibody, as monotherapy in patients with metastatic breast cancer. *Ann Oncol* 2010; 21:275-282.
39. Litvinov SV, Bakker HA, Gourevitch MM, et al. Evidence for a role of the epithelial glycoprotein 40 (EpCAM) in epithelial cell-cell adhesion. *Cell Adhes Commun* 1994; 2:417-428.
40. Hussain S, Pluckthun A, Allen TM, et al. Antitumor activity of an epithelial cell adhesion molecule targeted nanovesicular drug delivery system. *Mol Cancer Ther* 2007; 6:3019-3027.
41. Osta WA, Chen Y, Mikhitarian K, et al. EpCAM is overexpressed in breast cancer and is a potential target for breast cancer gene therapy. *Cancer Res* 2004; 64:5818-5824.
42. Keller PJ, Lin A, Arendt LM, et al. Mapping the cellular and molecular heterogeneity of normal and malignant breast tissues and cultured cell lines. *Breast Cancer Res* 2010; 12:R87.

43. Low PS, Kularatne SA. Folate-targeted therapeutic and imaging agents for cancer. *Curr Opin Chem Biol* 2009; 13:256-262.
44. Hartmann LC, Keeney GL, Lingle WL, et al. Folate receptor overexpression is associated with poor outcome in breast cancer. *Int J Cancer* 2007; 121:938-942.
45. Parker N, Turk MJ, Westrick E, et al. Folate receptor expression in carcinomas and normal tissues determined by a quantitative radioligand binding assay. *Anal Biochem* 2005; 338:284-293.
46. Segal EI, Low PS. Tumor detection using folate receptor-targeted imaging agents. *Cancer Metastasis Rev* 2008; 27:655-664.
47. Meier R, Henning TD, Boddington S, et al. Breast cancers: MR imaging of folate-receptor expression with the folate-specific nanoparticle P1133. *Radiology* 2010; 255:527-535.
48. van Dam GM, Themelis G, Crane LM, et al. Intraoperative tumor-specific fluorescence imaging in ovarian cancer by folate receptor- α targeting: first in-human results. *Nat Med* 2011; 17:1315-1319.
49. Sabharanjak S, Mayor S. Folate receptor endocytosis and trafficking. *Adv Drug Deliv Rev* 2004; 56:1099-1109.
50. Ross JF, Chaudhuri PK, Ratnam M. Differential regulation of folate receptor isoforms in normal and malignant tissues *in vivo* and in established cell lines. Physiologic and clinical implications. *Cancer* 1994; 73:2432-2443.
51. Tafreshi NK, Bui MM, Bishop K, et al. Noninvasive detection of breast cancer lymph node metastasis using carbonic anhydrases IX and XII targeted imaging probes. *Clin Cancer Res* 2012; 18:207-219.
52. Wykoff CC, Beasley N, Watson PH, et al. Expression of the hypoxia-inducible and tumor-associated carbonic anhydrases in ductal carcinoma in situ of the breast. *Am J Pathol* 2001; 158:1011-1019.
53. Watson PH, Chia SK, Wykoff CC, et al. Carbonic anhydrase XII is a marker of good prognosis in invasive breast carcinoma. *Br J Cancer* 2003; 88:1065-1070.
54. Fink-Retter A, Gschwantler-Kaulich D, Hudelist G, et al. Differential spatial expression and activation pattern of EGFR and HER2 in human breast cancer. *Oncol Rep* 2007; 18:299-304.
55. Ohlschlegel C, Zahel K, Kradolfer D, et al. HER2 genetic heterogeneity in breast carcinoma. *J Clin Pathol* 2011; 64:1112-1116.
56. Yaziji H, Goldstein LC, Barry TS, et al. HER-2 testing in breast cancer using parallel tissue-based methods. *JAMA* 2004; 291:1972-1977.
57. Vogel UF. Confirmation of a low HER2 positivity rate of breast carcinomas - limitations of immunohistochemistry and *in situ* hybridization. *Diagn Pathol* 2010; 5:50.
58. Arapantoni-Dadioti P, Valavanis C, Gavrassa T, et al. Discordant expression of hormone receptors and HER2 in breast cancer. A retrospective comparison of primary tumors with paired metachronous recurrences or metastases. *J BUON* 2012; 17:277-283.
59. Yang YL, Fan Y, Lang RG, et al. Genetic heterogeneity of HER2 in breast cancer: impact on HER2 testing and its clinicopathologic significance. *Breast Cancer Res Treat* 2012; 134:1095-1102.
60. Moise M, Motoc A, Raducan A, et al. Human epidermal growth factor receptor 2 (HER2/neu) supraexpression in the mammary tumors. *Rom J Morphol Embryol* 2011; 52:1101-1105.
61. Recareanu F, Simionescu C, Georgescu CV, et al. Ductal invasive mammary carcinoma--clinicopathological prognostic factors related to immunohistochemical expression of hormonal receptors and HER2/neu oncoprotein. *Rom J Morphol Embryol* 2011; 52:1059-1064.
62. Laurinaviciene A, Dasevicius D, Ostapenko V, et al. Membrane connectivity estimated by digital image analysis of HER2 immunohistochemistry is concordant with visual scoring and fluorescence *in situ* hybridization results: algorithm evaluation on breast cancer tissue microarrays. *Diagn Pathol* 2011; 6:87.
63. Ambroise M, Ghosh M, Mallikarjuna VS, et al. Immunohistochemical profile of breast cancer patients at a tertiary care hospital in South India. *Asian Pac J Cancer Prev* 2011; 12:625-629.
64. Cuadros M, Cano C, Lopez FJ, et al. HER2 status in breast cancer: experience of a Spanish National Reference Centre. *Clin Transl Oncol* 2011; 13:335-340.

65. Thang VH, Tani E, Van TT, et al. HER2 status in operable breast cancers from Vietnamese women: Analysis by immunohistochemistry (IHC) and automated silver enhanced in situ hybridization (SISH). *Acta Oncol* 2011; 50:360-366.
66. Goddard KA, Weinmann S, Richert-Boe K, et al. HER2 evaluation and its impact on breast cancer treatment decisions. *Public Health Genomics* 2012; 15:1-10.
67. Owens MA, Horten BC, Da Silva MM. HER2 amplification ratios by fluorescence in situ hybridization and correlation with immunohistochemistry in a cohort of 6556 breast cancer tissues. *Clin Breast Cancer* 2004; 5:63-69.
68. Ogawa M, Kosaka N, Choyke PL, et al. *In vivo* molecular imaging of cancer with a quenching near-infrared fluorescent probe using conjugates of monoclonal antibodies and indocyanine green. *Cancer Res* 2009; 69:1268-1272.
69. Chernomordik V, Hassan M, Lee SB, et al. Quantitative analysis of HER2 receptor expression *in vivo* by near-infrared optical imaging. *Mol Imaging* 2010; 9:192-200.
70. Chopra A. Trastuzumab complexed to near-infrared fluorophore indocyanine green. In: Anonymous *Molecular Imaging and Contrast Agent Database (MICAD)*. 2004.
71. Sampath L, Kwon S, Ke S, et al. Dual-labeled trastuzumab-based imaging agent for the detection of human epidermal growth factor receptor 2 overexpression in breast cancer. *J Nucl Med* 2007; 48:1501-1510.
72. Leung K. IRDye 800-Labeled anti-epidermal growth factor receptor Affibody. 2010.
73. Guillemard V, Nedev HN, Berezov A, et al. HER2-mediated internalization of a targeted prodrug cytotoxic conjugate is dependent on the valency of the targeting ligand. *DNA Cell Biol* 2005; 24:350-358.
74. Press MF, Cordon-Cardo C, Slamon DJ. Expression of the HER-2/neu proto-oncogene in normal human adult and fetal tissues. *Oncogene* 1990; 5:953-962.
75. Ratcliffe N, Wells W, Wheeler K, et al. The combination of in situ hybridization and immunohistochemical analysis: an evaluation of HER2/neu expression in paraffin-embedded breast carcinomas and adjacent normal-appearing breast epithelium. *Mod Pathol* 1997; 10:1247-1252.
76. Beer AJ, Niemeyer M, Carlsen J, et al. Patterns of alphavbeta3 expression in primary and metastatic human breast cancer as shown by 18F-Galacto-RGD PET. *J Nucl Med* 2008; 49:255-259.
77. Gui GP, Wells CA, Browne PD, et al. Integrin expression in primary breast cancer and its relation to axillary nodal status. *Surgery* 1995; 117:102-108.
78. Pignatelli M, Cardillo MR, Hanby A, et al. Integrins and their accessory adhesion molecules in mammary carcinomas: loss of polarization in poorly differentiated tumors. *Hum Pathol* 1992; 23:1159-1166.
79. Berry MG, Gui GP, Wells CA, et al. Integrin expression and survival in human breast cancer. *Eur J Surg Oncol* 2004; 30:484-489.
80. Gasparini G, Brooks PC, Biganzoli E, et al. Vascular integrin alpha(v)beta3: a new prognostic indicator in breast cancer. *Clin Cancer Res* 1998; 4:2625-2634.
81. Damjanovich L, Fulop B, Adany R, et al. Integrin expression on normal and neoplastic human breast epithelium. *Acta Chir Hung* 1997; 36:69-71.
82. Koukoulis GK, Virtanen I, Korhonen M, et al. Immunohistochemical localization of integrins in the normal, hyperplastic, and neoplastic breast. Correlations with their functions as receptors and cell adhesion molecules. *Am J Pathol* 1991; 139:787-799.
83. Edwards WB, Akers WJ, Ye Y, et al. Multimodal imaging of integrin receptor-positive tumors by bioluminescence, fluorescence, gamma scintigraphy, and single-photon emission computed tomography using a cyclic RGD peptide labeled with a near-infrared fluorescent dye and a radionuclide. *Mol Imaging* 2009; 8:101-110.
84. Bunschoten A, Buckle T, Visser NL, et al. Multimodal interventional molecular imaging of tumor margins and distant metastases by targeting alpha(v) beta(3) integrin. *ChemBiochem* 2012; 13:1039-1045.
85. Lee H, Akers W, Bhushan K, et al. Near-infrared pH-activatable fluorescent probes for imaging primary and metastatic breast tumors. *Bioconjug Chem* 2011; 22:777-784.

86. Wang W, Ke S, Wu Q, et al. Near-infrared optical imaging of integrin alphavbeta3 in human tumor xenografts. *Mol Imaging* 2004; 3:343-351.
87. Liu Z, Jia B, Zhao H, et al. Specific Targeting of Human Integrin alpha(v)beta (3) with (111)In-Labeled Abegrin in Nude Mouse Models. *Mol Imaging Biol* 2011; 13:112-120.
88. Axelsson R, Bach-Gansmo T, Castell-Conesa J, et al. An open-label, multicenter, phase 2a study to assess the feasibility of imaging metastases in late-stage cancer patients with the alpha v beta 3-selective angiogenesis imaging agent ^{99m}Tc-NC100692. *Acta Radiol* 2010; 51:40-46.
89. Posey JA, Khazaeli MB, DelGrosso A, et al. A pilot trial of Vitaxin, a humanized anti-vitronectin receptor (anti alpha v beta 3) antibody in patients with metastatic cancer. *Cancer Biother Radiopharm* 2001; 16:125-132.
90. Sancey L, Garanger E, Foillard S, et al. Clustering and internalization of integrin alphavbeta3 with a tetrameric RGD-synthetic peptide. *Mol Ther* 2009; 17:837-843.
91. Gui GP, Wells CA, Browne PD, et al. Integrin expression in primary breast cancer and its relation to axillary nodal status. *Surgery* 1995; 117:102-108.
92. Chia SK, Wykoff CC, Watson PH, et al. Prognostic significance of a novel hypoxia-regulated marker, carbonic anhydrase IX, in invasive breast carcinoma. *J Clin Oncol* 2001; 19:3660-3668.
93. Hussain SA, Ganesan R, Reynolds G, et al. Hypoxia-regulated carbonic anhydrase IX expression is associated with poor survival in patients with invasive breast cancer. *Br J Cancer* 2007; 96:104-109.
94. Trastour C, Benizri E, Ettore F, et al. HIF-1alpha and CA IX staining in invasive breast carcinomas: prognosis and treatment outcome. *Int J Cancer* 2007; 120:1451-1458.
95. Colpaert CG, Vermeulen PB, Fox SB, et al. The presence of a fibrotic focus in invasive breast carcinoma correlates with the expression of carbonic anhydrase IX and is a marker of hypoxia and poor prognosis. *Breast Cancer Res Treat* 2003; 81:137-147.
96. Brennan DJ, Jirstrom K, Kronblad A, et al. CA IX is an independent prognostic marker in premenopausal breast cancer patients with one to three positive lymph nodes and a putative marker of radiation resistance. *Clin Cancer Res* 2006; 12:6421-6431.
97. Groves K, Bao B, Zhang J, et al. Synthesis and evaluation of near-infrared fluorescent sulfonamide derivatives for imaging of hypoxia-induced carbonic anhydrase IX expression in tumors. *Bioorg Med Chem Lett* 2012; 22:653-657.
98. Xu C, Lo A, Yammanuru A, et al. Unique biological properties of catalytic domain directed human anti-CAIX antibodies discovered through phage-display technology. *PLoS One* 2010; 5:e9625.
99. Zardawi SJ, Zardawi I, McNeil CM, et al. High Notch1 protein expression is an early event in breast cancer development and is associated with the HER-2 molecular subtype. *Histopathology* 2010; 56:286-296.
100. Yao K, Rizzo P, Rajan P, et al. Notch1 and Notch4 Receptors as Prognostic Markers in Breast Cancer. *Int J Surg Pathol* 2011; 19:607-613.
101. Ma D, Dong X, Zang S, et al. Aberrant expression and clinical correlation of Notch signaling molecules in breast cancer of Chinese population. *Asia Pac J Clin Oncol* 2011; 7:385-391.
102. Li Y, Burns JA, Cheney CA, et al. Distinct expression profiles of Notch1 protein in human solid tumors: Implications for development of targeted therapeutic monoclonal antibodies. *Biologics* 2010; 4:163-171.
103. Reedijk M, Odorcic S, Chang L, et al. High-level coexpression of JAG1 and NOTCH1 is observed in human breast cancer and is associated with poor overall survival. *Cancer Res* 2005; 65:8530-8537.
104. Parr C, Watkins G, Jiang WG. The possible correlation of Notch1 and Notch2 with clinical outcome and tumour clinicopathological parameters in human breast cancer. *Int J Mol Med* 2004; 14:779-786.
105. Hansson EM, Lanner F, Das D, et al. Control of Notch-ligand endocytosis by ligand-receptor interaction. *J Cell Sci* 2010; 123:2931-2942.
106. Li Y, Burns JA, Cheney CA, et al. Distinct expression profiles of Notch1 protein in human solid tumors: Implications for development of targeted therapeutic monoclonal antibodies. *Biologics* 2010; 4:163-171.

107. Zuo L, Li L, Wang Q, et al. Mammaglobin as a potential molecular target for breast cancer drug delivery. *Cancer Cell Int* 2009; 9:8.
108. Tafreshi NK, Enkemann SA, Bui MM, et al. A mammaglobin-A targeting agent for noninvasive detection of breast cancer metastasis in lymph nodes. *Cancer Res* 2011; 71:1050-1059.
109. Zehentner BK, Carter D. Mammaglobin: a candidate diagnostic marker for breast cancer. *Clin Biochem* 2004; 37:249-257.
110. Raica M, Cimpean AM, Meche A, et al. Analysis of the immunohistochemical expression of mammaglobin 1 in primary breast carcinoma and lymph node metastasis. *Rom J Morphol Embryol* 2009; 50:341-347.
111. Rehman F, Nagi AH, Hussain M. Immunohistochemical expression and correlation of mammaglobin with the grading system of breast carcinoma. *Indian J Pathol Microbiol* 2010; 53:619-623.
112. Sasaki E, Tsunoda N, Hatanaka Y, et al. Breast-specific expression of MGB1/mammaglobin: an examination of 480 tumors from various organs and clinicopathological analysis of MGB1-positive breast cancers. *Mod Pathol* 2007; 20:208-214.
113. Watson MA, Dintzis S, Darrow CM, et al. Mammaglobin expression in primary, metastatic, and occult breast cancer. *Cancer Res* 1999; 59:3028-3031.
114. Al-Joudi FS, Kaid FA, Ishak I, et al. Expression of human mammaglobin and clinicopathologic correlations in breast cancer: the findings in Malaysia. *Indian J Pathol Microbiol* 2011; 54:284-289.
115. Zafrakas M, Petschke B, Donner A, et al. Expression analysis of mammaglobin A (SCGB2A2) and lipophilin B (SCGB1D2) in more than 300 human tumors and matching normal tissues reveals their co-expression in gynecologic malignancies. *BMC Cancer* 2006; 6:88.
116. O'Brien N, Maguire TM, O'Donovan N, et al. Mammaglobin A: a promising marker for breast cancer. *Clin Chem* 2002; 48:1362-1364.
117. Fleming TP, Watson MA. Mammaglobin, a breast-specific gene, and its utility as a marker for breast cancer. *Ann N Y Acad Sci* 2000; 923:78-89.

Supplementary Table 3. Top 10 combinations of tumor markers and associated detection rates both observed and following bootstrap resampling to account for sampling variability in all 379 cases with information on all 10 evaluated markers. Results show that several combinations of tumor markers are possible with similar detection rates. Bootstrapping (2000-fold) was performed to evaluate robustness of the results. The existence of discrepancies between observed and bootstrapped rank indicate that the optimal marker combination as calculated for our study population might be an overestimation from the true situation, limiting generability.

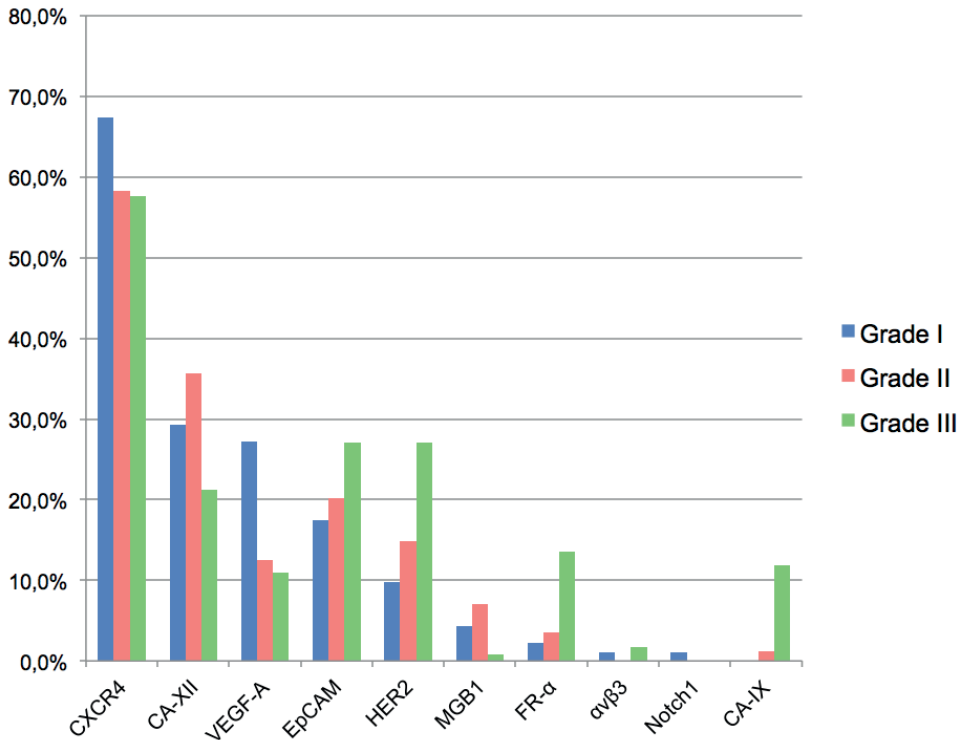
	Observed results		Bootstrap results (2000-fold)		Presence of marker in combination										
	Detection rate	Rank	Mean rank	Probability of top 10 ranking	CXCR4	CA-XII	EpCAM	HER2	VEGF	FR- α	MGB1	CA-IX	$\alpha v\beta 3$	Notch1	
Individual marker evaluation															
CXCR4	60.2%		1	1.0	Yes										
CA-XII	29.6%		2	2.0	1.00	Yes									
EpCAM	21.6%		3	3.1	1.00		Yes								
HER2	17.4%		4	4.2	1.00			Yes							
VEGF-A	15.6%		5	4.8	1.00				Yes						
FR- α	6.3%		6	6.2	1.00					Yes					
MGB1	4.5%		7	7.2	1.00						Yes				
CA-IX	4.2%		8	7.6	1.00							Yes			
$\alpha v\beta 3$	0.8%		9	9.0	1.00								Yes		
Notch1	0.3%		10	10.0	1.00									Yes	
Times individual marker in Top 10 out of 10 combinations:															
						1	1	1	1	1	1	1	1	1	1
Evaluation of all combinations of two markers															
CXCR4 CA-XII	69.9%		1	1.3	1.00	Yes	Yes								
CXCR4 EpCAM	68.1%		2	2.1	1.00	Yes	Yes								
CXCR4 HER2	67.3%		3	2.7	1.00	Yes		Yes							
CXCR4 VEGF-A	64.5%		4	4.0	1.00	Yes			Yes						
CXCR4 FR- α	62.0%		5	5.4	1.00	Yes				Yes					
CXCR4 MGB1	61.5%		6	6.0	1.00	Yes					Yes				
CXCR4 CA-IX	61.2%		7	6.7	1.00	Yes						Yes			
CXCR4 $\alpha v\beta 3$	60.4%		8	7.9	1.00	Yes							Yes		
CXCR4 Notch1	60.2%		9	9.0	1.00	Yes								Yes	
CA-XII EpCAM	46.7%		10	10.0	0.95		Yes	Yes							
Times individual marker in Top 10 out of 45 combinations:															
							9	2	2	1	1	1	1	1	1
Evaluation of all combinations of three markers															
CXCR4 CA-XII EpCAM	76.5%		1	1.5	1.00	Yes	Yes	Yes							
CXCR4 CA-XII HER2	76.3%		2	2.3	1.00	Yes	Yes	Yes							
CXCR4 EpCAM HER2	73.6%		3	8.9	0.72	Yes	Yes	Yes							
CXCR4 CA-XII VEGF-A	72.8%		4	6.1	1.00	Yes	Yes	Yes							
CXCR4 CA-XII FR- α	71.5%		5	6.7	0.92	Yes	Yes	Yes							
CXCR4 EpCAM VEGF-A	71.5%		6	9.9	0.63	Yes	Yes	Yes							
CXCR4 CA-XII MGB1	71.2%		7	7.4	0.83	Yes	Yes	Yes			Yes				
CXCR4 CA-XII CA-IX	71.0%		8	7.8	0.77	Yes	Yes	Yes				Yes			
CXCR4 HER2 VEGF-A	71.0%		9	15.0	0.13	Yes	Yes	Yes					Yes		
CXCR4 CA-XII $\alpha v\beta 3$	70.2%		10	7.6	0.78	Yes	Yes	Yes						Yes	
Times individual marker in Top 10 out of 120 combinations:															
						10	7	3	3	3	1	1	1	1	0

Evaluation of all combinations of four markers																		
CXCR4	CA-XII	EpCAM	HER2															
				81.3%	1	1.1	1.00	Yes	Yes									
CXCR4	CA-XII	EpCAM	VEGF-A	78.9%	2	4.8	0.98	Yes	Yes									
CXCR4	CA-XII	HER2	VEGF-A	78.6%	3	9.3	0.70	Yes	Yes									
CXCR4	CA-XII	EpCAM	MGB1	77.8%	4	7.2	0.85	Yes	Yes	Yes								
CXCR4	CA-XII	EpCAM	FR- α	77.6%	5	6.0	0.91	Yes	Yes									
CXCR4	CA-XII	EpCAM	CA-IX	77.0%	6	7.5	0.83	Yes	Yes	Yes								
CXCR4	CA-XII	HER2	MGB1	77.0%	7	11.1	0.58	Yes	Yes									
CXCR4	CA-XII	HER2	CA-IX	77.0%	8	12.1	0.55	Yes	Yes	Yes								
CXCR4	CA-XII	EpCAM	α v β 3	76.8%	9	8.3	0.79	Yes	Yes	Yes								
CXCR4	CA-XII	HER2	FR- α	76.8%	10	10.9	0.62	Yes	Yes	Yes								
Times individual marker in Top 10 out of 210 combinations:																		
							10	10	6	5	2	2	2	2	1	0		
Evaluation of all combinations of five markers																		
CXCR4	CA-XII	EpCAM	HER2	VEGF-A														
					83.1%	1	1.1	1.00	Yes	Yes	Yes							
CXCR4	CA-XII	EpCAM	HER2	MGB1	82.1%	2	4.0	0.98	Yes	Yes	Yes	Yes						
CXCR4	CA-XII	EpCAM	HER2	CA-IX	81.8%	3	4.3	0.97	Yes	Yes	Yes	Yes	Yes					
CXCR4	CA-XII	EpCAM	HER2	FR- α	81.5%	4	3.4	0.99	Yes	Yes	Yes	Yes	Yes	Yes				
CXCR4	CA-XII	EpCAM	HER2	α v β 3	81.5%	5	4.8	0.97	Yes	Yes	Yes	Yes	Yes	Yes	Yes			
CXCR4	CA-XII	EpCAM	HER2	Notch1	81.3%	6	6.4	0.96	Yes	Yes	Yes	Yes	Yes	Yes	Yes			
CXCR4	CA-XII	EpCAM	VEGF-A	FR- α	79.9%	7	11.6	0.71	Yes	Yes	Yes	Yes	Yes	Yes	Yes			
CXCR4	CA-XII	EpCAM	VEGF-A	MGB1	79.9%	8	13.1	0.62	Yes	Yes	Yes	Yes	Yes	Yes	Yes			
CXCR4	CA-XII	EpCAM	VEGF-A	CA-IX	79.4%	9	14.5	0.55	Yes	Yes	Yes	Yes	Yes	Yes	Yes			
CXCR4	CA-XII	HER2	VEGF-A	CA-IX	79.4%	10	27.0	0.04	Yes	Yes	Yes	Yes	Yes	Yes	Yes			
Times individual marker in Top 10 out of 252 combinations:																		
								10	10	10	9	7	5	2	2	3	1	1

α v β 3, *alpha v beta 3 integrin receptor*; *CA-IX*, *carbonic anhydrase IX*; *CA-XII*, *carbonic anhydrase XII*; *CXCR4*, *C-X-C chemokine receptor 4*; *EpCAM*, *epithelial cell adhesion molecule*; *FR- α* , *folate receptor alpha*; *HER2*, *human epidermal growth factor receptor 2*; *MGB1*, *mammaglobin 1*; *VEGF-A*, *vascular endothelial growth factor A*.

Supplementary Table 4. Ligands available for tumor-targeted optical imaging applications. This table provides an overview of the different targets and their corresponding targeted agents that are currently available in the clinic or are in clinical trial phase. The availability of clinical grade targeted agents might greatly enhance the translation of new targeted optical imaging agents towards clinical use.

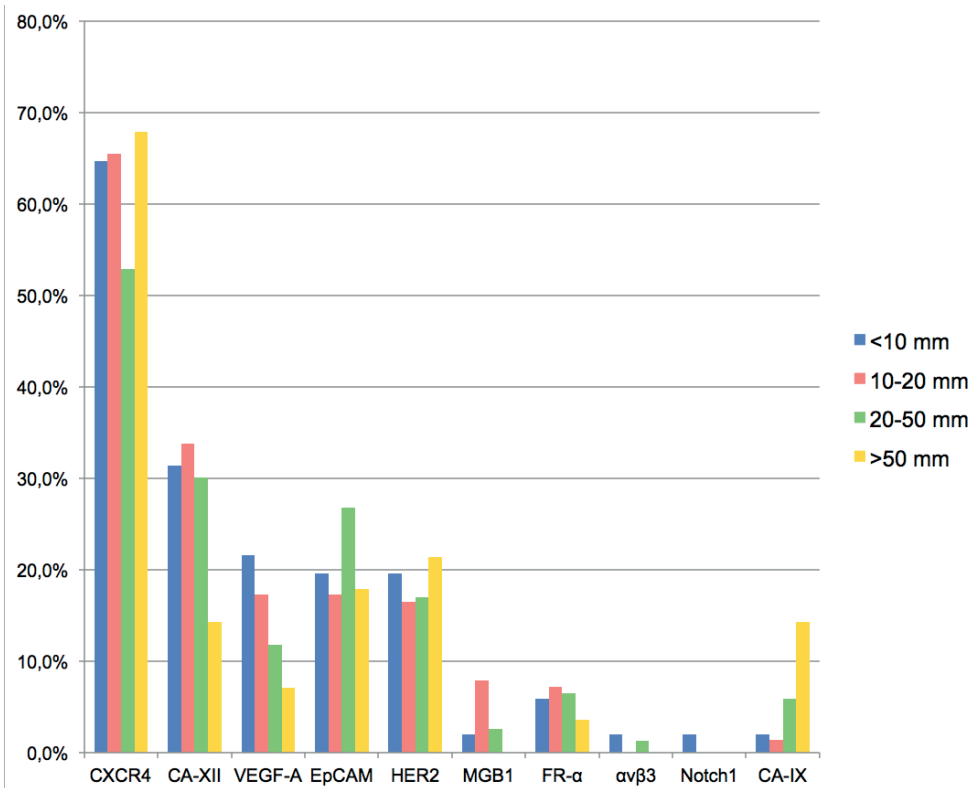
Target	Therapeutic	FDA approval	EMEA approval	Indication	Company	In clinical trial	Phase	Company
FR- α						UNII-2009BG00WA / Farletuzumab / MORAB-003 Folate-FITC / EC17	Phase III Phase II	Morphotek Inc. Endocyte Inc.
HER2 / ErbB2	Trastuzumab / Herceptin TM Pertuzumab / Perjeta TM	Yes Yes	Yes Yes	Breast neoplasms; Stomach Neoplasms Treatment of HER2 positive metastatic breast cancer	Genentech Inc. Genentech Inc.			
VEGF-A	Bevacizumab / Avastin TM Ranibizumab / Lucentis TM	Yes Yes	Yes Yes	Colorectal neoplasms Macular Edema; Wet Macular Degeneration; Diabetes Complications	Genentech Inc.			
EpCAM / CD326	Catumaxomab / Removab TM Edrecolomab / Panorex TM	No No	Yes No	Ascites; Ovarian cancer Colorectal neoplasms	Fresenius Biotech / Trion Pharma Glaxo Wellcome / Centocor	Proxinium / Vicinium / VB4-845 Adecatumumab / MT201	Phase III Phase II	Viventia Micromet Inc.
$\alpha v \beta 3$ integrin / Vitronectin receptor						Ertumaxomab / Rexomum TM 3622W94 / hu323/A3 ING-1 / heMAB MT-110 Etaracizumab / MEDI-522 / Etaratuzumab / Abegrin / Vitaxin TM EMD 66203 / cRGD peptide OMP-52W51 / Anti-Notch1	Phase II Phase I Phase I Phase I Phase II Phase II Phase I	Fresenius Biotech Glaxo Wellcome Inc. XOMA Inc. Micromet Inc. Medimmune Inc. Merck OncoMed Pharmaceuticals Inc.
Notch1 receptor						AVEO's humanized Notch1 antibody	Phase I	AVEO Pharmaceuticals Inc.
CXCR4	Plerixafor / AMD3100 / JM 3100 / Mozobil TM	Yes	Yes	Multiple Myeloma; Hematopoietic Stem Cell Transplantation; Lymphoma	Genzyme Inc.	AMDI11070 / AMD070	Phase II	Genzyme Inc.
CA-IX / CA-9						MSX-122 BKT-140 ALX-0651 BMS-936564/MDX-1338 WXCAREX [®] / cG250	Phase I Phase II Phase I Phase I Phase III	Metastatic Inc. Biokine Therap. Abylrx Bristol-Myers Squibb WILEX AG
CA-XII / CA-12						EXO-6A10	Phase I	Helmholtz Zentrum



Tumor marker	Grade I	Grade II	Grade III	P-value
CXCR4	67.4%	58.3%	57.6%	0.170
CA-XII	29.3%	35.7%	21.2%	0.041
VEGF-A	27.2%	12.5%	11.0%	<0.001
EpCAM	17.4%	20.2%	27.1%	0.168
HER2	9.8%	14.9%	27.1%	0.004
MGB1	4.3%	7.1%	0.8%	0.036
FR-α	2.2%	3.6%	13.6%	<0.001
αvβ3	1.1%	0.0%	1.7%	0.274
Notch1	1.1%	0.0%	0.0%	0.234
CA-IX	0.0%	1.2%	11.9%	<0.001

αvβ3, alpha v beta 3 integrin receptor; CA-IX, carbonic anhydrase IX; CA-XII, carbonic anhydrase XII, CXCR4, C-X-C chemokine receptor 4; EpCAM, epithelial cell adhesion molecule; FR-α, folate receptor alpha; HER2, human epidermal growth factor receptor 2; MGB1, mammaglobin 1; VEGF-A, vascular endothelial growth factor A.

Supplementary Figure 1. Tumor marker expression levels subdivided to grade of differentiation. FR-α (P<0.001), CA-IX (P<0.001), and HER2 (P=0.004) are more frequently expressed in less differentiated breast carcinoma. On the contrary, VEGF-A (P<0.001), MGB1 (P=0.036), and CA-XII (P=0.041) showed higher expression levels in well-differentiated tumors.



Tumor marker	<10 mm	10–20 mm	20–50 mm	>50 mm	P-value
CXCR4	64.7%	65.5%	52.9%	67.9%	0.075
CA-XII	31.4%	33.8%	30.1%	14.3%	0.251
VEGF-A	21.6%	17.3%	11.8%	7.1%	0.031
EpCAM	19.6%	17.3%	26.8%	17.9%	0.871
HER2	19.6%	16.5%	17.0%	21.4%	0.643
MGB1	2.0%	7.9%	2.6%	0.0%	0.513
FR-α	5.9%	7.2%	6.5%	3.6%	0.585
αvβ3	2.0%	0.0%	1.3%	0.0%	0.464
Notch1	2.0%	0.0%	0.0%	0.0%	0.228
CA-IX	2.0%	1.4%	5.9%	14.3%	0.111

αvβ3, alpha v beta 3 integrin receptor; CA-IX, carbonic anhydrase IX; CA-XII, carbonic anhydrase XII, CXCR4, C-X-C chemokine receptor 4; EpCAM, epithelial cell adhesion molecule; FR-α, folate receptor alpha; HER2, human epidermal growth factor receptor 2; MGB1, mammaglobin 1; VEGF-A, vascular endothelial growth factor A.

Supplementary Figure 2. Tumor marker expression levels subdivided to tumor size. Tumors were found less likely to express VEGF-A with increasing tumor size ($P=0.031$). A trend was seen between increasing tumor size and CA-IX expression, although not reaching statistical significance ($P=0.111$). The same accounts for the trend between decreasing tumor size and CA-XII expression ($P=0.251$).

Chapter

9

Submitted

Identifying tumor markers in lymph node metastases for targeted imaging applications in breast cancer patients

R.G. Pleijhuis
B. van der Vegt
L.M.A. Crane
S.G. Elias
T. van der Sluis
J. de Vries
J. Bart
G.M. van Dam

ABSTRACT*Introduction*

In breast cancer patients with a positive sentinel lymph node, an axillary lymph node dissection (ALND) is generally performed. In 50-80% of these patients, no additional positive axillary lymph nodes are found, suggesting substantial overtreatment. Near-infrared fluorescence (NIRF) imaging has the potential to enable noninvasive intraoperative detection of lymph node metastases and may thereby lead to a reduction in unnecessary removal of non-metastatic lymph nodes. We aimed to identify viable tumor markers for targeted NIRF imaging of lymph node metastases in breast cancer patients.

Methods

A panel of 10 membranous and/or extracellular tumor markers were assessed on tissue microarrays from 104 lymph node macrometastases and their corresponding primary tumors. Markers included $\alpha\beta3$ integrin receptor, CXCR4, CA-IX, CA-XII, EpCAM, FR- α , HER2, MGB1, Notch1 receptor, and VEGF-A. Tumor markers were prioritized based on a modified *target selection criteria* (TASC) scoring system consisting out of ten items, with scores ≥ 25 indicating viable markers.

Results

A total of 98 (94,2%) patients for whom histological material was available for both lymph node metastases and their corresponding primary tumor were eligible for analysis. Modified TASC scores were 25 for both EpCAM and CA-XII. At least one of these markers was expressed in 57.4% of the study population. Modified TASC scores for HER2, FR- α , CA-IX, CXCR4, MGB1 and VEGF-A were 22, 21, 21, 20, 18, and 13, respectively. No membranous and/or extracellular marker expression of sufficient intensity was observed for $\alpha\beta3$ integrin receptor and Notch1 receptor.

Conclusion

We systematically assessed the potential of ten tumor markers for targeted optical imaging of lymph node metastases in breast cancer patients. On the basis of ten tumor marker characteristics, EpCAM and CA-XII are considered promising markers for targeted NIRF imaging, allowing for a one-stage intraoperative evaluation of the tumor burden of lymph nodes.

INTRODUCTION

Assessing the presence of tumor in axillary lymph nodes (ALNs) of patients with breast cancer is an important aspect in clinical staging of the disease.¹ Tumor cells migrating from the primary tumor tend to metastasize to the first draining lymph node, also known as the sentinel lymph node (SLN), before spreading to other lymph nodes.² After removal, the SLN is assessed by a pathologist using step sectioning and immunohistochemistry.³ In the case of a positive SLN, an axillary lymph node dissection (ALND) is performed.⁴ However, in 47% of the patients who underwent ALND, the SLN is found to be the only lymph node containing metastasis.⁵ In these patients, ALND can be considered overtreatment with the known accompanying risks of nerve injury, lymph edema, shoulder dysfunction, and seroma formation.^{6,7} To reduce comorbidity associated with the unnecessary removal of non-metastatic ALNs, information on the tumor burden status of (sentinel) lymph nodes should ideally be available prior to or during surgery. Hereto, novel approaches are being developed that could enable noninvasive targeted imaging of lymph node metastases. In particular, near-infrared fluorescence (NIRF) optical imaging seems of interest for this purpose as it may allow for noninvasive assessment of the SLN and surrounding lymph nodes, potentially eliminating the need for extensive lymphadenectomy for assessment of the axillary lymph node status.

NIRF optical imaging makes use of a fluorescent optical contrast agent that emits light in the near-infrared (NIR) spectral range.⁸ The use of NIR light minimizes autofluorescence (i.e., intrinsic fluorescent activity of tissues) and photon absorption and scattering, while tissue penetration of photons in the NIR spectral range is maximized.⁹ Because NIR light is invisible to the human eye, a dedicated camera system is needed to detect the fluorescent signal.¹⁰

NIRF optical imaging is considered safe, inexpensive, fast, and uses non-ionizing radiation.¹¹ Already, several studies reported on the clinical feasibility of NIRF imaging to localize the SLN noninvasively in breast cancer patients.¹²⁻¹⁷ In these studies, patients were injected peritumorally with the nonspecific fluorescent dye indocyanine green (ICG), which distributes randomly across the lymphatic system, providing an anatomic map of lymph vessels and nodes instead of detecting cancer cells.¹⁸ For noninvasive assessment of the tumor burden of lymph nodes, however, fluorescent contrast agents have to be developed that are targeted specifically to tumor markers expressed by lymph node metastases.

As the portfolio of tumor markers that are known to be associated with breast cancer is still expanding and the development of targeted fluorescent probes is costly and time-consuming, we aimed to identify those tumor markers that are of particular interest for targeted NIRF imaging of lymph node metastases in breast cancer patients. Tissue microarrays were used to enable high-throughput analysis of a large sample of lymph node metastases and their corresponding primary tumors.

METHODS

Selection of tumor markers

A total of 10 tumor markers were selected that are known from literature for their role in breast cancer. Because targeted NIRF imaging requires the use of relatively large molecules that are unlikely to enter cancer cells (i.e., fluorescent contrast agents conjugated to a target-specific molecule), only membranous and/or extracellular markers were selected to ensure adequate marker accessibility. Selected tumor markers included C-X-C-chemokine receptor 4 (CXCR4),

alpha v beta 3 ($\alpha v\beta 3$) integrin receptor, carbonic anhydrase (CA) IX and XII, epithelial cell adhesion molecule (EpCAM), folate receptor alpha (FR- α), human epidermal growth factor receptor 2 (HER2), mammaglobin 1 (MGB1), Notch1 receptor, and vascular endothelial growth factor A (VEGF-A).

Selection of patients

Patients with lymph node macrometastasis (defined as metastasis ≥ 2.0 mm) were selected from previously described cohorts of invasive breast carcinoma specimen collected between 1996 and 2005 at the University Medical Center Groningen (UMCG).^{19,20} Patients for whom insufficient paraffin-embedded tissue was available for lymph node metastases and/or their corresponding primary tumor were excluded. Clinical and histopathological data of eligible patients were reviewed from pathology reports and medical charts. All data were anonymized and the study was conducted in accordance with the Declaration of Helsinki and with the rules and regulations posed by the Institutional Review Board of the UMCG.

Construction of tissue microarrays

Tissue microarrays (TMAs) were constructed to enable high-throughput immunohistochemical analysis of a large amount of lymph node metastases and their corresponding primaries simultaneously. Paraffin-embedded tissue from eligible patients was obtained from the archives of the Department of Pathology and Medical Biology from the UMCG. Slides from all sample blocks were evaluated for representative areas containing tumor tissue. TMAs were prepared as previously described.²¹ In brief, the most representative area of lymph node metastasis or invasive carcinoma was marked on the original haematoxylin and eosin (H&E) stained section. With this marked section for orientation, three 0.6 mm punches were taken from the selected area in the donor blocks and mounted in a recipient block using a tissue arrayer (Beecher Instruments, Sun Prairie, USA).

Immunohistochemistry

Semiquantitative immunohistochemistry (IHC) for all 10 biomarkers was performed on TMAs from lymph node metastases and their corresponding primary tumors. Briefly, 3 μm thick TMA sections were deparaffinized with xylene and gradually rehydrated through changes of graded ethanol from 100% to distilled water. Endogenous peroxidase activity was blocked by incubating TMA sections in phosphate-buffered saline pH 5.8 containing 0.3% H_2O_2 for 30 min. In the case of VEGF-A, endogenous biotin was additionally blocked using a Blocking Kit (Vector Laboratories, Burlingame, USA).

Primary antibodies against CXCR4 (ab2074, Abcam, Cambridge, UK) 1:50; $\alpha v\beta 3$ integrin (ab7166, clone BV3, Abcam, Cambridge, UK) 1:100; CA-IX (SAB1300310, Sigma Aldrich, Zwijndrecht, The Netherlands) 1:200; CA-XII (HPA008773, Sigma Aldrich, Zwijndrecht, The Netherlands) 1:50; EpCAM (IR637, clone Ber-EP4, DAKO) 1:100; FR- α (mAb-343, clone 3D2, a generous gift from prof. P.S. Low) 1:500; HER2 (RM9103S, clone SP3, Neomarkers, Duiven, The Netherlands) 1:80; MGB1 (ab101137, clone 31A5, Abcam, Cambridge, UK) 1:100; Notch1 (ab44986, clone A6, Abcam, Cambridge, UK) 1:50; and VEGF-A (sc-152, Santa Cruz Biotechnology, Heidelberg, Germany) 1:50 were diluted in PBS containing 1% bovine serum albumin and incubated at room temperature for 1 h. FR- α sections were incubated with mouse MACH3 (Biocare Medical, Walnut Creek, USA) for 3 h. Sections were then washed in phosphate-buffered saline and incubated with secondary and tertiary antibodies where appropriate. For visualization of the antibody-antigen complex, 3,3'-diaminobenzidine was used. After a final

wash with distilled water, counterstaining was performed with haematoxylin. Sections were then dehydrated through rising concentrations of ethanol, mounted with mounting medium, and coverslipped. Negative controls consisted of sections processed in the same way but with omission of the primary antibody step. Positive control tissue was included as usual.

Digitalization of slides

TMA slides were digitalized using the ScanScope GL Scanner (Aperio Technologies Inc., Vista, USA), creating high-resolution files suitable for image analysis. All slides were produced with core images linked to a Microsoft Access™ database containing relevant tissue core information. After importing the digital slides in ImageScope® (Aperio Technologies Inc., Vista, USA), each individual TMA section on the slide was captured, coded, and exported as a separate industry-standard TIFF file.

Assessment of tumor-to-background ratio

Tumor markers for targeted NIRF imaging should provide adequate tumor-to-background ratios (TBRs) to discriminate between lymph node metastases and normal lymphatic tissue. For this reason, expression of all 10 tumor markers was also evaluated in a set of 25 normal lymph node specimens using IHC. The TBR was calculated by multiplying the mean staining intensity with the proportion of stained tumor cells (three-item severity score; TIS-score) for lymph node metastases and dividing it by the TIS-score for normal lymphatic tissue. A TBR ≥ 3 was considered adequate for imaging purposes.²²

Scoring of immunohistochemistry

Manual IHC scoring was performed on digital TMA sections to allow for randomization of TMA cores, thereby minimizing bias effects. Tumor marker expression was assessed by evaluating the staining pattern (diffuse or focal) as well as the proportion of cancer cells showing no (0), weak (1+), moderate (2+), or strong (3+) membranous and/or extracellular staining. Evaluation of staining pattern (diffuse or focal) was performed both on a microscopic (within spot) and a macroscopic (between spots) level. To account for tumor heterogeneity, the average proportion and staining intensity was calculated for each tumor. An average membranous staining intensity of $\geq 2+$ in $\geq 10\%$ of tumor cells was considered positive. For CXCR4 and VEGF-A, only cases that showed an average membranous staining intensity of 3+ in $\geq 10\%$ of tumor cells were considered positive due to high background staining. Lymph node metastasis or primary tumor specimens were excluded from analysis in the event that all (3 out of 3) TMA sections were missing.

Marker expression in metastases and primary tumors

To account for potential heterogeneity in marker expression, expression levels were evaluated separately for lymph node metastasis and their corresponding primary tumor. Agreement of marker expression between lymph node metastasis and primary tumor was assessed separately for each individual tumor marker.

Modified target selection criteria scoring system

The scoring system used in the present study was based on the *target selection criteria* (TASC) scoring system, as recently introduced by van Oosten et al.²³ In brief, TASC provides a method for identifying markers that are of specific potential for targeted optical imaging of tumors by assigning points to each individual marker on the basis of seven characteristics:

I) tumor marker localization; II) expression pattern; III) tumor-to-background ratio; IV) target expression rate; V) reported successful use *in vivo*; VI) enzymatic activity, and VII) internalization of the marker upon binding of its ligand.

Because the focus of the current study is on lymph node metastasis instead of the primary tumors, some adjustments were made to the TASC scoring system. First, the amount of points awarded to tumor markers with a TBR >10 was increased from 3 to 6 points as a high TBR is important to obtain an adequate overall image resolution when imaging small structures like lymph node metastases. Second, the amount of points awarded for marker expression rate was altered. The original TASC score is dominated by the percentage of tumors that express the tumor marker on their cell membranes or in the extracellular matrix adjacent to tumor cells. Up to 6 points are assigned to expression rates as high as 90%, whereas expression rates below 50% are assigned no points. For targeted imaging applications, however, tumor markers expressed in less than 50% of the lymph node metastasis can still be of value as long as other characteristics crucial for optical imaging are favorable. Markers were therefore granted 0, 3, 5, or 6 points based on expression rates of 0–10%, 10–25%, 25–50%, or 50–100%, respectively (Supplementary Table 1).

Lastly, we complemented TASC with three additional selection criteria regarding marker expression of both lymph node metastasis and the corresponding primary tumor (Supplementary Table 1). In brief, points are granted for a high level of marker expression agreement and the possibility to apply a single tumor marker for targeted NIRF imaging of both lymph node metastases and their corresponding primary tumor. Moreover, points are granted when marker expression of lymph node metastases can be predicted by analyzing a sample of the primary tumor prior to surgery (e.g., by core needle biopsy).

The modified TASC score for each individual marker serves as a directive to objectify the value of different tumor markers for targeted NIRF imaging. Individual tumor markers can be awarded a total of 30 points at maximum. A total score of ≥ 25 points indicates that the tumor marker is of potential interest and justifies further exploration.

Statistical analysis

Descriptive statistics including medians and frequencies were utilized for the description of clinicopathological characteristics. Agreement of marker expression between lymph node metastases and corresponding primaries was assessed using the Kappa statistic. Kappa values of 0.41–0.60, 0.61–0.80, and 0.81–0.99 were considered to resemble moderate, substantial, and almost perfect agreement, respectively.²⁴ A *P*-value of ≤ 0.05 was considered statistically significant. All calculations were performed using Excel (Microsoft® Office Professional Edition 2003 SP3, Microsoft Corporation, Redmond, USA), SPSS 12.01 (SPSS Inc., Chicago, USA), and R version 3.0.1 (R Foundation for Statistical Computing, Vienna, Austria).²⁵

RESULTS

A total of 104 out of 439 (23.7%) patients with invasive breast carcinoma had lymph node macrometastases. Histologic material of lymph node metastases and corresponding primary tumors was retrieved from the pathology archive of the UMCG. Two out of 104 (1.9%) patients were excluded due to insufficient histologic material of the primary tumor for TMA construction, an additional 4 (3.8%) patients were excluded due to insufficient histologic material of lymph node metastases. A total of 98 out of 104 (94.2%) patients were therefore eligible for analysis. Clinicopathological characteristics of the study group are shown in Table 1.

Table 1. Clinicopathological characteristics of 98 breast cancer patients with lymph node metastases eligible for analysis.

Characteristics	N	%
Age (years), median (range)	56 (27–89)	
<45	13	13.3
45–65	60	61.2
>65	25	25.5
Tumor size (mm), median (range)	25 (5–140)	
<20	30	30.9
20–50	60	61.9
>50	7	7.2
Lymph node metastasis size (mm), median (range)	4.5 (1–23)	
<5 mm	34	34.7
5–10 mm	19	19.4
>5 mm	45	46.0
Number of metastasis, median (range)	3 (1–33)	
Number of excised lymph nodes, median (range)	11 (1–36)	
Histological type		
Invasive ductal carcinoma	93	94.9
Other types	5	5.1
In situ carcinoma present		
Yes	54	55.1
No	44	44.9
Histological grade		
I	14	14.3
II	30	30.6
III	53	54.1
Progesterone receptor		
Positive	51	52.0
Negative	42	49.9
Unknown	5	5.1
Estrogen receptor		
Positive	60	61.2
Negative	32	32.7
Unknown	6	6.1
Extranodal growth		
Yes	52	53.1
No	46	46.9

Manual immunohistochemistry scoring

A representative immunohistochemistry image indicating membranous and/or extracellular staining intensities for both lymph node metastasis and their corresponding primary tumor is shown in Fig. 1. For all 98 eligible patients, acceptable IHC (defined as at least one of the three cores stained sufficiently) differed between stains and was obtained for 97.9% to 100% of the lymph node metastases and 92.2% to 96.6% of the breast carcinoma specimen (Table 2). The percentage of available double and triple cores ranged from 16–21% and 65–74% between stains, respectively.

Marker expression in lymph node metastasis

An overview of the expression rates for each individual tumor marker is provided in Table 2. The most frequently expressed tumor marker in lymph node metastases was CXCR4 (49.5%), followed by HER2 (48.05%), CA-XII (37.1%), and EpCAM (28.9%). Expression rates for CA-IX, FR- α , MGB1, and VEGF-A ranged from 5.1% to 16.5%. No membranous or extracellular tumor marker expression of sufficient intensity (moderate to strong) was observed for Notch1 receptor and $\alpha\text{v}\beta\text{3}$ integrin receptor. Supplementary Table 2 provides a summary of marker expression rates as reported in the literature for lymph node metastases in breast cancer patients.

Marker expression related to primary tumor

Tumor marker expression was evaluated separately for lymph node metastases and corresponding primaries to evaluate heterogeneity (Table 2). The level of agreement of between both categories ranged from 0.44 to 0.81 for individual tumor markers (Table 3). Moreover, we evaluated whether marker expression in the primary tumor predicted for expression of the same marker in lymph node metastases (Table 4). Predictability of marker expression in lymph node metastases ranged from 53.8% to 78.7% for FR- α , CXCR4, and VEGF-A. For EpCAM, CA-XII, MGB1, HER2, and CA-IX, predictability ranged from 80.0% to 100.0%.

Tumor-to-background ratio

Mean TIS-scores were calculated for individual tumor markers using the aforementioned formula. Mean TIS-scores for lymph node metastases were 0.0 for $\alpha\text{v}\beta\text{3}$ integrin receptor, 0.13 for CA-IX, 0.71 for CA-XII, 1.27 for CXCR4, 0.58 for EpCAM, 0.04 for FR- α , 1.23 for HER2, 0.23 for MGB1, 0.0 for Notch1 receptor, and 1.85 for VEGF-A. For normal lymphatic tissue, mean TIS-scores were 0.25 for $\alpha\text{v}\beta\text{3}$ integrin receptor, 0.02 for CA-IX, 0.04 for CA-XII, 1.24 for CXCR4, 0.01 for EpCAM, 0.0 for FR- α , 0.38 for HER2, 0.0 for MGB1, 0.0 for Notch1 receptor, and 1.43 for VEGF-A. TBRs were calculated for each individual tumor marker and are provided in Table 4.

Modified target selection scores

Modified TASC scores were calculated for each individual tumor marker (Table 4) on the basis of ten aforementioned marker characteristics. EpCAM and CA-XII were identified as the most promising markers for targeted NIRF imaging of lymph node metastasis, fulfilling the criteria of a total score ≥ 25 points. At least one of these two markers was expressed in 57.4% of the study population. Modified TASC scores for HER2, FR- α , CA-IX, CXCR4, MGB1, and VEGF-A were 22, 21, 21, 20, 18, and 13, respectively. No modified TASC score could be calculated for $\alpha\text{v}\beta\text{3}$ integrin receptor and Notch1 receptor because no membranous and/or extracellular marker expression of sufficient intensity was observed.

Table 2. Expression rates for a panel of extracellular/membranous tumor markers in primary breast carcinoma and their corresponding lymph node metastasis as assessed by immunohistochemistry.

Target	Lymph node metastasis						Corresponding primary tumor						
	Evaluated cores			Negative			Evaluated cores			Positive			
	N	% of total	%	N	%	%	N	% of total	%	N	%	N	%
avβ3	98	100.0	0.0	98	100.0	100.0	93	94.9	0.0	0	0.0	93	100.0
CA-IX	96	97.9	10.4	86	89.6	89.6	91	92.9	7.7	7	7.7	84	92.3
CA-XII	97	99.0	37.1	61	62.9	62.9	94	95.9	27.7	26	27.7	68	72.3
CXCR4	97	99.0	49.5	49	50.5	50.5	95	96.9	64.2	61	64.2	34	35.8
EpCAM	97	99.0	28.9	69	71.1	71.1	92	93.9	17.4	16	17.4	76	82.6
FR-α	98	100.0	5.1	93	94.9	94.9	93	94.9	7.5	7	7.5	86	92.5
HER2	98	100.0	48.0	51	52.0	52.0	93	94.9	25.8	24	25.8	69	74.2
MGB1	97	99.0	8.2	89	91.8	91.8	92	93.9	4.3	4	4.3	88	95.7
Notch1	98	100.0	0.0	98	100.0	100.0	93	94.9	0.0	0	0.0	93	100.0
VEGF-A	97	99.0	16.5	81	83.5	83.5	95	96.9	14.7	14	14.7	81	85.3

avβ3, alpha v beta 3 integrin receptor; CA-IX, carbonic anhydrase IX; CA-XII, carbonic anhydrase XII; CPT, corresponding primary tumor; CXCR4, C-X-C chemokine receptor 4; EpCAM, epithelial cell adhesion molecule; FR-α, folate receptor alpha; HER2, human epidermal growth factor receptor 2; LNM, lymph node metastasis; MGB1, mammaglobin 1; VEGF-A, vascular endothelial growth factor A.

Table 3. Level of agreement between tumor marker expression of lymph node metastasis and the corresponding primary tumor.

Target	Valid cases		Positive cases						Kappa	P		
	N	% of total	Solely LNM	Solely CPT	LNM & CPT	Negative cases						
	N	%	N	%	N	%	N	%				
avβ3	93	94.9	0	0.0	0	0.0	0	0.0	93	100.0	-	-
CA-IX	90	91.8	3	3.3	0	0.0	7	7.8	80	88.9	0.806	<0.001
CA-XII	93	94.9	13	14.0	5	5.4	20	21.5	55	59.1	0.553	<0.001
CXCR4	94	95.9	0	0.0	13	13.8	48	51.1	33	35.1	0.722	<0.001
EpCAM	91	92.9	13	14.3	3	3.3	13	14.3	62	68.1	0.513	<0.001
FR-α	93	94.9	1	1.1	3	3.2	4	4.3	85	91.4	0.644	<0.001
HER2	93	94.9	20	21.5	0	0.0	24	25.5	49	52.7	0.558	<0.001
MGB1	92	93.9	3	3.3	0	0.0	4	4.3	85	92.4	0.711	<0.001
Notch1	93	94.9	0	0.0	0	0.0	0	0.0	93	100.0	-	-
VEGF-A	94	95.9	7	7.4	6	6.4	7	7.4	74	78.8	0.438	<0.001

avβ3, alpha v beta 3 integrin receptor; CA-IX, carbonic anhydrase IX; CA-XII, carbonic anhydrase XII; CPT, corresponding primary tumor; CXCR4, C-X-C chemokine receptor 4; EpCAM, epithelial cell adhesion molecule; FR-α, folate receptor alpha; HER2, human epidermal growth factor receptor 2; LNM, lymph node metastasis; MGB1, mammaglobin 1; VEGF-A, vascular endothelial growth factor A.

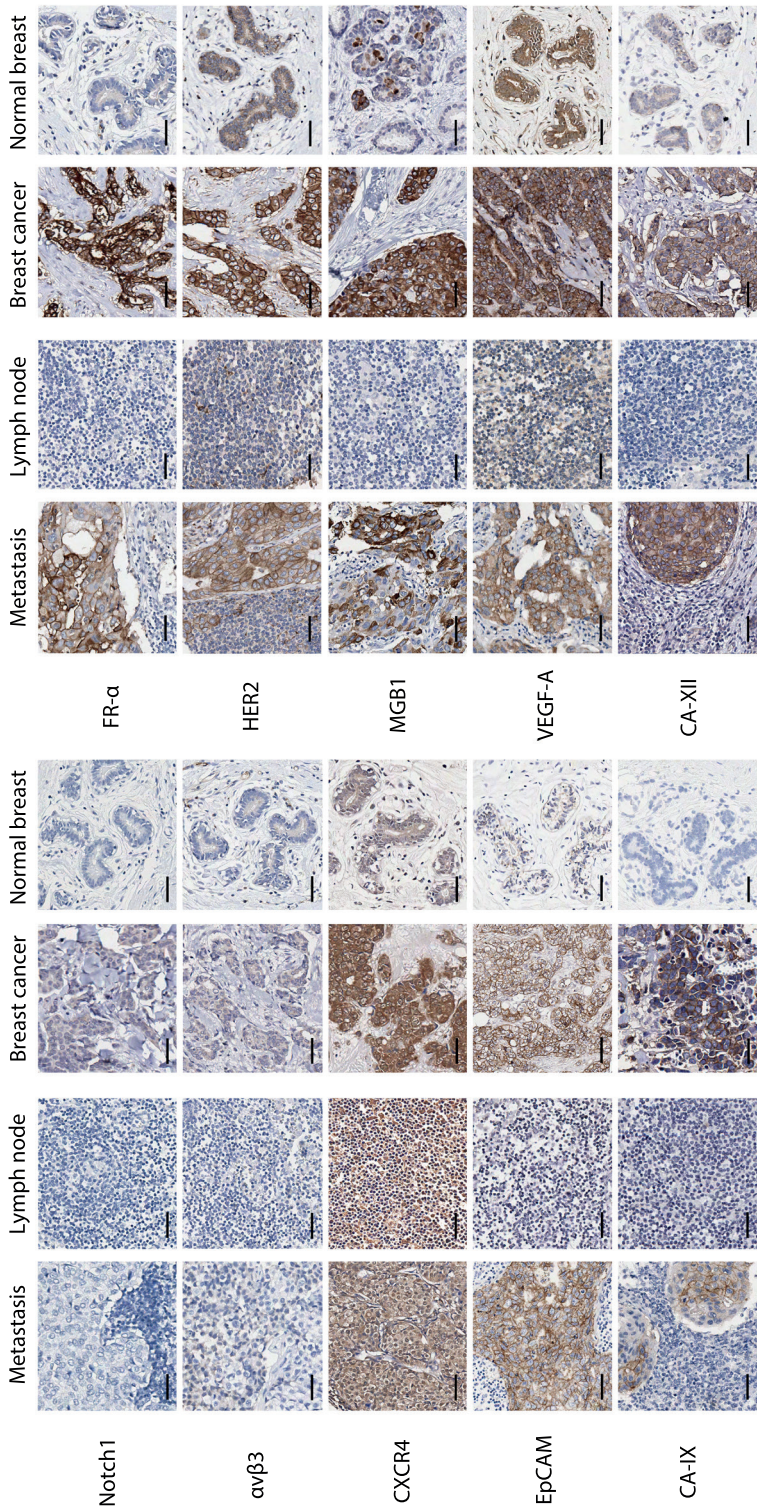
Table 4. Ranking of tumor markers for targeted optical imaging of lymph node metastases in breast cancer patients.

Tumor marker	Target Selection Criteria (TASC)										Added selection criteria			
	I	II	III	IV	V	VI	VII	VIII	IX	X	Agreement with CPT	Dual expression	Predictability of marker expression	Total marker score
<i>Max points</i>	5	4	6	6	2	1	1	3	1	1	3	1	1	30
EpCAM	Membranous	Diffuse	>10.0	28.9% membranous	Yes	Not described	Yes	0.513	50.0%	81.3%	0.513	50.0%	81.3%	25
CA-XII	Membranous	Diffuse	>10.0	37.1% membranous	Yes	Yes	Not described	0.553	60.6%	80.0%	0.553	60.6%	80.0%	25
HER2	Membranous	Diffuse	3.2	48.0% membranous	Yes	Not described	Yes	0.558	54.5%	100.0%	0.558	54.5%	100.0%	22
FR-α	Membranous	Diffuse	>10.0	5.1% membranous	Yes	Not described	Yes	0.644	80.0%	57.1%	0.644	80.0%	57.1%	21
CA-IX	Membranous	Mostly diffuse, some focal	6.6	10.4% membranous	Yes	Yes	Yes	0.806	70.0%	100.0%	0.806	70.0%	100.0%	21
CXCR4	Membranous	Diffuse	1.24	49.5% membranous	Yes	Not described	Yes	0.722	100.0%	78.7%	0.722	100.0%	78.7%	20
MGB1	Membranous	Mostly diffuse, some focal	>10.0	8.2% membranous	Yes	Not described	Not described	0.711	57.1%	100.0%	0.711	57.1%	100.0%	18
VEGF-A	Extracellular	Diffuse	1.43	16.5% extracellular	Yes	Not described	Not described	0.438	50.0%	53.8%	0.438	50.0%	53.8%	13
αvβ3	None observed	N/A	N/A	N/A	Yes	Not described	Yes	N/A	N/A	N/A	N/A	N/A	N/A	N/A
Notch1	None observed	N/A	N/A	N/A	Yes	Not described	Yes	N/A	N/A	N/A	N/A	N/A	N/A	N/A

αvβ3, alpha v beta 3 integrin receptor; CA-IX, carbonic anhydrase IX; CA-XII, carbonic anhydrase XII; CPT, corresponding primary tumor; CXCR4, C-X-C chemokine receptor 4; EpCAM, epithelial cell adhesion molecule; FR-α, folate receptor alpha; HER2, human epidermal growth factor receptor 2; MGB1, mammaglobin 1; TBR, tumor-to-background ratio; VEGF-A, vascular endothelial growth factor A.

Marker characteristics were evaluated through immunohistochemical analysis of tissue microarrays. In addition, marker characteristics reported in the literature were taken into account if available. Marker prioritization was based on the *target selection criteria* (TASC) scoring system, complemented with selection criteria regarding marker expression of both lymph node metastases and corresponding primary tumors. Individual tumor markers can be awarded 30 points at maximum. Markers that are awarded ≥25 points are regarded promising targets for targeted optical imaging of lymph node metastasis. Details on the awarding of points are available online (Supplementary Table 1).

*Modified thresholds were used for T/B ratio and tumor marker expression rate (Supplementary Table 1).



$\alpha v \beta 3$, alpha v beta 3 integrin receptor; CA-IX, carbonic anhydrase IX; CA-XII, carbonic anhydrase XII; CXCR4, C-X-C chemokine receptor 4; EpCAM, epithelial cell adhesion molecule; FR- α , folate receptor alpha; HER2, human epidermal growth factor receptor 2; MGB1, mammaglobin 1; VEGF-A, vascular endothelial growth factor A.

Figure 1. Immunohistochemical staining of lymph node metastases and corresponding primary breast carcinoma. Representative specimen of normal lymphatic tissue and glandular breast tissue were included for comparison. HER2 and VEGF-A showed weak background staining in the majority of lymphatic tissue specimen. For CXCR4, high background staining in lymphatic tissue was observed. In primary breast carcinoma, weak to moderate background staining was observed for CXCR4, VEGF-A, and HER2. Scalebar equals 50 μm .

DISCUSSION

In the present study, we aimed to identify viable tumor markers for targeted NIRF imaging of lymph node metastases in breast cancer patients. A total of 10 membranous and extracellular tumor markers that are reported in the literature for their role in breast cancer were evaluated. For all markers assessed, targeted moieties are already in clinical trial or available for clinical use, facilitating clinical translation. By conjugating these moieties with fluorescent optical contrast agents that emit light in the near-infrared spectral range, fluorescent probes are obtained for targeted NIRF imaging.

Markers for imaging lymph node metastasis

The most potential tumor markers identified using our modified TASC scoring system were EpCAM and CA-XII, which were both awarded a total of 25 points.

EpCAM is a transmembrane protein that is involved in cell-cell adhesion in normal epithelial cells, while in cancer it can actually loosen cell-cell adhesions by functioning as an antagonist to E-cadherin.²⁶ In breast cancer, EpCAM expression is associated with poor prognosis in node-positive patients.²⁷ To date, several humanized monoclonal antibodies are available for targeted imaging of EpCAM in patients (e.g., catumaxomab and edrecolomab), facilitating clinical translation.

CA-XII is an extracellular enzyme involved in the regulation of the microenvironment acidity and tumor malignant phenotype.^{28,29} A humanized monoclonal antibody, known as EXO-6A10, was recently developed for specific targeting of CA-XII in patients (European patent 2384766) and is awaiting approval.

Although not identified as a marker of particular interest (i.e., modified TASC score ≥ 25 points), HER2 contains favorable marker characteristics for targeted NIRF imaging. HER2 is a well-known marker for breast cancer that is overexpressed in 25–30% of all breast carcinoma and is associated with a poor prognosis. In patients with tumor-positive lymph nodes, even higher rates of HER2 expression are reported.³⁰ In the current study, HER2 expression was moderate to strong in 48.0% of the lymph node metastases compared to 25.8% of the corresponding primary tumors. When a primary tumor was HER2 positive, its corresponding lymph node metastases also showed moderate to strong membranous HER2 expression in all cases. This observation is in accordance with the literature and indicates that HER2 expression profiling of the primary tumor (e.g., by core needle biopsy) can be used to select those patients suitable for HER2 targeted imaging of lymph node metastases.³¹ In 21.5% of the patients with HER2 positive lymph node metastases, the primary tumor was negative for HER2, suggesting that a substantial amount of patients with HER2 positive lymph node metastases would be missed when marker expression is solely based on the expression level of the corresponding primary tumor.

FR- α is a transmembrane receptor that shows limited expression in normal tissue but is over-expressed on a variety of human cancers, including breast cancer.³² Although, FR- α and its ligand (folic acid) seem an attractive ligand/receptor combination for targeted imaging of cancer cells, FR- α was not identified as a potent marker for the detection of lymph node metastases due to heterogeneity in marker expression and low expression rate.

CXCR4 is a transmembrane chemokine receptor that allows for migration of hematopoietic cells from the bone marrow to the peripheral lymph nodes.³³ It has been implicated in the invasion and metastasis of breast cancer.³⁴ Although CXCR4 was identified as a promising marker for targeted NIRF imaging of primary breast carcinoma,^{35,36} the applicability of CXCR4

for targeted imaging of lymph node metastases seems limited. First, we found the TBR of CXCR4 positive lymph node metastasis to be insufficient for imaging purposes due to the expression of CXCR4 on the surface of T lymphocytes that are abundantly present in lymph nodes. Moreover, CXCR4 expression was found to decrease as breast cancer cells metastasize to the lymph nodes. Shim et al. reported that 45 out of 74 (61%) primary tumors showed strong ($\geq 3+$) CXCR4 expression, while for lymph node metastases this was only 6 out of 20 (30%; $P < 0.001$).³⁷ In our study a similar trend was observed with strong staining being present in 49.5% (primary tumors) and 64.3% (lymph node metastases) of the patients ($P < 0.001$). The difference in expression of CXCR4 may be mediated by high levels of SDF-1 in the lymph nodes that lead to CXCR4 internalization and degradation through the lysosome pathway.³⁸ Moreover, CXCR4 levels in the primary tumor may be high due to the relatively hypoxic environment in primary tumors compared with metastases in the lymph nodes.³⁷ Taken together, although suitable for targeted imaging of primary breast carcinoma, we recommend not to use CXCR4 as a marker for targeted NIRF imaging of lymph node metastases.

MGB1 expression is reported in 40% to 84% of the lymph node metastases and corresponding primary tumors, with the expression pattern being primarily cytoplasmic (Supplementary Table 3).³⁹ Because only moderate to strong membranous and extracellular marker expression was counted as positive, the MGB1 expression rate in our study is considerably lower (8.2%). No difference in MGB1 expression was found between primary and metastatic breast carcinoma, which is in agreement with the literature.⁴⁰

VEGF-A is an endothelial growth factor that plays a key role in tumor angiogenesis and is associated with invasive tumor growth, metastasis, and reduced survival.⁴¹⁻⁴⁴ VEGF-A can be either membrane-bound or present in the interstitial cell space with highest concentrations observed in close proximity of tumor cells.⁴⁵ To date, several preclinical studies have reported good results using VEGF-A as a marker for targeted imaging of primary tumors.^{46,47} At our institution, a clinical study is currently being performed in order to detect primary breast carcinoma using bevacizumab labeled with the fluorescent dye IRDye 800CW (NCT01508572). For targeted imaging of lymph node metastases, however, VEGF-A seems less suitable due to heterogeneity in marker expression and a relatively low TBR (Table 4).

No membranous and/or extracellular staining of sufficient intensity was observed in any of the lymph node metastases and corresponding primaries for both $\alpha v \beta 3$ integrin receptor and Notch1 receptor, while positive controls were adequate. As integrins regulate the interaction between epithelial cells and the extracellular matrix, a decrease in the expression of $\alpha v \beta 3$ integrin could make cancer cells more prone to metastasize to the lymph nodes.⁴⁸ This could explain the low $\alpha v \beta 3$ integrin expression level observed in our study population of node-positive patients. Indeed, several studies reported a significant loss of integrin receptor expression on primary breast cancer cells in the presence of axillary metastasis.^{49,50} Conversely, in bone metastases, $\alpha v \beta 3$ integrin receptor was reported to be overexpressed.^{51,52}

As for $\alpha v \beta 3$ integrin receptor, no membranous and/or extracellular Notch1 receptor expression of sufficient intensity was observed in any of the 98 evaluated lymph node metastases. To our knowledge, no other studies previously reported on Notch1 receptor expression in lymph node metastasis from breast cancer patients. Zhu et al. evaluated expression of Notch1 receptor in hematologic metastases and corresponding primary tumors for several cancers, including breast cancer.⁵³ At least 10% of the cancer cells was reported to show moderate to strong Notch1 receptor expression in 1 out of 5 (20%) evaluated metastases. No assessment of lymph node metastases was performed. Further studies are therefore desirable to confirm our findings concerning the weak expression of Notch1 receptor in lymph node metastases.

Assessment of marker expression

We used manual IHC scoring to assess functional membranous and/or extracellular expression of 10 different tumor markers in lymph node metastases and their corresponding primaries. Although IHC is easy to perform on a variety of tumor samples and is considered a predominant method for evaluating functional tumor marker expression in clinical practice, there also are a number of drawbacks with IHC. The most important drawback is the lack of assay standardization and variance in the interpretation of the IHC staining.^{54,55} Given the lack of quantifiable internal reference standards for calibration, results obtained using IHC stains should be considered semiquantitative, comparing the staining intensity and number of positive cells with other cases.⁵⁶

With the exception of HER2 receptor and MGB1, only limited data is available on the expression of different tumor markers in lymph node metastases (Supplementary Table 2). When marker expression as observed in the current study is compared with data reported in the literature, overall expression rates are quite similar. Differences can be largely explained by the semiquantitative nature of IHC, different thresholds that were used for marker positivity, and the small sample size of some studies. Moreover, the majority of studies did not differentiate between cytoplasmic and membranous staining, the latter being of particular interest for targeted optical imaging as imaging agents will only be able to bind those biomarkers situated on the exterior of tumor cells. Because the focus of our study was on the identification of tumor markers suitable for targeted NIRF imaging, cytoplasmic staining was not taken into account when assessing marker expression.

Targeted imaging of lymph node metastasis

Targeted NIRF imaging holds great promise to improve breast cancer care by providing the surgeon with a high-resolution noninvasive imaging modality for the detection of lymph node metastases. Several animal and clinical studies have already shown the potential of targeted optical imaging to improve the therapeutic outcome of surgery.

Tafreshi et al. successfully applied a high-resolution NIRF imaging system to noninvasively detect lymph node metastases in a xenograft bioluminescent breast cancer model.⁵⁷ NIRF imaging was performed 24 hours following injection of a near-infrared fluorescent dye conjugated to a monoclonal antibody targeted towards MGB1. One year later, the same group reported on the applicability of CA-IX and CA-XII as markers for targeted imaging of lymph node metastases in mice.³⁰ Again, targeted probes were developed by conjugation of monoclonal antibodies specific for CA-IX and CA-XII to a near-infrared fluorescent dye. Results indicated that the targeted dye was retained in positive lymph nodes for up to at least 7 days postinjection. As few as 1,000 breast cancer cells could be detected in the lymph nodes, indicating the high sensitivity of targeted NIRF imaging.

Wu et al. reported on a fluorescent probe targeted against HER2 receptor to differentiate metastatic lymph nodes from non-metastatic nodes.⁵⁸ Using an animal model, they showed that lymph node metastases were easily distinguishable from surrounding normal (lymphatic) tissue with sensitivity and specificity rates of 78% and 100%, respectively.

According to our modified TASC scoring system, HER2, CA-IX, and MGB1 (awarded 22, 21, and 18 points, respectively) have rather favorable characteristics for targeted optical imaging, but should not be prioritized for clinical translation. CA-XII and EpCAM, on the other hand, seem of particular interest for clinical translation based on our current findings.

To our knowledge, no clinical studies have yet been published concerning the detection of lymph node metastases using targeted NIRF imaging in humans. There has been some early

work, however, towards targeted NIRF imaging in a clinical setting. In 2011, the first-in-human use of intraoperative tumor-specific NIRF imaging was reported by our group, concerning the real-time surgical visualization of tumor tissue in patients undergoing an exploratory laparotomy for suspected ovarian cancer.⁵⁹ It was shown that intraoperative NIRF-guided imaging allowed the surgeon to detect tumor spots of less than 1 millimeter in diameter that were undetected with visual inspection alone. For targeted NIRF imaging of lymph node metastases, the same principle could be applied to support surgeons during lymph node status assessment by pinpointing suspicious lymph nodes.

Preoperative assessment of marker expression

Nowadays, core needle biopsy of the primary tumor is a common procedure for IHC analysis of ER, PR, and HER2 expression as a lead for patient-tailored therapies. Using IHC, those markers that are expressed throughout the tumor could be identified and used to predict marker expression of lymph node metastases that originated from the same tumor. This information could then be used to select matching optical contrast agents that are targeted specifically to the marker of choice. However, to prevent false negative results, heterogeneity in tumor marker expression should be taken strictly into account.

Marker expression between lymph node metastases and their corresponding primary tumor was evaluated separately in our study and was found to closely match for some markers, while differing substantially for others (Table 2–4).

CONCLUSION

Using a modified TASC scoring system as a directive, we identified EpCAM and CA-XII as tumor markers of particular interest for targeted NIRF imaging of lymph node metastases in breast cancer patients, covering with the highest chance of success both the primary tumor and potential lymph node metastases with one and the same tracer. Moderate to strong membranous expression was observed for at least one of these two markers in 57.4% of the evaluated patients. Further studies are needed to validate our findings *in vivo* and to evaluate the applicability of a one-stage intraoperative evaluation of the tumor burden of lymph nodes.

ACKNOWLEDGEMENTS

The authors wish to thank the Groningen University Fund, the Groningen Ubbo Emmius Fund, and the Junior Scientific Masterclass for financial support.

REFERENCES

1. Veronesi U, Paganelli G, Viale G, et al. A randomized comparison of sentinel-node biopsy with routine axillary dissection in breast cancer. *N Engl J Med* 2003; 349:546-553.
2. Mabry H, Giuliano AE. Sentinel node mapping for breast cancer: progress to date and prospects for the future. *Surg Oncol Clin N Am* 2007; 16:55-70.
3. Weaver DL. Pathology evaluation of sentinel lymph nodes in breast cancer: protocol recommendations and rationale. *Mod Pathol* 2010; 23 Suppl 2:S26-32.
4. Lyman GH, Giuliano AE, Somerfield MR, et al. American Society of Clinical Oncology guideline recommendations for sentinel lymph node biopsy in early-stage breast cancer. *J Clin Oncol* 2005; 23:7703-7720.
5. Kim T, Giuliano AE, Lyman GH. Lymphatic mapping and sentinel lymph node biopsy in early-stage breast carcinoma: a metaanalysis. *Cancer* 2006; 106:4-16.
6. Ivens D, Hoe AL, Podd TJ, et al. Assessment of morbidity from complete axillary dissection. *Br J Cancer* 1992; 66:136-138.
7. Kwan W, Jackson J, Weir LM, et al. Chronic arm morbidity after curative breast cancer treatment: prevalence and impact on quality of life. *J Clin Oncol* 2002; 20:4242-4248.
8. Ntziachristos V, Yoo JS, van Dam GM. Current concepts and future perspectives on surgical optical imaging in cancer. *J Biomed Opt* 2010; 15:066024.
9. Ntziachristos V. Fluorescence molecular imaging. *Annu Rev Biomed Eng* 2006; 8:1-33.
10. Themelis G, Yoo JS, Soh KS, et al. Real-time intraoperative fluorescence imaging system using light-absorption correction. *J Biomed Opt* 2009; 14:064012.
11. Luker GD, Luker KE. Optical imaging: current applications and future directions. *J Nucl Med* 2008;49:1-4.
12. Kitai T, Inomoto T, Miwa M, et al. Fluorescence navigation with indocyanine green for detecting sentinel lymph nodes in breast cancer. *Breast Cancer* 2005; 12:211-215.
13. Ogasawara Y, Ikeda H, Takahashi M, et al. Evaluation of breast lymphatic pathways with indocyanine green fluorescence imaging in patients with breast cancer. *World J Surg* 2008; 32:1924-1929.
14. Tagaya N, Yamazaki R, Nakagawa A, et al. Intraoperative identification of sentinel lymph nodes by near-infrared fluorescence imaging in patients with breast cancer. *Am J Surg* 2008; 195:850-853.
15. Hirche C, Murawa D, Mohr Z, et al. ICG fluorescence-guided sentinel node biopsy for axillary nodal staging in breast cancer. *Breast Cancer Res Treat* 2010; 121:373-378.
16. Murawa D, Hirche C, Dresel S, et al. Sentinel lymph node biopsy in breast cancer guided by indocyanine green fluorescence. *Br J Surg* 2009; 96:1289-1294.
17. Troyan SL, Kianzad V, Gibbs-Strauss SL, et al. The FLARE intraoperative near-infrared fluorescence imaging system: a first-in-human clinical trial in breast cancer sentinel lymph node mapping. *Ann Surg Oncol* 2009; 16:2943-2952.
18. Sevick-Muraca EM, Sharma R, Rasmussen JC, et al. Imaging of lymph flow in breast cancer patients after microdose administration of a near-infrared fluorophore: feasibility study. *Radiology* 2008; 246:734-741.
19. van der Vegt B, de Bock GH, Bart J, Zwartjes NG, Wesseling J. Validation of the 4B5 rabbit monoclonal antibody in determining HER2/neu status in breast cancer. *Mod Pathol*. 2009; 22(7):879-86.
20. van der Vegt B, de Roos MA, Peterse JL, Patriarca C, Hilken J, de Bock GH, et al. The expression pattern of MUC1 (EMA) is related to tumour characteristics and clinical outcome of invasive ductal breast carcinoma. *Histopathology*. 2007; 51(3):322-35.
21. Kononen J, Bubendorf L, Kallioniemi A, et al. Tissue microarrays for high-throughput molecular profiling of tumor specimens. *Nat Med* 1998; 4:844-847.
22. Vermeulen JF, van Brussel AS, van der Groep P, et al. Immunophenotyping invasive breast cancer: paving the road for molecular imaging. *BMC Cancer* 2012; 12:240.

23. van Oosten M, Crane LM, Bart J, et al. Selecting Potential Targetable Biomarkers for Imaging Purposes in Colorectal Cancer Using Target Selection Criteria (TASC): A Novel Target Identification Tool. *Transl Oncol* 2011; 4:71-82.
24. Viera AJ, Garrett JM. Understanding interobserver agreement: the kappa statistic. *Fam Med* 2005; 37:360-363.
25. R Core Team (2013). R: A language and environment for statistical computing. R Foundation for Statistical Computing, Vienna, Austria. Available at: <http://www.R-project.org/>.
26. Cimino A, Halushka M, Illei P, et al. Epithelial cell adhesion molecule (EpCAM) is overexpressed in breast cancer metastases. *Breast Cancer Res Treat* 2010; 123:701-708.
27. Spizzo G, Went P, Dirnhofer S, et al. High Ep-CAM expression is associated with poor prognosis in node-positive breast cancer. *Breast Cancer Res Treat* 2004 ;86:207-213.
28. Hsieh MJ, Chen KS, Chiou HL, et al. Carbonic anhydrase XII promotes invasion and migration ability of MDA-MB-231 breast cancer cells through the p38 MAPK signaling pathway. *Eur J Cell Biol* 2010; 89:598-606.
29. Watson PH, Chia SK, Wykoff CC, et al. Carbonic anhydrase XII is a marker of good prognosis in invasive breast carcinoma. *Br J Cancer* 2003; 88:1065-1070.
30. Cabioglu N, Yazici MS, Arun B, et al. CCR7 and CXCR4 as novel biomarkers predicting axillary lymph node metastasis in T1 breast cancer. *Clin Cancer Res* 2005; 11:5686-5693.
31. Carlsson J, Nordgren H, Sjostrom J, et al. HER2 expression in breast cancer primary tumours and corresponding metastases. Original data and literature review. *Br J Cancer* 2004; 90:2344-2348.
32. Segal EI, Low PS. Tumor detection using folate receptor-targeted imaging agents. *Cancer Metastasis Rev* 2008; 27:655-664.
33. Hiller D, Chu QD. CXCR4 and axillary lymph nodes: review of a potential biomarker for breast cancer metastasis. *Int J Breast Cancer* 2011; 2011:420981.
34. Muller A, Homey B, Soto H, et al. Involvement of chemokine receptors in breast cancer metastasis. *Nature* 2001; 410:50-56.
35. Meincke M, Tiwari S, Hattermann K, et al. Near-infrared molecular imaging of tumors via chemokine receptors CXCR4 and CXCR7. *Clin Exp Metastasis* 2011; 28:713-720.
36. Nimmagadda S, Pullambhatla M, Stone K, et al. Molecular imaging of CXCR4 receptor expression in human cancer xenografts with [64Cu]AMD3100 positron emission tomography. *Cancer Res* 2010; 70:3935-3944.
37. Shim H, Lau SK, Devi S, et al. Lower expression of CXCR4 in lymph node metastases than in primary breast cancers: potential regulation by ligand-dependent degradation and HIF-1 α . *Biochem Biophys Res Commun* 2006; 346:252-258.
38. Tafreshi NK, Enkemann SA, Bui MM, et al. A mammaglobin-A targeting agent for noninvasive detection of breast cancer metastasis in lymph nodes. *Cancer Res* 2011; 71:1050-1059.
39. Han JH, Kang Y, Shin HC, et al. Mammaglobin expression in lymph nodes is an important marker of metastatic breast carcinoma. *Arch Pathol Lab Med* 2003; 127:1330-1334.
40. Signorel N, Oldridge J, Pelchen-Matthews A, et al. Phorbol esters and SDF-1 induce rapid endocytosis and down modulation of the chemokine receptor CXCR4. *J Cell Biol* 1997; 139:651-664.
41. Arias-Pulido H, Chaheer N, Gong Y, et al. Tumor stromal vascular endothelial growth factor A is predictive of poor outcome in inflammatory breast cancer. *BMC Cancer* 2012; 12:298.
42. Dhakal HP, Naume B, Synnestvedt M, et al. Expression of vascular endothelial growth factor and vascular endothelial growth factor receptors 1 and 2 in invasive breast carcinoma: prognostic significance and relationship with markers for aggressiveness. *Histopathology* 2012; 61:350-364.
43. Cimpean AM, Raica M, Suciuc C, et al. Vascular endothelial growth factor A (VEGF A) as individual prognostic factor in invasive breast carcinoma. *Rom J Morphol Embryol* 2008; 49:303-308.
44. Ghosh S, Sullivan CA, Zerkowski MP, et al. High levels of vascular endothelial growth factor and its receptors (VEGFR-1, VEGFR-2, neuropilin-1) are associated with worse outcome in breast cancer. *Hum Pathol* 2008; 39:1835-1843.

45. Konecny GE, Meng YG, Untch M, et al. Association between HER-2/neu and vascular endothelial growth factor expression predicts clinical outcome in primary breast cancer patients. *Clin Cancer Res* 2004; 10:1706-1716.
46. Terwisscha van Scheltinga AG, van Dam GM, Nagengast WB, et al. Intraoperative near-infrared fluorescence tumor imaging with vascular endothelial growth factor and human epidermal growth factor receptor 2 targeting antibodies. *J Nucl Med* 2011; 52:1778-1785.
47. Nagengast WB, de Vries EG, Hospers GA, et al. *In vivo* VEGF imaging with radiolabeled bevacizumab in a human ovarian tumor xenograft. *J Nucl Med* 2007; 48:1313-1319.
48. Gui GP, Puddefoot JR, Vinson GP, et al. Altered cell-matrix contact: a prerequisite for breast cancer metastasis? *Br J Cancer* 1997; 75:623-633.
49. Gui GP, Wells CA, Yeomans P, et al. Integrin expression in breast cancer cytology: a novel predictor of axillary metastasis. *Eur J Surg Oncol* 1996; 22:254-258.
50. Gui GP, Wells CA, Browne PD, et al. Integrin expression in primary breast cancer and its relation to axillary nodal status. *Surgery* 1995; 117:102-108.
51. Liapis H, Flath A, Kitazawa S. Integrin alpha V beta 3 expression by bone-residing breast cancer metastases. *Diagn Mol Pathol* 1996; 5:127-135.
52. Pola C, Formenti SC, Schneider RJ. Vitronectin-alpha v beta 3 Integrin Engagement Directs Hypoxia-Resistant mTOR Activity and Sustained Protein Synthesis Linked to Invasion by Breast Cancer Cells. *Cancer Res* 2013; 73:4571-4578.
53. Zhu H, Zhou X, Redfield S, et al. Elevated Expression of Notch1 Is Associated With Metastasis of Human Malignancies. *Int J Surg Pathol* 2013; 21:449-454.
54. Spizzo G, Fong D, Wurm M, et al. EpCAM expression in primary tumour tissues and metastases: an immunohistochemical analysis. *J Clin Pathol* 2011; 64:415-420.
55. Camp RL, Chung GG, Rimm DL. Automated subcellular localization and quantification of protein expression in tissue microarrays. *Nat Med* 2002; 8:1323-1327.
56. Taylor CR, Levenson RM. Quantification of immunohistochemistry--issues concerning methods, utility and semiquantitative assessment II. *Histopathology* 2006; 49:411-424.
57. Tafreshi NK, Bui MM, Bishop K, et al. Noninvasive detection of breast cancer lymph node metastasis using carbonic anhydrases IX and XII targeted imaging probes. *Clin Cancer Res* 2012; 18:207-219.
58. Wu J, Ma R, Cao H, et al. Intraoperative imaging of metastatic lymph nodes using a fluorophore-conjugated antibody in a HER2/neu-expressing orthotopic breast cancer mouse model. *Anticancer Res* 2013; 33: 419-424.
59. van Dam GM, Themelis G, Crane LM, et al. Intraoperative tumor-specific fluorescence imaging in ovarian cancer by folate receptor-alpha targeting: first in-human results. *Nat Med* 2011; 17:1315-1319.

Supplementary Table 1. Modified target selection criteria (TASC) scoring system for the selection of tumor markers for targeted optical imaging of lymph node metastasis in breast cancer patients. Items I-VII were imported from the original TASC scoring system, items VIII-X are complementary.

Item	Marker characteristics according to the TASC scoring system*	Score
I	Membranous (extracellular domain)	5
	In close proximity of tumor cell (extracellular matrix)	3
	Cytoplasmic	0
II	Diffuse expression throughout the tumor	4
	Mostly diffuse, some focal staining	2
	Mostly focal staining	0
III	TASC definition	Adjusted definition**
	TBR: >10	TBR: >10
	TBR: <3	TBR: 3–10
IV	TASC definition	Adjusted definition**
	>90%	>90%
	70–90%	25–50%
	50–69%	10–25%
V	10–49%	0–10%
	Percentage of patients in which the marker is expressed	6
V	Previously imaged with success <i>in vivo</i>	5
VI	Enzymatic activity	3
VII	Internalization	0
VIII	Almost perfect agreement (Kappa: >0.80)	6
	Substantial agreement (Kappa: 0.60–0.80)	5
	Moderate agreement (Kappa: 0.40–0.60)	3
IX	Poor to fair agreement (Kappa: <0.40)	0
	Percentage of patients with positive lymph node metastasis in who the corresponding primary tumor is also positive	1
X	Predictability of positive primary tumor for the presence of positive lymph node metastases.	0
	Maximum amount of points	30

* Modified from: Oosten M, Crane LM, Bart J, van Leeuwen FW, van Dam GM. Selecting potential targetable tumor markers for imaging purposes in colorectal cancer using target selection criteria (TASC): a novel target identification tool. *Transl Oncol* 2011; 14:71–82.

** Modified TASC score based on alternative thresholds for tumor-to-background ratio (TBR) and tumor marker expression level.

Supplementary Table 2. Tumor marker expression in lymph node metastases from breast cancer patients as reported in the literature.

Target	Expression rate (%)	Method	Number of patients	Reference	Year
αvβ3	NR	-	-	-	-
CA-IX	13%	IHC	49	Tafreshi et al. ¹	2012
	22%	IHC	60	van den Eynden et al. ²	2005
CA-XII	19%	IHC	49	Tafreshi et al. ¹	2012
CXCR4	30%	IHC	20	Shim et al. ³	2006
	60%	IHC	5	Muller et al. ⁴	2001
EpCAM	40%	IHC	5	Spizzo et al. ⁵	2011
FR-α	36%	IHC	61	O'Shanessy et al. ⁶	2012
HER2	55%	IHC	47	Carlsson et al. ⁷	2004
	25%	IHC	76	Tsutsui et al. ⁸	2002
	28%	IHC	46	Tanner et al. ⁹	2001
	25%	IHC	125	Simon et al. ¹⁰	2001
	38%	IHC	21	Shimizu et al. ¹¹	2000
	32%	IHC	56	Masood et al. ¹²	2000
MGB1	45%	IHC	50	Tafreshi et al. ¹³	2011
	76%	IHC	41	Wang et al. ¹⁴	2009
	60%	IHC	10	Sasaki et al. ¹⁵	2007
	69%	IHC	29	Bhargava et al. ¹⁶	2007
	84%	IHC	70	Han et al. ¹⁷	2003
Notch1	40%	IHC	5	Zhu et al. ¹⁸	2013
VEGF-A	48%	IHC	90	Maloney et al. ¹⁹	2007

αvβ3, alpha v beta 3 integrin receptor; CA-IX, carbonic anhydrase IX; CA-XII, carbonic anhydrase XII; CXCR4, C-X-C chemokine receptor 4; EpCAM, epithelial cell adhesion molecule; FR-α, folate receptor alpha; HER2, human epidermal growth factor receptor 2; IHC, immunohistochemistry; MGB1, mammaglobin 1; NR, not reported; VEGF-A, vascular endothelial growth factor A.

REFERENCES WITH SUPPLEMENTARY TABLE 2:

1. Tafreshi NK, Bui MM, Bishop K, et al. Noninvasive detection of breast cancer lymph node metastasis using carbonic anhydrases IX and XII targeted imaging probes. *Clin Cancer Res* 2012; 18:207-219.
2. Van den Eynden GG, Van der Auwera I, Van Laere SJ, et al. Angiogenesis and hypoxia in lymph node metastases is predicted by the angiogenesis and hypoxia in the primary tumour in patients with breast cancer. *Br J Cancer* 2005; 93:1128-1136.
3. Shim H, Lau SK, Devi S, et al. Lower expression of CXCR4 in lymph node metastases than in primary breast cancers: potential regulation by ligand-dependent degradation and HIF-1alpha. *Biochem Biophys Res Commun* 2006; 346:252-258.
4. Muller A, Homey B, Soto H, et al. Involvement of chemokine receptors in breast cancer metastasis. *Nature* 2001; 410:50-56.
5. Spizzo G, Fong D, Wurm M, et al. EpCAM expression in primary tumour tissues and metastases: an immunohistochemical analysis. *J Clin Pathol* 2011; 64:415-420.
6. O'Shannessy DJ, Somers EB, Maltzman J, Smale R, Fu Y. Folate receptor alpha (FRA) expression in breast cancer: identification of a new molecular subtype and association with triple negative disease. *SpringerPlus* 2012, 1:22 doi:10.1186/2193-1801-1-22.
7. Carlsson J, Nordgren H, Sjostrom J, et al. HER2 expression in breast cancer primary tumours and corresponding metastases. Original data and literature review. *Br J Cancer* 2004; 90:2344-2348.
8. Tsutsui S, Ohno S, Murakami S, et al. EGFR, c-erbB2 and p53 protein in the primary lesions and paired metastatic regional lymph nodes in breast cancer. *Eur J Surg Oncol* 2002; 28:383-387.
9. Tanner M, Jarvinen P, Isola J. Amplification of HER-2/neu and topoisomerase IIalpha in primary and metastatic breast cancer. *Cancer Res* 2001; 61:5345-5348.
10. Simon R, Nocito A, Hubscher T, et al. Patterns of her-2/neu amplification and overexpression in primary and metastatic breast cancer. *J Natl Cancer Inst* 2001; 93:1141-1146.
11. Shimizu C, Fukutomi T, Tsuda H, et al. c-erbB-2 protein overexpression and p53 immunoreaction in primary and recurrent breast cancer tissues. *J Surg Oncol* 2000; 73:17-20.
12. Masood S, Bui MM. Assessment of Her-2/neu overexpression in primary breast cancers and their metastatic lesions: an immunohistochemical study. *Ann Clin Lab Sci* 2000; 30:259-265.
13. Tafreshi NK, Enkemann SA, Bui MM, et al. A mammaglobin-A targeting agent for noninvasive detection of breast cancer metastasis in lymph nodes. *Cancer Res* 2011; 71:1050-1059.
14. Wang Z, Spaulding B, Sienko A, et al. Mammaglobin, a valuable diagnostic marker for metastatic breast carcinoma. *Int J Clin Exp Pathol* 2009; 2:384-389.
15. Sasaki E, Tsunoda N, Hatanaka Y, et al. Breast-specific expression of MGB1/mammaglobin: an examination of 480 tumors from various organs and clinicopathological analysis of MGB1-positive breast cancers. *Mod Pathol* 2007; 20:208-214.
16. Bhargava R, Beriwal S, Dabbs DJ. Mammaglobin vs GCDFP-15: an immunohistologic validation survey for sensitivity and specificity. *Am J Clin Pathol* 2007; 127:103-113.
17. Han JH, Kang Y, Shin HC, et al. Mammaglobin expression in lymph nodes is an important marker of metastatic breast carcinoma. *Arch Pathol Lab Med* 2003; 127:1330-1334.
18. Zhu H, Zhou X, Redfield S, et al. Elevated Expression of Notch1 Is Associated With Metastasis of Human Malignancies. *Int J Surg Pathol* 2013; 21:449-454.
19. Maloney, Katherine F., Expression of Vascular Endothelial Growth Factor Subtypes in Mammary Invasive Ductal Carcinoma and their Relationship to Tumor Progression. 2007. University of Massachusetts Medical School. Senior Scholars Program. Paper 45.

Chapter

10

Summary

R.G. Pleijhuis

Combining innovative molecular biology and chemistry, scientists in the field of cancer research have developed optical imaging modalities for visualization of a wide variety of cellular and molecular processes *in vivo*. Whereas optical imaging has primarily been used in the last decade for research in cells and small laboratory animals, the next frontier is to translate this technology towards a clinical setting. Already, vibrant developments have been made in both imaging systems and fluorescent probes. This thesis provides an overview of the technical and biological requirements for NIRF imaging, with the emphasis on potential imaging applications to complement the surgical treatment of breast cancer.

A general introduction on optical imaging and its potential applications in breast cancer treatment is provided in **Chapter 1**. In the case of clinical $T_{1-2}N_0M_{0-x}$ breast carcinoma, breast-conserving surgery followed by radiotherapy is considered standard treatment. Inadequate removal of the primary tumor results in positive surgical margins, which is considered to be one of the most important risk factors of local recurrence. More than focal positive margins therefore form an indication for additional surgery and, consequently, adverse effects on delay of adjuvant treatment, cosmesis, psychological distress, and health costs. NIRF-guided surgery may reduce the frequency of positive surgical margins following lumpectomy by providing the surgeon with real-time feedback on surgical margin status during the surgical procedure.

Chapter 2 comprises a review of the different pre- and intraoperative techniques that are currently available as well as potential future techniques for obtaining negative surgical margins following breast-conserving surgery. The percentage of patients reported with positive surgical margins following lumpectomy ranges from 20% to 40% in the majority of studies. Efforts to reduce the number of positive margins should focus on optimizing the surgical procedure itself, as the main problem is the lack of real-time intraoperative feedback on the presence of positive surgical margins during lumpectomy. Innovative intraoperative approaches, such as positron emission tomography, magnetic resonance imaging, radioguided occult lesion localization, and NIRF optical imaging, could complement breast-conserving surgery by providing real-time feedback on surgical margin status during lumpectomy.

To identify whether patients at high risk for positive surgical margins could be identified prior to breast-conserving surgery, a multicenter study was conducted within twenty hospitals in the Northern- and Eastern region of the Netherlands. **Chapter 3** describes the development of a predictive tool (nomogram) based on preoperative variables from 1185 patients, enabling preoperative estimation of the risk of positive margins on an individual basis. The nomogram was validated in an independent dataset consisting of 331 patients, showing adequate discrimination and calibration. To facilitate the use of our prediction tool in the clinic, a userfriendly web-based application was developed as an alternative to a graphical nomogram.

Chapter 4 focuses on the potential of NIRF imaging in demarcating cancerous tissue as a step-up towards NIRF-guided breast-conserving surgery. With the current diversity in fluorescent agents and the accompanying differences in biodistribution, we aimed to develop a methodology that enables correction for discrepancies in tumor demarcation as a result of the application of different imaging systems and fluorescent probes in NIRF imaging. Bioluminescence and NIRF imaging were performed in a xenograft breast cancer mouse model using different imaging systems and fluorescent probes in separate groups. Bioluminescence served as a gold standard for cancerous tissue. *Segmentation-based comparative analysis of planar optical signals* (SCAPOS) was applied as a novel methodology to correct for false negative NIRF signals in each group.

Chapter 5 describes a technical feasibility study for pre- and intraoperative NIRF imaging applications using tissue-like breast phantoms. Breast-shaped phantoms were produced with optical properties that closely match those of normal breast tissue. Fluorescent tumor-like inclusions containing indocyanine green were positioned at predefined locations in the phantoms to allow for simulation of (i) preoperative tumor localization, (ii) real-time NIRF-guided tumor resection, and (iii) intraoperative margin assessment. Optical imaging was performed using a customized clinical prototype NIRF intraoperative camera. Tumor-like inclusions in breast phantoms could be detected up to a depth of 21 mm using the intraoperative camera system. Real-time NIRF-guided resection of tumor-like inclusions proved feasible. Moreover, intraoperative NIRF imaging reliably detected residual disease in case of inadequate resection. Clinical studies are needed to further validate these results.

Chapter 6 outlines a clinical study investigating the technical feasibility of NIRF-guided visualization of the sentinel lymph node using a nonspecific fluorescent dye in ten patients with biopsy-proven cT₁₋₂N₀ breast carcinoma. All patients underwent the standard sentinel lymph node procedure, consisting of a preoperative injection with radiolabeled colloid and intraoperative injection with vital blue dye. In addition, all patients received a peritumoral injection with 1 ml (0.5 mg/ml) indocyanine green intraoperatively. The sentinel node was successfully identified in all patients using a customized multispectral fluorescence camera system. The total number of lymph nodes detected with radiolabeled colloid, vital blue dye, and indocyanine green was 18, 9, and 14, respectively. The use of the NIRF camera system did not interfere with the standard operative procedure. No adverse reactions were encountered following administration of indocyanine green.

Chapter 7 comprises a systematic review of current techniques used for sentinel lymph node mapping in breast cancer and melanoma. Pooled detection rates using radiocolloid alone gradually increased from 92% in 1995 to 98% in 2012, which is likely to be attributable to a gradual sophistication of the technique over time. Addition of vital blue dye did not increase sentinel lymph node detection rates compared to the use of radiocolloid alone, while its use led to allergic reactions in up to 5% of the patients. Addition of the nonspecific fluorescent dye indocyanine green to radiocolloid increased detection rates to 100%. No anaphylactic reactions were described when indocyanine green was applied.

Chapter 8 describes the assessment of tumor marker characteristics from 10 preselected markers using the recently introduced *target selection criteria* (TASC) scoring system. The scoring system is based on seven favorable target characteristics for imaging purposes for which each marker is scored: I) extracellular tumor marker localization; II) expression pattern; III) tumor-to-normal ratio (T/N); IV) target expression rate; V) reported successful use *in vivo*; VI) enzymatic activity, and VII) internalization. Evaluated tumor markers included alpha v beta 3 ($\alpha v \beta 3$) integrin receptor, C-X-C-chemokine receptor 4 (CXCR4), carbonic anhydrase (CA) IX and XII, epithelial cell adhesion molecule (EpCAM), folate receptor alpha (FR- α), human epidermal growth factor receptor 2 (HER2), mammaglobin 1 (MGB1), Notch1 receptor, and vascular endothelial growth factor A (VEGF-A). All ten tumor markers were assessed on tissue microarrays of invasive breast carcinomas from 439 eligible patients using immunohistochemistry. CXCR4, CA-XII, and EpCAM were identified as the most potent tumor markers for probe development according to TASC.

Chapter 9 focuses on tumor marker expression in lymph node metastases from 98 breast cancer patients, evaluating the same panel of ten tumor markers mentioned in Chapter 8. To evaluate whether a single targeted fluorescent probe could be applied for simultaneous imaging of both lymph node metastases and the primary tumor, marker expression levels were compared between lymph node metastases and their corresponding primaries. CXCR4 was deemed unsuitable for targeted imaging of lymph node metastasis due to expression of CXCR4 on the outer membrane of lymphocytes, resulting in high background signals in lymph nodes. CA-XII and EpCAM were identified as the most potent markers for targeted imaging of lymph node metastases.

Chapter

11

Conclusions & future perspectives

R.G. Pleijhuis

In this thesis, we describe intraoperative NIRF imaging as a novel and highly promising technique to complement the surgical treatment of breast cancer. Optical imaging modalities have become essential for studying small animal models, providing unique insights into disease pathogenesis, drug development, and effects of therapy. Herein, the concept of using NIR light has proven a crucial step in the development of optical technologies that can offer high integration in a clinical setting. Further development of intraoperative imaging systems should be directed towards maximizing signal penetration of optical signals in deep tissues and enabling accurate, quantitative imaging that eliminates the appearance of false negatives or positives. Although challenges will continue to arise, optical imaging has the potential to become a powerful and practical tool for a wide array of applications in cancer research and treatment, including detection of early-stage cancer, image-guided biopsies and surgical procedures, and therapeutic monitoring of cancer.

Targeted NIRF imaging in animals

The incidence of breast cancer is expected to rise to 17,500 newly diagnosed cases in 2020, indicating that breast cancer will continue to be the most common malignancy in women in the Netherlands in the years to come.¹ Intraoperative NIRF imaging offers a promising technique for real-time fluorescence-guided surgery that is safe, simple to operate, fast, relatively inexpensive, makes use of non-ionizing radiation, and enables imaging at high resolution (as low as 10 μm).² Application of tumor-targeted fluorescent probes could differentiate malignancy from surrounding breast tissue, enabling NIRF-guided resection of the primary tumor as well as sites of regional disseminated disease without unnecessary damage to healthy tissue.³ Indeed, animal studies reported the outcome of cancer surgery to improve when real-time NIRF imaging feedback was enabled during surgery using tumor-targeted fluorescent probes.⁴ Confirmatory *ex vivo* imaging, bioluminescence imaging, and histopathology were used to validate the *in vivo* findings. NIRF imaging detected all tumors and successfully guided total tumor excision by effectively detecting small tumor residuals, which occasionally were missed by the surgeon. It should be mentioned, however, that a xenograft animal model was used with subcutaneously implanted tumors that do not necessarily exhibit the same invasiveness and disease characteristics as in humans. Caution should therefore be used when extrapolating these results to humans.

Targeted NIRF imaging in humans

Recently, our group reported on the first-in-human use of intraoperative tumor-specific NIRF imaging in patients undergoing an exploratory laparotomy for suspected ovarian cancer.⁵ The potential value of intraoperative NIRF imaging for the detection of tumor tissue in ovarian cancer was assessed using the targeted fluorescent probe folate-FITC, which was synthesized by conjugating folate (a vitamin) to the fluorescent dye fluorescein isothiocyanate (FITC). Folate-FITC is targeted specifically towards folate receptor α , which is overexpressed in 90-95% of the malignant ovarian carcinoma.⁶ The targeting ligand, folate, is especially attractive as it is non-toxic, inexpensive, and relatively easy conjugated to a fluorescent dye. However, its applicability in breast cancer seems limited due to the relatively low expression of folate receptor α in breast tumors (Chapter 8) and the unfavorable emission wavelength of FITC (~ 500 nm), reducing penetration depth of the optical signal to several millimeters. Moreover, there are concerns regarding potential toxicity of folate-FITC on the long term, as the

compound is internalized in living cells upon binding to its receptor. Alternative tumor markers are therefore needed as well as fluorescent agents in the near-infrared spectral range for successful NIRF imaging in breast cancer. So far, the only two fluorescent agents that made it towards the process of clinical translation are IRDye 800CW (LI-COR Biosciences, Lincoln, USA) and ZW800-1 (The FLARE Foundation, Wayland, USA). Both agents have favorable toxicity profiles and are expected to be applied for NIRF imaging of different solid cancers in the near future. At the University Medical Center of Groningen and Utrecht, the BIRDye CTMM MAMMOTH optical imaging study (NCT01508572) is currently being performed, in which the tracer bevacizumab-IRDye 800CW will be administered to 20 breast cancer patients prior to surgery.⁷ The tracer consists of the near-infrared fluorescent dye IRDye 800CW conjugated to the VEGF-A targeting humanized monoclonal antibody bevacizumab. VEGF-A has proven to be a valid target for molecular imaging with radioactive labeled tracers.⁸ However, in view of radiation safety, infrastructure, costs, and stability, fluorescent labeling of bevacizumab has potential advantages over radioactive labeling. The purpose of the BIRDye study is to provide insight in the uptake of bevacizumab-IRDye 800CW in breast cancer tissue, surrounding healthy tissue, tumor margins, and lymph nodes. Also, the safety will be assessed as well as the intraoperative detectability of the bevacizumab-IRDye 800CW fluorescent signal.

Tumor markers for targeted NIRF imaging

In addition to VEGF-A, alternative tumor markers are available that are of particular interest for tumor-targeted imaging in breast cancer (Chapter 8), including CXCR4, EpCAM, and CA-XII. For the majority of tumor markers, humanized monoclonal antibodies are already available that can be conjugated with NIR fluorescent agents, facilitating clinical translation. As NIRF optical contrast agents translate from preclinical studies to patients, applications of optical imaging in clinical care are expected to expand rapidly.

Whether or not a specific marker is expressed, can be assessed prior to surgery by performing immunohistochemistry on a core needle biopsy. Through the assessment of multiple markers simultaneously using a preoperative marker panel, the most suitable tumor marker and its corresponding fluorescent probe can be selected for each individual patient. Several hours to days after injection with the selected probe, tumor-targeted NIRF-guided surgery can be performed. Implementation of such a preoperative marker panel is considered an important step towards patient-tailored imaging.

NIRF-guided sentinel lymph node mapping

Although the sentinel node detection rate is already 97% using the current standard technique of radiocolloid combined with vital blue dye (Chapter 7), the true added value of NIRF imaging lies in its potential to visualize lymph node metastasis. By using a multispectral imaging system, multiple fluorescent agents can be used simultaneously as long as their emission wavelengths are distinct.⁹ For example, the nonspecific fluorescent dye indocyanine green could be combined with a tumor-targeted fluorescent dye for visualization of the sentinel lymph node and potential lymph node metastasis, respectively (Fig. 1).

Tafreshi et al. showed the feasibility of targeting lymph node metastases using a NIRF imaging system in a xenograft breast cancer mouse model.^{10,11} NIRF imaging was performed 24 hours following injection of a NIR fluorescent dye conjugated to a monoclonal antibody targeted towards mammoglobin 1, carbonic anhydrase IX, or carbonic anhydrase XII. Results indicated

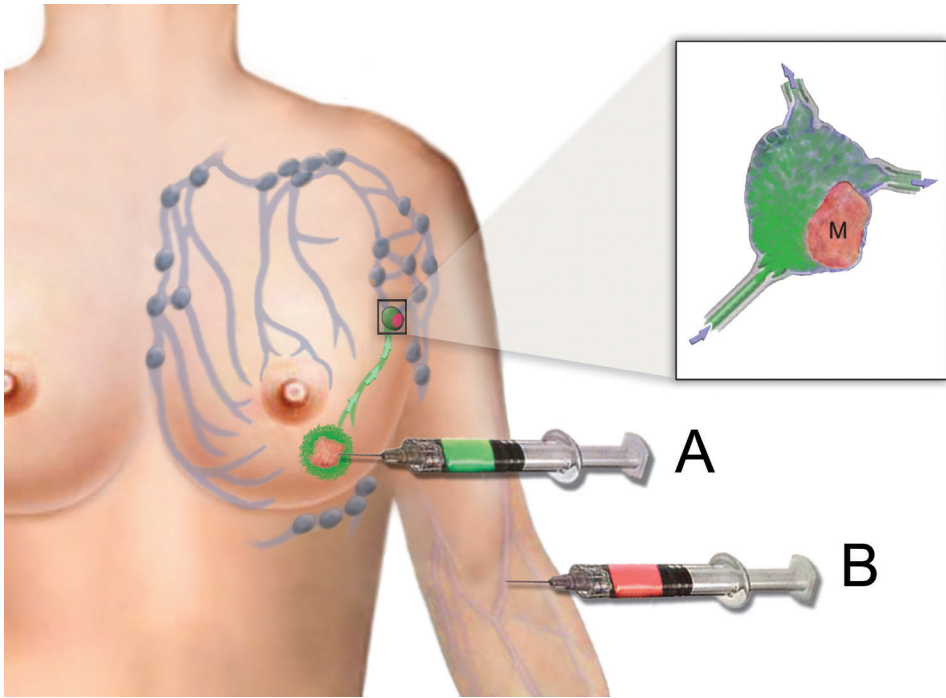


Figure 1. NIRF-guided lymph node mapping using a dual probe approach in combination with a multispectral imaging system. After localization of the sentinel lymph node using a nonspecific fluorescent probe (**A**), the identified lymph node is scanned for the presence of the tumor-targeted probe (**B**) bound to metastases (**M**).

that the fluorescent probe was only retained in the primary tumor and lymph node metastases. As few as 1,000 breast cancer cells could be detected in the lymph nodes, indicating the high sensitivity of this methodology. Theoretically, this approach offers considerable potential for the staging of breast cancer. Already, tumor markers were identified that are of particular interest for targeted imaging of lymph node metastasis (Chapter 9). However, extensive scientific testing is needed to confirm this hypothesis.

Technical improvements to NIRF imaging systems

Several NIRF epi-illumination systems have been developed for interventional imaging applications, providing the surgeon with real-time information concerning the distribution of fluorescent molecules in tissue. Imaging over a range of NIR wavelengths enables correction for photon-tissue interaction and spectral unmixing of multiple fluorescent signals.¹²

To date, three new intraoperative camera systems have been developed that can detect and unmix NIRF signals in real-time. The T3-platform[®] (SurgOptix Inc., Redwood Shores, USA) resolves true fluorescence biodistribution, eliminating false positive and negative results common to other epi-illumination fluorescence imaging systems. The implementation is based on the use of three cameras operating in parallel, utilizing a common main objective that allows for the concurrent collection of color, fluorescence, and light attenuation images from the same field of view.¹³ The T3-platform is currently in clinical trial related to breast cancer patients (NCT01508572).

The second camera system is the Artemis™ (Quest Medical Imaging, Middenmeer, The Netherlands), which is a real-time stereoscopic imaging system that combines visible light with NIR light images. The Artemis™ creates multispectral images by using a five-channel prism (covering the range from 400–1000 nm), enabling the capture of five different color bands simultaneously.³

The third intraoperative camera is the *fluorescence-assisted resection and exploration* (FLARE™) system, which acquires color video and NIR fluorescence images simultaneously in real-time.¹⁴ The FLARE™ system underwent considerable refinements over the years, including the addition of hands-free operation and the integration of high-power, multi-channel, and computer-controlled LED light source required for human surgery.

The current intraoperative NIRF imaging systems enable superposition of the fluorescent signal on a color video of the surgical view, facilitating anatomical positioning of the optical signal.² The current frame-rate of about 10–20 frames per second enables video-rate visualization of the fluorescent signal. Although some groups are working on holographic projections of the fluorescent signal on the surgical field, this methodology seems prone to artefacts due to movement of the patient. Because nowadays all surgeons are trained in laparoscopic surgery and are therefore used to working with 2D screens, visualizing the fluorescent signal as an overlay image on the operating room monitor seems the most straightforward approach. In addition, a NIRF camera was integrated into robotic systems like the da Vinci Si HD™ system (Intuitive Surgical Inc., Sunnyvale, USA), providing a combination of technical and minimally invasive advantages.¹⁵ However, only a few articles have been published thus far regarding this technique which is still experimental and evolving.¹⁶⁻²¹

Photoacoustic imaging

Beyond epi-illumination fluorescence imaging, photoacoustic methods are emerging to offer high-resolution optical imaging through up to centimeters of depth.²² Photoacoustic imaging is based on the fact that local thermal expansion occurs directly following photon absorption by endogenous molecules or exogenously administered optical contrast agents. This local expansion results in the emission of ultrasound waves, which can be detected using an ultrasound transducer and used to generate a photoacoustic image.²³

Although photoacoustic imaging also suffers from depth limitation, the maximum signal penetration depth is inherently greater than that with conventional optical imaging techniques. At greater depths, the effect of light scattering and absorption by tissue decreases the photon flux reaching deep tissue, thereby weakening the ultrasound signal. Because ultrasound scatters orders of magnitude less than photons in tissue, high spatial resolutions can be preserved through millimeters to centimeters of tissue.²⁴ Some preliminary studies have already reported on the detection of suspected breast carcinoma based on increased absorption due to tumor vasculature.²⁵ In addition, handheld photoacoustic systems for noninvasive sentinel lymph node mapping are being developed.

REFERENCES

1. Dutch Cancer Society. Cancer in the Netherlands to 2020: Trends and prognoses [Kanker in Nederland tot 2020: Trends en prognoses]. 2011. www.kwfkankerbestrijding.nl
2. Mieog JS, Vahrmeijer AL, Hutteman M, et al. Novel intraoperative near-infrared fluorescence camera system for optical image-guided cancer surgery. *Mol Imaging*. 2010; 9(4):223-231.
3. Keereweer S, Kerrebijn JD, van Driel PB, et al. Optical image-guided surgery – where do we stand? *Mol Imaging Biol*. 2010; 13(2):199-207.
4. Themelis G, Harlaar NJ, Kelder W, et al. Enhancing surgical vision by using real-time imaging of $\alpha v\beta 3$ -integrin targeted near-infrared fluorescent agent. *Ann Surg Oncol*. 2011; 18(12): 3506-3513.
5. van Dam GM, Themelis G, Crane LM, et al. Intraoperative tumor-specific fluorescence imaging in ovarian cancer by folate receptor- α targeting: first in-human results. *Nat Med*. 2011; 17(10):1315-1319.
6. Markert S, Lassmann S, Gabriel B, et al. Alpha-folate receptor expression in epithelial ovarian carcinoma and non-neoplastic ovarian tissue. *Anticancer Res*. 2008; 28(6A):3567-3572.
7. BIRDye trail: <http://clinicaltrials.gov/ct2/show/NCT01508572>
8. Gaykema SB, Brouwers AH, Lub-de Hooge MN, et al. ^{89}Zr -Bevacizumab PET Imaging in Primary Breast Cancer. *J Nucl Med*. 2013; 54:1014-1018.
9. Zhou L, El-Deiry WS. Multispectral fluorescence imaging. *J Nucl Med*. 2009; 50(10):1563-1566.
10. Tafreshi NK, Enkemann SA, Bui MM, Lloyd MC, Abrahams D, Huynh AS. A mammaglobin-A targeting agent for noninvasive detection of breast cancer metastasis in lymph nodes. *Cancer Res*. 2011; 1(3):1050-1059.
11. Tafreshi NK, Bui MM, Bishop K, et al. Noninvasive detection of breast cancer lymph node metastasis using carbonic anhydrases IX and XII targeted imaging probes. *Clin Cancer Res* 2012; 18:207-219.
12. Ntziachristos V. Fluorescence molecular imaging. *Annu Rev Biomed Eng*. 2006; 8:1-33.
13. Themelis G, Yoo JS, Soh KS, Schulz R, Ntziachristos V. Real-time intraoperative fluorescence imaging system using light-absorption correction. *J Biomed Opt*. 2009; 14:064012.
14. Troyan SL, Kianzad V, Gibbs-Strauss SL, et al. The FLARE™ Intraoperative Near-Infrared Fluorescence Imaging System: A First-in-Human Clinical Trial in Breast Cancer Sentinel Lymph Node Mapping. *Ann Surg Oncol*. 2009; 16(10): 2943–2952.
15. Marano A, Priora F, Lenti LM, Ravazzoni F, Quarati R, Spinoglio G. Application of Fluorescence in Robotic General Surgery: Review of the Literature and State of the Art. *World J Surg*. 2013; 37(12):2800-2811.
16. Holloway RW, Bravo RA, Rakowski JA, et al. Detection of sentinel lymph nodes in patients with endometrial cancer undergoing robotic-assisted staging: a comparison of colorimetric and fluorescence imaging. *Gynecol Oncol*. 2012; 126:25–29.
17. Rossi EC, Ivanova A, Boggess JF. Robotically assisted fluorescence-guided lymph node mapping with ICG for gynecologic malignancies: a feasibility study. *Gynecol Oncol*. 2012; 124:78–82.
18. Buchs NC, Hagen ME, Pugin F, et al. Intraoperative fluorescent cholangiography using indocyanine green during robotic single site cholecystectomy. *Int J Med Robot*. 2012; 8:436–440.
19. Calatayud D, Milone L, Elli EF, Giulianotti PC. ICG-fluorescence identification of a small aberrant biliary canalculus during robotic cholecystectomy. *Liver Int*. 2012; 32:602.
20. Wagner OJ, Louie BE, Vallieres E, Aye RW, Farivar AS. Near-infrared fluorescence imaging can help identify the contralateral phrenic nerve during robotic thymectomy. *Ann Thorac Surg*. 2012; 94:622–625.
21. Tobis S, Knopf J, Silvers C, et al. Near-infrared fluorescence imaging with robotic assisted laparoscopic partial nephrectomy: initial clinical experience for renal cortical tumors. *J Urol*. 2011; 186:47–52.

22. Garcia-Allende PB, Glatz J, Koch M, Ntziachristos V. Enriching the interventional vision of cancer with fluorescence and optoacoustic imaging. *J Nucl Med.* 2013; 54(5):664-667.
23. Kim C, Favazza C, Wang LV. *In vivo* photoacoustic tomography of chemicals: high-resolution functional and molecular optical imaging at new depths. *Chem Rev.* 2010; 110:2756–2782.
24. Taruttis A, Ntziachristos V. Translational optical imaging. *AJR Am J Roentgenol.* 2012; 199(2):263-271.
25. Ermilov SA, Khamapirad T, Conjusteau A, et al. Laser optoacoustic imaging system for detection of breast cancer. *J Biomed Opt.* 2009; 14:024007.

Chapter

12

Nederlandse samenvatting

R.G. Pleijhuis

Door het combineren van moleculaire biologie en chemie, hebben wetenschappers in het veld van kankeronderzoek optische beeldvormingstechnieken ontwikkeld om een variëteit aan cellulaire en moleculaire processen zichtbaar te maken *in vivo*. Hoewel optische beeldvorming primair wordt toegepast voor wetenschappelijk onderzoek in cellijnen en proefdieren, zullen patiënten pas rechtstreeks baat hebben bij deze techniek wanneer deze vertaald wordt naar de kliniek. De laatste jaren hebben belangrijke ontwikkelingen plaatsgevonden van zowel de camerasystemen als de optische contrastmiddelen. Dit proefschrift verschaft een overzicht van de technische en biologische benodigdheden voor nabij-infrarood fluorescentie (NIRF) beeldvorming, met de nadruk op toepassingen van optische beeldvorming als aanvulling op de chirurgische behandeling van borstkanker.

Een algehele introductie met betrekking tot optische beeldvorming en de potentiële toepassingen hiervan bij de chirurgische behandeling van het mammacarcinoom is opgenomen in **Hoofdstuk 1**. Bij patiënten met een $T_{1-2}N_0M_{0-x}$ mammacarcinoom bestaat de standaard behandeling uit borstsparende chirurgie gevolgd door radiotherapie. Indien de tumor niet volledig is verwijderd is er sprake van positieve snijvlakken, welke worden beschouwd als een belangrijke risicofactor voor het optreden van een lokaal recidief. Meer dan focaal positieve snijvlakken vormen daarom een indicatie voor aanvullende chirurgie met als gevolg een nadelig effect op cosmetiek, een toegenomen psychologische belasting en een stijging in de kosten van de gezondheidszorg. Fluorescentiegeleide chirurgie zou de frequentie van positieve snijvlakken na borstsparende chirurgie mogelijk kunnen reduceren door de chirurg intraoperatief te voorzien van real-time feedback ten aanzien van de locatie en grootte van de tumor.

Hoofdstuk 2 omvat een uiteenzetting van de verschillende pre- en intraoperatieve technieken die heden ten dage beschikbaar zijn evenals potentieel toekomstige technieken voor het verkrijgen van vrije snijvlakken bij borstsparende chirurgie. Het merendeel van de wetenschappelijke studies rapporteren een percentage patiënten met positieve snijvlakken na borstsparende chirurgie variërend van 20% tot 40%. Inspanningen om dit relatief hoge percentage te reduceren zouden zich moeten richten op de chirurgische procedure zelf, waarbij het hoofdprobleem het ontbreken van real-time intraoperatieve feedback ten aanzien van de status van de snijvlakken wordt geacht. Innovatieve intraoperatieve toepassingen, waaronder positron emissie tomografie (PET), radiogeleide lokalisatie van occulte tumoren en nabij-infrarood fluorescentie beeldvorming, zouden een belangrijke aanvulling kunnen zijn op borstsparende chirurgie door de chirurg real-time feedback te verstrekken ten aanzien van de status van de snijvlakken.

Om patiënten met een hoog risico op positieve snijvlakken te identificeren voorafgaand aan borstsparende chirurgie, werd een multicenter studie verricht met medewerking van twintig ziekenhuizen in de regio Noord- en Oost-Nederland. **Hoofdstuk 3** beschrijft de ontwikkeling van een predictiemodel (nomogram), gebaseerd op preoperatieve variabelen van 1.185 patiënten, waarmee preoperatieve inschatting van het risico op positieve snijvlakken mogelijk wordt op individuele basis. Het nomogram werd gevalideerd in een onafhankelijke dataset bestaande uit 331 patiënten. Om gebruik van het predictiemodel in een klinische setting te faciliteren, werd een gebruiksvriendelijke internetapplicatie ontwikkeld als alternatief voor het grafische nomogram.

Hoofdstuk 4 focust op het potentieel van NIRF beeldvorming ten aanzien van het markeren van tumorweefsel als opstap naar NIRF-geleide borstsparende chirurgie. Gezien de diversiteit in beschikbare optische contrastmiddelen en de daarmee gepaard gaande verschillen in biodistributie, werd een methode ontwikkeld waarmee kan worden gecorrigeerd voor discrepanties in demarcatie van tumorweefsel ten gevolge van het gebruik van verschillende camerasystemen en/of optische contrastmiddelen. Bioluminescentie en NIRF beeldvorming werden verricht in een borstkanker model in muizen, waarbij per groep gebruik werd gemaakt van verschillende camerasystemen en optische contrastmiddelen. Bioluminescentie diende hierbij als gouden standaard voor de aanwezigheid van tumorweefsel. *Segmentation-based comparative analysis of planar optical signals* (SCAPOS) werd toegepast als nieuwe methode voor het corrigeren van vals negatieve signalen in elke groep.

Hoofdstuk 5 beschrijft een technische haalbaarheidsstudie naar de pre- en intraoperatieve toepassingsmogelijkheden van NIRF beeldvorming met behulp van weefsel-gelijkende borstfantomen. Fantomen met optische eigenschappen gelijkend op die van normaal mammaweefsel werden geproduceerd in de vorm van een vrouwelijke borst. Fluorescente tumor-gelijkende inclusies werden gepositioneerd op verschillende diepten in de borstfantomen voor het simuleren van (i) preoperatieve tumor lokalisatie, (ii) real-time NIRF-geleide tumor resectie, en (iii) intraoperatieve beoordeling van de chirurgische snijvlakken. Optische beeldvorming werd verricht door middel van een prototype NIRF camera. De tumor-gelijkende fluorescente inclusies konden worden gedetecteerd tot op een diepte van 21 mm in de borstfantomen. Real-time fluorescentie-geleide resectie van tumor-gelijkende inclusies bleek technisch haalbaar. Klinische studies zijn noodzakelijk om deze resultaten te valideren.

In **Hoofdstuk 6** wordt een klinische studie beschreven, waarin de technische haalbaarheid van fluorescentie-geleide detectie van de poortwachterklier met behulp van een non-specifiek fluorescent contrastmiddel in tien patiënten met een bewezen cT₁₋₂N₀ mammacarcinoom. Alle patiënten ondergingen de standaard poortwachterklier procedure, bestaande uit een preoperatieve injectie met radiogelabeld colloïd en intraoperatieve injectie met patent blauw. Daarnaast werden alle patiënten intraoperatief rondom de primaire tumor geïnjecteerd met 1 ml (0,5 mg/ml) indocyanine groen. De poortwachterklier kon succesvol worden geïdentificeerd in alle patiënten met behulp van een NIRF camera systeem. Het totaal aantal lymfeklieren dat werd gedetecteerd met radiogelabeld colloïd, patent blauw en indocyanine groen bedroeg 18, 9, en 14. Het gebruik van een NIRF camera systeem interfereerde niet met de standaard chirurgische procedure en er werden geen nadelige effecten waargenomen van het gebruik van indocyanine groen.

Hoofdstuk 7 behelst een systematische review van technieken die heden ten dage worden toegepast voor het detecteren van de poortwachterklier. Het percentage succesvolle poortwachterklierprocedures waarbij alleen radiocolloïd wordt gebruikt steeg van 92% in 1995 tot 98% in 2012, waarschijnlijk door toegenomen ervaring en een geleidelijke verbetering van de techniek. Toevoeging van blauwe kleurstof (patent blauw) leidde niet tot een toename van het percentage succesvolle poortwachterklierprocedures in vergelijking tot het gebruik van radiocolloïd alleen. Toevoeging van het nonspecifieke fluorescente contrastmiddel indocyanine groen aan radiocolloïd resulteerde in een lichte toename van het percentage gedetecteerde poortwachterklieren.

Hoofdstuk 8 beschrijft een beoordeling van de eigenschappen van tien voorgeselecteerde tumor markers aan de hand van het recent geïntroduceerde *target selection criteria* (TASC) evaluatie systeem. Deze methode is gebaseerd op zeven gunstige karakteristieken van tumor markers voor optische beeldvorming: I) extracellulaire lokalisatie van de tumor marker, II) expressie patroon, III) tumor/achtergrond ratio, IV) mate van marker expressie, V) succesvolle toepassing van de marker *in vivo*, VI) enzymatische activiteit, en VII) internalisatie. De geëvalueerde tumor markers waren: alpha v beta 3 ($\alpha\text{v}\beta\text{3}$) integrine receptor, C-X-C-chemokine receptor 4 (CXCR4), koolzuuranhydrase (CA) IX en XII, epitheliaal cel adhesie molecuul (EpCAM), folaat receptor alfa (FR- α), humane epidermale groei factor receptor 2 (HER2), mammaglobine 1 (MGB1), Notch1 receptor en vasculair endotheliale groei factor A (VEGF-A). De beoordeling van tumor markers vond plaats middels immunohistochemische analyse van tissue microarrays (TMA's) van 439 patiënten met een invasief mammacarcinoom. CXCR4, CA-XII en EpCAM werden aan de hand van TASC geïdentificeerd als markers met de meeste potentie voor de ontwikkeling van tumor-gerichte fluorescente contrastmiddelen.

Naast fluorescentie-geleide resectie van de primaire tumor, zou pre- en/of intraoperatieve identificatie van lymfekliermetastasen een belangrijke toepassing kunnen zijn van tumor-gerichte NIRF beeldvorming. **Hoofdstuk 9** focust op de expressie van tumor markers in lymfekliermetastasen van 98 patiënten met mammacarcinoom, waarbij dezelfde markers werden beoordeeld als besproken in Hoofdstuk 8. Om te evalueren of een specifiek fluorescent contrastmiddel gelijktijdig zou kunnen worden toegepast voor het detecteren van zowel de lymfekliermetastasen als de primaire tumor, werd de expressie van tumor markers in beide groepen vergeleken. CXCR4 werd ongeschikt geacht voor gerichte beeldvorming van lymfekliermetastasen door de hoge mate van CXCR4 expressie op de membraan van lymfocyten, wat resulteert in een hoog achtergrond signaal in de lymfeklier zelf. CA-XII en EpCAM werden geïdentificeerd als markers met de meeste potentie voor gerichte NIRF beeldvorming van lymfekliermetastasen.

Addendum

Addendum

List of abbreviations

Dankwoord

Curriculum vitae

List of publications

LIST OF ABBREVIATIONS

AIC	Aikaike's information criterion
$\alpha\beta3$	Alpha v beta 3
ALN	Axillary lymph node
ALND	Axillary lymph node dissection
AUROC	Area under the receiver-operating characteristic curve
BC	Breast cancer
BCS	Breast-conserving surgery
BCT	Breast-conserving therapy
BI-RADS	Breast imaging reporting and data system
BLI	Bioluminescence imaging
CA-IX	Carbonic anhydrase IX
CA-XII	Carbonic anhydrase XII
CAL	Cryoprobe-assisted localization
CCD	Charge-coupled device
CCMO	National committee for clinical research
CI	Confidence interval
CNB	Core needle biopsy
CT	Computed tomography
CXCR4	C-X-C chemokine receptor 4
DAB	3,3-Diaminobenzidine
DARE	Database of abstracts of reviews of effects
DCIS	Ductal carcinoma in situ
EpCAM	Epithelial cell adhesion molecule
ER	Estrogen receptor
FDA	Food & drug administration
FDG	Fluoro-desoxyglucose
FISH	Fluorescent in situ hybridization
FITC	Fluorescein isothiocyanate
FLARE	Fluorescence-assisted resection and exploration system
FNR	False negative rate
FPS	Frames per second
FR- α	Folate receptor alpha
FRI	Fluorescence reflectance imaging
FSA	Frozen section analysis
FWHM	Full width at half maximum
GLUT1	Glucose transporter 1
HCL	Hydrochloric acid
H&E	Haematoxylin and eosin
HER2	Human epidermal growth factor receptor 2
ICD	International classification of diseases
ICG	Indocyanine green
IDC	Invasive ductal carcinoma
IHC	Immunohistochemistry
IOTPC	Intraoperative touch preparation cytology

IOUS	Intraoperative ultrasound
IR	Identification rate
IRB	Institutional review board
IVIS	<i>In vivo</i> imaging system
LED	Light-emitting diode
LND	Lymph node dissection
LR	Local recurrence
MGB1	Mammaglobin 1
MMP	Matrix metalloproteinase
MRI	Magnetic resonance imaging
MSAP	Multifunctional single attachment point
MVA	Multivariate regression analysis
NIR	Near-infrared
NIRF	Near-infrared fluorescence
OR	Odds ratio
PB	Patent blue
PBS	Phosphate-buffered saline
PET	Positron emission tomography
PR	Progesterone receptor
QUADAS	Quality assessment of diagnostic accuracy studies
RCT	Randomized controlled trial
ROI	Region of interest
ROLL	Radioguided occult lesion localization
RSL	Radioguided seed localization
SCAPOS	Segmentation-based comparative analysis of planar optical signals
SD	Standard deviation
SLN	Sentinel lymph node
SLNB	Sentinel lymph node biopsy
SLNM	Sentinel lymph node mapping
SN	Signal-to-noise
SPECT	Single-photon emission computed tomography
TBR	Tumor-to-background ratio
TBS	Tris-buffered saline
TFT	Thin-film transistor
TIS	Three-item severity score
TMA	Tissue microarray
US	Ultrasound
VEGF-A	Vascular endothelial growth factor A
WGL	Wire-guided localization

DANKWOORD

De afgelopen vier jaren heb ik mij gedurende mijn MD/PhD-traject afwisselend ingezet voor co-schappen en wetenschappelijk onderzoek. Het is een mooie en leerzame tijd geweest die ik zo weer over zou doen, ondanks de nodige tegenslagen gedurende de rit. Vanaf deze plek wil ik iedereen bedanken die heeft meegewerkt aan de totstandkoming van dit proefschrift. Een aantal mensen noem ik daarbij persoonlijk.

Prof. Dr. G.M. van Dam, beste Go, met je passie voor wetenschappelijk onderzoek en je ontembare enthousiasme heb je mij geleerd dat alles mogelijk is, zolang je er maar in blijft geloven en er voor de volle honderd procent voor gaat. Op verscheidene terreinen ben je een voorbeeld voor mij geweest. Ik dank je voor het vertrouwen dat je vanaf het begin in mij hebt gesteld. Je stimuleerde mij uit mijn comfort-zone te komen en nieuwe uitdagingen aan te gaan. Iets wat ik ook in de toekomst zal blijven nastreven.

Prof. dr. T. Wiggers, beste Theo, ik waardeer onze overleggen, waarbij je mij het vertrouwen hebt gegeven dat het voorliggende project haalbaar zou zijn in de beperkte tijdsduur van een MD/PhD-traject. Je constructieve feedback en bemoedigende woorden maken dat ik hier met goede herinneringen aan terugdenk.

Mijn dank gaat uit naar de leden van de leescommissie voor het beoordelen van het manuscript: **prof. dr. P.J. van Diest**, **prof. dr. C.W.G.M. Löwik** en **prof. dr. E.G.E. de Vries**.

Dr. W. Helfrich, beste Wijnand, dank voor je interesse gedurende het onderzoekstraject, innovatieve ideeën en constructieve feedback.

Van de afdeling pathologie wil ik met name **Jos Bart**, **Bert van der Vegt** en **Tineke van der Sluis** bedanken. Beste Jos, de besprekingen met jou resulteerden dikwijls in nieuwe ideeën en bliezen de projecten nieuw leven in. Beste Bert, gezamenlijk namen we stapels coupes door, op zoek naar geschikte lymfekliermetastasen voor nadere analyse. Beste Tineke, dank voor het kleuren van een indrukwekkende hoeveelheid TMA's en het geven van een kijkje in de keuken van het pathologielaab.

Dr. S. Siesling, beste Sabine. Dank voor je begeleiding gedurende het traject en je positieve instelling. Je ziet altijd mogelijkheden en hebt daarmee vele kansen gecreëerd, waarmee we het nomogram project tot een succes hebben kunnen maken. Ook wil ik **Annemiek Kwast** bedanken voor haar inzet en interesse. De statistische exercitie voor de ontwikkeling van het (digitale) nomogram was niet mogelijk geweest zonder jouw inspanningen.

I would like to thank **prof. dr. V. Ntziachristos**, **George Themelis**, **Thanos Sarantopoulos**, **Jürgen Glatz**, and **Maximilian Koch** from the Technical University of Munich. George, Thanos, Jürgen, and Maximilian, thank you for the technological assistance when operating the fluorescence camera system. It has been a pleasure working and dining with you.

Liesbeth Jansen en Jaap de Vries, beste Jaap en Liesbeth, dank voor jullie betrokkenheid gedurende het traject en voor het grondig reviseren van enkele papers.

Sjoerd Elias, beste Sjoerd, je kennis van statistiek en enthousiasme maken dat de samenwerking met jou altijd zeer prettig is verlopen. Levendige telefoongesprekken resulteerden in nieuwe ideeën, waarmee onze gezamenlijke papers naar een hoger niveau werden getild.

Gedurende het traject heb ik deel uit mogen maken van een enthousiaste onderzoeksgroep onder leiding van prof. dr. van Dam: **Hans de Jong, Wendy Kelder, Lucy Crane, Tim Buddingh, Marleen van Oosten, Niels Harlaar, Arash Motekallemi, Brenda Samaniego, Niels Langhout, Esther de Boer** en **Arwin Timmermans**. De onderlinge sfeer was altijd goed. Allen bedankt voor de prettige samenwerking en de inspirerende (onderzoeks)besprekingen.

Alle medewerkers van het Chirurgisch Onderzoekslaboratorium wil ik bedanken, in het bijzonder **Jacco Zwaagstra**. Beste Jacco, dank voor je bereidheid om mij wegwijs te maken op het Chirurgisch Onderzoekslaboratorium en mijn vragen te beantwoorden. Ik waardeer je nuchterheid, humor en consequente handhaving van de regels.

Van de kamer- en ganggenoten uit het Triadegebouw wil ik een aantal mensen apart bedanken: **Jeffrey Damman, Deborah van Dijk, Isalien Bakker, Kevin Wevers, Edris Alkozai, Mark Kirschbaum, Hilde Hoving, Geert van Rijt, Justin Smit** en **Maarten Speijers**.

Greg Hugenholtz, beste Greg, als kamergenoten hebben we aan elkaar een goede stimulans gehad om hard aan de slag te gaan. Ik waardeer je humor en brede kijk op de wereld. **Maarten Niebling**, beste Maarten, verscheidene uren hebben we besteed aan het verzamelen en doorlezen van artikelen voor onze systematische review, wat een monsterklus bleek. Dank voor je geduld tijdens mijn semi-arts stage en je positieve instelling. **Kevin Wevers**, beste Kevin, je creativiteit en vindingrijkheid zullen mij op positieve wijze bijblijven.

Paranimfen **Kasper Veldhuis** en **Arnoud Potgieser**. Lieve Kasper, de afgelopen jaren ben jij mijn steun en toeverlaat geweest en heb je alle onderzoeksverhalen moeten aanhoren. Ik hoop dat er nog vele jaren samen zullen volgen. Beste Arnoud, hoewel ik je pas heb ontmoet tijdens mijn co-schappen is het alsof we elkaar al jaren kennen. Ik hoop dat onze band nog vele jaren mag blijven bestaan.

Tjitte Verbeek, beste Tjitte, het is een plezier om met je te kunnen samenwerken en te brainstormen over innovaties in de gezondheidszorg, wat inmiddels geresulteerd heeft in enkele interessante projecten. Ik hoop dat er in de nabije toekomst nog vele volgen!

Graag wil ik enkele vrienden bedanken voor hun interesse in mijn werkzaamheden en de gezellige avonden als broodnodige ontspanning naast de studie en promotie: **Joep Kamphuis, Nick Marsman, Arden Jurgens, Emil Ronhaar, Kirsten Braamhaar, Joyce Lubbers, Sharyna Piek, Guus Jannink, Tim Jannink, Laura de Wijs, Sander Beldman, Marco Korte, Desiree Oldenhof, Bastiaan Meijer, Harm Brouwer, Silke Spit** en **Elmar Jagers**. Ook bedank ik de leden van tutorgroep 42, waarmee ik begon aan de opleiding geneeskunde en wat tot jaren daarna een hechte groep zou blijven: **Lejan Schultinge, Marloes Prins, Erika Droogsma, Marleen Hennink, Louis Prins, Marco Gaster, Jaap Eeuwema, Alie den Hartogh, Narmi Sollie, Christiaan Verhulst** en **Nienke van der Werff**.

Erik Verbeek, beste Erik, de afgelopen jaren heb jij je bewezen als trouwe vriend en heb je een onmisbare bijdrage geleverd aan de realisatie van onze gezamenlijke ICT-projecten.

Jan en Angelien Pleijhuis, mijn lieve ouders, bedankt voor jullie onvoorwaardelijke interesse en ondersteuning. Zonder jullie zou dit alles niet mogelijk zijn geweest. Ik had mij geen betere ouders kunnen wensen!

Groningen, januari 2014

Rick Pleijhuis

LIST OF PUBLICATIONS

1. van Dam GM, Themelis G, Crane LM, Harlaar NJ, [Pleijhuis RG](#), Kelder W, Sarantopoulos A, de Jong JS, Arts HJ, van der Zee AG, Bart J, Low PS, Ntziachristos V. Intraoperative tumor-specific fluorescence imaging in ovarian cancer by folate receptor- α targeting: first in-human results. *Nat Med.* 2011; 17(10):1315-9.
2. Crane LM, van Oosten M, [Pleijhuis RG](#), Motekallemi A, Dowdy SC, Cliby WA, van der Zee AG, van Dam GM. Intraoperative imaging in ovarian cancer: fact or fiction? *Mol Imaging.* 2011; 10(4):248-57.
3. [Pleijhuis RG](#), Langhout GC, Helfrich W, Themelis G, Sarantopoulos A, Crane LM, Harlaar NJ, de Jong JS, Ntziachristos V, van Dam GM. Near-infrared fluorescence (NIRF) imaging in breast-conserving surgery: assessing intraoperative techniques in tissue-simulating breast phantoms. *Eur J Surg Oncol.* 2011; 37(1):32-9.
4. [Pleijhuis RG](#), Kwast AB, Jansen L, de Vries J, Lanting R, Bart J, Wiggers T, van Dam GM, Siesling S. A validated web-based nomogram for predicting positive surgical margins following breast-conserving surgery as a preoperative tool for clinical decision-making. *Breast.* 2013; 22(5):773-779.
5. Crane LM, Themelis G, Buddingh K, Harlaar NJ, [Pleijhuis RG](#), Sarantopoulos A, van der Zee AG, Ntziachristos V, van Dam GM. Multispectral real-time fluorescence imaging for intraoperative detection of the sentinel lymph node in gynecologic oncology. *J Vis Exp.* 2010; (44). pii:2225.
6. Crane LM, Themelis G, [Pleijhuis RG](#), Harlaar NJ, Sarantopoulos A, Arts HJ, van der Zee AG, Ntziachristos V, van Dam GM. Intraoperative multispectral fluorescence imaging for the detection of the sentinel lymph node in cervical cancer: a novel concept. *Mol Imaging Biol.* 2011; 13(5):1043-9.
7. [Pleijhuis RG](#), Graafland M, de Vries J, Bart J, de Jong JS, van Dam GM. Obtaining adequate surgical margins in breast-conserving therapy for patients with early-stage breast cancer: current modalities and future directions. *Ann Surg Oncol.* 2009; 16(10):2717-30.
8. Verbeek T, [Pleijhuis RG](#), van Kleef AJG, Stegmann ME, Schultinge L, Sillius AW, Bos FM, Molenaar WM. Ervaringen met een Basiskwalificatie Onderwijs voor studenten (BKO-S). *TMO.* 2011; 30(6):272-282.
9. [Pleijhuis RG](#), Stegmann ME, Schultinge L, Verbeek T, van Kleef AJG, Sillius AW, Bos FM, Molenaar WM. Studenten trainen medestudenten in didactische vaardigheden. *TMO.* 2011; 30(4):143-151.
10. Gaykema SB, Brouwers AH, Lub-de Hooge MN, [Pleijhuis RG](#), Timmer-Bosscha H, Pot L, van Dam GM, van der Meulen SB, de Jong JR, Bart J, de Vries J, Jansen L, de Vries EG, Schröder CP. 89Zr-Bevacizumab PET imaging in primary breast cancer. *J Nucl Med.* 2013; (7):1014-8.
11. [Pleijhuis RG](#), Siesling S, van Dam GM. Digitaal nomogram voor positieve snijvlakken bij borstsparende chirurgie. *Oncologie up-to-date.* 2013; 4:25-26.
12. [Pleijhuis RG](#), Timmermans AC, de Boer E, de Jong JS, Ntziachristos V, van Dam, GM. Tissue-simulating phantoms for assessing potential near-infrared fluorescence imaging applications in breast cancer surgery. (*Accepted, awaiting publication*).

BOOKCHAPTERS

1. [Pleijhuis RG](#), Crane LM, van Oosten M, Ntziachristos V van Dam GM. Optical imaging applications in cancer research and treatment. 2013 *Cancer - Cares, Treatments, and Preventions*. ISBN: 978-1477554-99-9. iConcept Press.
2. Crane LM, [Pleijhuis RG](#), van Oosten M, van Dam GM. Molecular imaging of ovarian carcinoma. (*Accepted, awaiting publication*).

CURRICULUM VITAE (English)

Rick Pleijhuis was born on August 26th 1987 in Almelo, the Netherlands. In 2005, he graduated from high school at the Pius X College in Almelo, the Netherlands. After graduation, he enrolled in medical school at the State University of Groningen in 2005.

In the years that followed, Rick participated in many extracurricular activities and as a member of the committee on medical education, committee on education- and research, and the research advisory committee. In the second year of his study, Rick took part in a research project on optical imaging within the research group of prof. G.M. van Dam. The project served as the basis for the writing of his scientific thesis, for which he received an award for best thesis from the Nijbakker Morra Foundation in March 2010. Moreover, Rick applied for an ambitious MD/PhD-program on intraoperative near-infrared fluorescence imaging in breast cancer, which was granted in the same year.

In 2012, Rick received a talent grant for his research project from the Junior Scientific Masterclass and the Ubbo Emmius Fund and was installed in the Groningen Talent Group. After completing two years of internships, Rick graduated from medical school *cum laude* in April 2013. In the same year, he completed a four year training program on medical education and received the student of the year award from the Faculty of Medical Sciences at the State University of Groningen.

After defending his PhD thesis, Rick will start with a clinical training program to become a medical specialist in internal medicine.

CURRICULUM VITAE (Nederlands)

Rick Pleijhuis werd op 26 augustus 1987 geboren in Almelo. De middelbare school doorliep hij aan het Pius X College te Almelo, waar hij in 2005 slaagde voor het eindexamen gymnasium. Aansluitend startte hij met de studie geneeskunde aan de Rijksuniversiteit Groningen.

In de jaren die volgden was hij actief binnen Medische Faculteitsvereniging Panacea en verschillende medezeggenschaps-gremia, waaronder de opleidingscommissie geneeskunde (OCG), de onderwijs- en onderzoeksraad (O&O-raad) en de research advisory committee (RAC). Wetenschappelijke interesse ontstond in het tweede studiejaar. Rick verrichtte wetenschappelijk onderzoek op de afdeling chirurgie, waar hij binnen de onderzoeksgroep van prof. dr. G.M. van Dam een project kreeg toegewezen naar optische beeldvorming van het mammacarcinoom. Dit zou tevens het onderwerp worden van zijn wetenschappelijk stage, waarvoor hij in maart 2010 de Nijbakker Morra Scriptieprijs ontving. Hetzelfde onderzoek diende als basis voor een MD/PhD-traject, dat eveneens in 2010 werd gehonoreerd.

Gedurende het MD/PhD-traject combineerde Rick zijn co-schappen met wetenschappelijk onderzoek. Daarnaast verzorgde hij onderwijs voor jongerejaars studenten en participeerde in diverse didactische trainingen in het kader van een vierjarig opleidingsprogramma ter verkrijging van de basiskwalificatie onderwijs voor studenten (BKO-S). In 2012 ontving Rick een Talent Grant van de Junior Scientific Masterclass en het Ubbo Emmius Fonds. Kort daarop werd hij op voordacht van de Junior Scientific Masterclass geïnstalleerd in de Groningen Talent Group. In april 2013 studeerde Rick *cum laude* af als arts. Drie maanden later ontving hij uit handen van het Groninger Universiteit Fonds de GUF-100 prijs voor beste student van de Faculteit Medische Wetenschappen (kalenderjaar 2012–2013). In oktober 2013 sloot Rick zijn didactische opleidingsprogramma succesvol af met het behalen van de BKO-S.

Na afronding van zijn promotie zal Rick in februari 2014 starten met de opleiding tot medisch specialist in de interne geneeskunde.